Measuring the neutral temperature in railway track during installation and use

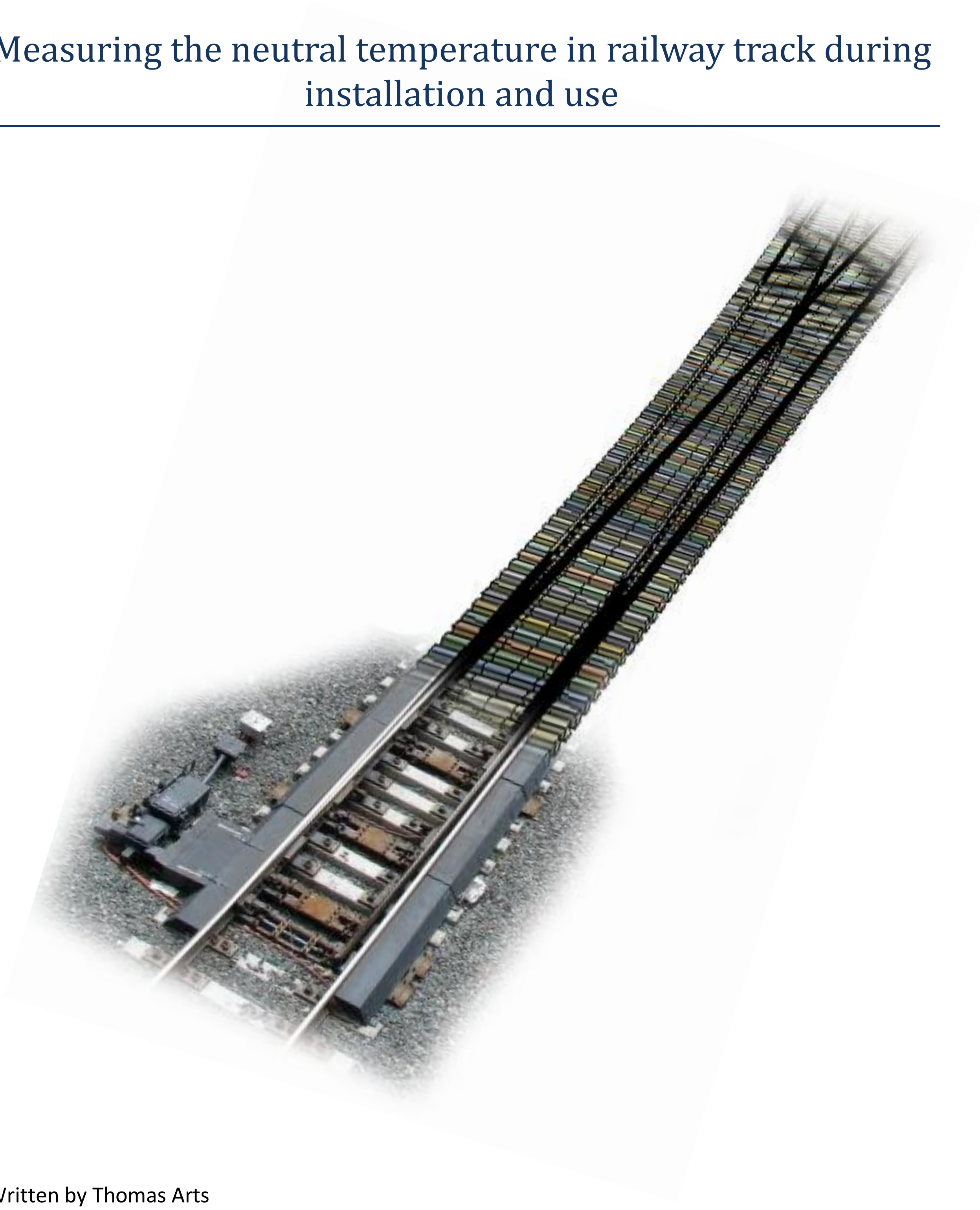

Written by Thomas Arts
Technical University Delft
Faculty of Civil Engineering and Geosciences
Section Road and Railway Engineering

Contact:

Student:
T.M.H. Arts
Thomas_moi@hotmail.com
06 53 49 49 77

Thesis committee:
Prof.dr.ir. A.A.A. Molenaar
TU Delft, section Road and Railway Engineering
A.A.A.Molenaar@tudelft.nl

Dr. V.L. Markine
TU Delft, section Road and Railway Engineering
V.L.Markine@tudelft.nl

Dr. Ir. P.C.J. Hoogenboom
TU Delft, section Construction Mechanics
P.C.J.Hoogenboom@tudelft.nl

Dr. I. Y. Shevtsov
ProRail, Asset Management
Ivan.shevtsov@prorail.nl

Preface

Before the reader lies the product of eleven months of research and testing. This report summarises all the findings and actions related to the graduation project I have undertaken. I have written this project as a student of the Faculty of Civil Engineering and Geosciences, at the Road and Railway section. The research in this report was done for the railway network operator ProRail in the Netherlands. The goal is to provide insight in the mechanics of producing "stress free" rail, and to provide the basis for producing new guidelines. It comprises theory, laboratory tests, practical tests and a finite element model and combines these elements to increase the fundamental knowledge of track behaviour. On a national level, this research has provided new insights and knowledge and has confirmed or disproven several theories.

Thanks go out to Ivan Shevtsov for his supervision of my work at ProRail, and his assistance in the dealings with all the outside actors and companies this project requires. A word of thanks to the entire asset management department of ProRail is also in place, as they have facilitated my research, and have been very friendly in the process.
Thanks also go out to Valeri Markine, for his assistance with the modelling software Ansys®.

For the laboratory test, I would like to thank Maarten Vaandrager (Stork FDO Inoteq) for his expertise in setting up and executing the laboratory test. Thanks also go out to Gianluca Cescon (Stork FDO Inoteq) for setting up and executing the practical tests.

Finally, I would like to thank my family and friends for their support, their company during the last six years of my study, the distraction they offered, and their help in proofreading this report. I would especially like to thank Ilse Schelling for her unconditional support during the long process of writing this Thesis.

Delft, July 22th 2011

Summary

The current guideline in use by ProRail, the rail network operator in the Netherlands, for the application of continuous welded rail in the Netherlands ("RLN 00120 Het voegloos maken van spoor, wissels en kruisingen") is considered difficult to execute in practice. The goal of this research is to provide insight in rail mechanics that will allow ProRail to improve their guideline, and to change it from a prescriptive guideline to a result-based guideline. To improve the understanding of the behaviour of turnouts under thermal loading a finite element model was developed. Next to the development of this model, practical tests were performed gathering data about the behaviour of pieces of replacement rail in the track.

The used finite element model was developed in ANSYS® using parameters established by earlier research. It was validated by referencing it with the LONGSTAB software that is currently used to analyse rail behaviour. Using the model, several thermal load situations were analysed, as well as the practices prescribed by the ProRail guideline. Results from the model indicate that the prescribed actions of ProRail have a positive effect on the stresses in the turnout. This model is usable in further research to improve the guidelines, and provides a basis for modelling larger turnout complexes and crossings.

To validate theoretical assumptions and predictions several practical tests were drawn up and executed. These include a laboratory test to verify sensor accuracy, a small test to experiment with displacement measurements and two tests to be conducted during rail maintenance. The first of these in situ tests was executed on a 6-meter piece or replacement rail, measuring the strains and displacements taking place during the replacement. After replacement long term monitoring of the strain behaviour was started. Unfortunately, one of the planned practical tests on the replacement rails was not executed in the process of this research. This is due to delays, such as sensor delivery time, problems getting permission from the regional ProRail departments, and budget cuts. However, the test has been prepared during the course of this research, the plan for the test was drawn up, all the equipment has been acquired and the laboratory test has been executed to validate the sensor output.

The laboratory test proved that the application of strain gauges was a viable method to measure the strains in the track; their accuracy was well within the desired margins as stated by ProRail. Furthermore, the laboratory test provided valuable insight into the temperature effects on strain gauge outputs.

The practical test on a 6-meter replacement rail provided interesting outcomes, validating some theories and refuting one. The theory that the cooling of welds increases the neutral temperature of the rail was validated, as well as the idea that the shrinkage of each weld was around 1.5 mm. The theory that the adjacent track would be fixed in position by the fasteners was refuted, movement appeared to be possible quite easily.

Furthermore, a number of problems occurring during the practical measurements were isolated and solutions to these problems were engineered. These problems include data logger errors, placement problems for some displacement sensors and temperature influences. The found solutions to these

problems will allow ProRail to perform the larger 30-meter replacement rail test, which involves a larger amount of sensors and more locations that will be monitored to be conducted without running into the problems encountered during this first test. Lastly, ProRail can then perform measurements on a turnout, and use these measurements for validation and improvement of the theoretical model, and allowing future investigations to be performed using the model, saving valuable time and money compared to having to execute these tests in situ.

During the practical tests, it was established that the temperature – force relation is not a constant one for this location. At lower temperatures, the rail can expand almost freely and no force is build up in the rail. When temperatures become higher, this expansion becomes more difficult and that leads to an increase of internal forces.

At the end of this research almost all of the original research questions have been answered (with the exception of the relation between a turnout in situ and the theoretical model), and much greater insight was collected into the mechanics of rail behaviour. This insight concerns the behaviour of track in practice, and a turnout theoretically, under temperature influences, and the influences of welds on a replacement rail. A number of ProRail suspicions and theories have been validated in the process, and can now be explained using the theoretical model or the practical measurement results. The guideline itself has not yet been adapted, but the knowledge gathered has already revealed possible improvements and a validation for the current regulations considering turnout construction.

It can be summarised that the conducted research provides a solid basis upon which ProRail can execute the further tests as described. These tests will provide even further insight into rail mechanics and will most likely lead to improvements in the guidelines. It is therefore strongly recommended to conduct the 30-meter rail test, and to perform a test on a turnout. This will allow validation of the finite element model, and will open up a cost efficient and fast way to test possible guideline improvements.

The application of sensors as during this test does not lend itself to large-scale application (due to its lack of robustness); however, suggestions for an optimised approach can be found in the conclusions. The foundation for the application of strain or stress sensors in the rail has been laid down in this report, thereby bringing ProRail one step closer to its ideal of “Smart Track”.

Samenvatting

De huidige richtlijn in gebruik door ProRail, de rail netwerk manager in Nederland, voor het toepassen van voegloos spoor (“RLN 00120 Het voegloos maken van spoor, wissels en kruisingen”) wordt als moeilijk uitvoerbaar beschouwd. Het doel van dit onderzoek is het leveren van inzicht in het gedrag van spoor. Deze inzichten zullen ProRail in staat stellen hun richtlijn te verbeteren, en deze te veranderen van een voorschrijvende richtlijn naar een richtlijn die op resultaten stuurt. Ten einde het inzicht in het gedrag van wissels onder warmtebelastingen te verbeteren is een eindige elementen model ontwikkeld. Naast het ontwikkelen van dit model zijn ook een aantal praktijkproeven uitgevoerd waarin gegevens verzameld werden die het gedrag van een passtuk in de rails beschrijven.

Het eindige elementen model werd ontwikkeld met behulp van parameters die door eerder onderzoek tot stand zijn gekomen. Het model werd gevalideerd door deze te correleren aan de LONGSTAB software welke op dit moment gebruikt wordt om het gedrag van spoor te voorspellen. Met behulp van dit model werden verschillende warmte belastingen geanalyseerd, evenals de situatie die ontstaat door het gebruik van de ProRail richtlijnen. De resultaten van het model geven aan dat de voorgeschreven handelingen door ProRail inderdaad een gunstig effect hebben op de spanningen in een wissel. Dit model kan in toekomstig onderzoek gebruikt worden om de richtlijnen te verbeteren, en levert een basis waarop grotere wissel complexen en kruisingen kunnen worden gemodelleerd.

Voor het bewijzen van de theoretische aannames en voorspellingen zijn een aantal praktijkproeven opgesteld en uitgevoerd. Hieronder valt een laboratorium proef om de nauwkeurigheid van de sensoren vast te stellen, een kleine proef om de verplaatsingsmeter uit te testen en twee praktijkproeven tijdens onderhoudswerkzaamheden. De eerste van deze twee praktijkproeven behelsde het plaatsen van een 6 meter lang passtuk, waarbij de rekken en verplaatsingen tijdens het plaatsen gemeten werden. Na het plaatsen van het passtuk werd vervolgens over gegaan op over lange termijn vastleggen van de verandering in rekken. Helaas kon een van de geplande praktijkproeven niet gedurende de loop van dit onderzoek uitgevoerd worden. Dit heeft te maken met vertragingen, zoals de levertijd van sensoren, problemen met het verkrijgen van toestemming van het regio beheer van ProRail en bezuinigingen. Deze test is echter al wel voorbereid tijdens dit onderzoek, een plan voor de uitvoering van de test is opgesteld, de meetinstrumenten zijn aangeschaft en deze zijn in de laboratoriumproef gevalideerd.

Met behulp van de laboratoriumproeven is bewezen dat rekstroken toegepast kunnen worden als methode om de rek te meten. Er werd vastgesteld dat hun nauwkeurigheid ruim binnen de door ProRail gewenste marge viel. Daarnaast heeft de laboratoriumproef waardevolle informatie opgeleverd met betrekking tot de temperatuur gevoeligheid van rekstroken.
De praktijkproef op het 6 meter lange passtuk heeft een aantal interessante resultaten opgeleverd, waarmee een aantal theorieën bewezen werden en een theorie weerlegd werd. De theorie dat het koelen van de las de spanning in het passtuk opdrijft werd bewezen, evenals het gegeven dat een las ongeveer 1.5 mm krimpt. De theorie dat de aan het passtuk vast gelasten spoorstaaf niet zou kunnen verplaatsen vanwege de bevestigingen werd weerlegd, verplaatsingen bleken zeer goed mogelijk.

Naast het vergaren van metingen werden tijdens de praktijkproeven ook een aantal problemen vastgesteld, en werden er voor deze problemen oplossingen bedacht. Deze problemen omhelsden problemen met de data logger, plaatsingsproblemen voor de verplaatsingssensoren en temperatuurs effecten in de data logger. De gevonden oplossingen kunnen door ProRail gebruikt worden om de metingen op een passtuk van 30 meter, waarop meer sensoren geplaatst worden en op meer locaties gemeten wordt, uit te voeren zonder dat deze problemen zich nog eens voordoen. Hierna kan het onderzoek afgesloten worden met een praktijkmeting op een wissel, waarmee hopelijk het eindige elementen model gevalideerd en verbeterd kan worden. Dit stelt ProRail in staat om toekomstig onderzoek digitaal uit te voeren, waarmee kostbare tijd en geld bespaard kunnen worden.

Tijdens de praktijkproef is gebleken dat de relatie tussen temperatuur en kracht in de rail niet constant is. Bij lagere temperaturen kan de rail bijna vrij uitzetten en wordt er geen kracht opgebouwd in de rail. Als de temperatuur hoger wordt, wordt deze uitzetting moeilijker. Dit leidt tot een toename van de krachtverhoging door temperatuurverschillen.

Bij sluiting van dit onderzoek zijn bijna alle van de originele onderzoeksvragen beantwoord (met uitzondering van de relatie tussen een wissel in de praktijk en het theoretische model). Tijdens dit proces is veel inzicht verkregen in het gedrag van spoor. Dit inzicht behelst het gedrag van het spoor in de praktijk, hoe een wissel zich theoretisch gedraagt onder temperatuur invloeden, en de invloed van lassen op een passtuk. Een aantal van de vermoedens en theorieën die de ronde deden bij ProRail zijn hiermee bevestigd, en kunnen nu met behulp van het model en de meetgegevens verklaard of onderbouwd worden. De richtlijn zelf is nog niet aangepast, maar de kennis die verzameld is heeft al een aantal verbeterpunten mogelijk gemaakt. De juistheid van de huidige richtlijnen voor het aanleggen van wissels zijn in dit onderzoek bevestigd.

Samenvattend kan gesteld worden dat het uitgevoerde onderzoek een solide basis heeft gecreëerd waarop ProRail verdere proeven kan baseren. Deze proeven zullen het inzicht in het gedrag van spoor nog verder vergroten, en zullen vrijwel zeker tot verdere verbetering van de richtlijn leiden. Daarom is het van zeer groot belang dat de proef op het 30 meter passtuk, en een proef op een wissel nog uitgevoerd zullen worden. Deze laatste proef kan het eindige elementen model valideren en zal daarmee een goedkope en snelle manier leveren om de richtlijnen nog verder te verbeteren.

Het toepassen van sensoren zoals gedurende dit onderzoek is gedaan leent zich niet voor grootschalige toepassing (dit door het kwetsbare systeem), maar suggesties voor een verbeterde toepassing zijn in de conclusie van dit rapport weergegeven. De basis voor het gebruik van rek of spannings sensoren is in dit onderzoek gelegd, hiermee is ProRail weer een stap dichterbij hun ideaal van “Slim Spoor”.

Table of contents

Contact: 2
Preface 3
Summary 4
Samenvatting 6
Table of contents 8
1 Definitions 11
1.1 Terminology 11
1.2 Definitions: 11
1.3 Decimals and thousands 11
2 Introduction 12
3 Project approach: 13
3.1 Problem definition 13
3.2 Goal 13
3.3 Research questions 14
3.4 Assumptions 14
3.5 Actors 14
3.6 Time span and locations 15
3.7 Scope 15
3.8 Budget cuts 15
4 Problem analysis 17
4.1 The track structure 17
4.2 The rails 17
4.3 Jointed and continuous welded rail 19
4.4 Track failure 19
4.5 Temperature force theory 22
4.6 Plastic shear resistance theory 23
4.7 Achieving neutral temperature in rail 24
4.8 Welding methods 26
4.9 Turnouts components 28
5 State of the art in procedures 30
5.1 Rail replacement procedure 30
5.2 Turnouts and crossings 31
5.3 In practice 32
6 Procedure proposal 33
7 Overview of considered measuring methods 34
7.1 Cutting method 34
7.2 Lifting method 34
7.3 Deformation methods 35
7.4 Ultrasonic methods 35
7.5 X ray method 36
7.6 Vibration method 37
7.7 Magnetic method 37
8 Measurement method and sensor types 38
8.1 Strain gauge basics 38

8.2 Reference point from zero measurement ... 38
8.3 Reference point from secondary measurement method ... 39
8.4 Difficulties encountered by using strain gauges ... 40
8.5 Behaviour of the strain gauge under temperature influences ... 42
9 Selecting the measurement equipment ... 43
9.1 Procedure of selecting the measuring system ... 43
9.2 Measurement precision ... 43
9.3 Comparison of proposed sensors ... 44
10 Modelling the rail ... 46
10.1 The straight track model ... 46
10.1.1 Stiffness determination ... 46
10.1.2 Comparison to LONGSTAB model ... 50
10.1.3 Non-linear model ... 52
10.2 Turnout ... 54
10.2.1 Model parts and materials ... 54
10.2.2 Model preparation ... 61
10.2.3 Modelled situations ... 61
10.2.4 Limitations ... 63
11 Model results ... 64
11.1 Numerical outcomes of the basic model ... 65
11.1.1 Stresses and strains ... 65
11.1.2 Displacements ... 68
11.2 Numerical outcomes of the linear 2/3 fixed model ... 69
11.2.1 Stresses and strains ... 69
11.2.2 Displacements ... 71
11.3 Numerical outcomes of the non-linear 2/3 fixed model ... 73
11.3.1 Stresses and strains ... 73
11.3.2 Displacements ... 74
11.4 Practical situation ... 76
11.4.1 Situation after construction ... 77
11.4.2 Situation at 40 degrees turnout temperature ... 79
11.5 Conclusions ... 83
12 Practical tests ... 85
12.1 The laboratory tests ... 85
12.1.1 Description: ... 85
12.1.2 Preparation ... 87
12.1.3 First laboratory test execution: ... 89
12.1.4 Second laboratory test execution ... 90
12.1.5 Final test execution ... 92
12.1.6 Evaluation of all laboratory tests ... 92
12.1.7 Accuracy ... 101
12.1.8 The measurements compared to the theory ... 104
12.2 The first in-situ test - planning ... 107
12.2.1 Set up ... 107
12.2.2 Preparation ... 109

12.2.3 Placement of the rail ... 110
12.3 The first in-situ test - execution ... 113
12.3.1 Location ... 113
12.3.2 Installation procedure ... 116
13 Test results ... 121
13.1 Rail replacement ... 121
13.1.1 Basics ... 121
13.1.2 Strain gauge ... 121
13.1.3 DVRT ... 125
13.1.4 Temperature ... 127
13.1.5 Incidents ... 130
13.2 Long term measurements ... 131
14 Conclusions ... 136
15 Recommendations ... 142
15.1 Improved strain sensor implementation ... 143
16 References ... 145

1 Definitions

1.1 Terminology

Because multiple definitions are used in literature and various countries, a short definition and determination of terms to be used in this report shall be given below.

Track - The structure of rails, sleepers and substructure that support the train.

Rail - The metal beams of the track, which are in direct contact with the wheels of the trains.

Turnout - The piece of track where trains can change direction. In America this is referred to as a switch, while in England it is called a turnout.

1.2 Definitions:

CWR – Continuous welded rail.

Sleeper – The wooden or concrete support of the track usually placed every 60 cm.

Buckling – A sudden and large lateral movement in a beam caused by compression.

Stress free temperature or neutral temperature – Rail is constructed with a stress situation that is equal to the stresses which would occur naturally at this temperature. For the Netherlands this temperature is 25 °C. By constructing to this temperature (which is about the average of the temperature extremes) it is unlikely that the stresses in the steel will become too high or too low. If for example temperatures range between -10 and 60, all rails should be constructed at 25°C to minimise temperature stresses.

Data logger – A device to collect the outputs of the measuring devices.

LVDT – Linear variable differential transformer. A sensor to determine displacements of the probing head. This type of sensor is based on a full electrical bridge set up.

DVRT – Differential variable reluctance transducer. A sensor similar to a LVDT, but with an increased temperature compensation system.

Point machine – Actuator that moves and locks the switchblade. (In Dutch Wisselsteller, ALD in European codes)

Spring back – Displacement of the rails (retreating or springing back) from the cutting location due to tensile temperature stresses.

1.3 Decimals and thousands

Decimal numbers are denoted by a “. “ For example: 0.5

Thousands are separated by a “,” for example: 100,000

The American system of separation marks is used instead of the Dutch system because of personal preference by the author.

2 Introduction

The rail network in the Netherlands is an essential asset for its economy and the mobility of its inhabitants. With a growing economy and increasing mobility, it is therefore subject to an increase in demand of its capacity. To be able to live up to this demand it is vital that rail conditions and maintenance schedules are optimum. This is the reason ProRail has drawn up regulations for all the aspects concerning the maintenance and construction on its network. The current regulation[1] concerning the application of continuous welded rail on both straight track and turnout (arrangements) and crossings is considered “hard to execute”.

ProRail would like to append its current regulations and change them from being very prescriptive, concerning every action, to being a standard to comply to. This standard would set demands for the geometry and neutral temperature of the turnout or crossing construction. There are already systems in place to measure the geometry, but none are developed to determine the neutral, or stress free, temperature. This raises the problem for ProRail on how to measure neutral temperature in an implementable and economical fashion. Already some companies are developing systems to measure the stresses in the rail. These systems however only output the data of a single spot of rail. A complete model that would relate these outputs to the behaviour of turnouts and crossings is however still lacking.

This is one of the reasons for this master thesis to be commissioned, providing ProRail with models that proof that the neutral temperature can be deducted from measurements. Next to this, these would also need to provide insight into how turnouts or turnout systems behave. This will then provide ProRail with a way to check the constructions that were put in place by its subcontractors, allowing ProRail to draw up new regulations. These regulations would give the subcontractors more freedom to optimise their actions, while still applying the current high standard of the result. This would be one of the first steps towards an intelligent rail system, in which all the rail stresses are known at all times. The benefit being that lengths of track subject to a high risk of buckling or tensile breaking can be identified and that incidents occurring because of these actions can be prevented at all times.

Another reason is to provide ProRail with a foundation on which to base their choice of a measurement system, and to enable them to draw up a well-argued list of demands for this new system. By having a better insight in the behaviour of the system, the tools to be applied on the system can be further fine-tuned.

[1] RLN00120 Richtlijn het voegloos maken van sporen, wissels en kruisingen

3 Project approach:

In this chapter, an overview of the problem definition as described by ProRail is provided, alongside the long-term and direct goals. The related research questions, assumptions and all the actors of this research are presented as well. Furthermore, the geographical locations of practical tests, the scope of this research and the influence of budgets cuts are discussed.

3.1 Problem definition

To prevent the problems discussed in chapter 4.4 ProRail has set up guidelines, which must be followed by the contractors performing maintenance on the rail. Rail maintenance parties would like to simplify current guidelines for the replacement of turnouts and crossings, and change these from prescriptions per action to a guideline for the result. ProRail agrees with this sentiment and wants to transform their current extensive manual to a document stating the (geometrical and neutral temperature (chapter 4.4)) demands that would have to be met. This approach will grant ProRail's contractors more freedom in their work methods, allowing the current "hard to execute" guideline to be replaced by one which is easier to implement, and therefore enjoys more support among contractors.

To reach this goal ProRail wants to use a new measuring system for the neutral rail temperature (theoretical information about rail neutral temperature can be found in chapter 4.5). A simple, direct and always executable check for the stress free temperature is not yet developed. Though methods are available, these are often hard to implement or are of a complicated nature. ProRail is therefore looking for a more simple and workable solution to check stresses in the rail. For measuring the geometrical qualities systems are readily available and already in use.

3.2 Goal

The goal is to provide ProRail with the possibility to measure stresses in a turnout or turnout complex. This entails developing a method to determine the stress free temperature, and the current temperature, and to use these references to determine stresses. Considerations are given to an instrument, which measures the strain in the track, by which the stresses can be deduced. These stresses must then be processed to allow a calculation of the stress free temperature. The difficulty in this approach is that the strains in the rail due to temperature changes are suppressed by the support structure of the rail. Strains will therefore not develop according to theory of free rail expansion, while stresses will develop. However, these cannot be measured. This is due to stress being a fabricated parameter, not a natural parameter that is present and measurable in nature.

Next to this, a model must be developed which provides insight into the distribution of the stress in the rail in turnouts, which can then be used for larger turnout complexes. This model is used to link the calculations and the data found in the practical experiments. This model also allows the determination of the critical locations for measurement, which will allow minimisation of the number of measuring devices.

The ultimate goal is that ProRail can determine the stresses in its network at any time, and the new system to allow ProRail to accept or refuse newly build or replaced turnouts.

Sub goals

1. To provide measurements (to the contractor) during the welding of continuous track, with the goal to provide insight, control and improvement on the results of the used procedure and welding sequence.
2. To be able to check track and turnouts neutral rail temperature (by an inspector) at any moment after welding without prior knowledge of work method or weld sequence.

3.3 Research questions

- What is the best workable method to determine the neutral temperature?
- Which type of sensors can help ProRail accomplish its goal, what are the drawbacks and costs of these sensors, and which implementation offers the best practical alternative?
- What are the critical locations in turnouts and turnout complexes with respect to stresses in the rail?
- How is rail temperature loading distributed in stresses and deformations?
- Does the theory match the practical experiments?

3.4 Assumptions

1) The measuring devices will be commercially available in due time. During this research, strain gauges are used to collect data. The eventual measuring instrument could be based on a different principle, but will provide the same type of output.
2) Ballast properties for the finite element model are assumed as determined by others earlier, for example by S. Boogaerdt [2] and M.A. Van. [3]
3) It is not allowed to cause damage to the rail, drill holes or weld sensors to the rail.

3.5 Actors

Involved parties in this research are:

ProRail, as the rail network operator in the Netherlands, has worded the wish to have a better understanding of the processes involved in turnouts due to temperature stresses. They have formulated the goal of this research and supplied the knowledge, funding and guidance to reach this goal.

The TUDelft, for providing knowledge and support needed for the development of the finite element model. They have facilitated the use of the finite element software, as well as guidance and expertise concerning all manner of technical details.

Bienfait, as the provider of the data logger and strain gauge protective casings.

Stork FDO Inoteq, the party contracted by ProRail to facilitate the lab test and the installation of sensors for this test.

Strukton, as a contractor for ProRail they have provided the rail and have allowed measurements to be taken on the rail on which they perform rail maintenance.

3.6 Time span and locations

The time span of this research is from September 6th, 2010 until August 19th 2011.

Practical tests were performed at the following locations.

Test 1:
Lab test (chapter 12.1 and appendix X)
Location: Stork FDO Inoteq, Amsterdam[1]
Date: December 22nd 2010, and a second execution January 14th 2011.

Test 2:
DVRT mounting test (appendix chapter XII)
Location: Diemen[2]
Date: March 3th 2011

Test 3
6-Meter replacement rail (chapter 12.2 and 12.3)
Location: Amsterdam Central – Amsterdam Sloterdijk[3]
Date: 15th of June 2011

Still to be conducted (due to time limits and budget cuts):

- 30-Meter replacement rail
- Measurements during turnout placement

3.7 Scope

The goal of this research is to provide insight in the mechanics of temperature forces occurring in turnouts and crossings. Its scope is therefore limited to the development of stresses and strains in these constructions. The Thesis includes development of a number of finite element models and their outcomes, performing some practical experiments, and producing this report.

Not included in this research are; research into the ballast properties, buckling behaviour of straight track, and the behaviour of continuous welded track on bridges.

The scope of this thesis extends to supporting ProRail during the process of introducing this new measurement system into their work procedures. This includes providing support during the decision of what measurement device to be used by ProRail and providing knowledge to be used during the drafting of a new guideline. In addition, an active role is assumed in the preparation for lab tests and practical tests, as well as in the discussions with different actors.

3.8 Budget cuts

Nearing the execution of the first practical test budget cuts at ProRail were announced. Unfortunately, this project was one of those affected. The necessary funds for the third (and key) practical test, the measurements on an actual turnout, were not available anymore. This means that

[1] In the digital version of the report this is a link to the Stork FDO Inoteq website
[2] In the digital version of this report this is a link to google maps pinpointing the site
[3] In the digital version of this report this is a link to google maps pinpointing the site

there is no opportunity anymore to validate the finite element model of the turnout and that the goal of the project, finding a method to establish stresses in a turnout, can no longer be accomplished. This Master Thesis will describe all the actions and findings up until the point where the turnout test would have been executed. However, a lot of insight has already been gained from the other tests and investigations conducted.

Even though the finite element model can no longer be verified by means of measurements in situ, the model is still verified by older models and research and can therefore still be of value in the research into the behaviour of turnouts, and turnout complexes. Unfortunately, the link to the real world situation can no longer be established in this Master Thesis.

It is the author's sincere wish that ProRail will be able to free up funds in the near future to complete this project. Thereby enabling them to gather a solid, well-founded, understanding of what goes on in the turnout.

4 Problem analysis

In this chapter, basic information regarding the rail structure, maintenance procedures and theoretical background is provided. This will further illustrate the problem and the structural makeup of the track system to allow readers new to rail mechanics to understand the general concepts. Professionals already working in the rail environment are suggested to read this chapter as well, to refresh their knowledge in order to understand the steps taken further along this research.

4.1 The track structure

The basic structure of the railway track, as displayed in Figure 4.1, consists of the sub grade, on top of which is a layer of sub-ballast (gravel). On this layer of sub-ballast, two layers of ballast are located. In the top layer, the sleepers are located, wedged in the ballast and thereby horizontally fixed to a degree. The lower ballast layers are used to transfer the vertical load to the sub grade. The sleepers in turn support the rail, and are connected to it by fasteners.

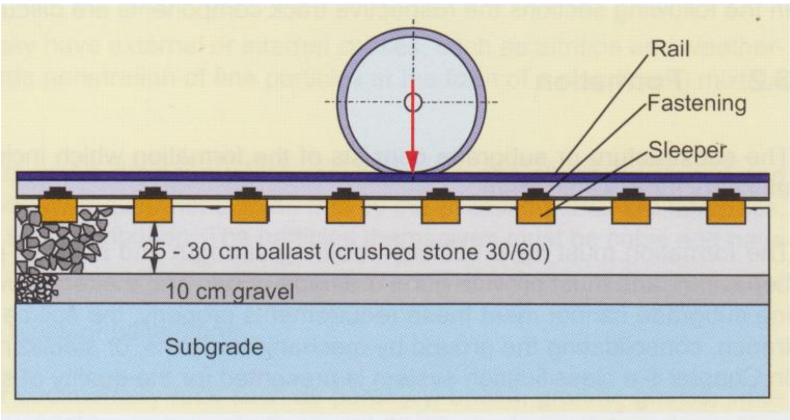

Figure 4.1 Typical track structure [4]

4.2 The rails

The rails are the focus of this research, and especially the longitudinal stresses in the rail are of concern. These depend greatly on the cross sectional area. Therefore, some more information is provided. For a metallurgical summary, please see appendix I.

There are several types of rails, the most commonly used one in the ProRail network is the flat-bottomed rail UIC 54E1. All rail referenced to in this Thesis is UIC54E1. Its geometry is depicted in Figure 4.2. The top of the rail is designed in such a way that good contact with the wheel profile is ensured. The thickness of the web is determined by the requirement stiffness against bending and buckling while keeping the material bill as low as possible. The rail foot is designed to provide stability, a greater moment of inertia in the lateral direction, to allow for fastening and to distribute the load on the sleeper.

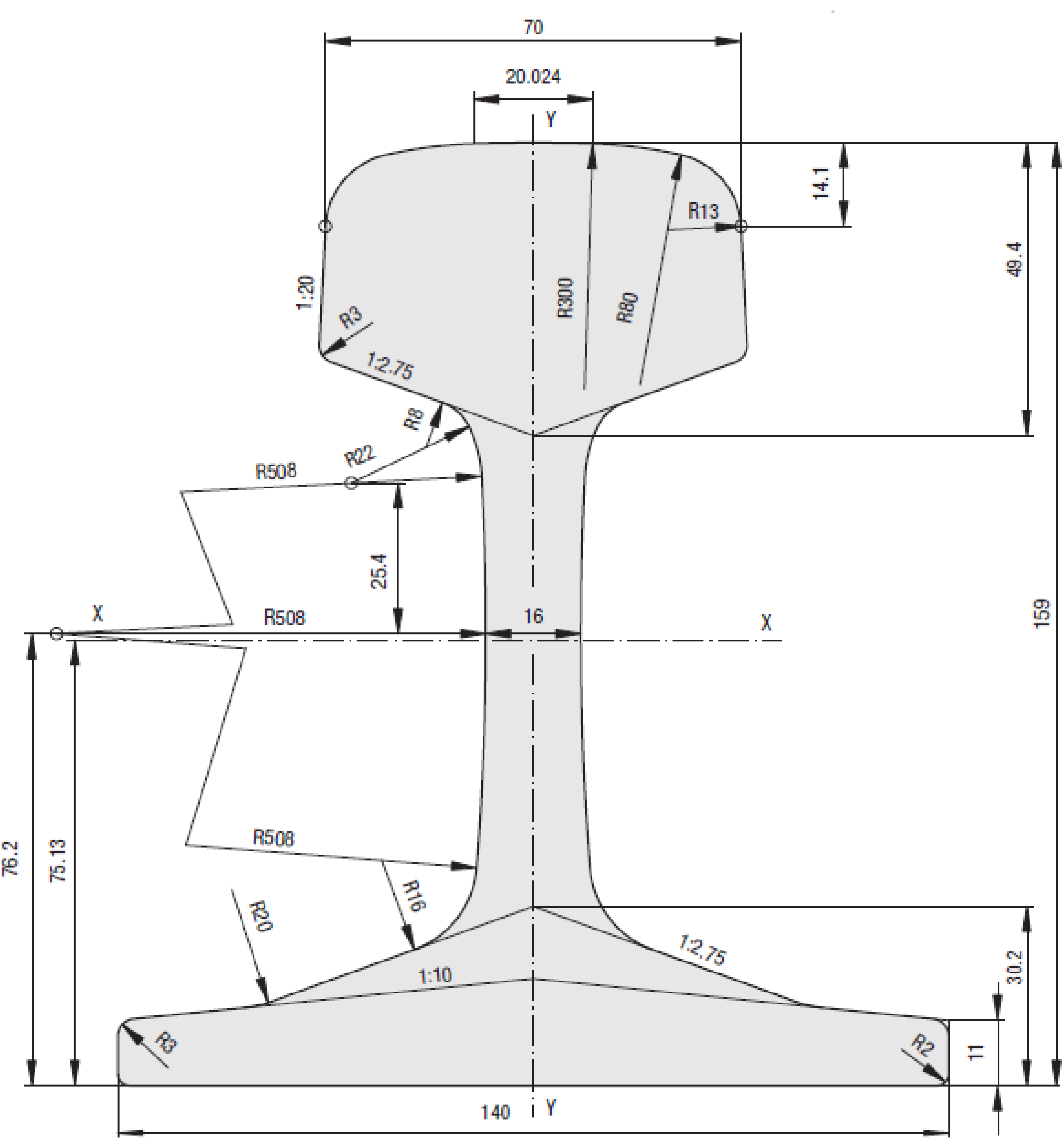

Figure 4.2 UIC 54E1 rail profile, sizes in mm, scale 1:1 [5]

4.3 Jointed and continuous welded rail

In the past jointed track was used. This consisted of small stretches of rail (typically 25 meters in length) which were joined together with a fishplate coupler (as illustrated in Figure 4.3). This type of rail has certain disadvantages. Some important ones are:

- High maintenance costs due to the high amount of joints and correlated plastic deformation on the joint edges
- Passenger discomfort
- High noise emission

A new type of track is therefore commonly applied nowadays. This is the so-called continuous welded rail and has become the standard in many countries. In this type of track the pieces of rail are not joined together using fishplates, but are joined by welds (for instance by thermite welding, Figure 4.4). This means the stretches of rail are longer and will need more room to expand. This is very impractical as large expansion joints are expensive. Therefore, another solution has been found. The expansion is prevented by fixing the rail to the sleepers. This causes each sleeper to prevent the rail to expand. This prevented expansion in turn causes high stresses in the rail itself.

Figure 4.3 Old fishplate joint [6]

Figure 4.4 Thermite weld

4.4 Track failure

The stresses that occur in the rail due to temperature influences are significant and can lead to failures. There are two types of failure commonly related to temperature influences.

Cold weather failure

The stresses due to cold weather could become higher than the tensile strength of the rail, causing it to rupture. This is usually not a very large issue (depending on the gap size); ruptured rail can still be operated on or can be temporarily strengthened by fishplate joints. The rupture will provide a jolt to passengers and a fast deterioration of the impact surface, but does not normally cause derailments or large damages.

Hot weather failure

The stresses due to hot weather can cause the entire structure to buckle (displace sideways). When this happens, the consequences are much more severe. Illustrated in Figure 4.5 is an example of track buckling. When a train would encounter such a defect at high speeds, the results are catastrophic. Buckling occurs when internal stresses keep increasing, until there are two possible static equilibrium situations, the non-deformed state, or a laterally deformed state. Buckling is a sudden process and often occurs in long stretches of straight rail, or near fixed points such as bridges. The exact moment of buckling, and the required force, depend on the lateral resistance that can be provided by the sleepers in the ballast. If the lateral resistance is no longer enough to prevent sideways movement buckling can happen. So long as sideways movement is prevented buckling will not occur, even though the stresses in the rail can become significantly high.

Figure 4.5 Buckling example [7]

In the digital version of this report, this page contains a movie showing buckling.

The possible failures discussed are why railway track needs to be constructed at a neutral temperature (25 °C in NL), a temperature that is in between the highest and lowest rail temperatures that might occur. In this way, the largest strength reserves are left in the rail (structure). Because it is not possible to construct the entire rail at a temperature of 25 degrees, artificial methods have been developed to raise this temperature parameter so construction at lower temperatures can take place. The theoretical background for these methods is discussed in chapter 4.5, while the methods themselves are discussed in chapter 4.7.

Buckling behaviour of the track and the behaviour of track on bridges[1] has been the subject of a lot of research and has been the focus of many papers and simulations [8,9,10,11]. There is however a lack of data and research concerning the behaviour of turnouts, crossings and turnout combinations in continuous welded rail under temperature differences.

[1] Bridges have a different rate of expansion due to temperature changes when compared to the rail. This causes complicated distributions of force when the rail is connected to the bridge with a very fixed connection.

4.5 Temperature force theory

When a material such as steel is heated, it will expand. Due to the application of CWR in modern railway track there is no room for the rails to expand. Because of the restrained expansion, stresses will occur in the rail.

Firstly, the definition of strain shall be provided:

$$\varepsilon = \frac{\Delta l}{l} \tag{1}$$

With:

ε = Strain in the object	[m/m]
Δl = change in length of the object	[m]
l = total length of the object	[m]

The relation between temperature and expansion is:

$$\varepsilon = \alpha * \Delta T \tag{2}$$

With:

α = Coefficient of thermal expansion of the material	[m/m/°]
ΔT = Change in temperature	[°]

The change in temperature is the difference between the current temperature of the object (rail in this case), and the temperature at the start of heating. For rail, the temperature at the start of heating is usually referred to as the neutral temperature, which is the temperature that corresponds to the average stress situation in the rail. To translate between stress and temperature relation (3) (Hooke's law) is used.

$$\sigma = E * \varepsilon \tag{3}$$

With:

σ = Stress in the object	[N/mm^2]
E = Elastic modulus of the material	[N/mm^2]

Replacing ε with relation (2) yields:

$$\sigma = E * \alpha * \Delta T \tag{4}$$

In which ΔT is the difference between the neutral temperature and the current temperature.

$$\Delta T = T_{rail} - T_{neutral} \tag{5}$$

The relation between stress in the rail and the current temperature is described by:

$$\sigma = E * \alpha * (T_{rail} - T_{neutral}) \tag{6}$$

When the stress is multiplied by the cross sectional area of the rail the relation between force in the rail and the temperature of the rail is found.

$$N = A * E * \alpha * (T_{rail} - T_{neutral}) \tag{7}$$

With:

E = Elastic modulus of steel	[200,000 N/mm²]
A = The cross sectional area of the rail	[mm²]
α = The linear expansion coefficient of steel	[0.000012 m/m/°]
T_{rail} = Rail temperature	[°]
$T_{neutral}$ = Neutral temperature	[°]

Observing these relations, one might understandably be under the impression that when the rail temperature is known, the force in the rail is known as well. This is however not the case, Hooke's law is valid for objects and materials that act as an (ideal) spring, converting strain to force in a direct fashion. In Hooke's law, one of the ends of the spring is on a fixed point, and expansion takes place in only a single direction, such as in Figure 4.6.

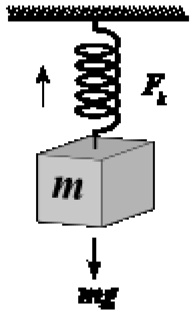

Figure 4.6 Hooke's law basic situation [6]

Track under compressive force does not behave as a spring, when a rail is under a compressive force it will move sideways or vertically as well. Consider the situation in a curve for example, when a temperature increase forces the rail to expand (relation 1) the rail will try to move out sideways, instead of remaining in its old position and converting the temperature increase to stresses. This is why relation (6) is only valid for prevented temperature expansion. If the rail is free to expand, there are no forces in the rail. If all the expansion is prevented, all of the temperature increase is converted into stresses.

$T_{neutral}$ is a very important parameter in rail engineering. The basic explanation behind this parameter can be found in chapter 4.4. In practice, this parameter is used to describe the stress situation in the rail. It is therefore not in essence a true temperature indication, but it is the stress level equivalent with the temperature of 25 degrees. The neutral temperature can therefore be raised in a piece of rail by applying tension, and then fixing it in place, or by heating it and welding it in place, after which it will cool down and tensions will develop as well. The most straightforward method is to place the rail at the right temperature and fix it in place. This is however hard to do as the rail temperature needs to be exactly 25 degrees, which does not happen often at night.

4.6 Plastic shear resistance theory

This theory can be used to explain the behaviour of rail near rail ends where free expansion can take place, it is visualised in Figure 4.7. It assumes that the resistance against expansion movement is constant over the rail length. This implies that where the rail ends (at the rail end, stress is zero) the force in the rail will decrease linearly from the maximum to zero. This reduction takes place over the "breathing length" of the rail, also referred to as anchorage length. It is an analytical model that simplifies the suspected rail behaviour. In the previously used LONGSTAB software this model has been implemented with the addition of friction between the track structure components [2]. To improve the understanding of rail behaviour, a theoretical finite element model (chapter 7) has been developed, as it is a more realistic approach to the behaviour than this simplification.

What this theory implies is that rail in straight track is not able to elongate due to temperature changes, and that these temperature changes are therefore converted into stresses, except at the outer ends of rail track.

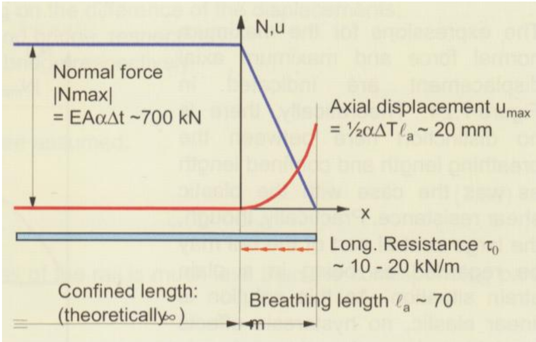

Figure 4.7 Force and expansion in continuous welded rail near an open end according to plastic shear theory [4]

4.7 Achieving neutral temperature in rail

When rail is being placed in the track while the rail temperature is lower than the neutral temperature required, the rail needs to be subjected to a tensile stress. This will bring it to the required neutral temperature (see chapter 4.5). The concept is simple, by elongating the rail and welding it in place the situation corresponds to the situation when the rail would be placed at a higher temperature (the rail length equals the length the rail would have at the neutral temperature). When the temperature is lower than the neutral temperature, the same tensile stress will be present in the replacement rail as in the original track, due to its elongation upon placement. There are two general methods to lengthen rail, one is heating and the other is mechanically lengthening the rail.

Heating

The rail is lengthened by applying heat. This can be done by using heat blankets (Figure 4.8) or a movable heater. The expanded rail is then welded in position. The amount of heating can surpass the neutral temperature. This way the piece of track will expand, which after connecting and cooling, will introduce a stress level in the adjacent rail (due to the cooling and related shrinkage). This stress level can be made to comply with the neutral temperature demanded for the connecting rail. When using a heating wagon the rail is heated from the top down. Care has to be taken that the temperature does not become too high in a single spot (the heater must stay mobile or must be turned off when stopped). Another aspect is that heating the top makes the rail bend downwards as the top will be warmer and therefore expand more than the bottom of the rail. More on this can be found in the appendix, chapter II.

Figure 4.8 Rail elongation by heating (using heating blankets) [12]

Mechanical stressing

This procedure involves putting a (mobile) hydraulic jack on the rail end (Figure 4.9). This jack is then either attached to the present rail or anchored in the ground (rarely). Using hydraulic pressure the jack is contracted, which expands the rail and via this expansion applies stress in the rail. When the proper amount of force is introduced to get the proper length, the rail is welded into its final position.

Figure 4.9 Rail elongation by hydraulic jack

4.8 Welding methods

There are two generally applied methods of rail welding. Both have advantages and disadvantages, which are described in the following chapters:

Thermite welding

Thermite welding is considered a fusion welding process. It consists of a preheated sand mould with a defined gap between the faces (Figure 4.10). [4] The pieces of rail are then welded together by allowing the molten steel to flow in the mould (Figure 4.11). The molten steel (Figure 4.12) is produced by the reducing effect of the aluminium on the heavy metal oxide. Its chemical reaction is:

$$Fe_2O_3 + 2\,Al \rightarrow Al_2O_3 + 2Fe + 850\,kj$$

Figure 4.10 Thermite mould

Figure 4.10 Igniting the thermite

Figure 4.12 Removing the mould

The iron obtained from this reaction is too soft for practical use. To compensate, steel-forming alloying additions are added to the mix. After solidification, the excess weld metal to compensate for shrinkage is removed while the weld is still red hot. This is normally done with a hydraulic shearing device (Figure 4.13). Subsequently the surface is ground with a grinding machine. Making a thermic weld is a (relatively) time consuming process, it can however be done with (relatively) simple and portable equipment. This makes it useful in situations where there is little space to manoeuvre.

Figure 4.11 Hydraulic shearing device (left) and grinder (right) [4]

Flash butt welding

Flash butt welding is an electrical resistance type of welding. It involves melting the rail ends with a high electrical current. The ends are consequently joined mechanically and allowed to cool. Modern flash butt welders are programmed in a very specific heat and pressure sequence, after which post weld treatments can be taken into account as well.

Mobile flash welding (illustrated in Figure 4.14) is the mobile form of the process, and can produce welds with an equal quality as the stationary machine. Modern mobile welders come fully equipped with railhead aligners and hydraulic systems that hydraulically stretch the rail to neutral temperature before closing the weld. Flash butt welding is a fast process, but it requires large pieces of machinery that make it less suitable for use in turnouts.

Figure 4.124 Mobile flash butt welding equipment [13]

4.9 Turnouts components

As this research is focused on the behaviour of temperature stresses in turnouts and crossings, some basic explanation of terms are provided. The locations of the components are illustrated in Figure 4.15.

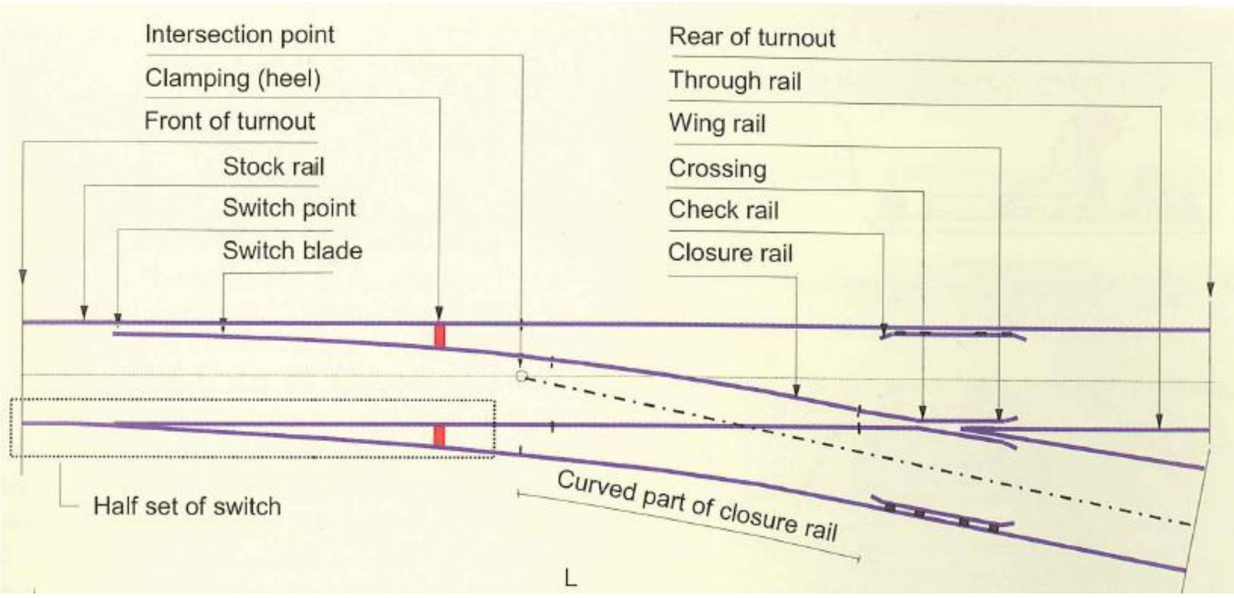

Figure 4.135 A turnout and its important parts [4]

Front of turnout:
This lies in the centre of the rail joint on the side of the non-divided track and indicates where the turnout structure starts.

Rear of turnout:
This lies at corresponding points on the side of the divided track.

Intersection point:
The point where the centre lines of the straight and divergent tracks intersect.

Crossing angle of the turnout:
The angle at which the centre lines intersect. Common values in the Netherlands are 1:9 and 1:15.

Stock rail:
The rail that continues through the turnout without being intersected.

Turnout point:
The tip of the turnout blade, where the change of direction starts.

Turnout blade:
The movable inner “rail” that supports and guides the train in the change of direction.

Clamping:
A device to control rail creep.

Wing rail and checkrail:
Guiding strips inside the rails. These prevent derailment and guide the train into the correct direction.

Closure rail:
The non-movable rail connected to the turnout blade, which guides the train over the latter part of the turnout.

Common crossing:
The structure where the two rails intersect also referred to as a frog or K-rail.

5 State of the art in procedures

This chapter will provide a short overview of the current maintenance procedures. This overview has been compressed to encompass only the basics needed by readers new to the subject to understand the procedure and execution of rail maintenance. For more information the reader is referred to RLN00120 “het voegloos maken van spoor en wissels” which is available at ProRail.

5.1 Rail replacement procedure

The current replacement procedure as determined by ProRail is as follows:

In the preparation stage, the amount of required elongation for reaching the desired neutral temperature must be determined, and a choice must be made between the different stretching techniques. These being: heating by induction or by thermal blankets, or stretching the rail mechanically using hydraulic pulling. This would then have to be included in the welding and neutralisation plan, which describes the method of elongation, the method of welding and the sequence in which the different welds are to be made.

Other important conditions are:

- Ballast profile must comply with standards
- Fastenings must be in good condition and correctly applied
- Sleepers must be in good condition

During the execution the prescribed actions are:

- Removing the dirt and ballast from the rails, sleepers and holes in the track. (Figure 5.1)
- Marking the current rail position on both the rail and the sleeper (Figure 5.2).
- Cutting the rail (Figure 5.1)

Figure 5.1 Cutting the rail

Figure 5.2 Marking rail positions

- Measuring the current rail temperature (shaded side) using a thermometer within 1 degree of error.
- Marking the distance the rail needs to be lengthened. This is a combination of both the current rail temperature and the neutral temperature to be established, and can be found in pre-calculated tables which are based on the length of inserted rail and the environmental temperature.
- Elongating the rail by the prescribed amount. (Figure 5.3)
- Welding the rail (thermite or flash butt). (Figure 5.3)

Afterwards the revised welding and neutralization plan needs to be provided to management.

Figure 5.3 Welding of a rail, with hydraulic elongation equipment present

5.2 Turnouts and crossings

In turnouts and crossings, there are some deviations from the procedure for renewing track or replacing track sections. For instance, hydraulic elongation of the rail inside the turnout is not allowed. This is due to the forces being applied to the turnout components causing displacements and potentially displacing the turnout beyond its tolerances. Furthermore, there are specific regulations regarding neutral temperature of different components in the turnout. For example, in ProRail regulations the closure rails (chapter 4.3) need to be heated to a temperature of 25 degrees before closing the welds. The same goes for the rail that connects to the turnout at its three ends. The rest of the turnout does not need to be heated.

Next to this it is prescribed to “weld from the inside out” to prevent the turnout from laterally deforming (bending out of plane) due to the welding stresses. This means that the closure welds in the centre of the turnout are welded first, working outwards welding the other connections. This way the centre of the turnout is fixed first, and the stresses due to the weld cooling are distributed equally along the turnout, both in location as in time. One can imagine that closing all the welds on for instance the curved closing rail will reduce its length, and therefore cause the straight stock rail opposite to “open up” (Figure 5.4). When closing the weld on this gap the result is a bend closure rail. More information can be found in chapter II.

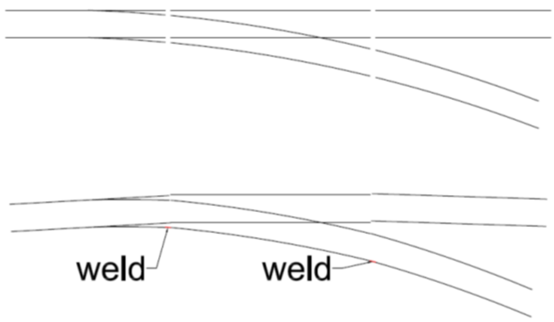

Figure 5.4 Turnout deformations

The stresses due to weld cooling can be quite significant, and can cause a deviation of the neutral temperature. This deviation is currently not taken into account.

5.3 In practice

In the practical situation, there are two main actors. On the one hand, there is ProRail; they are the owners and managers of the rail network. They want their network to be in good condition and want to know what happens in the rail during its lifetime, and how this influences performance and wear resistance. On the other hand, there are the contractors, who maintain the track for ProRail and want to know how to construct new rail, and how to perform maintenance operations. This boils down to ProRail wanting to know; theoretical behaviour, safety margins and costs, while the contractor wants to know practical values; how high should a pulling force be, what is the maximum deviation allowed and when is it considered acceptable. Both parties communicate via the guidelines set up by ProRail. A discussion is present between both parties, caused by discrepancies in theoretical background for the guidelines and practical observations.

By commissioning this research, ProRail hopes to increase their understanding of the rail, and use this understanding to engage in discussions with the contractors to create a better understanding of rail behaviour by bridging the gap between theory and practice.

6 Procedure proposal

The procedure followed during this Thesis is described in the following text.

Firstly, a type of measuring system is chosen. Afterwards conversations are scheduled with producers of these sensors. The chosen systems are then tested for compliance with the accuracy desired by ProRail. This is done in a controlled environment during a laboratory test. After verification that the sensors work as required, two practical tests on a straight piece of track are executed (6 and 30 meters), finally to be followed by a test on a turnout. This turnout test will be executed on a later date, not as part of this Thesis. This is due to budget cuts at ProRail. The practical procedural path is illustrated in Figure 6.2.

Parallel to this practical approach a piece of straight track is modelled in Ansys®; this is compared to the current track model (LONGSTAB, [18, 19]) When it is verified that both models yield the same output, a model of a full turnout is constructed. These models are used for comparing the practical tests to the theoretical output, and to yield insight in the behaviour of turnouts. The theoretical procedural path is illustrated in Figure 6.1.

Several meetings and discussions are held with people working in the welding or rail maintenance business. Amongst these were meetings with Strukton Rail and an interview with R. van Bezooijen from Id2 Engineering. A summary (in Dutch) of this last meeting can be found in appendix chapter II.

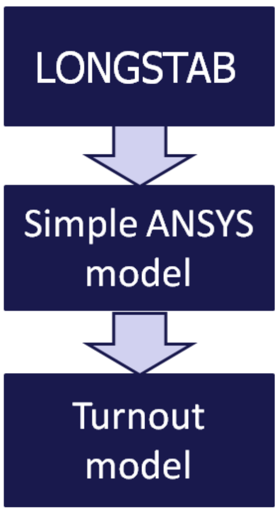

Figure 6.1 Theoretical procedural path

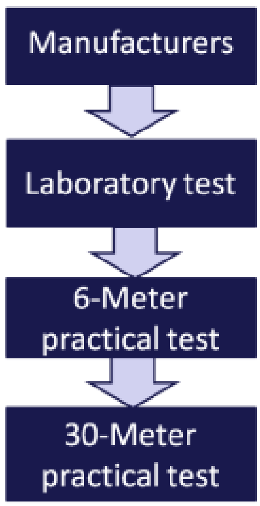

Figure 6.2 Practical procedural path

7 Overview of considered measuring methods

For this research, a practical measuring method must be chosen. A study of available techniques was therefore undertaken. There are many methods of determining the stresses and neutral temperatures in the rail. All of these methods have drawbacks. They are expensive, difficult, or inaccurate. A short exert from [1] is presented on the following pages. The methods are divided in direct measurements, in which tension can be calculated with a few parameters and the measurements on site, and indirect measurements, in which the resulting measurements need to be compared to a database of reference measurements to establish the stress state of the material.

7.1 Cutting method

A frequently used method is the cutting method (Figure 7.1). In this method, the rail is cut and the expansion/contraction is measured. By measuring the current temperature, the neutral temperature can be determined. This method is time-consuming and destructive [1]. It utilizes formula (1) (chapter 4.5) and (2) to establish the neutral temperature upon construction. The strain is calculated by dividing the displacement in the cut over the length of rail affected (anchorage length). For this method to work both the anchorage length and the stiffness of rail steel need to be known. This method has no need for a database of reference measurements and is therefore qualified as a direct measurement type.

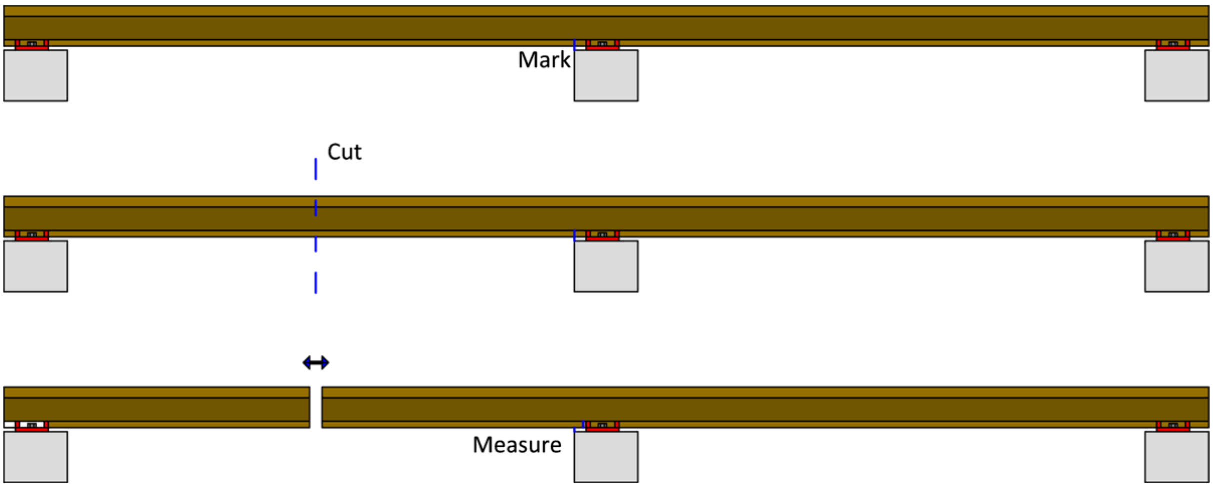

Figure 7.1 Cut and marking method

7.2 Lifting method

Another frequently used method is the lifting method as presented in Figure 7.2. About 30m of the rail is unclipped and the vertical force required to lift the rail a certain distance is measured. As the resistance depends on the force in the rail, the neutral temperature can be calculated. This method is semi-destructive, time-consuming and cannot be used if there are compressive stresses in the rail.[1] This method does not use any of the previously stated formula, but is based upon the relation between compressive force in a beam and the force needed to displace this beam for a certain distance. It is all based on geometry and force distribution triangles. This method measures the tension directly.

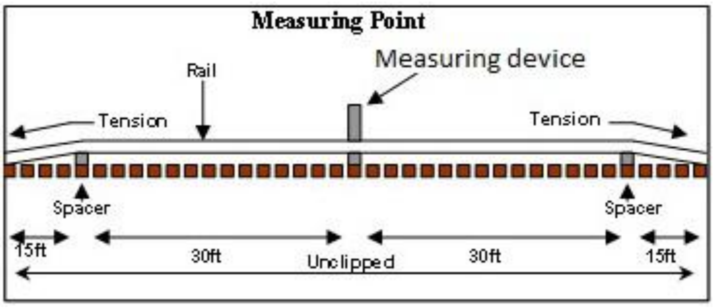

Figure 7.2 Stress measuring by the lifting method [14]

7.3 Deformation methods

Deformation measurements can be done with strain gauges (Figure 7.3) or by measuring the distance between two points. The time for installing this equipment can be rather long, and it is necessary to know the thermal strains at the time of installation. Drawbacks are the lack of strain variations during normal use; temperature does not have an effect on the strain in the rail as the rail is fixed in position [1]. This method uses formula (2) and (6) from chapter 4.5. By measuring the rail elongation and the temperature, it is possible not only to measure the elongation, but also to establish the part of the temperature influence that is present as stress. This method is a direct stress measuring method.

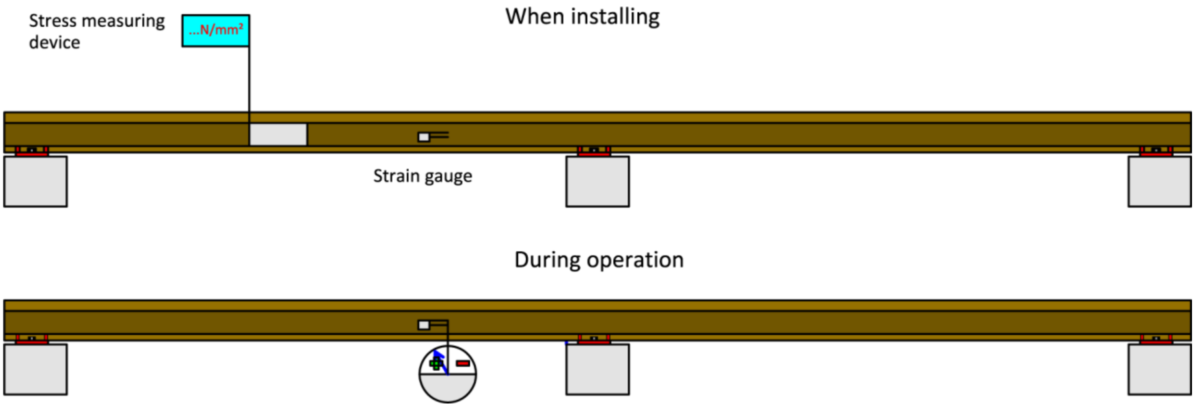

Figure 7.3 Deformation measurements with a strain gauge

7.4 Ultrasonic methods

Ultrasonic methods are also available; these are based on the phenomenon that the sound velocity in the rail is influenced by the stress state. The sound velocity in the rail is compared to the sound velocity in a rail without thermal stresses. The difference between these is assumed to be caused by thermal stresses. This is a rapid method, but the need for a reference measurement makes the results uncertain [1]. It is visualised in Figure 7.4. This method is an indirect method, which uses a database that encompasses the relations between sound velocity and rail material; it measures an elongation in an indirect fashion.

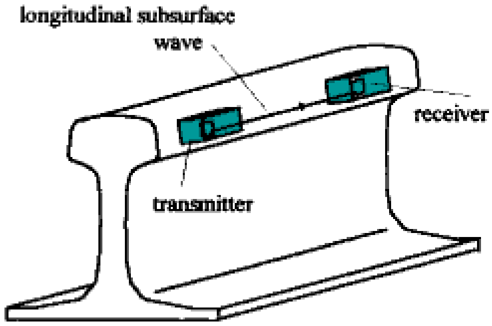

Figure 7.4 Ultrasonic measurements [15]

A similar principle has been successfully applied in a set up that resembles a strain gauge (SAW system, Figure 7.5); it consists of a piezoelectric substrate crystal upon which metal parts are mounted. An antenna enables the sensor/transponder to communicate with a transmitter and reader by radio. An elongation of the substrate can be translated into a delay in the response signal, thereby indicating elongation of the substrate. This is similar to the ultrasonic measurement, the material type is known and the delay in response can be translated into an elongation. This SAW system has been tested for temperature determinations and identification purposes, but has not yet been applied to measure strains, though the technology seems to be well suited to do so.

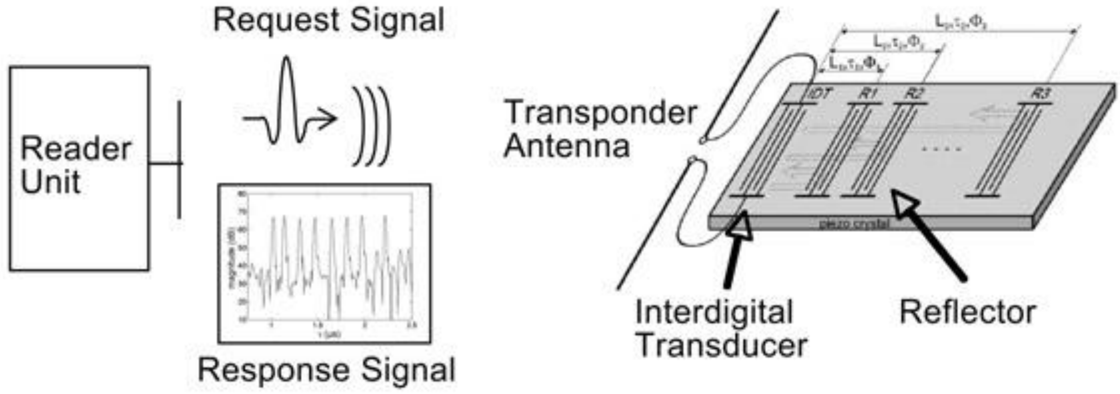

Figure 7.5 overview of the SAW system

7.5 X ray method

X-ray diffraction can be used for measuring the distance between two atomic planes in a crystal and this distance can be related to the stresses in the material. A drawback of the method is that it also measures the stresses in a small volume close to the surface [1]. This method is an indirect method; it requires a database that encompasses the distance data of the atomic planes in various materials at various stress states. Its principle is illustrated in Figure 7.6.

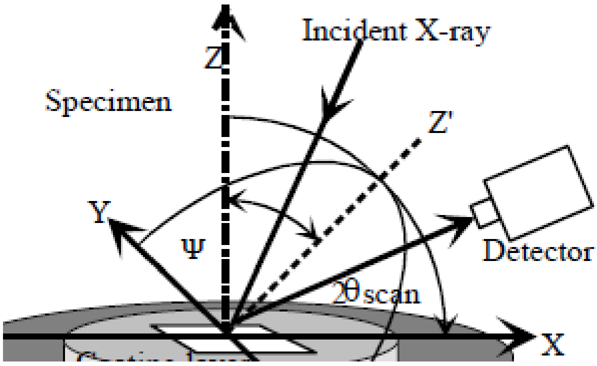

Figure 7.6 Principle behind x-ray stress measurements [1]

7.6 Vibration method

A vibration method, the guided wave technique, which is not sensitive to the boundary conditions, has been suggested and investigated. The results show that this is a method with potential for railway applications, but it has also been found that the method requires measurement with very high accuracy, advanced finite element (FE) calculations. Before the actual longitudinal load in the rail can be calculated from the measured vibrations, a rather tricky adaptation of the measured results has to be made [1]. This method is an indirect method; it requires reference calculations of the vibration states of the rail.

7.7 Magnetic method

A magnetic method has also been developed [16, 17]. This method uses non-contacting magnetic probes to generate an alternating magnetic field in the rail. This field interacts with the properties of the rail microstructure and produces magnetic (Barkhause) noise (Figure 7.7). The amplitude of the noise is related to the longitudinal stress in the rail. However, as with the ultrasonic methods, the measurements from the stressed rail must be compared with measurements from reference material. This method is an indirect method, as the Barkhause noise distribution is dependent on the exact composition of the steel.

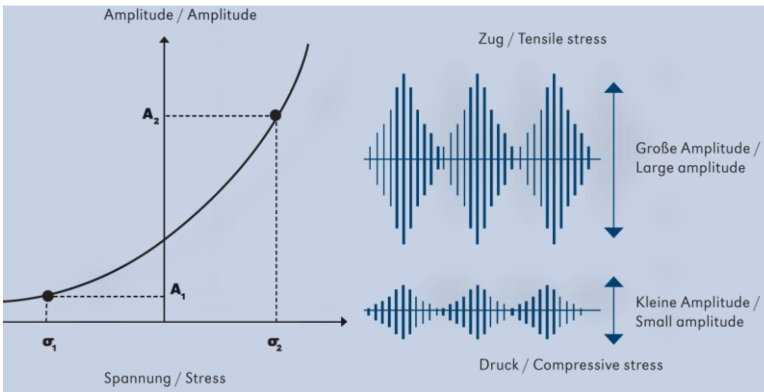

Figure 7.7 Principle behind the electromagnetic stress measurements

8 Measurement method and sensor types

For this Thesis, the chosen method of measurement is the deformation method. This is because strain gauges are a proven and lasting system. It will enable ProRail to conduct experiments for a long period in the rather hostile rail environment, without the need to stop rail traffic on the studied piece of track, such as is the case for electromagnetic and ultrasonic techniques on the market today. Drawbacks and hazards of using strain gauges are:

- Wiring which needs to be protected during tamping or other maintenance procedures
- A need for a reference measurement (to zero the measurements)
- The need for a professional to apply the strain gauge
- The required accuracy for the strain gauge is extremely high, and might be hard to reach in situ
- Temperature compensation needs to be applied

A particular situation needs to be addressed. The rail is connected with a very stiff connection, and in theory is not able to expand or contract (see chapter 4.6). This could raise questions concerning the usefulness of strain gauge application during long-term measurements. It should however be noted that when elongation is prevented, stresses in the rail rise, therefore the stresses can be determined from exactly this lack of elongation, all is needed is to know the temperature (using formula (2) and (4)). More on this can be found in chapter 4.5. Some further basic strain gauge behaviour is described in chapter 8.1.

The use of strain gauges, when it can be confirmed a high enough accuracy can be reached on-site, is an easy solution to measuring the amount of elongation of the rail when installing. An implementation of strain gauges and temperature sensors can therefore be used to provide the contractor with data concerning how close the new rail is to reaching the required stress free temperature. Strain gauges can also provide insight into the behaviour of the track during the cooling of the welds. After this moment, it is theorised that a strain gauge will not provide any more useful data. It is the goal of this research to find locations in the turnout, where useful measurements can still be conducted.

8.1 Strain gauge basics

A strain gauge has a certain electrical resistance. This resistance correlates to the deformation of the strain gauge. A deformation of the strain gauge would yield a change in voltage run through the strain gauge due to a change in resistance, indicating a certain amount of deformation in the stain gauge; this is recorded by a data logger as mV/V. Using the known relation between elongation and resistance this value can be converted back to strain. All strain gauges have a different starting resistance, for example due to differences in force applied on them during gluing (see appendix chapter VIII) for the installation procedure). To be able to use strain gauges it is therefore necessary to create a point of reference, linking resistance to strain in practice. This reference point would link the voltage from the strain gauge to the stresses in the material. A reference point can be created in two ways.

8.2 Reference point from zero measurement

This would imply that at a situation where the amount of stress in the material is guaranteed to be zero the voltage from the strain gauge would be read. (Figure 8.1) The later voltage output under strain can then be related to this zero reference, thereby indicating the change in deformation and the corresponding stress in the steel. In practice, this would boil down to a measurement being done in the factory, in which the temperature and voltage output are recorded. When the piece of rail is then transported from the factory to the site, another measurement would give the change in strain in the material. As the change in deformation due to the stress in the rail is known this will allow one to determine the equivalent temperature that would cause similar stresses. It can then be checked whether this temperature is in the range as prescribed by the regulations.

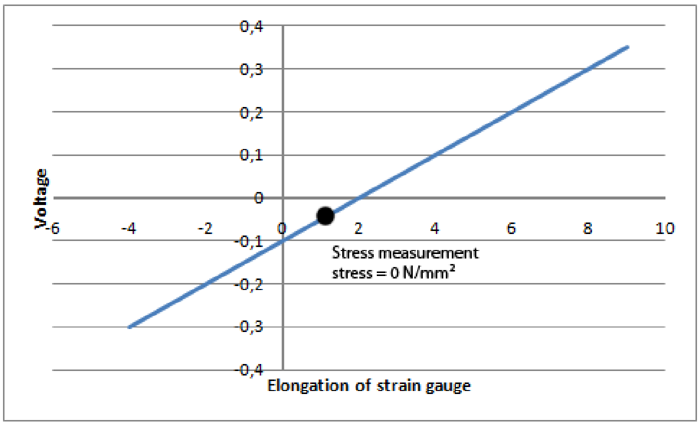

Figure 8.1 Using a zero stress reference

8.3 Reference point from secondary measurement method

This method would entail installing the strain gauge, and later using a separate method of determining the stress, for instance a mobile magnetic stress transducer, to correlate the voltage to a stress level (Figure 8.2). When temperatures change, or other actions influences the strain level in the rail, this can then be read from the strain gauge as a change in voltage output.

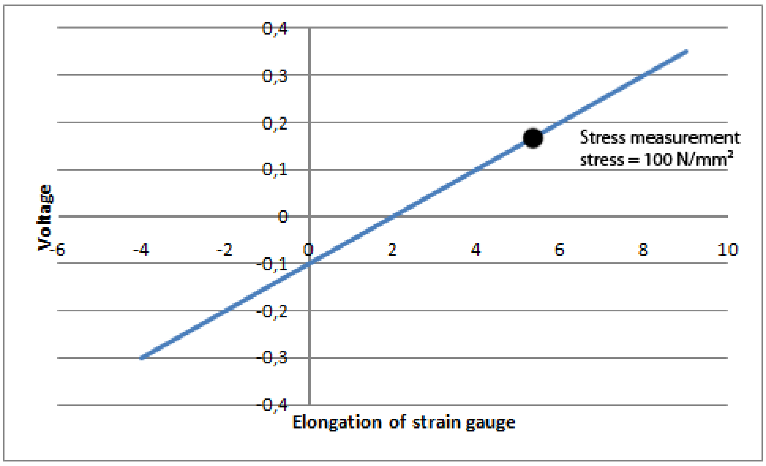

Figure 8.2 Using a stress measurement as reference

For this experiment, the first option has been chosen. Only one type of equipment is needed, so long as the strain gauges are applied in a zero-stress situation. This is for instance the case when the turnout is still in the workshop awaiting transportation or when a replacement rail is placed but not yet welded.

8.4 Difficulties encountered by using strain gauges

In the case of already constructed CWR, due to the fixing of the rail to the sleepers, changes in temperature will not directly translate into an elongation or compression of the rail. It is therefore theoretically impossible to measure stresses by only using strain gauges. Some changes might still be measured, such as breaks in the rail, changes in geometry due to constant braking or accelerating, or slight “settling” of the rail after placement. The expectation of ProRail is that some changes in strain can still be measured due to train-rail interaction, but this must be confirmed. When combining the use of strain gauges with temperature sensors enough of the variables in formula (4) are available to calculate stresses in the rail at any time.

The very stiff behaviour of rail structures is the reason why a theoretical model is constructed detailing a turnout, it will allow ProRail to establish the locations where slight displacements of the rail, and corresponding strains, will occur and can therefore be precisely measured with strain gauges, increasing their accuracy. A larger measurement range equals an increase in accuracy as the range is still divided into the same amount of equal parts. This knowledge can improve the effectiveness of the strain gauges greatly.

During the installation of a replacement rail, turnout or turnout parts, strain gauges can be used without fear of zero measurements. When one considers a turnout being installed, one can imagine that the rails to which the turnout is being connected need to be heated or stretched. The key difference in this situation is that the new piece of rail has room to expand, equal to the distance the adjacent rail retreats when heat is dissipated or stretching is stopped. The principles are illustrated in the following Figure 8.3, showing the deformation of the rail and the corresponding strain gauge output. An interesting aspect is the cooling of the weld. When the weld cools, it shrinks which causes additional strains and thereby an increase of the neutral temperature. This effect is quantified in chapter 13.1.2.

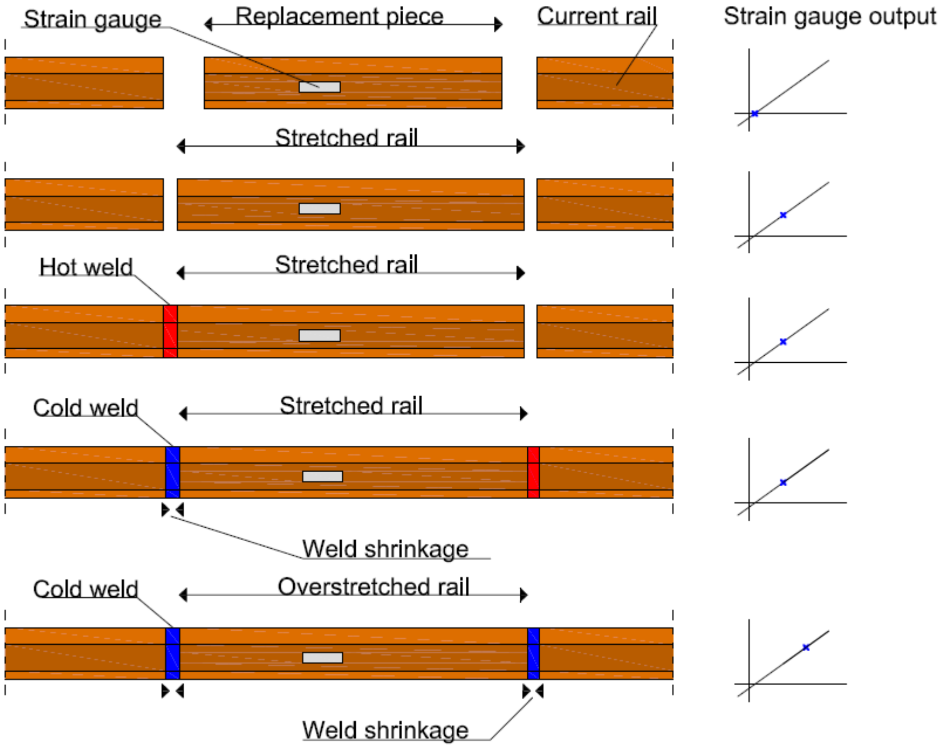

Figure 8.3 Overview of the strain development when placing a replacement rail

8.5 Behaviour of the strain gauge under temperature influences

Another important process to understand is the temperature compensation of the strain gauge. Two separate compensations have to be taken into account before the final strain value can be determined. The first one is the temperature compensation curve, which is discussed in chapter 12.1.6.1, this temperature compensation curve is a function of temperature and specific variables, which are provided, with each batch of strain gauges.

The second compensation in the strain gauge is a less visible process. Almost all modern strain gauges for use on steel are supplied with a standard temperature compensation for the free expansion of steel. This means that when the strain gauge is applied to a piece of steel able to undergo temperature expansion freely, its output signal is zero. This is done so that temperature effects are not measured as strain.

For most applications, this is the desired behaviour. However, when a strain gauge is applied to a piece of steel unable to undergo free temperature expansion it will provide a negative signal, which is in essence the temperature compensation. Consider the case of a piece of steel that is fully fixed and has a compensated strain gauge attached to it. When heating this piece of steel, a strain signal of -12 microstrains per degree of temperature increase (the approximate coefficient of thermal expansion of steel) is provided to the data logger by the strain gauge. Notice the sign of the signal, which is negative and thereby (falsely) indicates compression of the steel plate.

Now consider the situation on the rail, where it is unknown how much the rail can expand due to temperature. Two ultimate situations can be discerned. A fully free expansion shows up in the data as a constant value of strain (i.e. a coefficient of 0). A fully restrained expansion shows up as a temperature-strain relation with a coefficient of -12. Anything in between suggests a somewhat restricted expansion. This behaviour is used for analysing the forces in the rail and the rail behaviour under temperature changes. In Figure 8.4 these situations are illustrated, from left to right: normal situation, situation with a tensile force on all sides, temperature increase with free expansion, and temperature increase with prevented expansion by fixed supports on all sides.

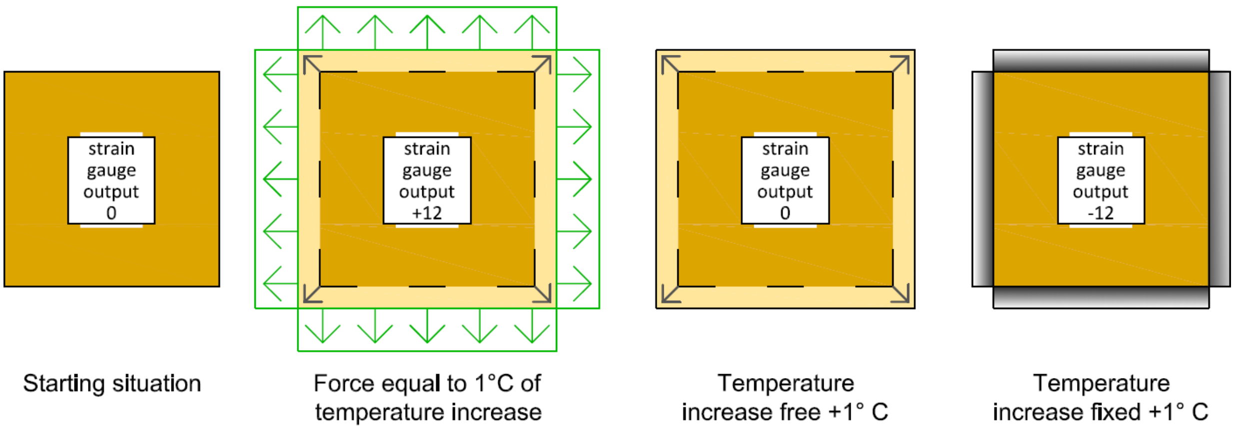

Figure 8.4 Strain gauge outputs

9 Selecting the measurement equipment

This chapter will encompass the procedure followed and how these led to the use of the systems in this test. Thanks go out to all of the companies that provided us with information and offers. Let it be clear that the comparison is not a judgement of worth for the different system, but merely an investigation into which system would match the best with the unique wishes and boundary conditions in this specific project.

9.1 Procedure of selecting the measuring system

Because of the commercial nature of the goal of the project, and the need for a sensor to be tested and produced, a number of producers of measuring instruments were approached with a request for information. Those that responded with a solution to our problem were then asked to explain their ideas in a meeting. This meeting was set up to allow ProRail to explain their problem, and the producers of the equipment to explain their solutions for this problem. Another two meetings were held with companies that use a mobile technique for stress measurements. These would not produce the future fixed sensors, but they were asked about their ability to check the measurements of the sensors during the practical test. The mobile techniques were not considered solutions to the research questions, as they require the piece of rail to be put out of service during measurements. ProRail's goal is to have a permanent and cost efficient technique that can provide feedback during operation as well. It is therefore opted not to consider the rather expensive mobile measuring techniques.

In total eight companies are approached. Two of these concerning the direct and mobile stress measurement techniques (Grontmij and ETS Spoor), two engineering firms (which do a lot of sensor-related work) were approached to provide their views and how they could contribute to this project (Stork and Cauberg-Huygen), and four manufacturers of sensors were approached (AE-Sensors, Bienfait, Feteris, HBM). A meeting with each of these companies (except for AE-Sensors, who were contacted by telephone) was held.

The aforementioned discussions took place over the course of two weeks. After the last discussion, the producers were sent an email containing extra information requested by them and the request to make an offer within the week. The request for an offer was accompanied by a request for an offer to use their laboratory, should they have one. A separate laboratory offer request was send to the TU Delft and the TU Eindhoven.

After receiving the replies an evaluation was made and it was opted to contact Stork to make an appointment for the laboratory test. The use of their laboratory would be combined with the use of Storks sensors used in-house (supplied by MicroMeasurement (MM)), and the test would be expanded to encompass the sensors produced by Bienfait, as well as the sensors provided by AE-Sensors.

9.2 Measurement precision

ProRail has the desire to measure the correctness of the neutral temperature to within an accuracy of one degree Celsius. Using the relationship between the expansion of the rail and the increase in temperature the required accuracy of the measurement system can be determined. Should this elongation be measured by a strain measuring system such as a strain gauge or a displacement transducer the required strain accuracy, or resolution, can be determined.

Using a coefficient of linear expansion (α) for steel of 0.000012 m/m/° and formula (2) from chapter 4.5, coupled with a desired 1 degree C, the required accuracy for the strain sensor can be determined to be equal to the coefficient of expansion. The sensor must therefore be able to have an accuracy of 12 microstrains (12μm/m or $12*10^{-6}$ m/m). This is a very strict demand, obtaining an accuracy as high as this is hard to achieve by use of a strain gauge, according to the sensor manufacturers.
Using formula 6, the increase of the stress due to an increase of temperature of one degree is therefore equal to 2.4N/mm². This is the required accuracy for a direct stress-sensor.

A temperature sensor that is combined with a strain or stress sensor would require an accuracy of 1 degree or preferably even better.

It is worth noting that even though an accuracy this high may be achieved, there are additional errors in the constants E and α, which are material dependent and deviate with each batch of rail produced and thereby introduce an additional error.

9.3 Comparison of proposed sensors

As discussed earlier, several companies were approached to provide a solution for the sensor problem. The original request for information was send to companies, which were known to work with strain gauges. In an attempt to broaden the field, the companies using direct stress measurements were also invited to a meeting. During the discussions, it became clear that there is no direct stress measurement device available small enough to be fitted on the rail. Therefore, the laboratory and practical tests would have to be performed with the use of more common sensors. Due to the tradition of stress measurements performed via strain gauges, this was the logical approach for most companies. Their suggested products ranged from simple strain gauges without any peripherals to readymade strain gauge/temperature-sensor combinations encased in a protective shell. One of the important considerations of ProRail were the distance at which the sensor data could be read out, wireless solutions were preferred. This would allow the readings to be done from some distance from the rail, thereby not hindering the train traffic.

A short overview of the different sensors is shown below. Only the specifications that vary largely between the different sensors are shown. The accuracy rating has been done using a 5 part rating, varying from (--) very poor, (-) poor, (+/-) average (able to reach 12μm/m), (+) good (proven to reach 12μm/m or better), (++) very good (smaller than 1μm/m possible). Other specifications that were not included in the table are frequency of measurements, approximate cost per data point, temperature range, power supply, type of wireless connection, method of installation, accuracy influence of temperature and many others.

Sensor supplier	HBM	MM	Bienfait	AE-sensors	Salient
Type of sensor	Strain gauge	Strain gauge	Strain gauge	DVRT	Strain gauge
Wireless	X	X	V	V	V
Accuracy	+/-	+	+/-	++	+/-
Combined temperature sensor	X	X	V	X	V
Protective casing	X	X	V	X	V
Electrical/magnetic interference	+	+	+	--	+

Of these sensors, the Bienfait and MM strain gauges were chosen as the two primary candidates for measuring strains in the practical application. The Bienfait sensor would be preferable, because of its robustness. Should it not prove to be accurate enough, then the MM sensor is plan B. For displacement measurements the AE sensors was chosen, due to its proven accuracy being well within what was required. Furthermore, the AE sensor is reusable, but can only be used for checking the elongation of new rail parts during installation. Its sensitivity to magnetic and electrical interference might render it useless for measurements when the rail is being used by the trains.

10 Modelling the rail

In the following chapter, the development of the finite element model is described. Its results can be found in chapter 11.

To improve insight in the mechanics beyond the scope of the analytical model as discussed in chapter 4.6 it was decided that it would be beneficial to have a finite element model of a turnout. This model would allow a visual representation of the stresses and strains in the turnout. Furthermore, it would incorporate the influence of sleeper displacements and differences in stiffness of various parts of the turnout, which would be very difficult to do in an analytical representation.

Because the current LONGSTAB software does not provide either a visual representation or the desired scaling (it needs to be very precise to be able to differentiate the stresses over the height of a rail, should this be necessary), using this software would mean having to expand it well beyond its current scope. It was opted to develop a new model in a different software package; with more inherent possibilities such as thermal loadings, visual representation of results, possibilities to expand the model for dynamic calculations and the ability to import very detailed components from 3d drawing software should this be necessary.

10.1 The straight track model

A simple straight track model was constructed. Its purpose is to establish the correctness of the newly used modelling software Ansys® by comparing it to the established LONGSTAB software. Unfortunately, the LONGSTAB software is limited in the details of its output. Therefore, it is felt that a model in Ansys® would provide more insight in the details of the turnout under thermal loads.

For the straight track model, the stiffness of different parts and supports would have to be determined. Using values, which were established, by M.A. Van [3] and S. Boogaerdt [2], the model was constructed. This model was made with respect to the elastic behaviour of the material, it is considered unlikely that parts of the turnout will deform by large enough amounts to cause non-linear behaviour. This is something that has to be considered when reviewing the calculation results. Non-linear track structure behaviour starts at deformations of the ballast bed exceeding five millimetres.

By using this straight track model and comparing it to the LONGSTAB model it is verified that the stiffness of the various springs are modelled correctly (the behaviour of both systems should be identical). These verified springs are then used in the model of the turnout.

Two separate loading conditions were compared, one with a tensile load on both rails, one with a tensile load on only one rails. The first situation will verify the longitudinal behaviour while the second will verify the rotational behaviour. The results from the calculations were compared to the outcome of an established modelling tool (LONGSTAB), thereby verifying the correctness of the new software and the used spring stiffness.

10.1.1 Stiffness determination

The first model that was developed was a basic situation, detailing a piece of straight track (Figure 10.1) subject to external forces. This model was developed both in Ansys® as in LONGSTAB and was used to relate both software packages.

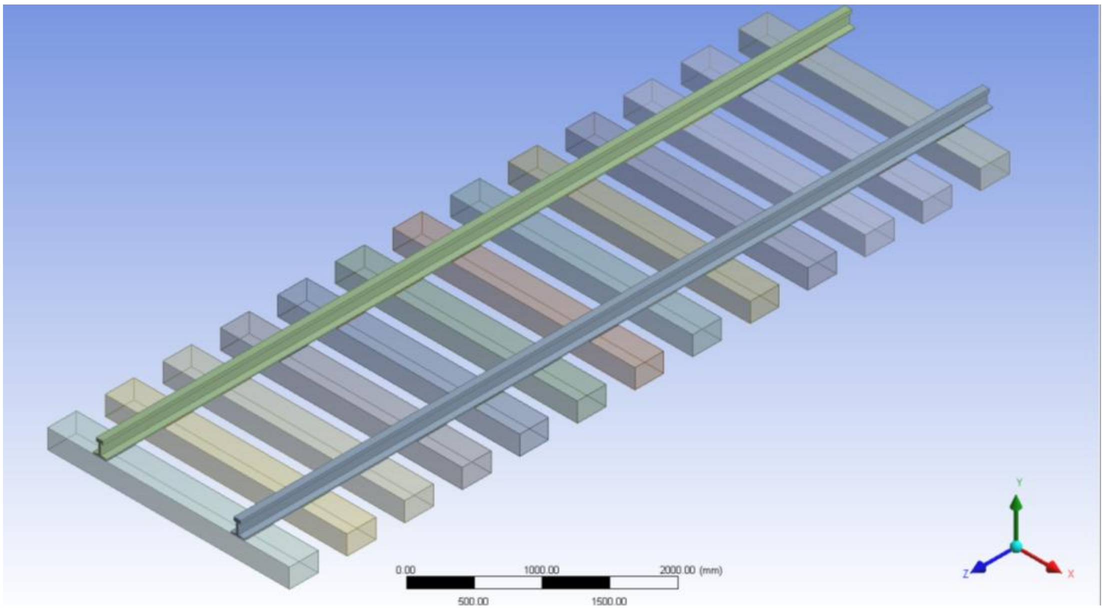

Figure 10.1 Model overview

The properties for fasteners and ballast are taken from the master thesis report by S. Boogaerdt [2]. The values are summarised below:

Fastener properties:		
Longitudinal stiffness	17,140,000	N/m
Lateral stiffness	25,0000,000	N/m
Rotational stiffness	100,000	Nm/rad

Ballast properties:		
Lateral stiffness	1,800,000	N/m
Longitudinal stiffness	2,400,000	N/m
Vertical stiffness	100,000,000	N/m

These values are valid per meter of track and per fastener. Therefore, they have to be converted to values per surface in the model. These calculations are given below:

Vertical stiffness. The bottom area of the sleepers is equal to 2.5 meters by 0.3 meters. With a sleeper every 0.6 meters this means that per meter of track 1.25m² is available for the vertical support. Dividing the vertical stiffness from the second table by 1.25 yields a stiffness of 79.998.400 N/m³ to be applied in the model.

Lateral stiffness. The side area of the sleepers is equal to two times 0.2 meters by 0.3 meters. With a sleeper every 0.6 meters this means that per meter of track 0.2 m² is available for the vertical support. Dividing the lateral stiffness from the second table by 0.2 yields a stiffness of 9.000.000 N/m³ to be applied in the model.

Longitudinal stiffness. The side area of the sleepers is equal to two times 2.50 meters by 0.2 meters. With a sleeper every 0.6 meters this means that per meter of track 1.667 m² is available for the longitudinal support. Dividing the longitudinal stiffness from the second table by 1.667 yields a stiffness of about 1.440.000 N/m³ to be applied in the model.

Fastener stiffness. The determination of the fastener stiffness to be used in the model is somewhat different. Because of the rather complex design of fasteners, involving clamping forces, friction and complicated geometry it is opted to use a simplification. Instead of modelling the actual clamp and applying the clamp forces, the behaviour of the fasteners is modelled using the “railpad”. This is a 3d solid, nothing more than a box with a height of 7 mm and sides of 140 by 300 mm. The material of this railpad is adjusted and tweaked so it behaves according to the stiffness in various directions as established by M.A. Van.

In practice this means that a single sleeper is modelled and fixed in place, upon which rests a railpad, which has a piece of rail of 300 mm on top of it. A force is then applied to the piece of rail in the x or y direction, and the amount of deformation of the top of the railpad (and thus the rail) is calculated. This process is illustrated in Figure 10.2.

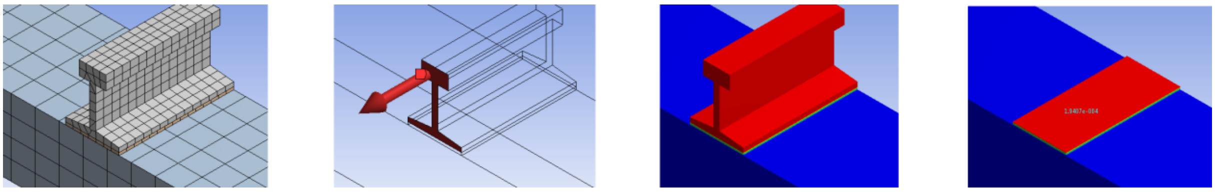

Figure 10.2 The spring stiffness determination

Using this displacement the stiffness of the railpad in that direction can easily be determined by dividing the force over the resulting displacement. This is done in all three directions, even though the vertical stiffness is probably of lesser importance. Because the rotational stiffness of the fastener has to be modelled correctly as well, the shear modulus of the railpad material is adjusted until a moment applied on the surface of the railpad yields the appropriate rotation.

The stiffness is determined by calculating the directional displacement in x-direction at the outer edge of the railpad. Using the fact that the railpad is 140 mm wide, the inverse sine of the displacement at the edge, divided by half the width (70mm), yields the angle of rotation. Dividing the applied moment by this rotation yields the rotational spring stiffness of the railpad. This process is illustrated in Figure 10.3.

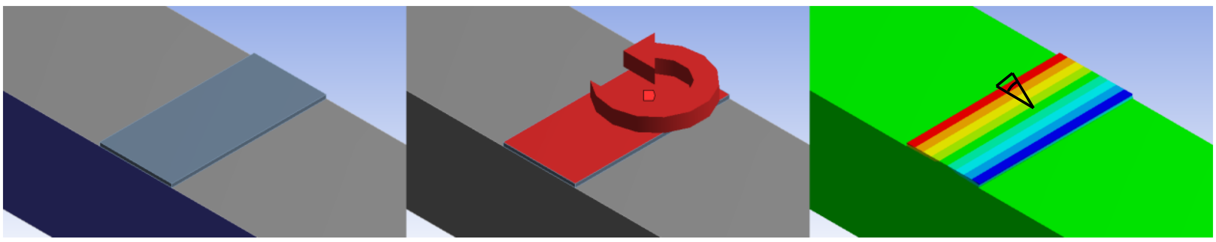

Figure 10.3 Left to right: geometry, rotational load, displacement in X direction

The longitudinal and lateral fastener stiffness is provided in N/m per meter of rail. This means that with a sleeper every 0.6 meters, and two fasteners per sleeper the values provided have to be divided by 2 and $\frac{1}{0.6}$. This leads to the following stiffness to be modelled:

Springs	Value to be obtained:	
Lateral:	75,000,000	N/m
Longitudinal:	5,142,000	N/m
Rotational:	100,000	Nm/rad

After a parameter study, and an iterative process, the values given in the table below are established for the stiffness in the lateral, longitudinal and rotational direction. The material properties used to fine tune the stiffness were the shear moduli and the stiffness moduli. Reaching the appropriate stiffness in lateral direction could not be accomplished by adjusting the material properties alone; correcting the lateral stiffness would introduce an error in the rotational stiffness. Therefore, a spring has been added in the lateral direction to compensate. This spring is positioned to have an effect on only the lateral stiffness.

Results

After several iterations, the following values for the stiffness were obtained. The lateral stiffness was used as a "wildcard" to make sure the rotational stiffness would be correct. The lateral spring would add the needed lateral stiffness. These springs are the grey lines across the sleepers.
The obtained values were:

Direction	Stiffness	Stiffness target	Absolute difference	Percentage difference
Lateral [N/m]	75,125,836	75,000,000	-125,836	-0.17
Longitudinal [N/m]	5,155,436	5,142,000	-13,436	-0.26
Rotational [Nm/Rad]	99,702	100,000	298	0.30

The other parameters were:
Railpad size: 300x140x7 mm
Sleeper size: 300x200x2500 mm
Lateral spring stiffness: 6.30E+07 N/m
Railpad material:

Orthotropic Elasticity	
Young's Modulus X direction	5,e+007 Pa
Young's Modulus Y direction	4,8e+007 Pa
Young's Modulus Z direction	2,8e+006 Pa
Major Poisson's Ratio XY	0,42
Major Poisson's Ratio YZ	0,42
Major Poisson's Ratio XZ	0,42
Shear Modulus XY	2,03e+006 Pa
Shear Modulus YZ	8,6e+005 Pa
Shear Modulus XZ	9,6e+006 Pa
Thermal Expansion	2,3e-004 1/°C

Figure 10.4 Railpad material

10.1.2 Comparison to LONGSTAB model

After running a calculation with these stiffness parameters, the results are compared to the ones that are calculated with the LONGSTAB model. Displacement measurements were performed at the approximate locations of the nodes in the LONGSTAB model. Measurements were performed in two situations, one with a pulling force on both rails, one with a pulling force on only one rail. The pulling force was set at 1000 N in both Ansys® and LONGSTAB. An example of the outcomes is given in Figure 10.5.

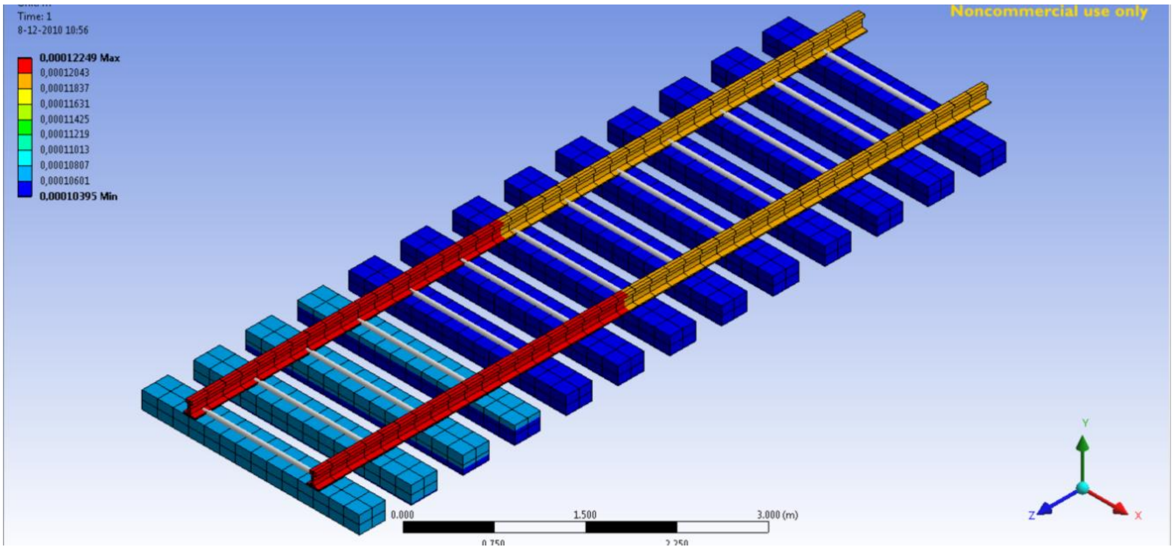

Figure 10.5 Straight track model, with a force on both rail ends.

The behaviour of the model was established to remain linear for forces not exceeding a pulling force of 30kN; corresponding to a displacement larger than 5 mm. Due to the linearity, it suffices to compare only a single loading. The results were:

Displacement due to 1000 N of force on both rails

	X direction			
	Left rail	**Right rail**	**Sleeper under right rail**	**Sleeper under left rail**
Longstab [mm]	0.00012	0.00012	0.0001076	0.0001076
Ansys [mm]	0.00012	0.00012	0.00010656	0.00010656
Difference [%]	0.4	0.4	1.0	1.0

Displacement due to 1000 N of force on the "right" rail

	X direction				Y direction			
	Left rail	**Right rail**	**Sleeper under right rail**	**Sleeper under left rail**	**Left rail**	**Right rail**	**Sleeper under right rail**	**Sleeper under left rail**
Longstab [mm]	0.0106	0.1120	0.0971	0.0105	0.0113	0.0113	0.0112	0.0112
Ansys [mm]	0.0117	0.1102	0.0952	0.0114	0.0108	0.0108	0.0108	0.0108
Difference [%]	-10.9	1.6	1.8	-8.0	4.8	4.8	3.7	3.7

It is clear from the results that the longitudinal behaviour in Ansys® corresponds very nicely with the behaviour of the LONGSTAB model. The deviation of 1% can be explained by the slight deviation of stiffness, and the slight difference in parameters such as the surface area of the rails, which has a slight deviation as well. The situation is somewhat different when the rotation is concerned. In the Ansys® model the stiffness of the spring is spread out over the total surface area of the sleeper. In contrast, the LONSTAB model employs two single longitudinal springs right in the nodes corresponding to the sleepers under the rail. Because of these different types of supports, the rotational stiffness of the sleeper is different, while the longitudinal stiffness remains correct. This difference explains the larger deviation under the left rail. This is proven in the table below, where the output is displayed when the elastic areas are replaced by longitudinal springs. Any remaining deviation is due to the difficulty in measuring the exact position of the LONGSTAB node in Ansys®.

Displacement due to 1000 N of force on the "right" rail with adjusted rotational stiffness

	X direction				Y direction			
	Left rail	Right rail	Sleeper under right rail	Sleeper under left rail	Left rail	Right rail	Sleeper under right rail	Sleeper under left rail
Longstab [mm]	0.0106	0.1120	0.0971	0.0105	0.0113	0.0113	0.0112	0.0112
Ansys [mm]	0.0109	0.1116	0.0968	0.0107	0.0111	0.0111	0.0109	0.0109
Difference [%]	-2.1	0.3	0.3	-1.4	1.7	1.7	2.4	2.4

However, the aim is not to exactly recreate the output of the LONGSTAB, but to model reality as best as possible referenced to the LONGSTAB model. An elastic area is a better approximation of the real situation, and therefore no springs are used in longitudinal direction.

10.1.3 Non-linear model

When one of the turnout ends is not fixed, and the turnout is heated or loaded by a force, the sleepers can expand beyond the modelled linear behaviour of the ballast (up to 5mm [3]). A separate model has been made for these situations. This consists of a new spring element connected to the sleepers. This element is positioned in the longitudinal direction of the turnout. In ANSYS® a non-linear spring is not a readily available object. Therefore normal elastic springs were used, which were transformed into general linear elements using ANSYS® commands. On these elements, it is possible to prescribe the force-displacement diagram using another command. The force displacement relation is based on a combination of the LONGSTAB theory (linear resistance until 5 mm displacement) and the measurements performed by S. Boogaerdt (ballast yields at 14400 Pa, or 7200 N), this behaviour is visualised in Figure 10.6.

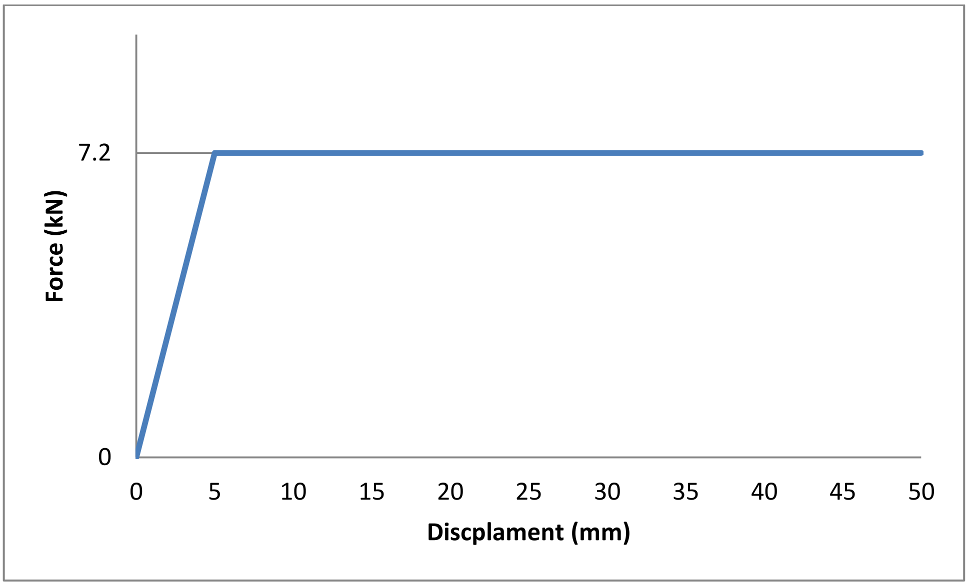

Figure 10.6 Force displacement relation of the non-linear spring element

In earlier research [2, 3] it has been determined that the ballast behaviour is linear elastic until a sleeper displacement of 5 mm. The plastic behaviour continues until a displacement of 50mm, after this amount of displacement the ballast internal structure collapses. The used non-linear model behaves like the ballast for the first 5 mm; afterwards its resistance to displacement is constant. It does not however collapse after a 50mm displacement (Ansys® does not allow a negative slope for the force-displacement graph). This makes the non-linear model valid for sleeper displacements up to 50 mm, but not beyond. In the model this means that the spring keeps resisting up to a force that causes a 5 mm displacement, a higher force displaces the material infinitely, while it keeps resisting with the same force that causes the 5mm displacement. When the sleepers are coupled with the rails this infinite displacement is no longer possible, and the whole structure reacts as established in earlier research.

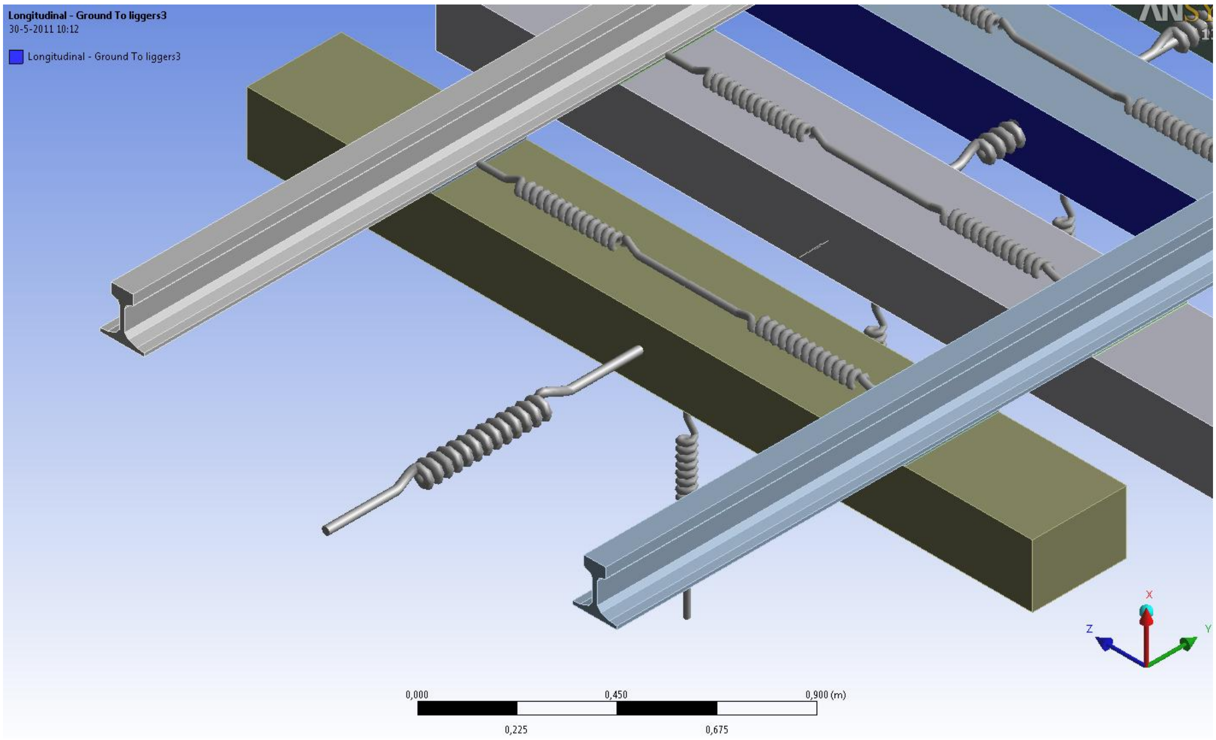

Figure 10.7 Springs in the model

Visible on the print screen of the model (Figure 10.7) are the bi-linear longitudinal springs, shown in the Y direction. The rotational springs are shown underneath the sleepers, positioned in the X direction with a rotational stiffness around the X-axis. These are needed to compensate for the lack of rotational stiffness that was lost when the elastic surface supports were lost. These springs were tuned to have the same behaviour as the elastically supported surfaces used in the linear mode. Every sleeper has its own unique rotational stiffness due to its length varying. The springs in the Z direction are the sleeper-railpad springs, needed to model the connection between rail and sleeper.

10.2 Turnout

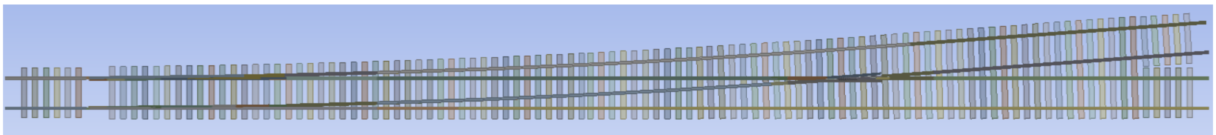

Figure 10.8 Turnout overview

The turnout is modelled using AutoCAD® drawings. It has been opted to model a 1:15 turnout with a radius of 725 meters (Figure 10.8). This is the newest type of turnout ProRail uses and the expectation is that it will become widely used in the Netherlands. The geometry of the turnout was drawn in 3-d in AutoCAD®. This was then imported in Solidworks® and converted to a .step file. This in turn could be imported into Ansys®. Even though this sounds simple on paper, in reality the complicated geometry and the sometimes “stubborn” software posed problems in all stages of the process.

Using this model, predictions can be made for the practical experiment. The output from the practical experiment can then be compared to the theoretical output from the model. This helps to enhance the accuracy of the model, and the theoretical model in turn yields insight in the practical situation.

Two-dimensional drawings of the turnout and its components were provided by the engineering firm Arcadis. These were then redrawn into a 3d drawing consisting of solids in Ansys®. A 3-d model of a common crossing (frog) was supplied by Wisselbouw Nederland. This was adjusted and converted to fit in the Ansys® model. However, this model was of a composite common crossing contained some errors and therefore was not used. For the final used model, a different solid cast crossing was modelled based on the AutoCAD® drawings. The reason behind this was it was preferable to model every aspect from the same crossing, and not to start mixing different parts from separate crossings.

10.2.1 Model parts and materials

The model consists of four separate geometrical parts. These are the sleepers, the railpads, most of the rail, and the two curved rail pieces. These last ones were made separately in Ansys® as its geometry posed problems when converting from the drawing to the .step file. In all probability, the double curved surfaces were probably the cause of conversion errors. The CAD system in Ansys® is adequate to model these curved rail pieces, but its user unfriendliness does not encourage the entire turnout to be modelled in Ansys®.

The sleepers are supported by elastic springs, the values of which are discussed previously. The material assigned to them is structural concrete with the properties as displayed in Figure 10.9.

Young's Modulus	3,e+010 Pa
Poisson's Ratio	0,18
Density	2300, kg/m³
Thermal Expansion	1,4e-005 1/°C
Tensile Yield Strength	0, Pa
Compressive Yield Strength	0, Pa
Tensile Ultimate Strength	5,e+006 Pa
Compressive Ultimate Strength	4,1e+007 Pa

Figure 10.9 Sleeper material

The railpads are assigned the corresponding material (as determined previously), and springs have been added at each fastener location in lateral direction. The rails are modelled as being structural steel with the properties as displayed in Figure 10.10.

Young's Modulus	2,e+011 Pa
Poisson's Ratio	0,3
Density	7850, kg/m³
Thermal Expansion	1,2e-005 1/°C
Alternating Stress	
Strain-Life Parameters	
Tensile Yield Strength	2,5e+008 Pa
Compressive Yield Strength	2,5e+008 Pa
Tensile Ultimate Strength	4,6e+008 Pa
Compressive Ultimate Strength	0, Pa

Figure 10.10 Rail material

Below are some screenshots to illustrate the model:

Turnout geometry:

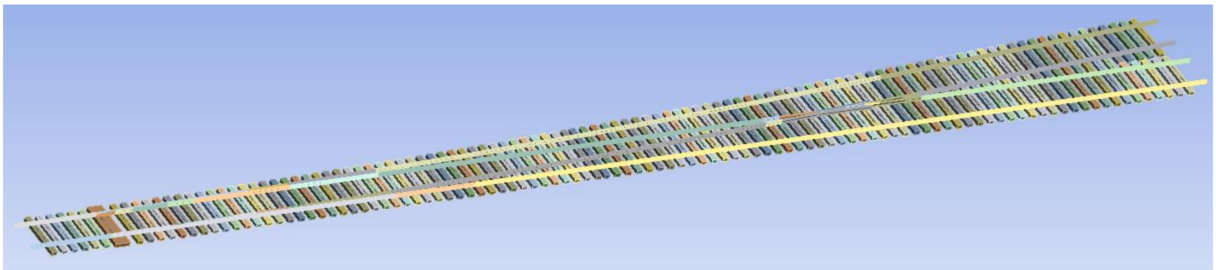

Common crossing close up:

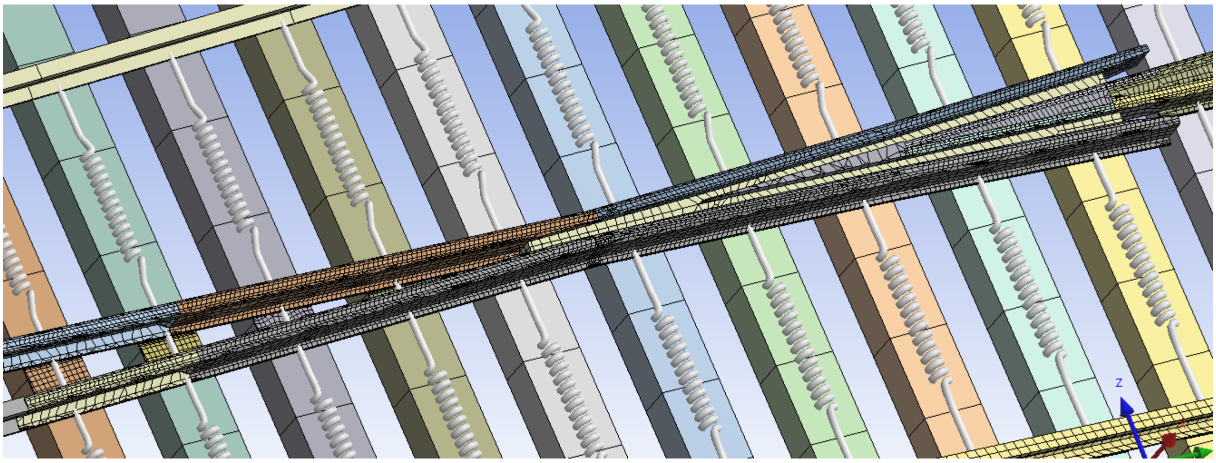

The small areas between the rails on the left side, with the fine mesh inside, are the iron connecting plates that connect both rails before and after the common crossing.

Switchblade close-up:

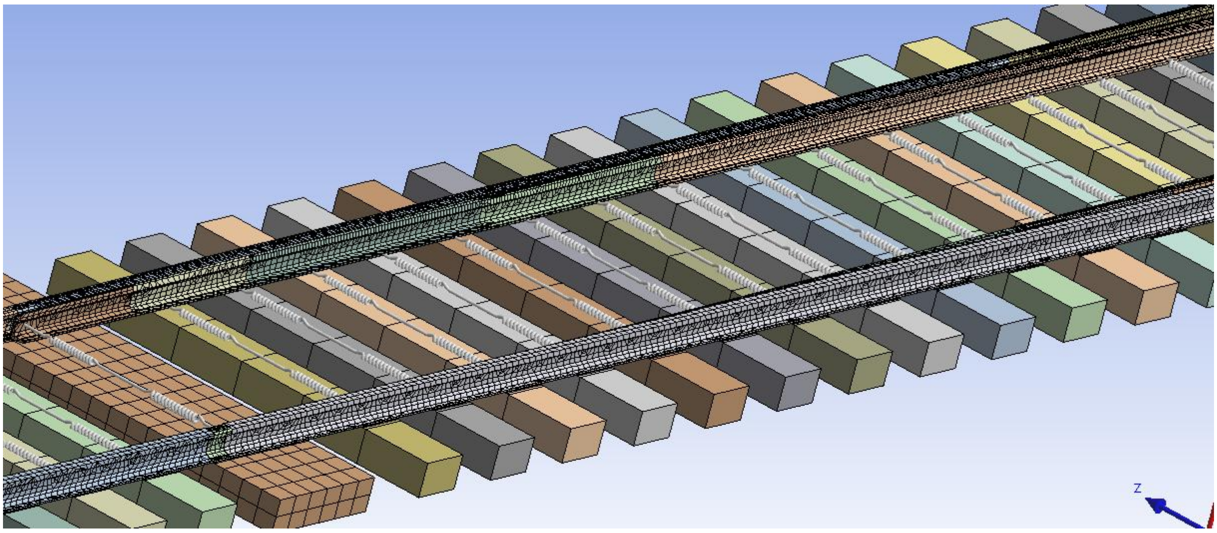

Railpad close up:

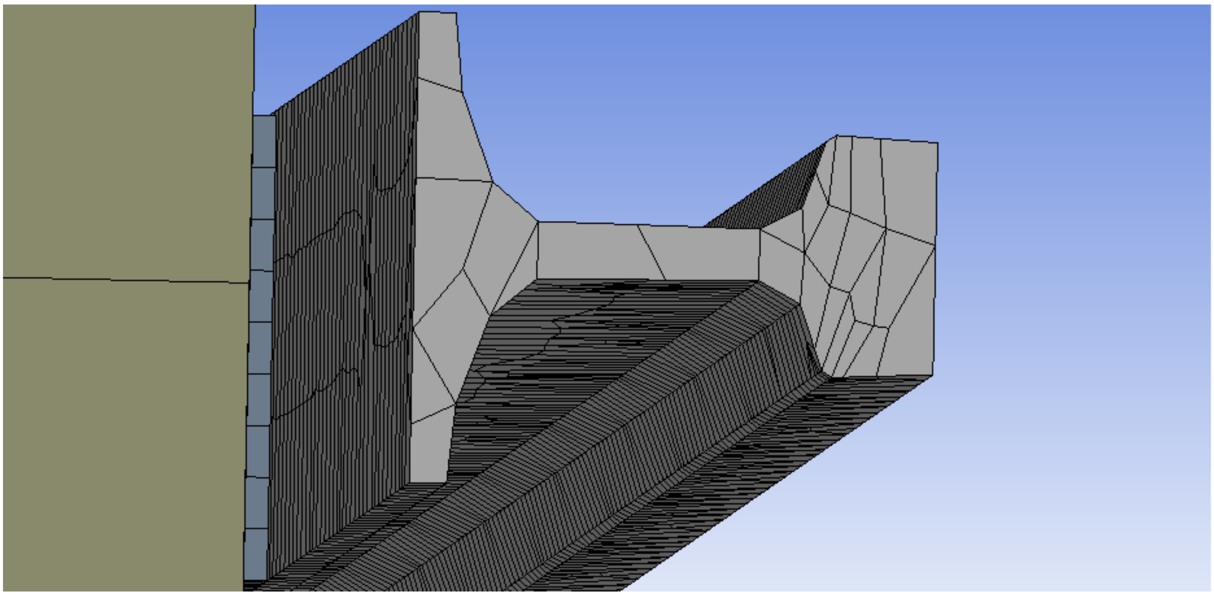

10.2.1.1 Switch blade boundary conditions

The switchblade and its boundary conditions are one of the most interesting sections of the turnout. In practice, the switchblade is manoeuvred from and to its corresponding stock rail with the aid of horizontal greased up sliding plates, which are positioned next to the stock rail, and support the switchblade in the vertical direction. The vertical support was modelled as a frictionless support in the vertical direction, as the friction coefficient of the horizontal sliding plate is not known but assumed very low.

When the switchblade is opened completely it is fixed to its end position by means of the point machine, with the outer side of the switchblade resting against the outer side of the sliding plate (Figure 10.11). In the fully closed position it is again locked into place by the point machine, while its side rests against metal blocks (called heel blocks) attached to the stock rail (Figure 10.12). This ensures the switchblade has the correct curvature when it is closed.

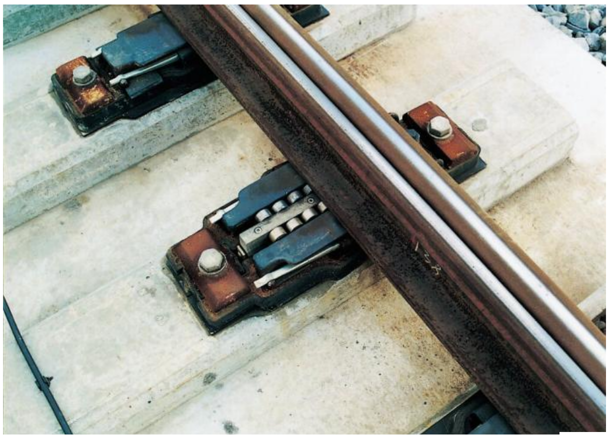

Figure 10.111 Slide plates

Figure 10.2 Heel block

Modelling this situation realistically was a challenge. Several possible solutions were tried. The first was using a frictionless contact zone but, due to the complicated geometry, the solution solver software needed a large amount of iterations with very small steps to converge to a solution. This went as far as needing more than 48 hours of calculation time (57 iterations) for a single model.

Another solution tried was using a LINK180 element with some custom settings (this is basically a connection between two nodes). This element is able to “open” when it is subjected to a tensile force thereby not transferring any force, while it is able to transfer a compressive force when it is “closed”. By positioning these elements between the switchblade and stock rail, a satisfactory behaviour could be achieved. Moving the switchblade away from the stock rail opens these LINK180 elements, allowing this movement to be performed without the force being absorbed by the LINK180 connection. When the switchblade is pressed against the stock rail the LINK180 element closes and transfers the forces and deformations to the stock rail. This behaviour corresponds to the situation in practice. It was however noted that in the case of the switchblade itself expanding due to temperature changes the LINK180 elements are rotated slightly towards the closed position instead of opening, and start transferring some of the force generated by the switchblade to the stock rail. Furthermore, when the link is closed the connection also has a bending stiffness and thereby influences the free expansion of the switchblade.

An analysis of the forces involved and the benefits and drawbacks of the different solutions led to the conclusion that for the specific purpose of this model it would be most advantageous not to model this contact. This means that the loads from the switchblade to the stock rail are not transferred in their appropriate locations (instead they are transferred through the point machine); this allows the switchblade to bend slightly towards the stock rail (1-3 mm). While this behaviour is not the behaviour as in practice, the forces exerted on the stock rail by the switchblade are sufficiently small (between 1.7 and 3.5 kN for several different load configurations) that neglecting them would not cause unrealistic results. These forces are spread out over a length of about 6 meters, resulting in an average sleeper displacement due to these forces of approximately 1E-5 m. To verify, a calculation with the frictionless contact areas was compared to the solution without these contacts, please refer to appendix VII for more details.

These displacements are deemed sufficiently small as to allow ignoring of the contacts between switchblade and stock rail. This causes a minor inaccuracy in the model, but allows it to remain linear, and thereby calculable in approximately 20 minutes. A much more preferable solution compared to the 57 iterations and the 48.5 hours calculation period when using frictionless contact surfaces, or the greater inaccuracies in the switchblade displacement when modelling the contact using the LINK elements. This option is therefore considered the best configuration, balancing calculability and accuracy of the model. Properties of the different modelling methods are presented in Figure 10.13.

	No contact	Frictionless contact	LINK180 elements
Drawbacks	Unrealistic switchblade lateral deformation	Nonlinear solution needed	Not limited to compressive resistance, resulting in inaccurate switch blade results
	Forces in switch blade not taken into account at appropriate locations	Complicated rail geometry makes proper contact definition difficult	
Benefits	Linear solution	Realistic behaviour	Compressive behaviour can be defined
			Linear solution
Calculation time	20 minutes	48+ hours	20 minutes
Iterations	1	57	1

Figure 10.12 Modelling methods properties

In the digital version of this report, this page contains an interactive copy of the turnout model.

10.2.2 Model preparation

Contact regions have been automatically generated and were checked manually. The tolerance was set very low, so only the direct contacting regions would be automatically generated. Some faulty generated regions were removed, and some missing regions were added. The faulty ones included connections between the switchblade and the non-movable rail. These were set to frictionless contact, allowing the blade to expand freely, or no contact, depending on the model.

10.2.2.1 Mesh

The mesh was generated using the "mechanical" and a hex dominant meshing setting. The size of the mesh was set to 0.05 meters, a setting which would allow detailed meshing of the complex geometry while at the same time trying to keep the amount of nodes as low as possible. Some of the less complex geometry, such as the sleepers, was set to a larger element size as to reduce the number of equations to be solved.

10.2.2.2 Boundary conditions

The boundary conditions at the rail ends were set to fixed, as it is assumed the rails connected to them is properly constructed and therefore cannot displace. The assumption that a fixed connection is a good approximation has been investigated in appendix chapter IV.ii

10.2.2.3 Common crossing

The support under the common crossing deviates from the rest of the turnout. Due to the rigidity of the common crossing, and the special fastening of it to the sleepers, it is not modelled using the spring-analogy material railpads, but it is connected to the supporting sleepers in all directions using structural steel railpad elements. This is considered a better representation of reality, as in practice the frog is connected to the sleepers by means of a fixed connection.

10.2.2.4 Ball and claw

The ball and claw system was modelled after the official drawings of the system used with this type of turnout. More specifically, the ball and claw system on this turnout are not two separate entities, but a single construction linking the switchblade to the strike rail. It is illustrated in Figure 10.14.

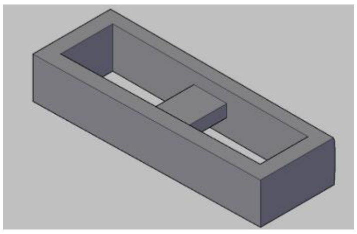

Figure 10.13 Ball and claw system of this turnout

10.2.3 Modelled situations

Several situations were modelled and calculated, to provide insight in the size of the stresses and the behaviour of the turnout.
These situations were:

- A temperature increase of 40 degrees on a turnout with fixed supports on all three sides as shown in Figure 10.15. In this situation, the connections to the straight rail tracks on all three legs of the turnout are modelled as fixed supports.

- A temperature increase of 40 degrees on a turnout with fixed supports on all three sides. In this situation the longitudinal springs between the fasteners and the rails were suppressed (not used in the calculation) to compare the results. This is due to the significantly reduced time needed for constructing new models when omitting the springs. Should the results not differ greatly it is much preferred to suppress the springs. See appendix chapter III for the results.

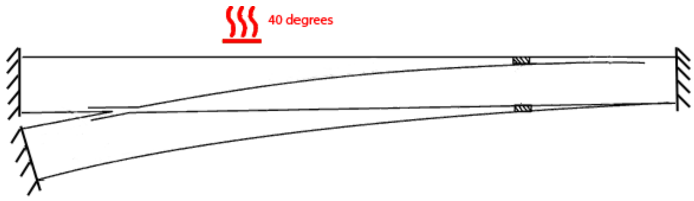

Figure 10.14 Turnout with fixed supports on all sides

- A temperature increase of 20 degrees on a fully supported turnout (Figure 10.16).

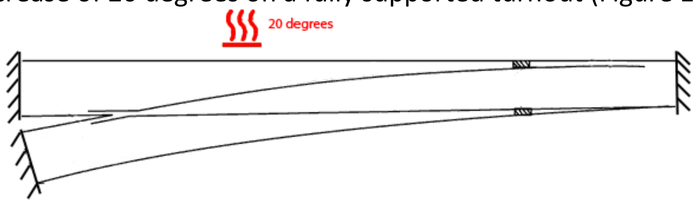

Figure 10.15 Heated turnout with fixed supports on all sides

- A temperature decrease of 40 degrees on a fully supported turnout (Figure 10.17)

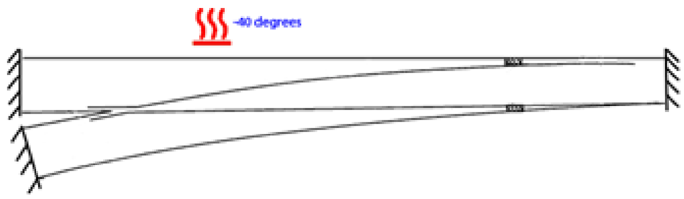

Figure 10.16 Cooled down turnout with fixed supports on all sides

- A temperature increase of 40 degrees on a 2/3 fixed support turnout with the turnout rails free to expand (Figure 10.18). This models displacement are larger than the linear model is valid for, it has therefore also been calculated a second time using the nonlinear model. This situation can occur during renewal, and is theoretically the only scenario in which one of the rail-ends can expand beyond the linear behaviour of ballast.

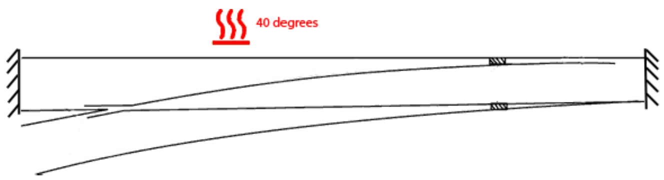

Figure 10.17 Heated turnout with 2 out of 3 supports fixed, and one free

- A temperature increase of 20 degrees, where the turnout is supported in 2/3 ends. This simulation was run three times, with a different turnout end left unfixed each time.

- A turnout installed following the ProRail guidelines, during an outside temperature of 0 degrees. This means that the closure rail (chapter 4.3) is heated to 28 degrees, as well as the connecting track. The effect of the cooling of the adjacent track was simulated by introducing a tensile force equal to 28 degrees of cooling. The other turnout parts are installed at 0 degrees (Figure 10.19)

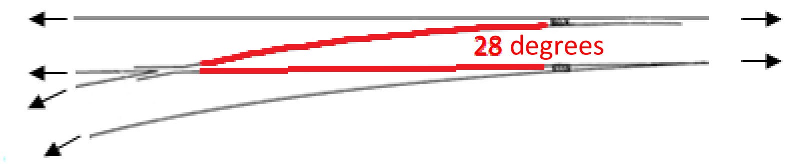

Figure 10.18 Turnout constructed according to the ProRail guideline

- The situation described previously, but followed by an increased temperature of 40 degrees in the entire turnout.

10.2.4 Limitations

Some limitations with the Ansys® model need to be addressed. The ballast behaviour is a key factor to the behaviour of the entire turnout, but this behaviour differs greatly from site to site. Because it is not possible to determine the ballast behaviour at the test site due to practical and economic issues the theoretical values mentioned in [2] and [3] are used.

The wing and check rails (chapter 4.9) are not modelled as their effect on the behaviour of the turnout is probably minor. In addition, the rails and connections are not modelled fully according to reality. The properties of the connections are approached by using corresponding stiffness, while the rail profile has been “straightened” up a little, all the actual curves and corners of the rounded rail profile have been turned into straight lines. This is to be able to make the mesh of the model coarser, thereby reducing calculating time. The change from curved to straight lines will not have a noticeable impact on the outcome of the calculation, as the inner rail surface area is kept constant. Furthermore, the rail profile used in practice can deviate, as there are deviations in the dimensions of the rail (they are rolled to within certain margins), and the wear and tear on the railhead will reduce its height as well.

Calculation was done using automated Ansys® settings, using the sparse solver (in INCORE mode). The model was calculated in a single iteration. Deviating from the automated settings was found not to give any notable increase in either calculation time or accuracy of the model.

11 Model results

In this chapter, the outcomes of the models are discussed briefly. Two further investigations into turnout behaviour can be found in appendix IV. These investigations discuss the linear behaviour of the turnout and the fixed connection boundary condition.

This chapter focuses only on the outcomes of the theoretical FEM model; these outcomes will not be related to measurements in practice. This chapter will refer to the different rails in the turnout by number. This numbering is shown in Figure 11.1, the sleeper numbering is presented in Figure 11.2.

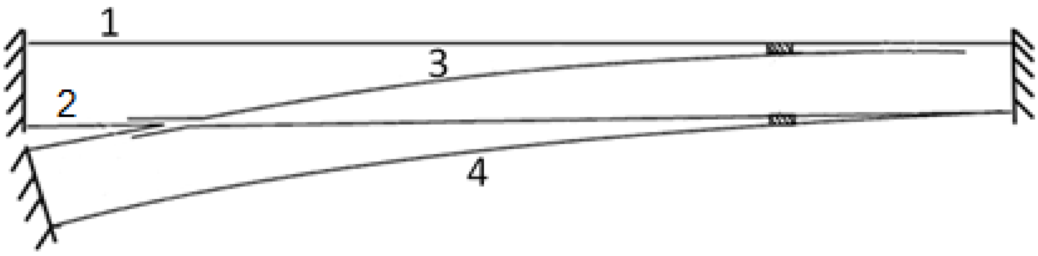

Figure 11.1 Rail numbering

Sleeper #

1 10 20 30 40 50 60 70 80 90 100

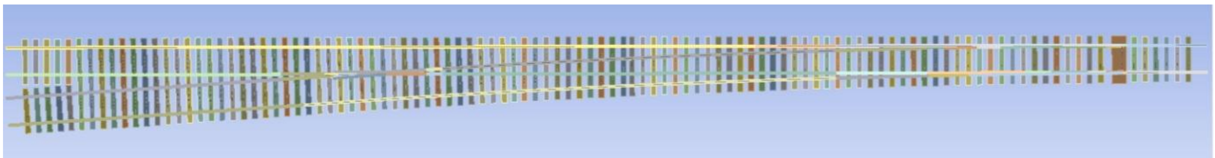

Figure 11.2 Top view of the turnout for reference

The data in the graphs in this chapter was collected by requesting the output from the program at the railhead every five sleepers. The exact location where the output was requested was the middle of the top of the rail profiles as illustrated in Figure 11.3. This is an acceptable location to request the data; in Figure 11.4, the distribution of strains over the height of the rail is presented. One can see that the difference between top and bottom of the rail is five microstrains maximum; this is in the situation where the rail is heated by 40 degrees. Getting the data from the top of the railhead is therefore representative for the strain in the entire rail cross section. However, the found strains are two or three microstrains too high. This does however not affect the distributions in the following graphs as these focuses on the distribution of strains throughout the entire turnout and the data was consistently requested at the same relative location. This behaviour suggest that further turnout models can be made with simpler representations of rail geometry.

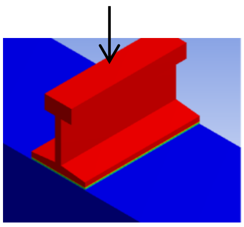

Figure 11.3 Data request location

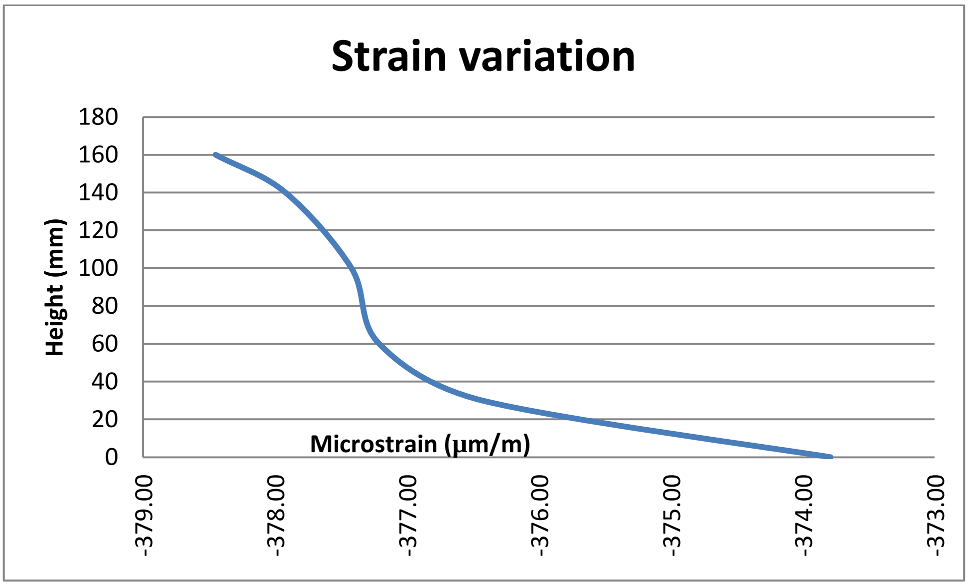

Figure 11.4 Strain variation over the height of the rail profile

11.1 Numerical outcomes of the basic model

The outcomes as calculated by Ansys® for the fully constrained turnout heated by 40 degrees are taken as reference (Figure 11.5). These results are discussed below.

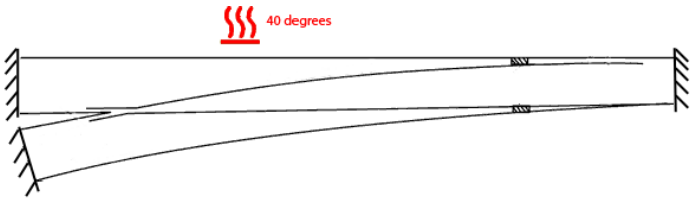

Figure 11.5 The boundary conditions for the model

11.1.1 Stresses and strains

A short overview of the strains and stresses calculated by the model is presented here. Rail 1 behaves similar to rail 4. Rail 2 behaves similar to rail 3. A number of conclusions can be drawn from the outcomes of this theoretical model (Figures 11.6 and 11.7). A direct relation between the strains and stresses is shown (mirrored around the X-axis).

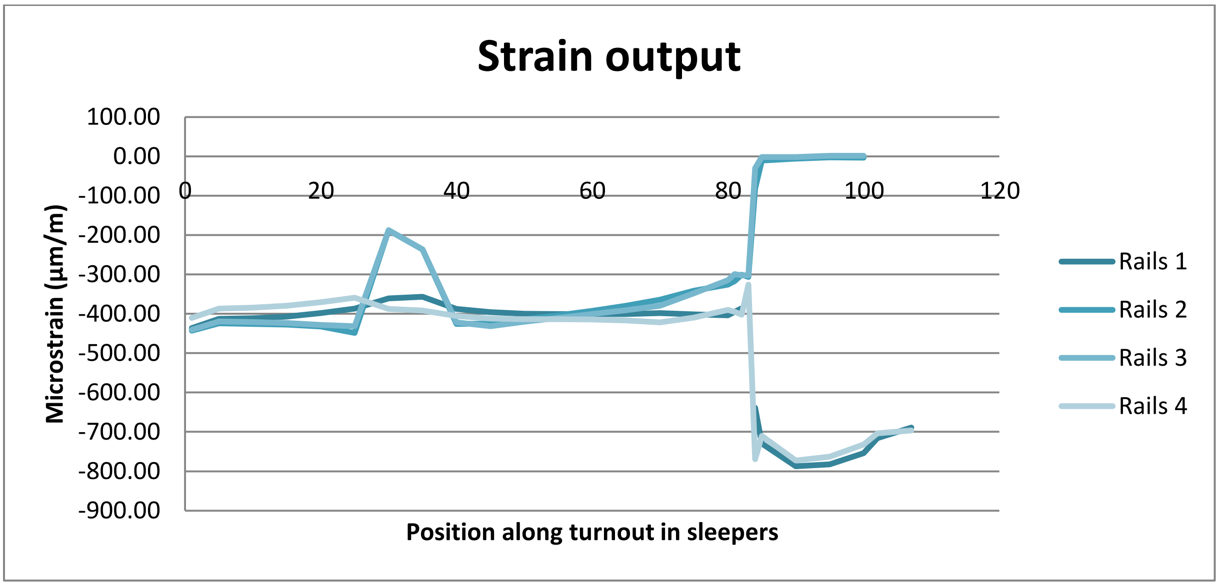

Figure 11.6 Uncorrected strain distribution in the model

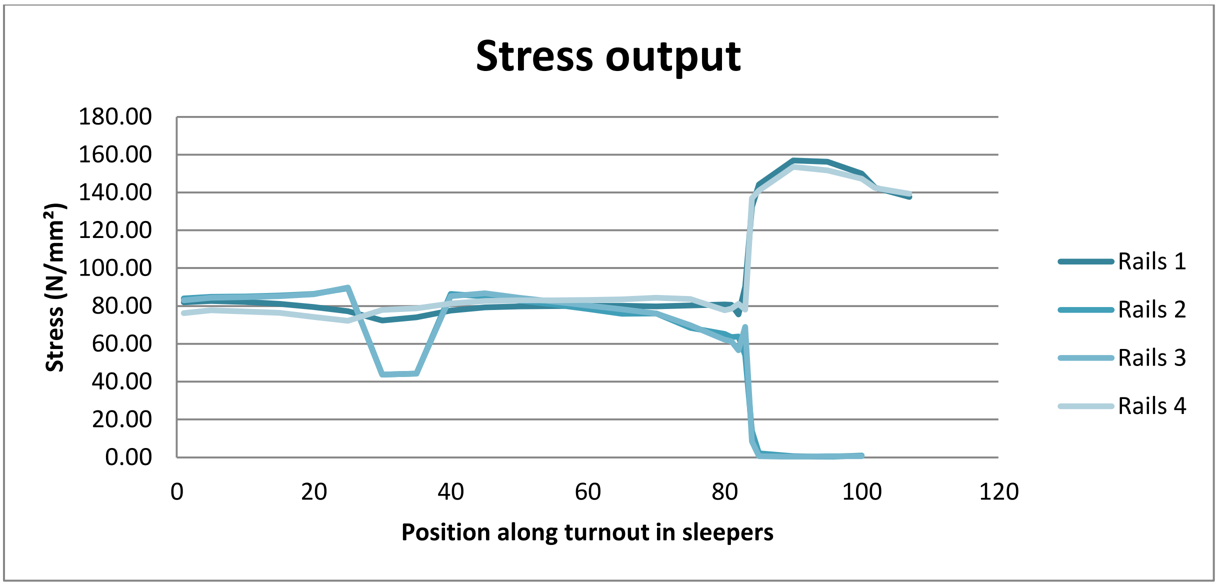

Figure 11.7 Stress distribution in the model

All strain values are negative, which is due to the way Ansys® presents its results; strains are made up of both thermal and structural strains. Ansys® presents these two separately. Because only the structural strains are plotted, the entire strain graph has a negative value. The total strain in the steel is the summation of both strains, where the structural strain has a minus sign. The thermal strain for the steel is constant at 480 microstrains (40 degrees of temperature difference, at a thermal expansion of 12 microstrains per degree). The compensated strain distribution is presented in Figure 11.8; all other strain outputs are presented corrected.

The stress graph does not need to be corrected; the shown stress values are the total stress values. The temperature increase of 40 degrees causes a stress of approximately 102 N/mm^2. Parts of the turnout with higher stresses as this reference stress are compressed, while those with lower stresses are expanding.

A note for strain gauge applications, when estimating strain gauge output use the corrected graph for rail without free expansion; use the uncorrected graph for rail with free expansion. Due to temperature correction a 480 microstrain reading on the switchblade (free expansion) would be compensated to zero by the temperature compensation of strain gauges.

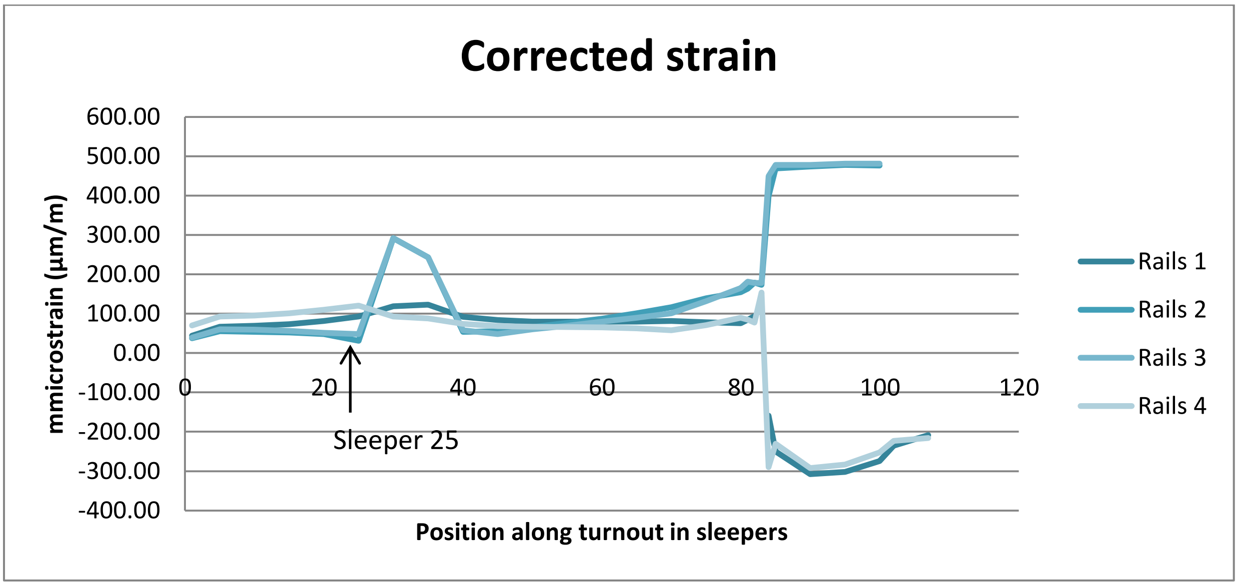

Figure 11.8 Corrected strain

Several locations have been identified and their behaviour analysed:

The common crossing

Starting around the 25th sleeper the strain line for rails 2 and 3 starts to increase, while at the same time the stress line starts to decrease. The decreasing stress indicates that there is less resistance against deformation of the common crossing, or that this resistance is spread over a larger area. The second statement can be proven false by observing the geometry of the common crossing. Its cross section is actually the smallest at the location where the stresses are lowest. This means that the decrease in stress, and the linked increase in strain, means that there is less resistance to deformation of the common crossing. This can be explained by the large bulk of the common crossing being heated causing a large force on the sleepers linked to it. This force is so large that it exceeds the resisting force, making the sleepers move, and thereby reducing the level of stress caused on the common crossing by the resistance. This allows the common crossing to expand more freely, thereby raising the amount of strain in the crossing.

Closure rail (chapter 4.3)

The closure rail is located between sleepers 35 and 80. In this area the stress and strains of rails 1 and 4 remains constant, while the strain of rails 2 and 3 (the closure rails) increase slightly, along with a decrease of stress in the rail. This means that the closure rail has a slightly higher rate of expansion than the rest of the turnout structure. This effect can be explained by the ball and claw clamping of this specific turnout deforming, therefore allowing the closure rail to expand more than its adjacent stock rail.

Ball and claw and switchblade

This is where the largest changes are observed. At this location, all the forces in the closure rail are transferred to the adjacent stock rail by means of the ball and claw system. This means that the stress in the switchblade becomes zero. The switchblade is free to expand with the coefficient of the steel resulting in a constant strain of 480 µm/m (40° x 12 E-6 m/m/°). At the meantime, the stresses in the adjacent stock rail are almost doubled. This causes the sign of the resulting strain of the stock rail to change, indicating compression. In other words: in contrast to the expansion of the rest of the turnout, the last part of the stock rail is compressed and becomes shorter. This is due to the fixed boundary conditions on all parts of the rail. A quick check also confirms that the total resultant of elongation and compression is zero, as it should be.

11.1.2 Displacements

The displacement of the rails in longitudinal direction is presented in Figure 11.9. The displacement of rails 1 and 4 is zero at the ends, and conforms to the fixed connections that are modelled there. The rails 2 and 3 show an extra displacement at the switchblade, this is the area of free expansion. Another observation is that the displacement slope increases over the common crossing. This corresponds to the higher strain at the common crossing as discusses earlier. It should be noted that the 5mm displacement limit for linear displacement is not reached.

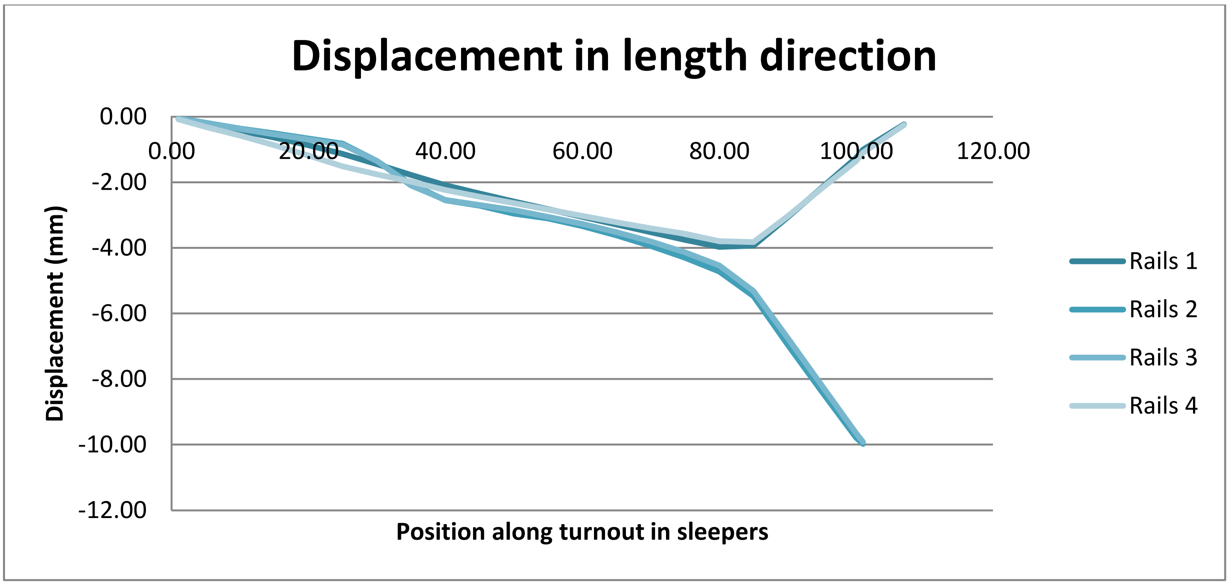

Figure 11.9 Displacement in length direction, along the turnout length

The displacement in lateral direction is presented in Figure 11.10. The (incorrect) displacement in lateral direction of the switchblade is filtered out, as it is not of interest and the outputs are not valid. The displacement of the point machine has been manually corrected, as its connection to the switchblade (in order to limit switchblade displacement) causes an exaggerated movement sideways.

The first thing that should be noted is the low values of the displacements, which are smaller than 1.1 mm. Furthermore, the sideways displacement happens very rapidly at the location of the common crossing. This is caused by the angled rails connecting to the stock rails at this location. This displacement is reduced slightly over the further length of the turnout. Near the rotating ball and claws some peaks are formed, this is due to the deformation of the ball and claw. The entire ball and claw system is rotated by the forces exerted on it, causing the peak in the purple line towards zero displacement. The other peaks are caused by this rotation being mirrored and damped further on in the turnout.

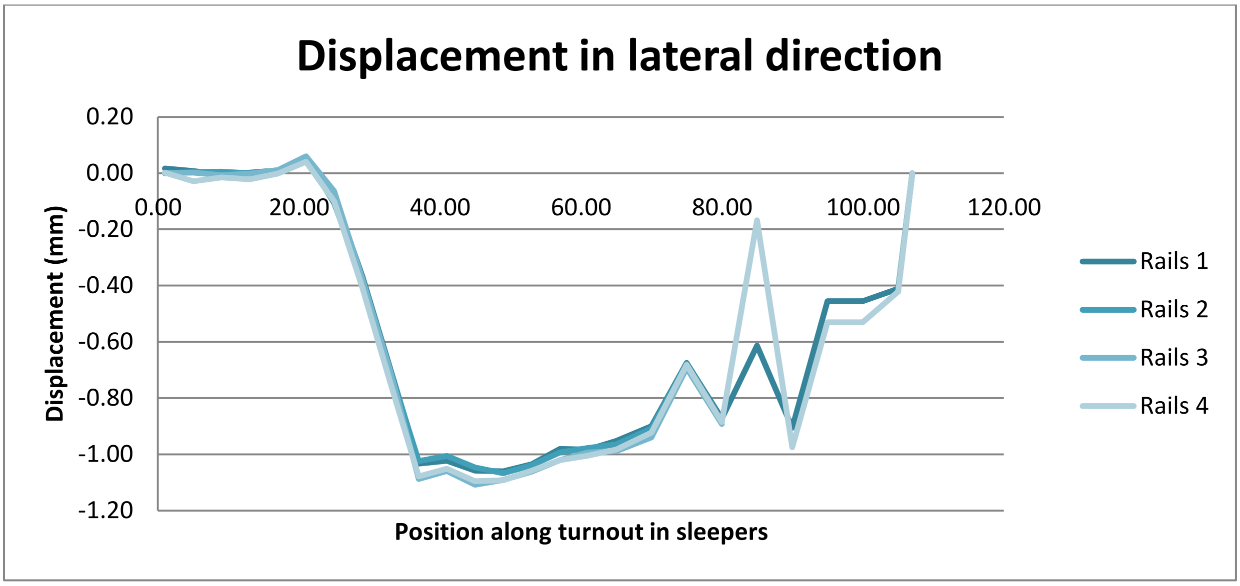

Figure 11.10 Lateral displacement in the model

11.2 Numerical outcomes of the linear 2/3 fixed model

The focus of the following models is on situations in which the turnout branch is free to expand or is loaded by a force (Figure 11.1). For more information and a sensitivity analysis, see appendix V.

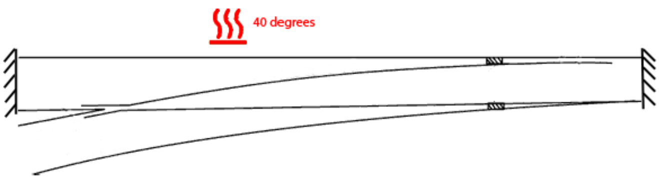

Figure 11.11 Boundary conditions of the model

In this situation, the turnout is modelled subjected to a temperature increase of 40 degrees. Furthermore, the turnout rail is modelled without a fixed boundary condition. This corresponds to a situation in real life where the turnout connection to the turnout rail is cut, for instance because of maintenance to this rail or an adjacent turnout, that is connected to this rail. This situation is very rare, but modelling this situation provides an opportunity to examine the behaviour of the turnout beyond the linear force-displacement behaviour of the ballast. To achieve this goal, two separate models are constructed. One is the basic model in which the ballast behaviour is modelled linearly, which is discussed in this chapter. In the next chapter, the outcome of a model with non-linear ballast behaviour is reviewed. The loading condition where the linear model is no longer valid lies around a temperature increase of 30 degrees.

11.2.1 Stresses and strains

The corrected strain graph (Figure 11.12) clearly shows that the strain behaviour on the right part of the graph is very similar to the situation where the turnout is fixed at all connecting rails. The difference lies in the left part, rails 4 and 3 obviously have a much higher strain, due to the expansion only being restricted by the sleeper-ballast interaction, and not being restricted by a connection with other rails. An interesting aspect of behaviour is shown at rail 2; this rail is in compression at the start, and quickly (within the space of five sleepers) moves to being in tension. This is due to the connections between rails 2 and 3 near the common crossing. They force rail 2 to deform along with rails 3 even before the bulk of the common crossing.

Rails 1 displays a lower strain value on the left side, this is due to the rotation of the sleepers being pivoted around these rail connections, thereby not displacing rail 1 and its sleepers. From the common crossing onward normal behaviour is displayed.

Rail 3 has a positive strain value throughout the entire structure, as it and rail 4 can expand freely on the left side. Beyond the ball and claw rail 4 is still fixed to the sleepers that halt its expansion, while rail 3 becomes the switchblade and can still expand freely.

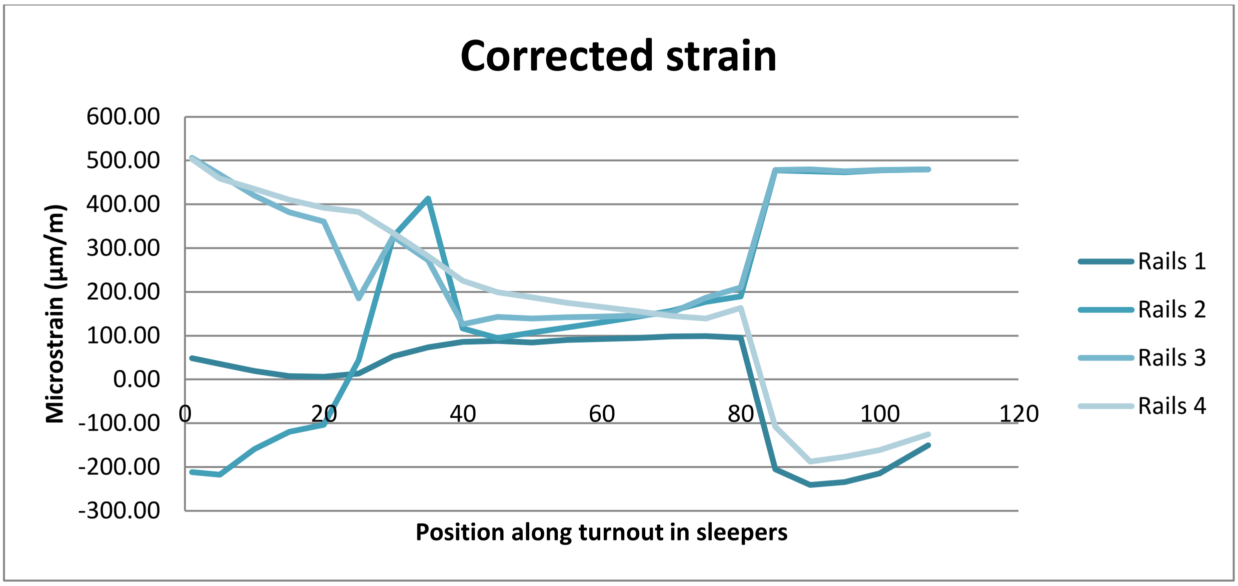

Figure 11.12 Corrected strain in the model

The stress graph (figure 11.13) shows stress behaviour that is an almost perfect mirror of the strain graph, just as with the basic model results. Highest stresses can be found in rails 2 and rails 1 and 4 after the ball and claw system.

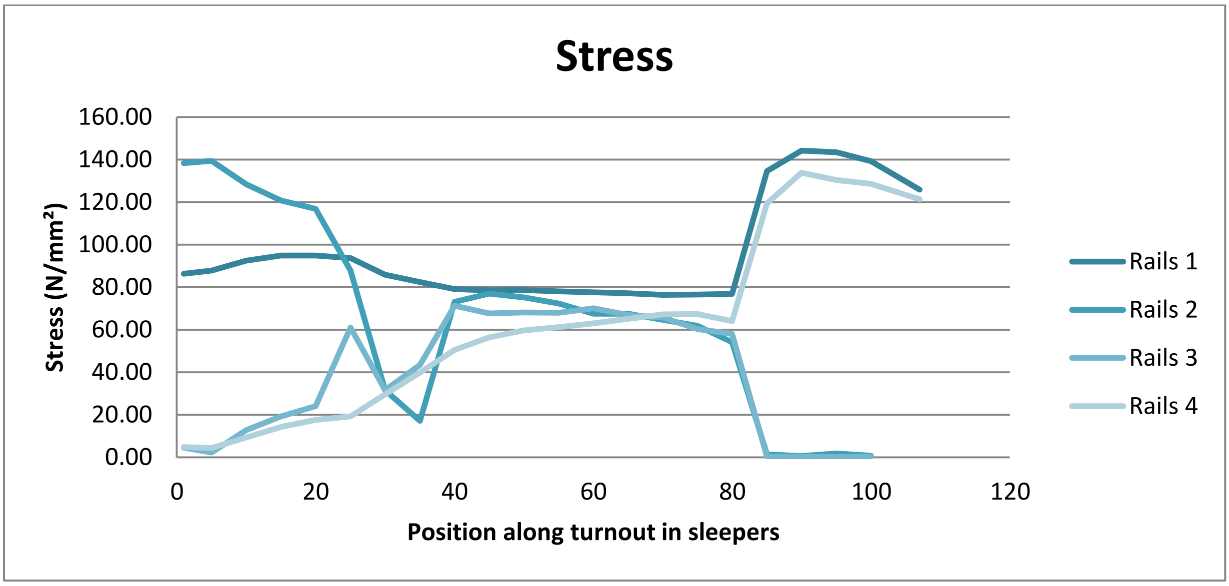

Figure 11.13 Stress in the turnout model

11.2.2 Displacements

The displacement in length direction (Figure 11.14) is straightforward. The only thing that needs to be noted is that the displacements are well above the 5 mm mark for which the linear model is valid (the sleeper displacements are closely related to the rail displacements). In lateral direction (Figure 11.15), the switchblade peaks on the right should be ignored. What is interesting is the behaviour before and after the common crossing (Figure 11.16). The common crossing itself does not move sideways much. The peaks are before and after the entire construction (including the connection plates between rails 2 and 3 before and after the crossing). This entire structure is so stiff that it rotates more or less as a single unit, causing the maximum and minimum displacements to be at the edges of this unit. For clarification, a print screen of the displacement results in lateral direction is added. Note that the displacements are increased by a factor of 100.

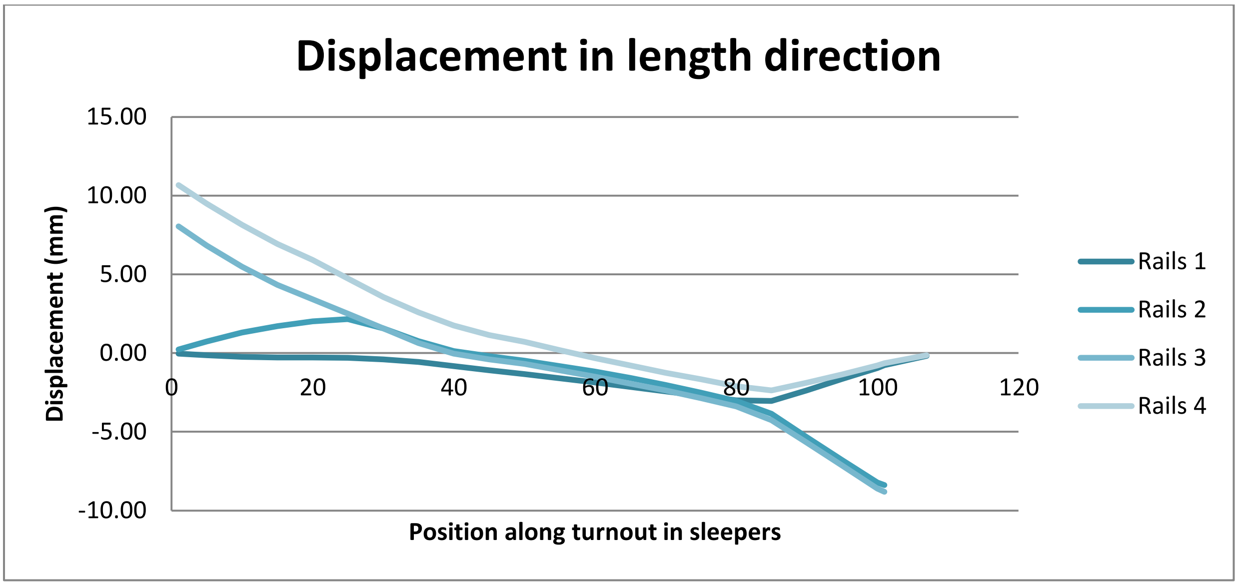

Figure 11.14 Displacement in length direction in the model

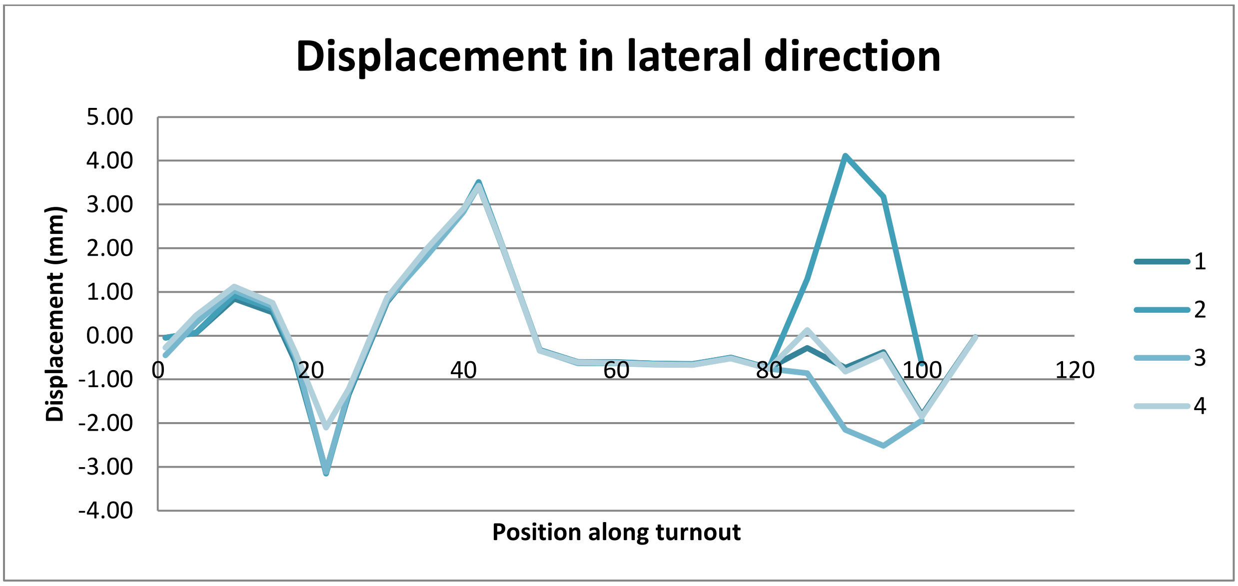

Figure 11.15 Displacement in lateral direction

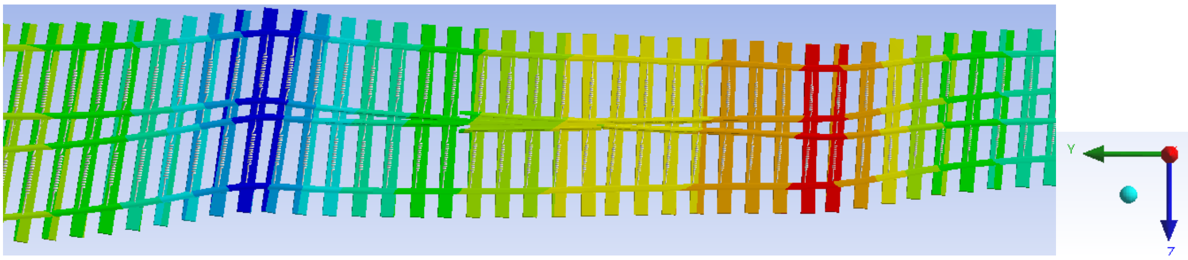

Figure 11.16 Displacement in the lateral (z) direction at the crossing. Red is maximum (positive) displacement, blue minimum (negative). Scale 1:200, displacement scaling 100x.

11.3 Numerical outcomes of the non-linear 2/3 fixed model

The discussed outcomes are based upon the turnout with the boundary conditions as in figure 11.17. The difference with the previous model is in the non-linear support of the sleepers.

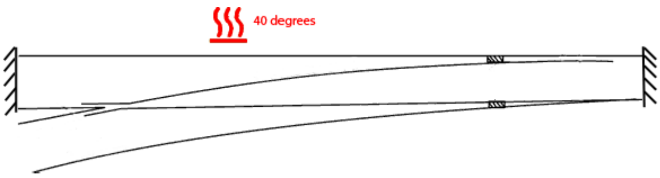

Figure 11.17 Boundary conditions of the turnout

11.3.1 Stresses and strains

The stresses and strains are almost identical to those of the linear model, and are displayed in Figure 11.18 and 11.19, plotted against their linearly supported model counterparts. A minor peak can be observed at the location of the common crossing, this peak is caused by a small deviation in the exact location where the strain output was measured. These small deviations (it was all done manually) also explain the slight deviations on the other parts of the graph. The numbers in the following graphs line names refer to the rail numbering.

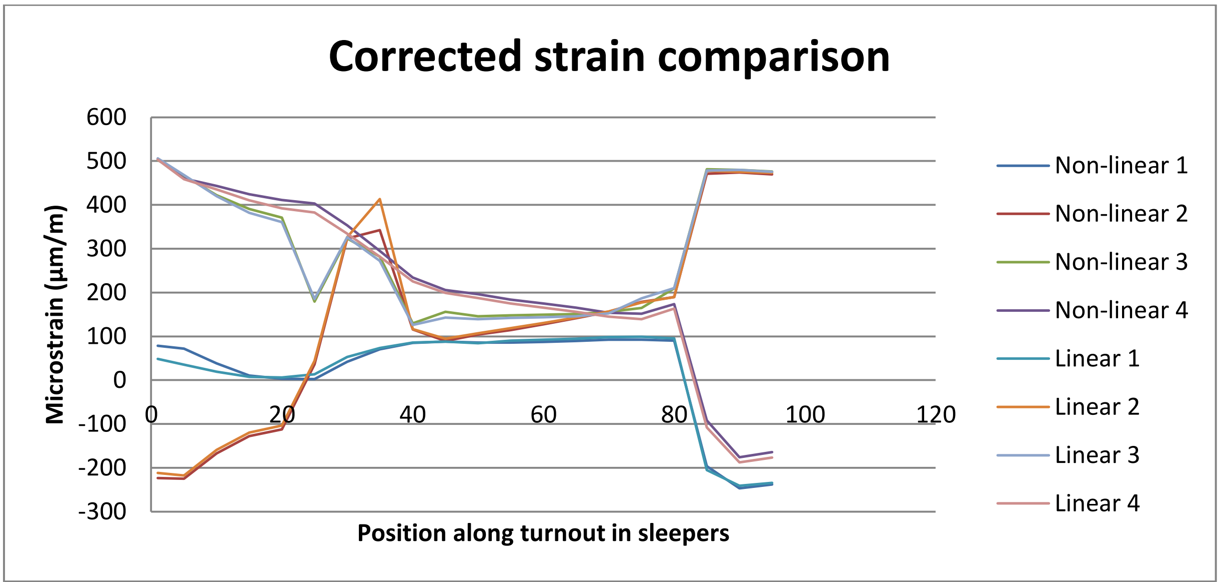

Figure 11.18 Comparison of strain between linear and non-linear supported model

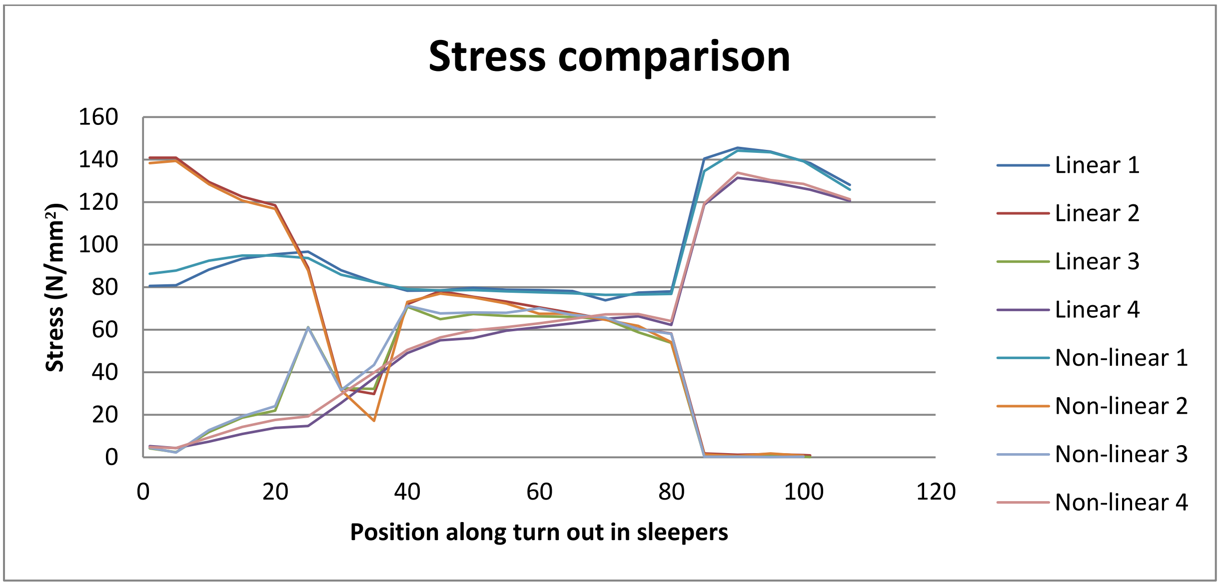

Figure 11.19 Stress comparison between linear and non-linear supported model

11.3.2 Displacements

The displacements are visualised below in Figures 11.20 and 11.21, once again plotted against their linearly supported model counterparts.

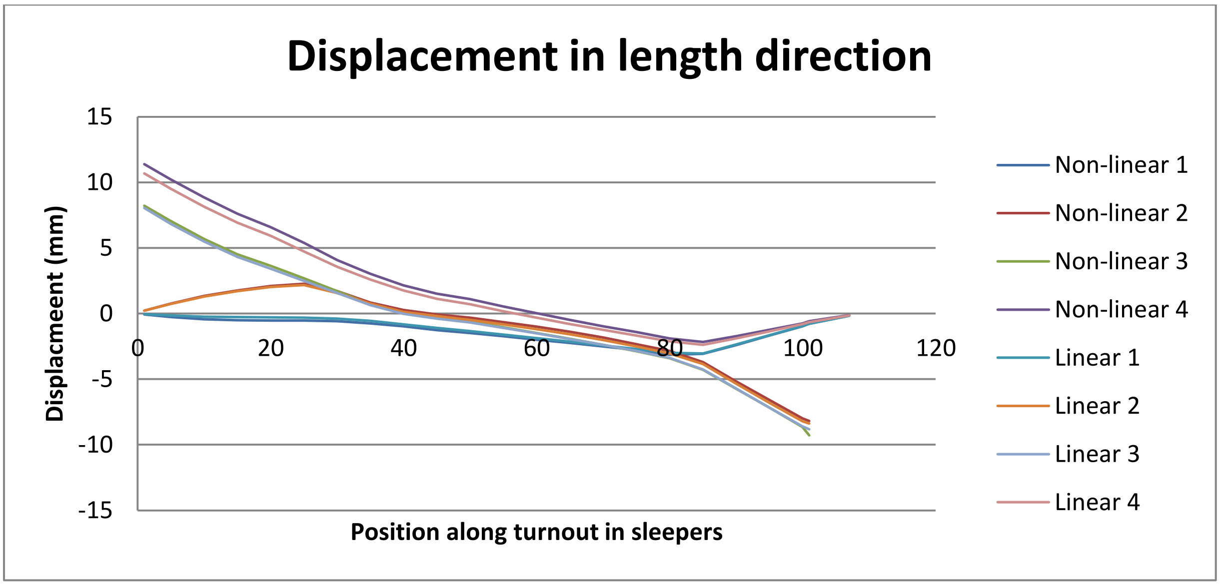

Figure 11.20 Comparison of displacement in length direction between the linear and non-linear supported models

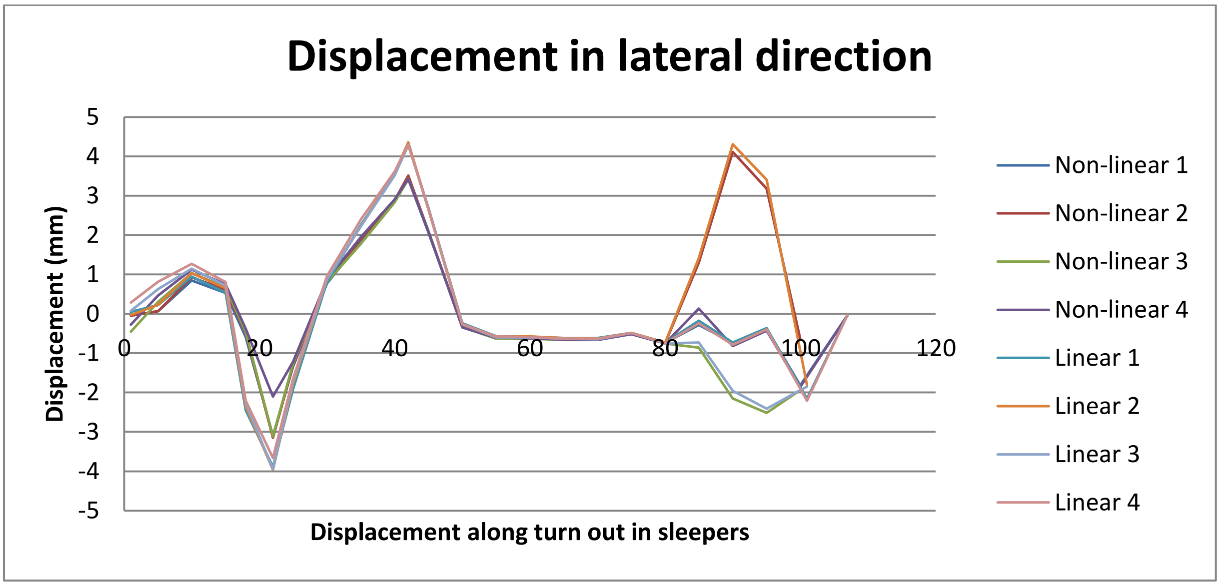

Figure 11.21 Comparison of the lateral displacement between the linear and non-linear model

These graphs of both the strain, stress and displacement outputs confirm that the non-linear model is valid (compared to the linear model), and that for small deviations above the 5 mm mark that the inaccuracy caused by the linear-elastic model is not significant. The only variable undergoing a noticeable deviation is the longitudinal displacement of rails 4. This means that the linear model can be used for almost all loading combinations, even those where the behaviour of certain sleepers might move into the non-linear region.

Note on graph lines: The lines have been reduced in thickness to increase the visibility of individual lines.

11.4 Practical situation

The boundary conditions of the linear model have been adjusted to conform to the guidelines in use by ProRail. These guidelines prescribe that when constructing a turnout between -5 and 25 degrees that the closure rails (chapter 4.3) must be heated to 28 degrees. Adjacent track that is connected to the turnout (the first 60 meters) needs to comply to a 28 degrees neutral temperature as well.

The modelled situation was a turnout placed with a temperature of 0 degrees for all turnout parts. The heated closure rail was modelled with the temperature of -28°C, as to conform to the situation when the turnout is switched in place and has cooled down. This is to simulate the tensions that occur in the closure rail as it cools down from 28°C to the air temperature of 0°C. At this time tensions will develop because the rail will want to compress, which is prevented by the rest of the turnout. The tensions that occur have been applied to the modelled parts by use of the thermal conditioning of these parts to -28 °C, Ansys® converts this boundary condition to equivalent thermal strains, thereby introducing the correct stresses.

The effect of the adjacent rail having a lower temperature was taken into account by placing a tension force on the rail ends, which corresponds to the tensile force that occurs when the rail cools down 28 degrees (490 kN). This situation corresponds to the newly constructed turnout of which the individual parts have cooled down.

A second model was made to correspond to a temperature of 40°C for all the turnout parts. This was done by assigning all the rail parts a temperature of 40 degrees, and the closure rail a temperature of 40 -28 = 12 degrees. The tensile forces were kept constant as the strain and stresses caused by the neutral temperature difference are maintained when the rail is fixed (hence the -28 in the closure rail as well).

11.4.1 Situation after construction

11.4.1.1 Stresses and strains

Displayed in Figures 11.22 and 11.23 are the strains and stresses when the turnout has been constructed and heated turnout components have cooled down.

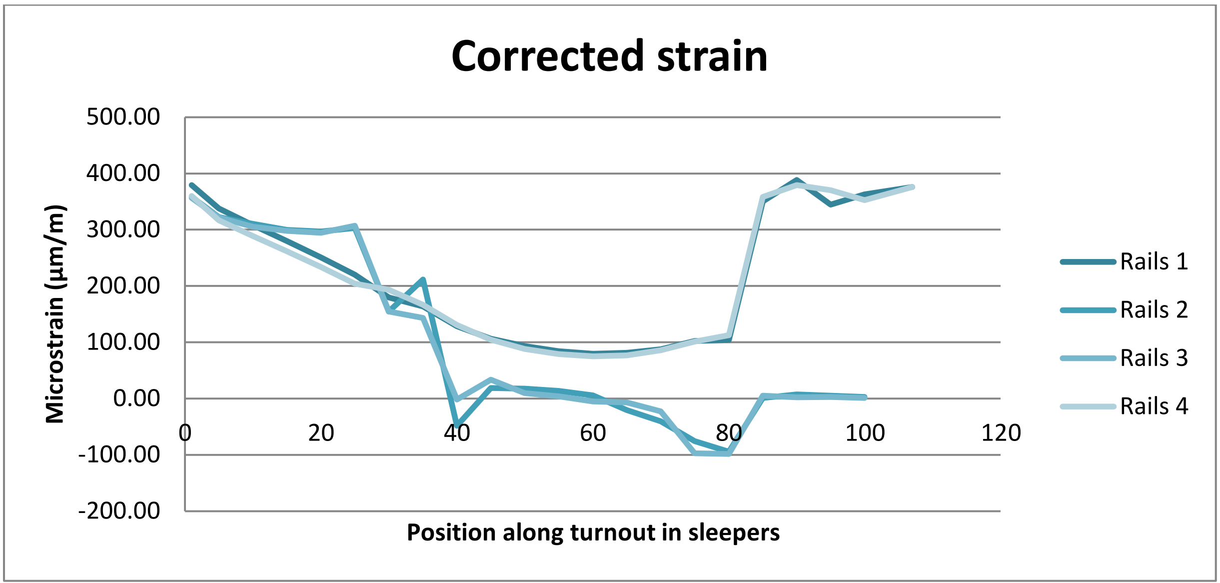

Figure 11.22 Corrected strain output in the turnout model

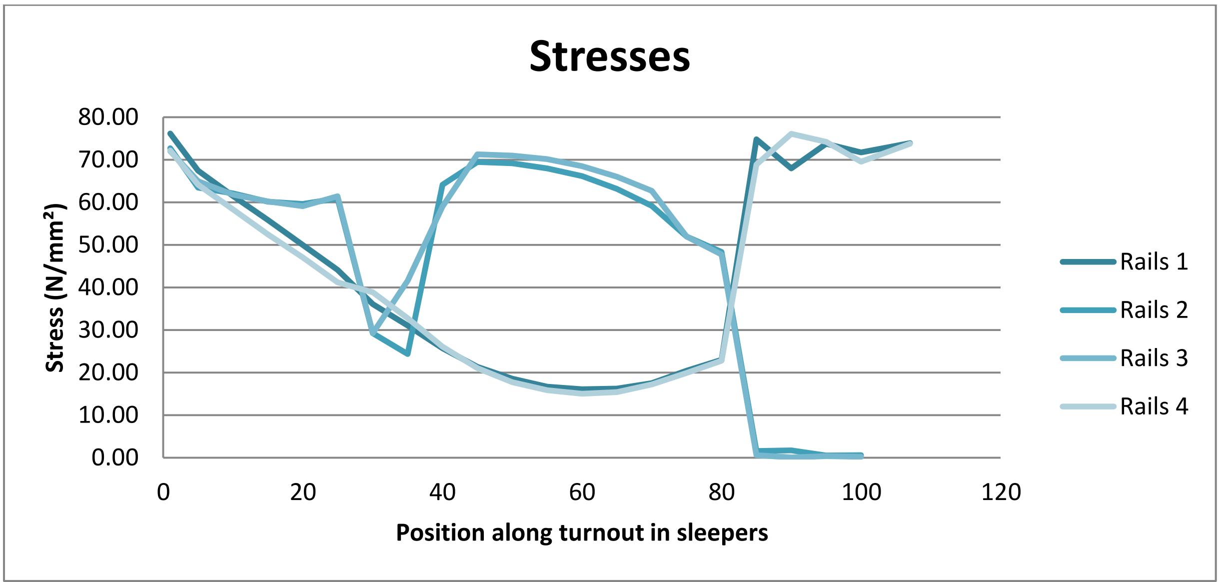

Figure 11.23 Stress distribution in the turnout model

The effect of the guidelines is clear; the entire turnout is being tensioned and lengthened by the tensile forces. This effect is countered in the closure rails by the heating of the closure rails. This causes an increase in stress; the total strain in the closure rail is around zero, while its stresses are equal to the very ends of the turnout where the force from the adjacent track is applied. It is once again noticeable that the stress level drops in the common crossing. The strains and stresses in Rails 1 and 4 are highest at the ends, and decrease gradually towards the middle of the turnout. This is due to the sleepers starting to counteract the applied stresses, resisting their displacement. The turnout is not long enough to reduce this force to zero entirely, and the effect of the tensile force on the other side starts to show past the halfway point. The behaviour at the ball and claw is once again the same.

11.4.1.2 Displacements

Displayed in Figures 11.24 and 11.25 are displacements in length and lateral direction when the turnout has been constructed and heated turnout components have cooled down.

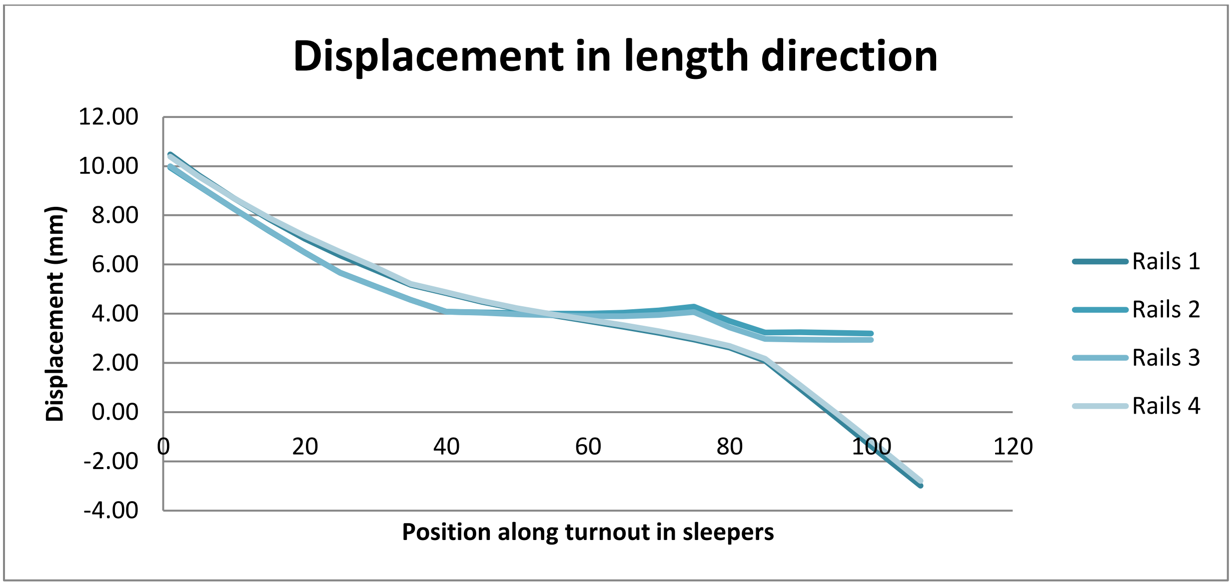

Figure 11.24 Displacement in length direction in the turnout model

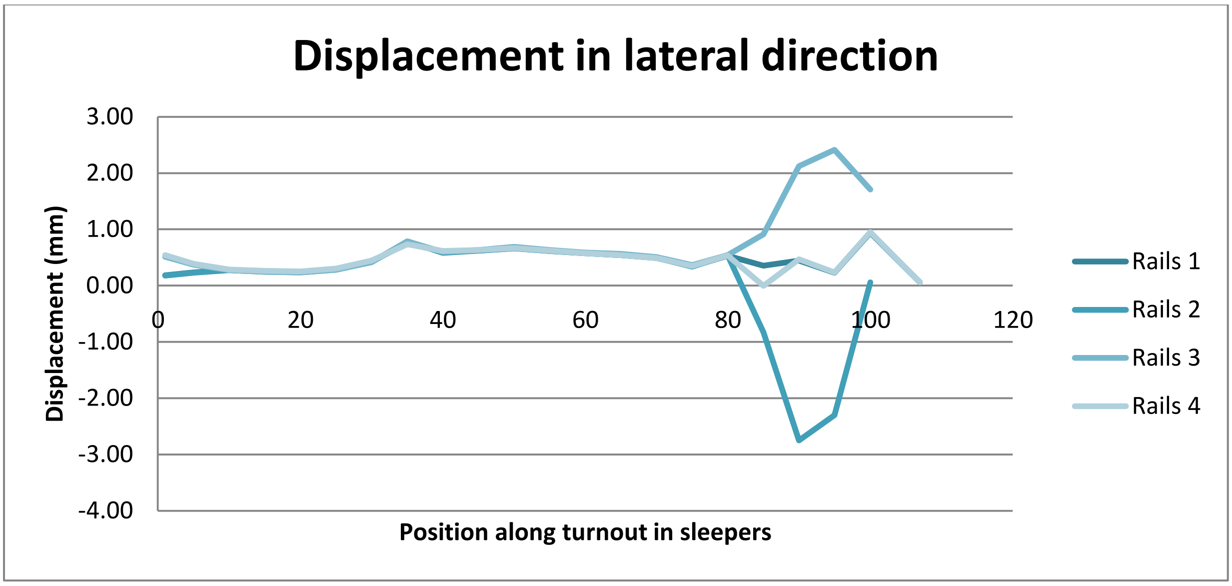

Figure 11.25 Lateral displacement in the turnout model

As can be seen, the lateral behaviour of the switchblade is still erroneous, and should be ignored. The linear model has simplified switchblade behaviour because of the reduced calculation time. Comparison with a more realistic model showed the differences in output to be minimal when applying this simplification. The behaviour of the entire turnout in lateral direction is nothing more than a slight shift towards the turnout branch. The amount of shift is somewhat constant, and no mayor or fast shifts take place (except at the point machine).

The displacement in length direction is somewhat more interesting. The zero displacement point is located far towards the right, which is caused by the closure rail (chapter 4.3) being heated in combination with the majority of the tensile forces being applied on the left. The focus of the tensile forces on the left causes the turnout to shift in this direction. In the area between the common crossing and the ball and claw system the closure rail moves as a single unit by 4 mm. The expansion is cancelled out by the temperature difference, as is visible in the strain graph. This temperature difference also lowers the strain of the stock rails in this section, causing their expansion to decrease and thereby moving the zero displacement point farther to the right of the graph in Figure 10.24.

11.4.2 Situation at 40 degrees turnout temperature

11.4.2.1 Stresses and strains

In Figures 11.26 and 11.27 the strains and stresses are displayed that occur when the previously constructed turnout, with heated components that have cooled down, is fully heated to 40 degrees.

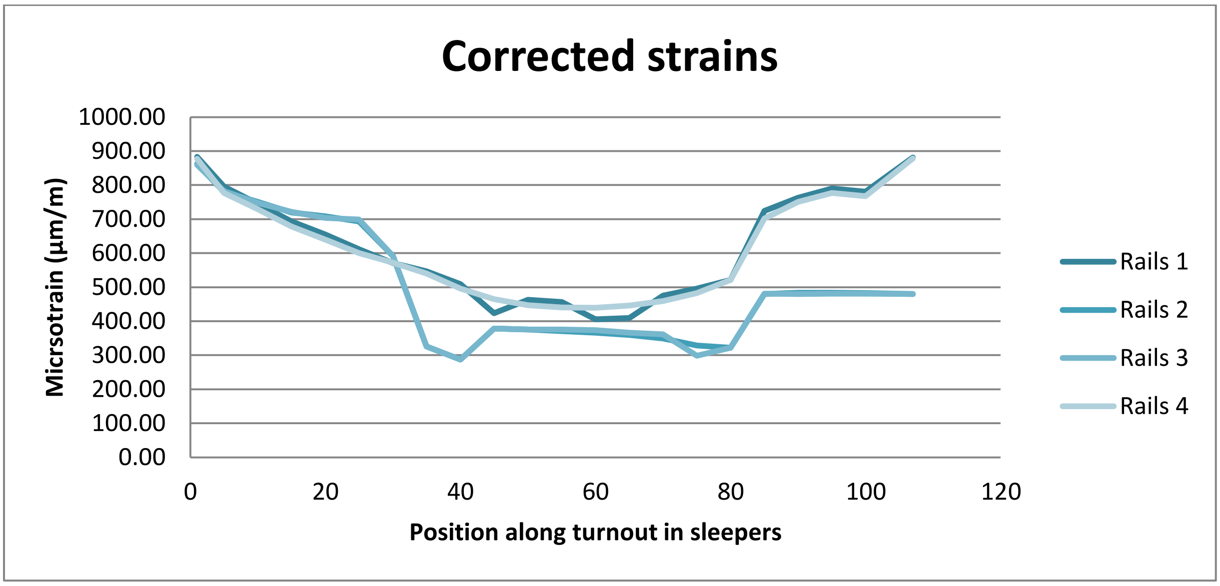

Figure 11.26 Corrected strains in the turnout model

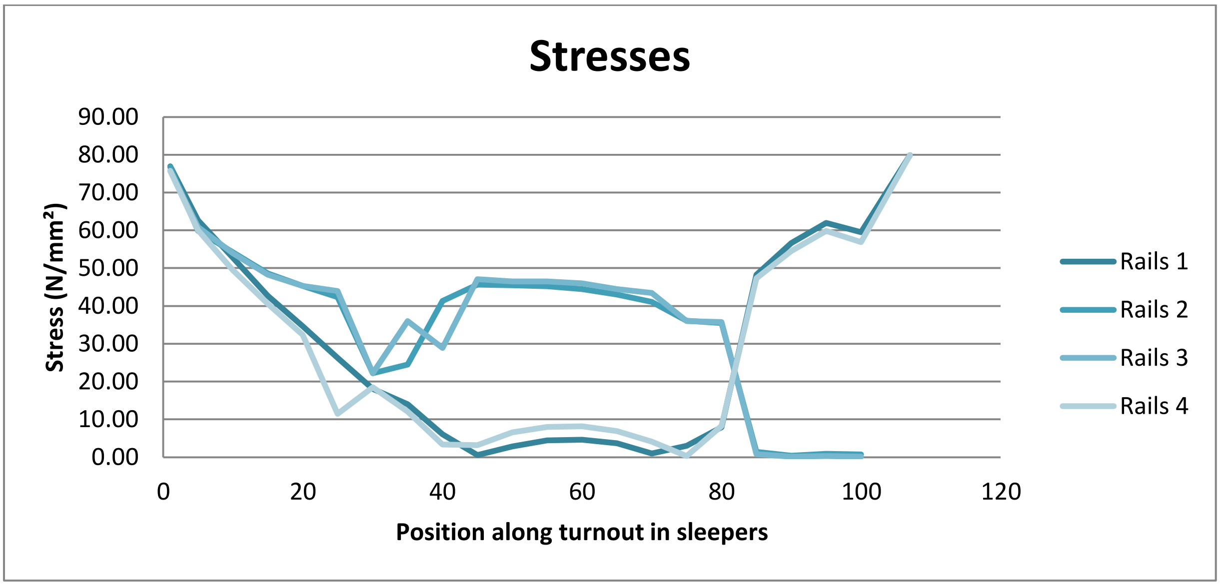

Figure 11.27 Stress distribution in the turnout model

This new situation causes the turnout to expand even further than its original expansion, a strain of 900 microstrains is reached, this is an expansion of 0.09%.The shape of the strain distribution is similar as in the previous case, just with higher values. The highest stress locations are at the ends of the turnout. These locations are therefore most at risk to buckling effects, however the simulation indicates that the stresses in these locations are not increased due to temperature effects in the turnout itself. In case of buckling occurring this would be caused by a stress from the adjacent rail being added to the stress already present in the turnout. It is recommended (see also chapter 15) to investigate this further.

At the stress distribution, some more interesting aspects can be observed, such as the actual decrease of stresses in the stock rail. The temperature increase and corresponding stresses are countered by the already present stresses and strains in the turnout. This is due to the expansion into the adjacent track, caused by the tensile forces. The stress is already present in the turnout because of this, when the turnout itself warms up it starts to move into the adjacent rail, causing relaxation of the stresses.

All the stresses in the turnout at a temperature increase of 40 degrees are much lower than with the basic situation (Figure 11.28), in which no measures were taken. These outcomes validate the ProRail guidelines. A comparison of stresses between these two situations is shown on the next page.

When the temperature change is increased to 60 degrees, it can be observed that the stress curves hardly change, except in the middle of the stock rail. This stress curve increases, but it is “anchored” around the common crossing and ball and claw location. See appendix VI for more information.

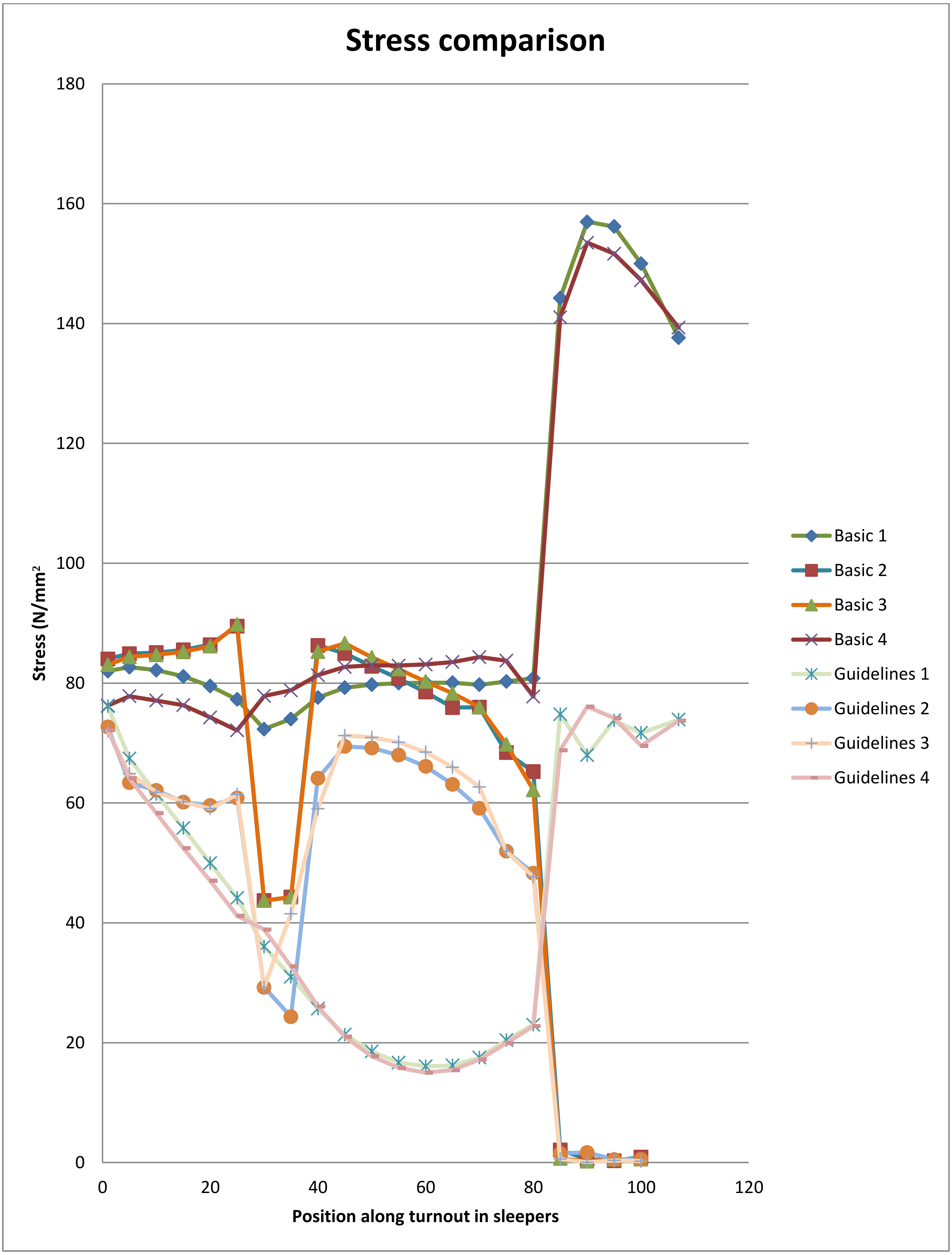

Figure 11.28 Stress distribution comparison between basic construction and following of the guidelines

11.4.2.2 Displacements

Displayed in Figures 11.29 and 11.30 are the displacements that occur when the previously constructed turnout, with heated components that have cooled down, is fully heated to 40 degrees.

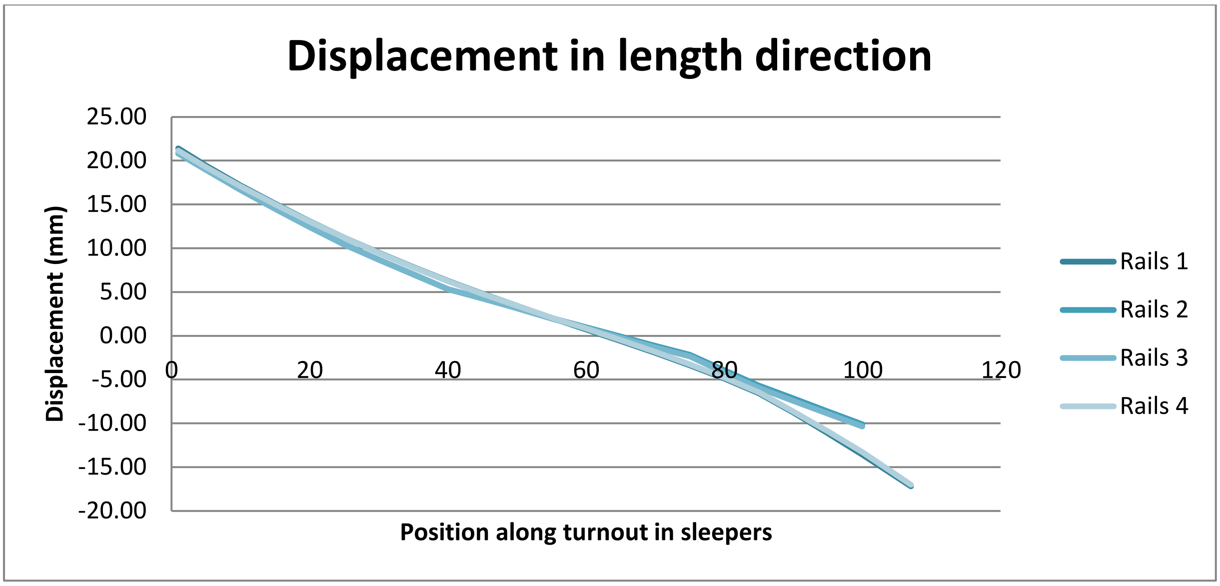

Figure 11.29 Displacement in length direction in the model

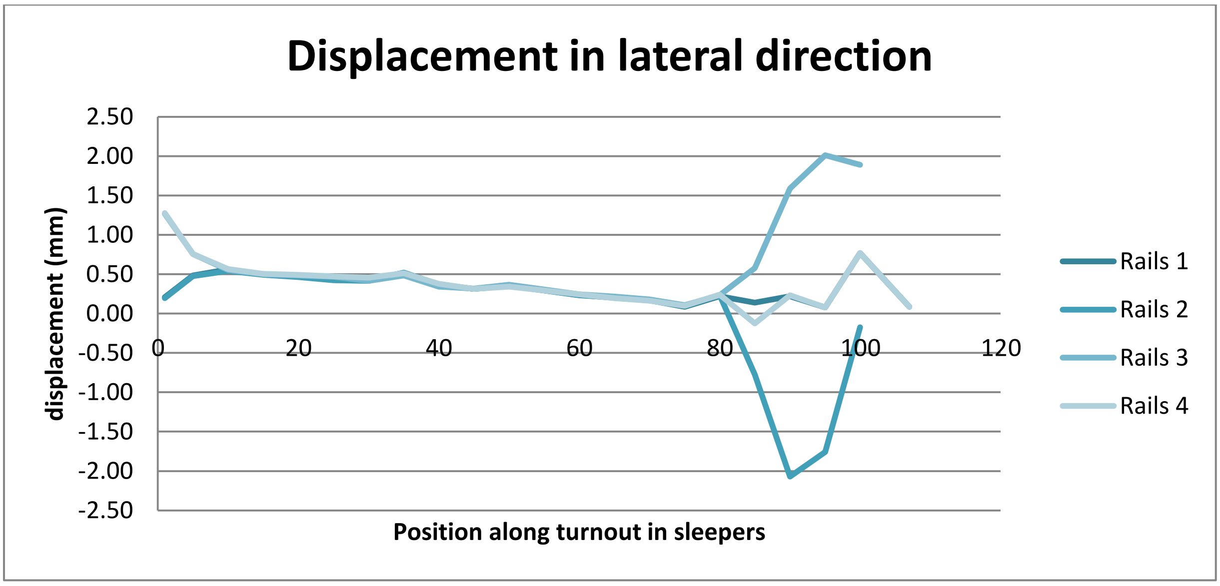

Figure 11.30 Displacement in lateral direction in the model

The displacements in lateral direction are slightly higher as with the basic model, but the deformations are still very small and well within acceptable margins.

Due to the high strains, and all the forces involved wanting to expand the turnout, the displacement in length direction is large, but still within the margins for the linear model. The zero point has shifted somewhat to the left, as the influence of the guideline measures is decreased due to the large influence of the temperature increase.

11.5 Conclusions

A short summary of the most important conclusions from the previous chapters is presented. These are presented per modeled situation. For the detailed situations, please refer to the appropriate subchapter.

Fully fixed situation

1) Strain gauges are perfectly able to measure these strains (assuming they are placed on the stock rail after the ball and claw they would need an accuracy of about 6-7 microstrain per degree)
2) The best locations for strain gauges are on the stock rail, after the ball and claw system, or on rails 1 and 4 (use the corrected graph, but for the switchblade observer that temperature strains are compensated by strain gauges i.e. on the end of the switchblade a strain gauge would output 0, not 480 µm/m.) By best location is meant the locations with the highest measurable strain, and the highest difference in strain with temperature changes, making these locations the more practical spots for accurate measurements.
3) The highest stresses occur where the (measurable) strain is highest as well.

2/3 Fixed situation

1) Turnout behaviour in this situation differs greatly from the fully fixed (reference) situation.
2) Rail 2 becomes one of the most stressed rails, next to rails 1 and 4 at the switchblades.
3) Even though the strain in rails 3 and 4 increases, but they become harder to measure in practice. This is due to the “free” expansion and strain gauge temperature compensation.
4) Rails 1 and 4 in the switchblade are still the best location for strain gauges.
5) Lateral displacement increases greatly.
6) The common crossing behaves like a solid unit, primarily rotating and hardly deforming.
7) The rotational direction of the common crossing is counter intuitive; it rotates away from the unfixed turnout rail. This is due to the longer rail 4 displacing more than rail 3, rotating the entire turnout branch.

2/3 Fixed situation, non-linear support

1) Very similar behaviour as the linear model.
2) Slight deviation in rail 4’s longitudinal displacement when compared to the linear supported model.
3) This model’s results are similar to the linear supported model outcomes.
4) Modelling non-linear situations does not necessarily require a non-linear supported model (errors are within acceptable margins). This error becomes larger when the temperature increase becomes higher.

Practical models

1) Medium strains and medium stresses are present upon completion of the turnout when compared to the other modelled situations and under operational temperatures.
2) Large strains and low stresses are found in the turnout when it is at higher temperatures. The guidelines allow for more movement in the turnout, by prestressing the turnout.
3) The highest stresses can be found in the closure rail (chapter 4.3), while the lowest stresses are present in stock rail.
4) With the prestressing of certain turnout components large displacements occur, but these remain well within linear behaviour.
5) The ProRail guidelines decrease stress values in the overall turnout, and can therefore be concluded to have a positive effect.

Note on turnout behaviour

These models and their outcomes clearly indicate that the behaviour of the track connected to the turnout is of great importance. The results from the 2/3 fixed model indicate that a lack of resistance (or a too high or low neutral temperature) in the adjacent track has great influence on the stress distributions in the rails or the deformation of the entire turnout. This is also confirmed by the practical situation model, in which the effect of stresses in the adjacent rail can be observed.

12 Practical tests

The practical tests, both laboratory and in situ, are discussed in detail in this chapter. The order in which these are discussed is chronologically. For these test the sensors discussed in chapter 9 were used. The results of the in situ test can be found in chapter 13. The laboratory results are discussed in this chapter, as their understanding is important for the choice of sensors to be applied during the in situ test.

12.1 The laboratory tests

The goal of the laboratory tests is to ensure the strain gauges can reach the accuracy desired by ProRail, being 12E-6 [m/m] (chapter 9.2), the equivalent of the free expansion of steel under a temperature increase of 1 degree Celsius. Its setup is reasonably simple; a piece of rail is heated and stressed while the sensor readings are logged. Using external reference sensors the strain in the rail is known to a high degree of accuracy. The strain gauge output is compared to these values. After establishing the accuracy of the strain gauges, conclusions are drawn concerning the usability of these sensors, and how realistic the demands in accuracy from ProRail are.

12.1.1 Description:

To ensure the sensors would yield accurate enough results to be used in practice a first experiment in a controlled environment was performed. In the test a setup was made that would allow ProRail to determine the maximum reachable accuracy of the strain gauge, and to compare different products on the market. Not only "normal" strain gauges were tested but also a ready-made product from the company of Bienfait and its corresponding data logger, as well as some DVRTs from the company of AE-sensors/Microstrain and its wireless data logging system. The DVRT is a linear displacement sensor, which only measures displacement in one direction, and can measure this displacement with a high degree of accuracy. The DVRTs were to be used to measure the displacement of the outermost sleepers and the rail in the practical tests, but as they already were available, it was decided to attach them in a strain measuring set up in the lab test as well.

The goal of this lab test was to allow ProRail to choose the best product to use in the course of these experiments. It would also provide data to be used when finding a permanent product, should ProRail decide to opt for this. Another reason for this test is to be able to provide the contractors, whose work would be checked using these kinds of sensors, with a well-founded study into these sensors. This would prevent discussions with the contractors concerning the reliability and accuracy of these sensors.

A number of different lab-setups were considered. Below is a description of the one that was chosen in consultation with the lab. The laboratory test was run by Stork FDO Inoteq, which was contracted to execute the test.

The goal is to determine the accuracy of the sensors when placed on a piece of rail. To this end, a piece of rail (length about 1.2 meters) was placed in a vertical position. The sensors were installed on the rail, three reference strain gauges in length direction and three reference strain gauges in lateral direction. This is to measure the expansion on both axes, and to be able to measure the expansion in lateral direction due to the Poisson ratio of the steel. The rail was then be heated electrically. The increase of temperature was from room temperature (18 degrees) to 60 degrees. During this heating, the rail was able to expand freely. Measurements from the sensors were taken the entire time. After reaching the 60-degree mark, the rail was stressed using hydraulic rams. The stressing force of these rams was in the order of 700 kN and was monitored. The rail was then compressed back to its original length. While keeping this force on the rail the rail was then allowed to cool down. This cycle is depicted in Figure 12.1.

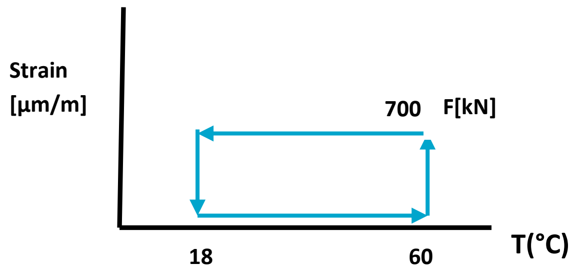

Figure 12.1 Loading and temperature cycle

The reason for compressing the rail was the sub goal of finding out whether it is possible to measure the strain in the rail (and thereby the stress) by measuring the expansion orthogonal to the rail direction. If the strain gauges were accurate enough to measure the strain due to the Poisson ratio that would open up further possibilities for determining the stress in the rail. These measurements could be used when the rail is not able to expand in its length direction. Ideally one would like to test this in the realistic setting in which the rail is clamped on both sides by fixed supports. Unfortunately, it is incredibly difficult to build a fixed support that is stiff enough not to deform while under these amount of stresses. By hydraulically compressing the rail back to its original length, the same results could be achieved. This way it could be explored whether or not measuring the expansion of the rail body in the vertical and lateral direction is a valid option to monitor rail stress. This would be useful for long term monitoring; it is not required for monitoring during the installation of replacement rail. Another benefit was the increase of the strain "path" of the test, and made it possible to test the accuracy of the strain gauges in compression as well as in extension. See also the strain distribution in chapter 12.1.2.1

After putting the rail through this cycle, the output of the sensors was compared. The reference sensors would provide a baseline, together with the tested LVDT sensor to measure the axial displacement of the rail. This would provide an accurate reference, which can be used to compare the new and untrested sensors.

The loading and heating part of the test were performed separately as well, to provide insight in both behaviours separately, without them influencing each other.

On the rail, there were three Bienfait sensors, three DVRTs from AE Sensors, and three LVDTs from Stork, three MM strain gauges in length-, and three in lateral direction. The choice for using multiple sensors of the same type was to be able to establish the variance between different sensor units. Three sensors will not be able to give a statistically sound overview of the sensor behaviour, but it is better than one sensor, while still being feasible.

12.1.2 Preparation

12.1.2.1 Theoretical output

The laboratory test was modelled in Ansys® prior to the execution of the test. This yielded an expected strain values pattern, data on the distribution between mechanical strain and thermal strain, and the general principles could be checked. After execution of the laboratory test the coefficient of thermal expansion and the Poisson ratio parameters in Ansys® can be updated to correspond to the values of the actual rails. The theoretical distribution is shown below in Figure 12.2, using the following load steps:

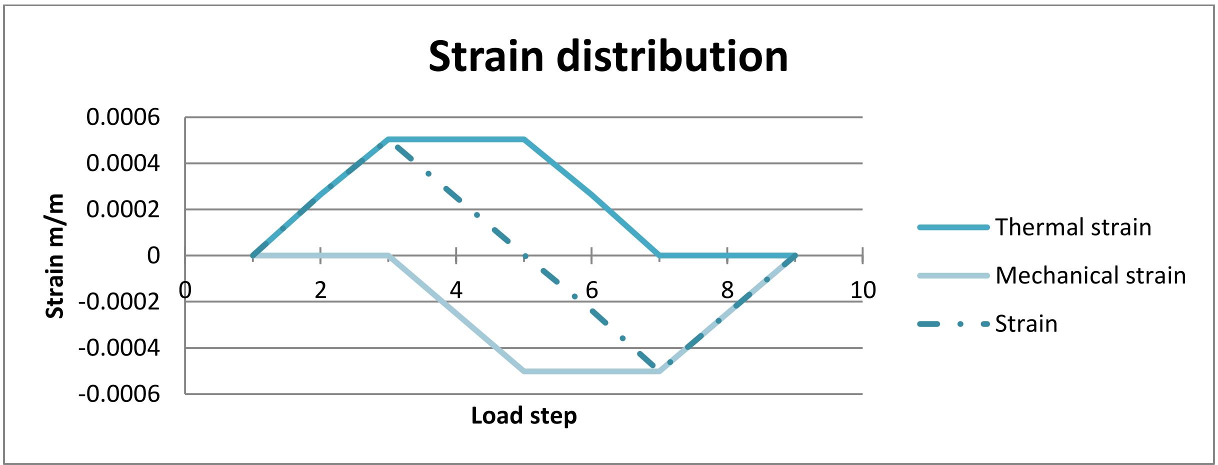

Figure 12.2 Strain distribution during laboratory test

Step [-]	1	2	3	4	5	6	7	8	9
Force [kN]	0	0	0	350	700	700	700	350	0
Temperature [°C]	18	40	60	60	60	40	18	18	18

12.1.2.2 Sensor placement

The sensors were placed in the centre of the rail specimen. On one side, combinations of two of each sensor type were placed, on the other side only one of each sensor (Figure 12.3). The Bienfait sensors were applied according to their application manual, while the normal strain gauges were fixed using the conventional method. This consists of grinding the rail, cleaning it, applying a glue accelerator, and finally gluing the strain gauge to the rail using the bonding agent. After setting the glue, the wires are soldered onto the sensors and connected to the data loggers. The application of the strain gauges was performed by Stork. A more detailed description of the sensor placement can be found in Appendix IIX and X.

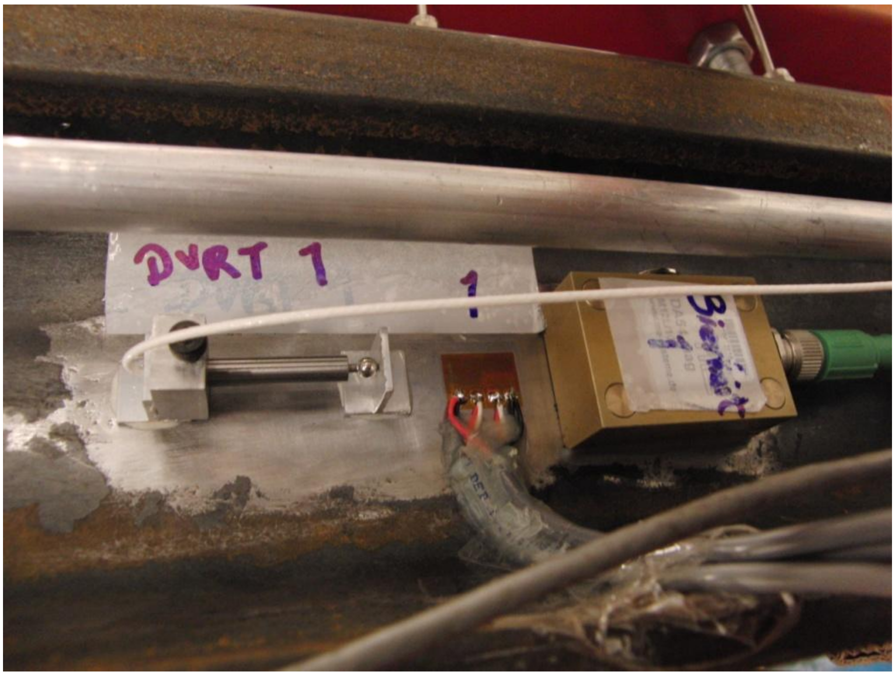

Figure 12.3 Sensor placement

12.1.2.3 DVRT solution

Even though the DVRTS were not going to be used for strain measurements, they were employed in this laboratory test in a special setup. This would provide information on how to use them and would give an indication of their accuracy. A special setup was constructed for them to be used.

DVRTs are displacement sensors; they measure displacement instead of strain. As such they are not usable for strain measurements “off the shelve”. To solve this issue, a special DVRT housing was constructed; it consists of two T shaped aluminium profiles. One of which has a small aluminium block attached to it, with a hole drilled through it. The DVRT is placed inside the hole and secured there by means of a screw-in clamp through another hole perpendicular to the DVRT. This device is shown in Figure 12.4.

By positioning these two pieces of T shaped profile at a set distance from each other, the difference in displacement can be measured over this distance. Hereby it is assumed that the centre line of the T profiles is the average movement of the flanges.

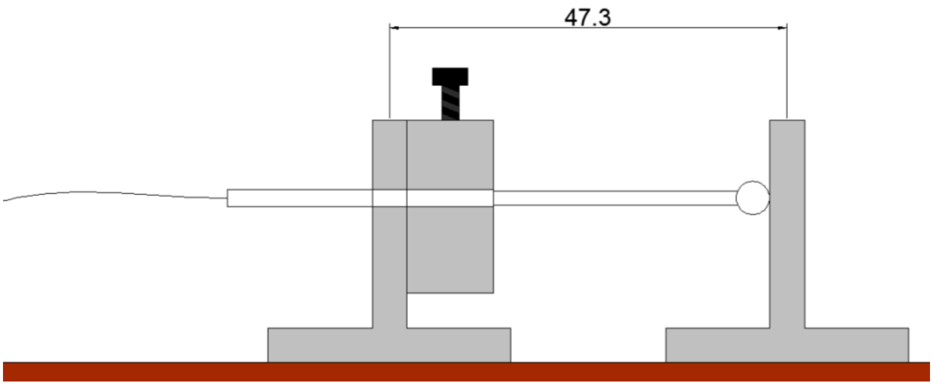

Figure 12.4 DVRT "strain" set up

Using the (known) distance between the two centre lines, the displacement measured by the DVRT can be translated to a strain measured. This would not work well with bending of the rail, but as only the longitudinal strain is of importance that is not an issue. It was found that even though the DVRT accuracy is very high, it was far from what was needed to function in this setup as a strain gauge. This setup did however provide experience with the operating of the DVRT and their accuracy.

12.1.3 First laboratory test execution:

The first laboratory test was executed on December 22nd 2010. This laboratory test concerned the loading cycle with the increase of temperature and cool down period. The average temperature cycle (of six temperature sensors) is depicted in Figure 12.5.

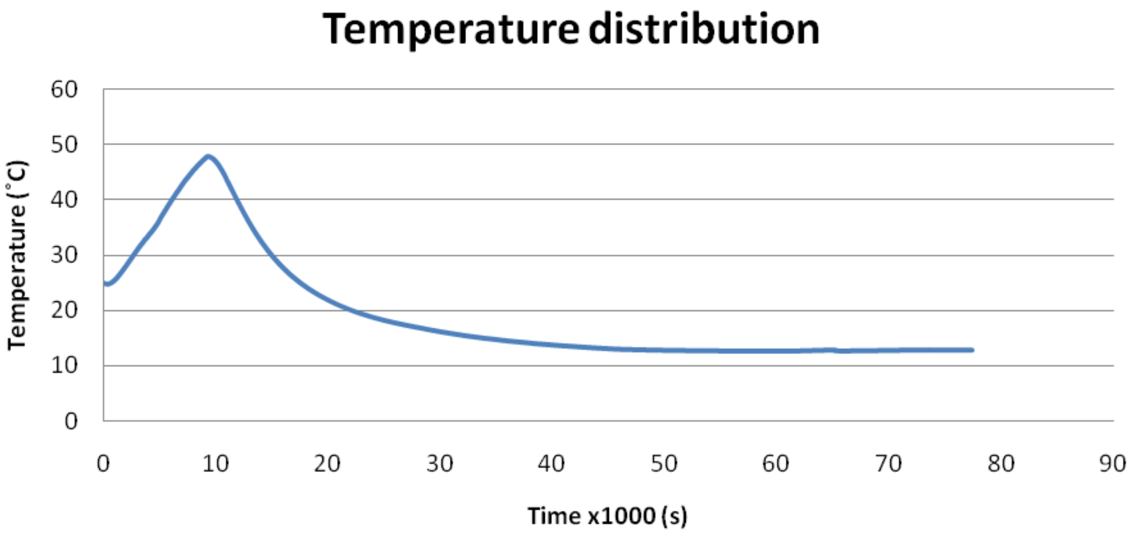

Figure 12.5 The temperature distribution during the first lab test (combined temperature and mechanical load)

This temperature loading was combined with a loading cycle of pure compressive force, see Figure 12.6.

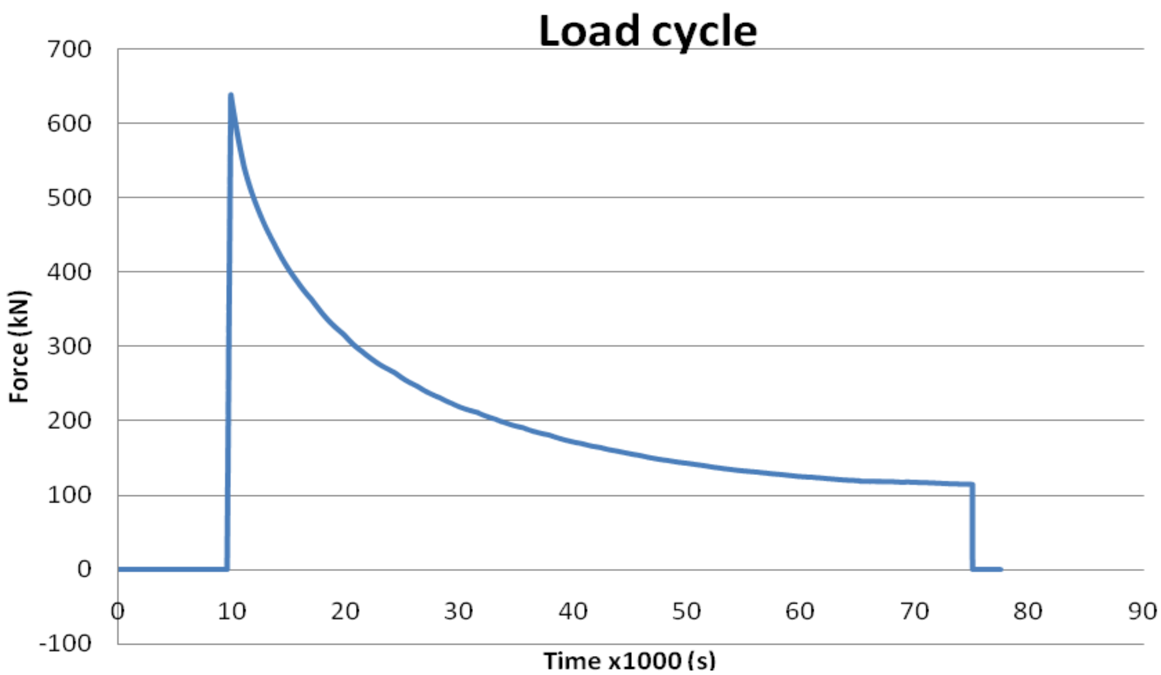

Figure 12.6 The load over time during the first lab test (combined temperature and mechanical load)

As one can see in Figure 12.6, the force is not held at a constant value after application, as was the original idea. This is because the pressure cylinder used by Stork had a pressure leak. This unfortunate circumstance makes the latter part of the load cycle very difficult to process. The goal was to identify the behaviour under temperature increase, then under a load increase, and then during cool down.
To study the temperature effects during cool down there are two options, to have no load, or to have a constant load. It was chosen to have the constant load, because this is more like the practical situation in the rail. Unfortunately, due to the pressure leak this was not possible. This means that in the latter part of the loading cycle both temperature effects and loading effects are present and cannot really be distinguished from each other. This prompted a new set up for the test, to have a pressure and a temperature cycle independent from each other; these cycles were applied during the second and third laboratory test.

It was assumed that the rail steel would be a good conductor of temperature, and that therefore the temperature distribution over the height of the rail would not differ much. Measurements did however establish that the heat conducting properties of the material were greatly overestimated. A temperature difference of almost 14 degrees over less than 40 cm was observed. In Figure 12.8, the heating area is illustrated. The heating wires are covered by brown paint, which is covered by white paper. These locations are heated, after which the head is transferred through the metal. In Figure 12.7, the resulting heating curve is shown. This was expected to have been distributed more equally. The real temperature distribution is important to know when calculating the theoretical expansion of steel, and when establishing the temperature coefficient of this steel. The found temperature distribution was used in all calculations.

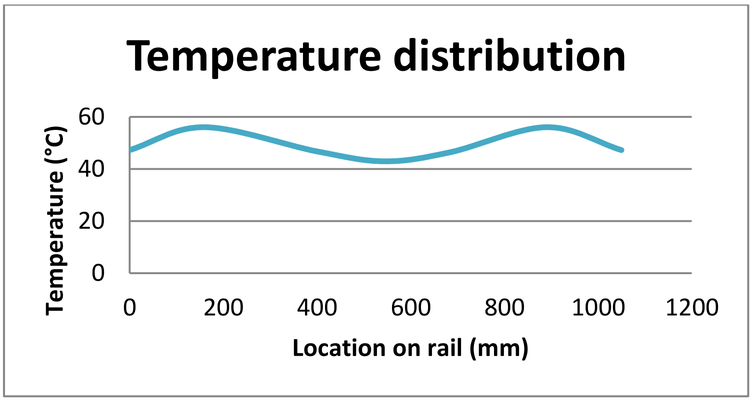

Figure 12.7 Temperature distribution

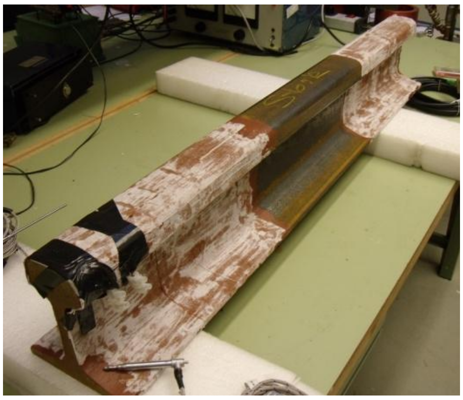

Figure 12.8 Test rail

12.1.4 Second laboratory test execution

A second test day was held on January 14th. During this day three tests were performed, the first and second consisting of three load cycles with loads of 600 kN. The last cycle was kept at load for a longer period to evaluate some sensor data as it was collected (Figure 12.9). The third test comprised only a single loading cycle.

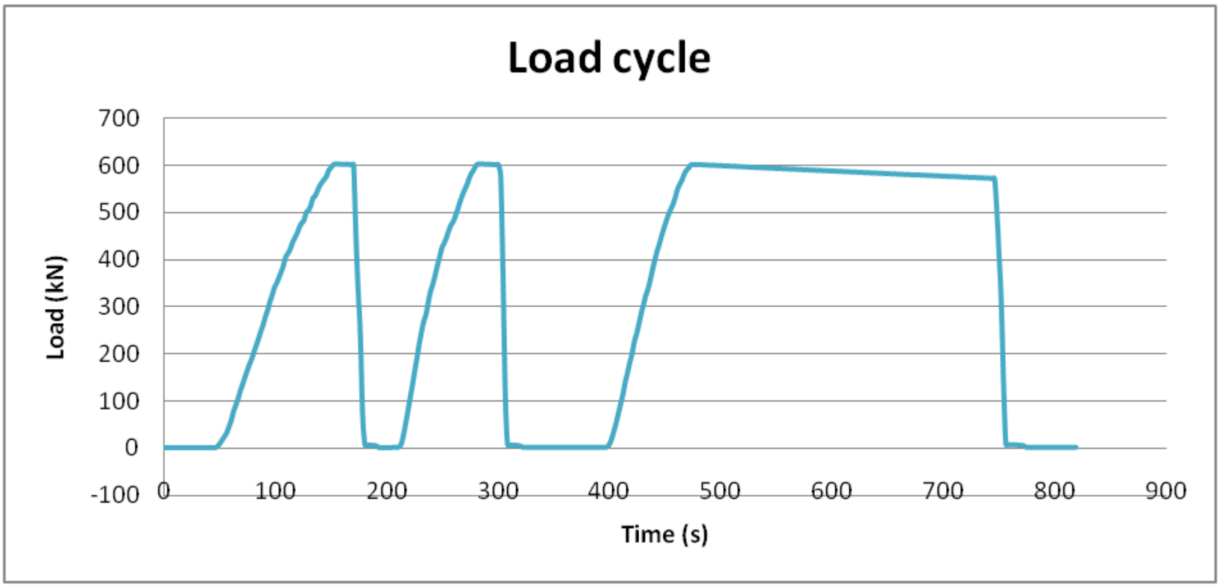

Figure 12.9 The load cycles during the second compression only test

Only one test was planned, but due to erroneous data-output during the first test, the test had to be repeated. As can be seen in Figure 12.10, LVDT1 shifted, probably during the first loading cycle, as the line remains horizontal for a period where it should not have been. This error rendered the LVDT values unusable, and prompted a rerun of this test.

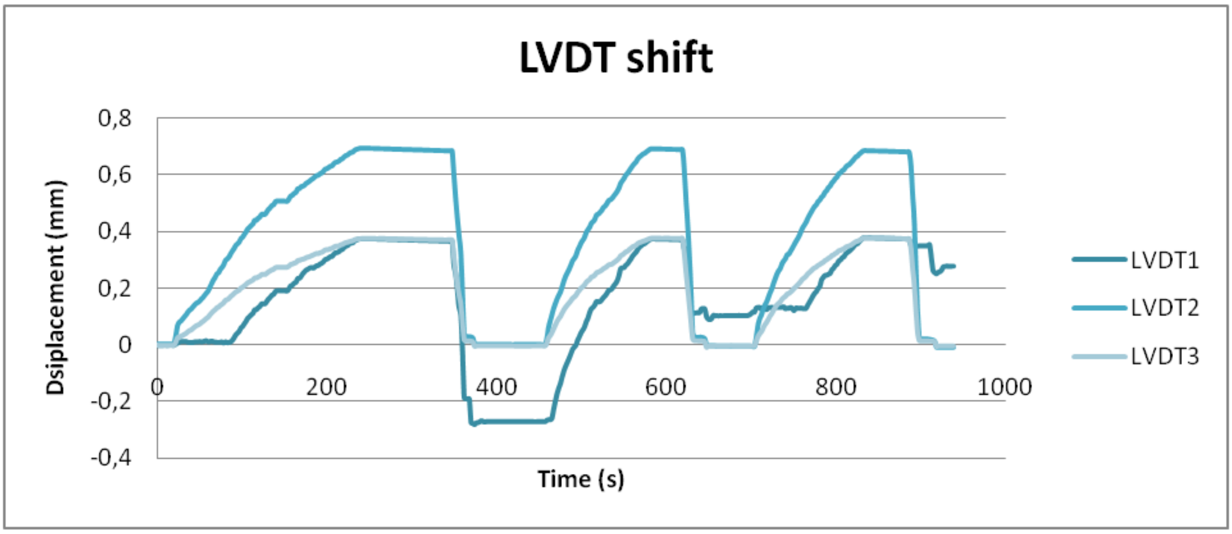

Figure 12.10 The LVDT readings during the first compression only test

At the end of the rerun, it was discovered that a setting in the data logger was not entered correctly. Even though this should, in theory, not have any influence on the outcome (except for scaling it with a factor 20) another loading test was executed to confirm this fact. This test did indeed confirm the setting did not have any influence on the output.

During this day some extra sensor calibrations took place as well, these calibration were prompted by unclear measurements that did not correspond to the output the theory predicted. All three LVDTs were tested using a micrometre. During this calibration, it was concluded that all LVDTs were working correctly.

A second calibration took place on the loading cell. During this calibration, it was found the loading cell had a deviation of 10kN over a 200kN range. This deviation was deemed too large. Stork however did not have the equipment to calibrate this loading cell, its calibration data has been send later and was used to correct the measurements.

12.1.5 Final test execution

The final temperature test, consisting of an increase of the rail temperature and a cool down period was performed on 17th of January. The goal was to establish the behaviour of the LVDTs and strain gauges under a change of temperature, as in practice temperature changes occur as well, especially during long term monitoring. The measurements were stopped before the cooling trajectory, due to the long time it takes the rail to cool down. The temperature is plotted against time in Figure 12.11.

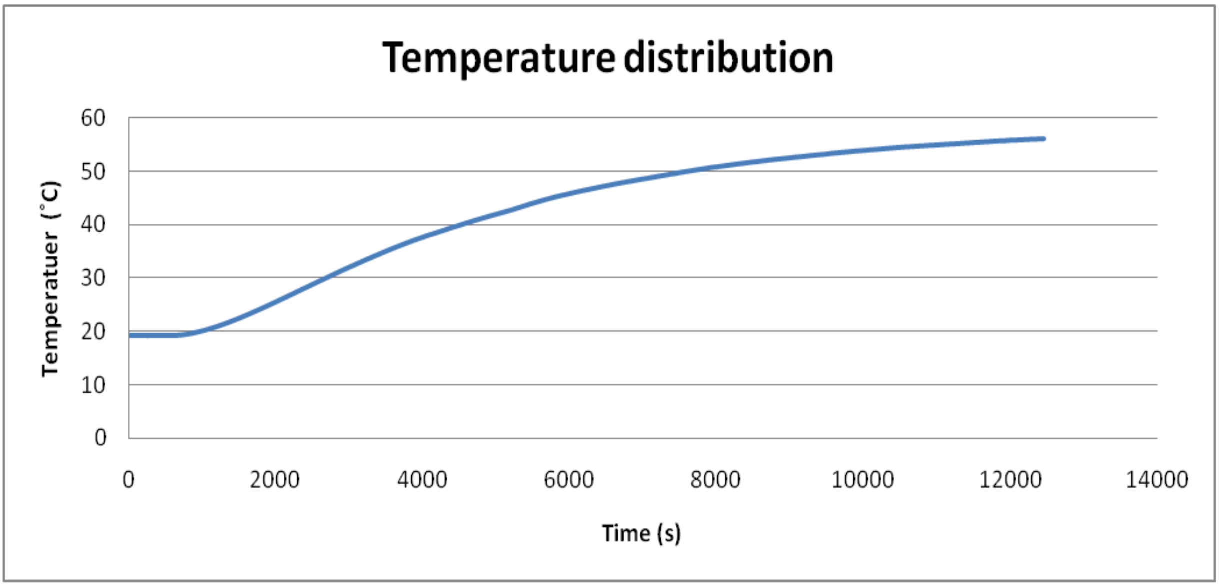

Figure 12.11 Temperature distribution during the third laboratory test (temperature load only)

12.1.6 Evaluation of all laboratory tests

12.1.6.1 Correction factors

Before any of the measured data could be analysed several factors would have to be taken in account. The first was the temperature compensation for the strain gauges. When a strain gauge is heated or cooled, it measures an apparent strain, which is caused by a change in electrical resistance of the gauge due to the changing temperature. The compensation curve is provided by the manufacturer of the strain gauge. The compensation curve for the MM strain gauges is shown in Figure 12.12.

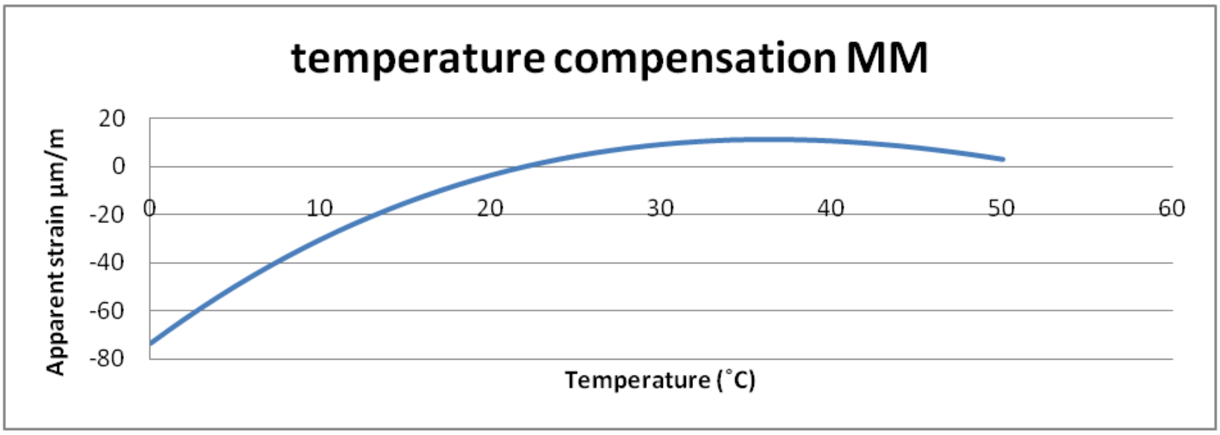

Figure 12.12 Temperature compensation curve prescribed by the manufacturer

The second factor that is important to take into account concerns the LVDTs, the displacement sensors that measure the extension and compression of the rail. These are mounted on aluminium bars that are positioned vertically, parallel to the rail. The choice for aluminium was based on its excellent heat conducting properties. By measuring the temperature of the aluminium bars in the middle it was assumed the aluminium bar has that temperature over its entire length (when the isolation is applied around the entire test set up). Every aluminium bar has its own temperature sensor. Using this temperature and the coefficient of thermal expansion of aluminium (23E-6 m/m/˚), the elongation or compression of the aluminium bar can be calculated. This was then added to the measurements conducted by the LVDT to get the absolute elongation or compression of the rail.

12.1.6.2 LVDT displacement

During the evaluation of the results, an irregularity was discovered. The average displacement measured by the three LVDTs was around 400, 750 and 700 micrometres. This did not correspond to the theoretical results that were predicted. Using the following relation and the measured forces a strain value could be calculated for the rail.

$$N = E * A * \varepsilon$$

With N measured by the load cell (630 kN), E = 210,000 N/mm² and A = 6977 mm²

This relation yields a theoretical strain of 430 µm/m. Using the rail length of 1050mm this would result in a theoretical shortening of the rail of 452 µm. Deviations in the stiffness of the metal (E) and the surface (A) cannot account for such a large difference. This posed quite a problem, and prompted us to calibrate the LVDTs to make sure their output was correct. The outcome of the calibration was that all the LVDTs were functioning normally and their readings were correct.

A closer study of the measurements of the LVDTs in the experiments performed, finally yielded a clue to what was happening. The three LVDTs were numbered and positioned as shown in Figure 12.13. Next to it is a graph showing the displacement (shortening) measured by the LVDTs during a single load cycle of one of the pressure tests on the second laboratory test day.

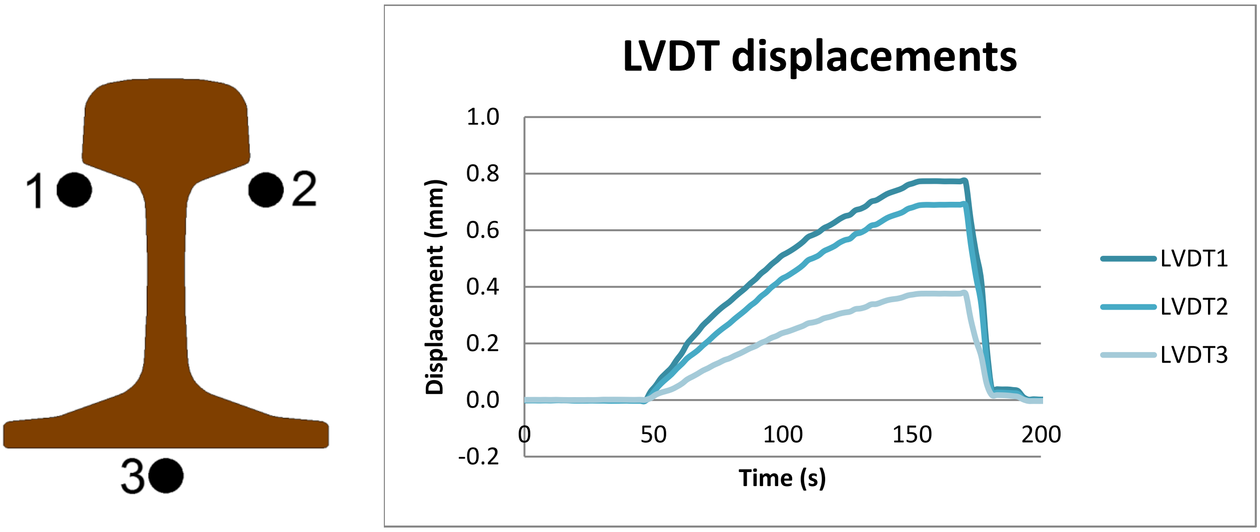

Figure 12.13 LVDT placement and displacements

When paring this graph to the location of the LVDTs it becomes clear that the rail is not only compressing. There is also a bending factor involved, more specifically in the direction of LVDT1 and 2, their larger values indicate a larger shortening of the rail in that position. Because this behaviour is constant during all the test performed, and even occurs (albeit very reduced) in reverse during the heating (and expansion) of the rail it is clear that bending is going to have to be considered. The reasons for this behaviour can be manifold. A deformation could have been formed during production. This was checked by comparing the straightness of the rail to a straight bar.
However, it is considered most likely that the cutting surfaces are not parallel to each other, which combined with an eccentric application of the force causes a deformation of the rail (Figure 12.14).

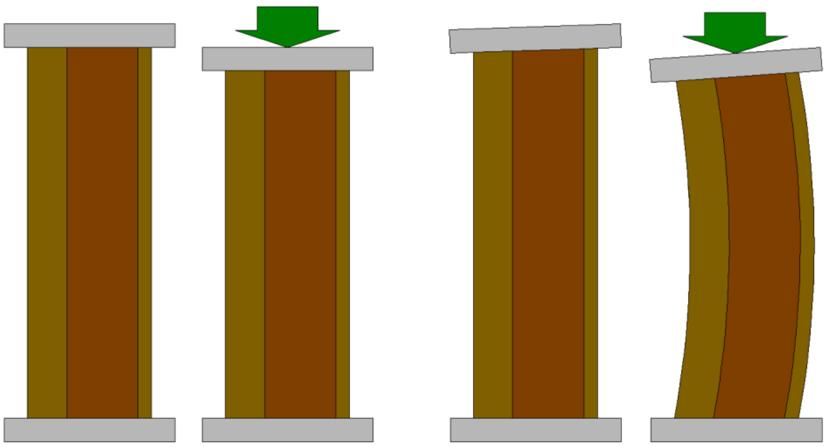

Figure 12.14 Deformation

Unfortunately this deformation is in a direction where bending was not expected. This means that no strain gauges are positioned correctly to measure this bending (bending on any of the other axes could be measured). To avoid such bending special supporting structures were used, which can be described as a bowl inside a bowl. This structure (Figure 12.15) would ensure that the rail could only be loaded by compression and not by a bending moment. It does not however safeguard against non-parallel cutting edges.

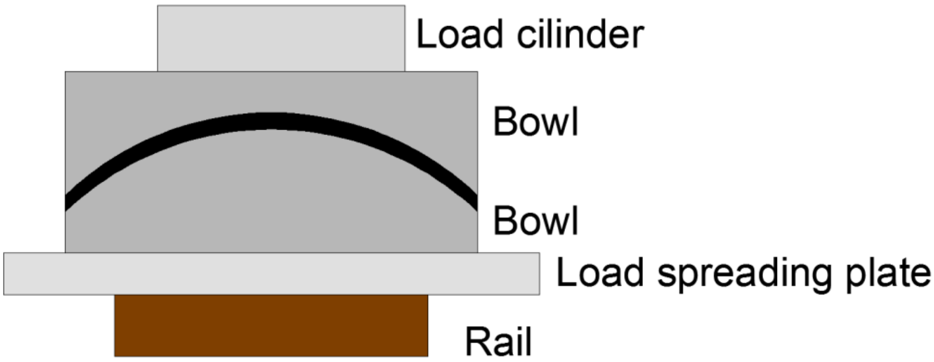

Figure 12.15 Double bowl structure

Attentive readers might wonder about bending in the other plane, as there is a difference between LVDT1 and LVDT2 as well. A closer examination of this difference reveals that it is constant for most of the loading period. Any bending in this direction would also be measured by our strain gauges; these however do not register any difference. This would suggest a slight displacement of the covering plate upon application of the load. This is another indication that both edges of the rail are not parallel to each other. Because there is no more difference in displacement after the initial change, it is considered very unlikely that there is bending in this direction as well.

Consequences

The consequences of the bending of the rail were quite severe. Instead of being able to simply average the displacement readings by the LVDT the bending deformation would have to be taken into account. This means that using the exact location of the LVDT measurements the strain variation over the height of the rail would have to be calculated, and using this variation and the position of the strain gauges, the actual strain would have to be calculated. This can then be used as the reference strain to which to compare the strain gauge output, finally yielding an indication of their accuracy.

When using this correction, based on the position of the measuring locations, the average LVDT reading was around 620 microstrains. This is still a far call from the theoretical measurements; the difference is still too large to be explained by a deviation of the area and stiffness values of the steel. When the Stork employees removed the rail from its load spreading plates they observed an imprint of the contact surface of the rail. This is very unfortunate, as it indicates that about 5% of the plate has been deformed plastically, which could lead to an unbalanced load distribution on the rail. This, coupled with a suspected deformation of the load spreading plates as illustrated in Figure 12.16, leads to the very unfortunate conclusion that the displacement measurements of the LVDTs cannot be used. The deformation of the loading plate is exactly on the locations of the displacement measurements.

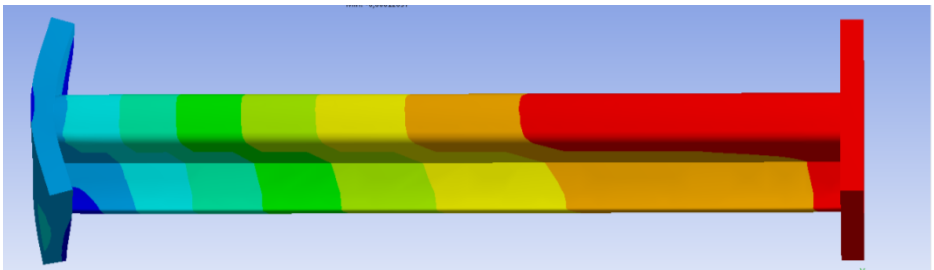

Figure 12.16 Loading plate deformation

It is impossible to correct for all these factors and thereby it is no longer possible to determine the exact elongation and compression of the rail. This is very unfortunate as this means that there is no longer an exact reference measurement for the strain gauges. In practice, this means that we cannot establish the exact accuracy of the strain gauges. We can only reference them to the theoretical values, and how much they deviate from them. This is unfortunate because in the theoretical calculations the stiffness E, the area A and the coefficient of expansion α are all taken from material tables. Would the LVDT readings be useful, these would have been known to a very high degree of certainty. Any statements about the performance of the sensors would have been well founded and well argued. As it is now the sensors have to be referenced using uncertain variables.

12.1.6.3 Strain gauge output - temperature

One of the surprising conclusions of the tests was the fact that the strain gauges measure almost no strain under a temperature change. We were expecting them to measure the strain caused by elongation of the rail, which would have to be corrected with the compensation curve. However, the strain gauges apparently were already compensated for the temperature expansion of the steel. It was known that these gauges existed, and that full bridges are always compensated, but not that the quarter bridge ones supplied by Stork had this built into them. The Stork employees were also unaware that this was the case, as they usually go to great lengths to exclude temperature effects and are rarely contracted to measure them, as this test is designed to do. It took a phone call to the supplier of the strain gauges to establish this fact. The strain gauge output during heating is shown in Figure 12.17.

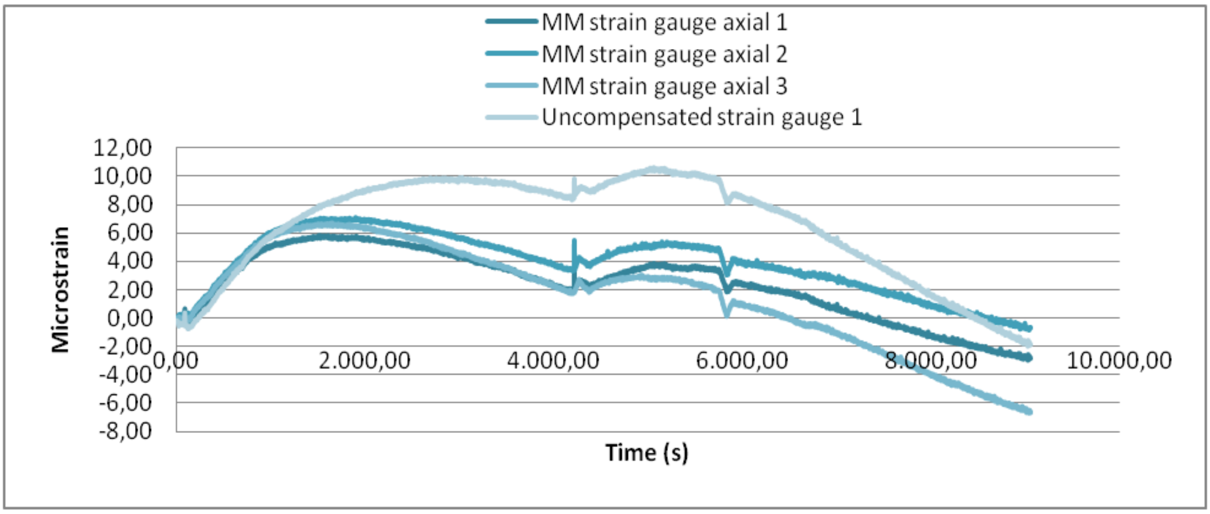

Figure 12.17 Strain gauges output during temperature changes[1]

As can be seen, the signal does vary from zero, even with the temperature compensation curve subtracted from it. Interestingly, when placing the power graph of the heating unit next to the strain measurements without temperature compensation a correlation can be found (Figure 12.18). Because this heating output is not directly correlated to a temperature increase or decrease (which takes a little longer to manifest) it is safe to say the heating device does have an impact on the readings provided by the strain gauge.

[1] Some graphs are lacking a title, this is done on purpose, and it is to optimise the area available for visual representation of the data.

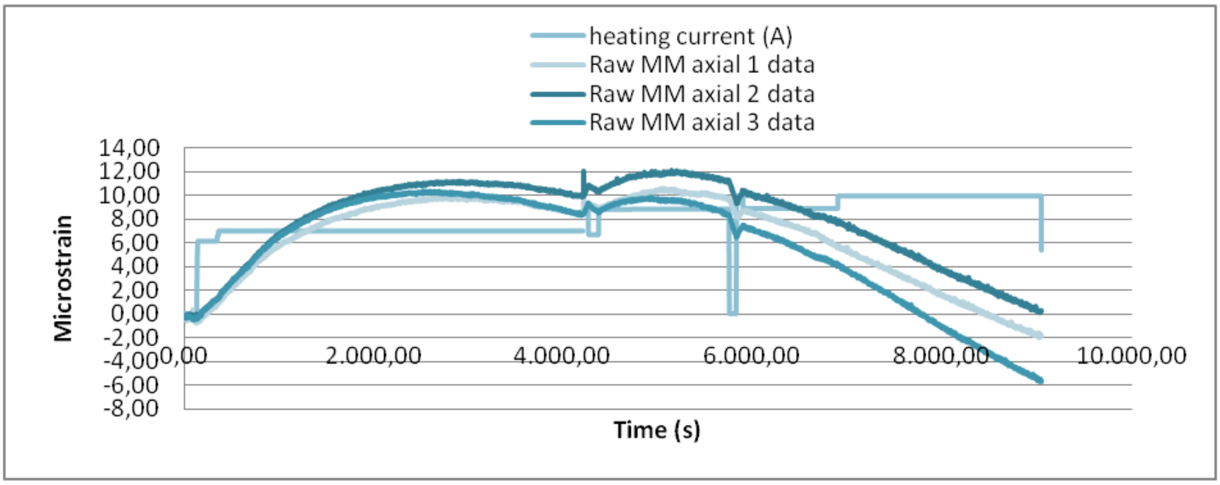

Figure 12.18 Strain gauge output with heating current influence

Comparing the MM strain gauges to the Bienfait strain gauges shows a large difference. The maximum deviations are much larger, and much greater negative values are reached. The irregularities caused by sudden changes in heating power output can also be seen here. Because the Bienfait strain gauges are positioned in a full bridge, they should be insensitive to temperature changes, and should register a zero strain output. The reason for this output to manifest itself is unknown. It could be due to wires heating up, or an increased influence of the heating power output as a full bridge is more sensitive. These measured values are still within the margins used for normal measurements, but because of the high accuracy of this test, these effects can be seen clearly (Figure 12.19).

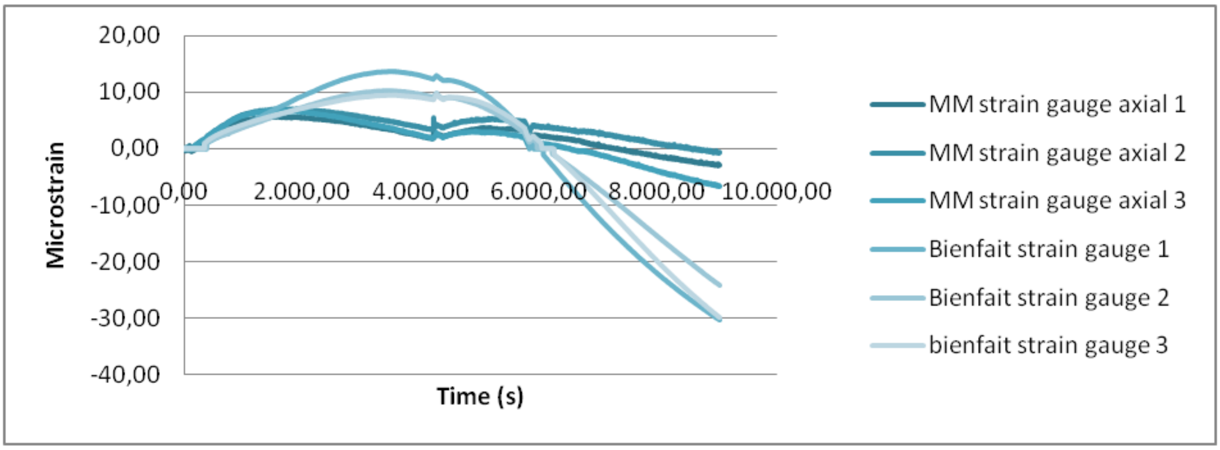

Figure 12.19 Difference between Bienfait and MM strain gauges under temperature changes

12.1.6.4 Strain gauge output - force

The strain gauge output due to force (Figure 12.20) is more straightforward, as the temperature during this test does not vary as much. Temperature differences still occur, and are still taken into account for the strain gauges and LVDT measurements, but these changes are much smaller and easily compensated. The overview of axial strain gauges is displayed below.

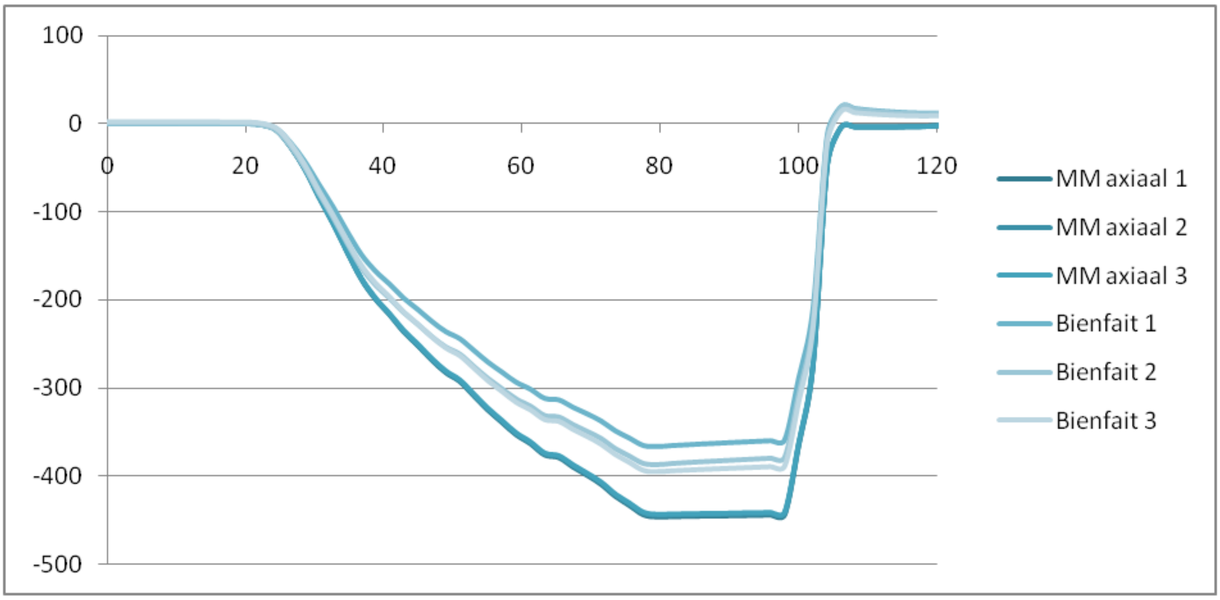

Figure 12.20 Strain gauge outputs under loading

A number of things can be noticed right away, the first is the very consist output of the three MM strain gauges; they all give the same read out. The second is the fact that the Bienfait strain gauges do not have this consistency, and that their values deviate from those of the MM strain gauges. A more detailed examination of the starting values is illustrated in the following graphs. During this time there is no load on the rail, and the strain output should be zero. This is an excellent opportunity to examine the natural "static" in the output of the strain gauges.

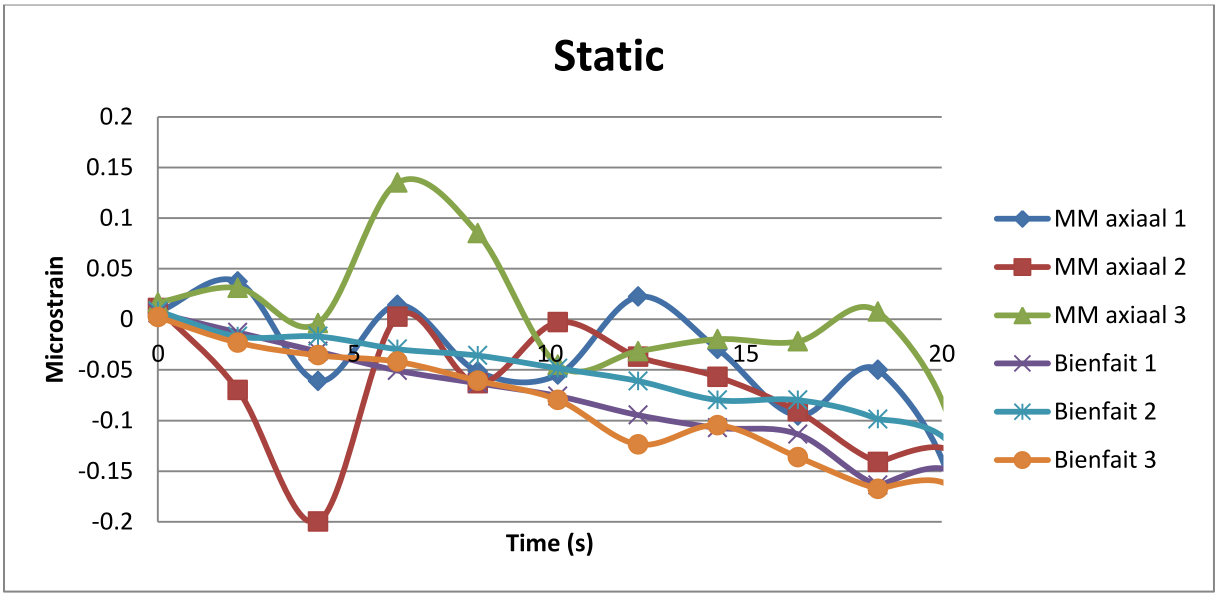

Figure 12.21 Strain gauge output variation under zero load[1]

The tangle of lines in Figure 12.21 is a bit confusing at first, but close examination reveals that the MM strain gauges have a greater variation than the Bienfait ones, who seem to have somewhat straighter lines. The scale of this graph is however negligible, influence of the static on the results of

[1] Some graphs have line colours that differ from the usual style of the report. This is done on purpose and is applied to those graphs where it is hard to identify the separate data sets otherwise.

the tests are therefore not to be expected. This graph provides evidence that the static is not an influencing factor on the readings.
A further analysis of the behaviour under maximum load is also prudent, as the differences between the Bienfait en MM type strain gauges is most profound in this zone, see Figure 12.22.

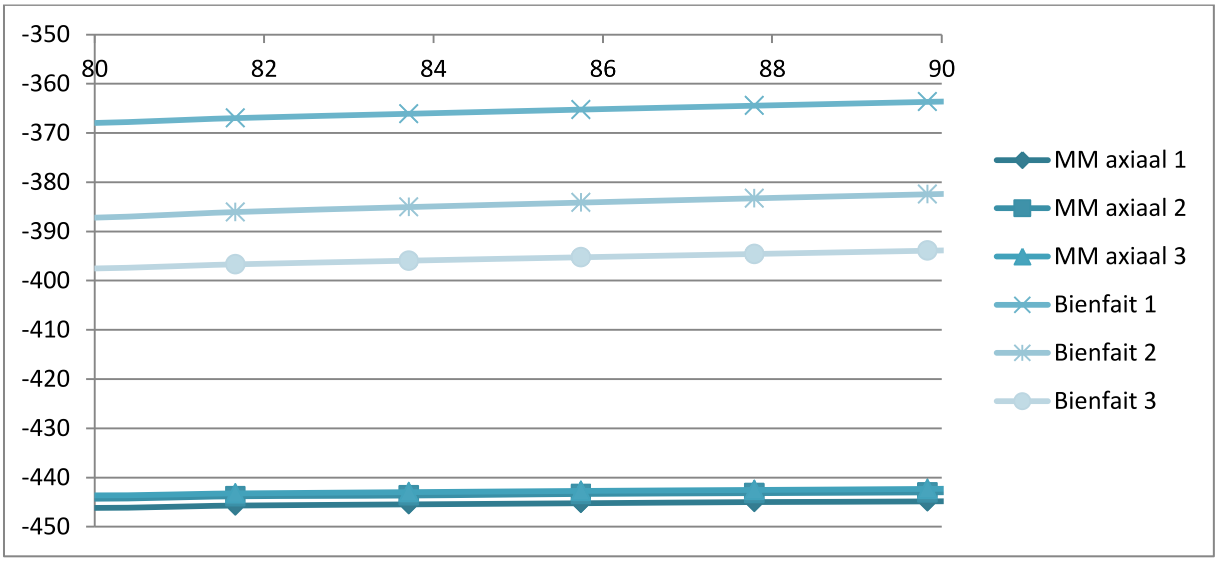

Figure 12.22 Strain gauge readings under maximum load

Even in the more detailed observation of the output (Figure 12.22), the MM strain gauges still are very close together. The difference between MM axial 2 and 3 is around one microstrain. These two strain gauges are glued on the rail at the same side. This means the readings from the gauges are very consistent, implying a good performance of these gauges.

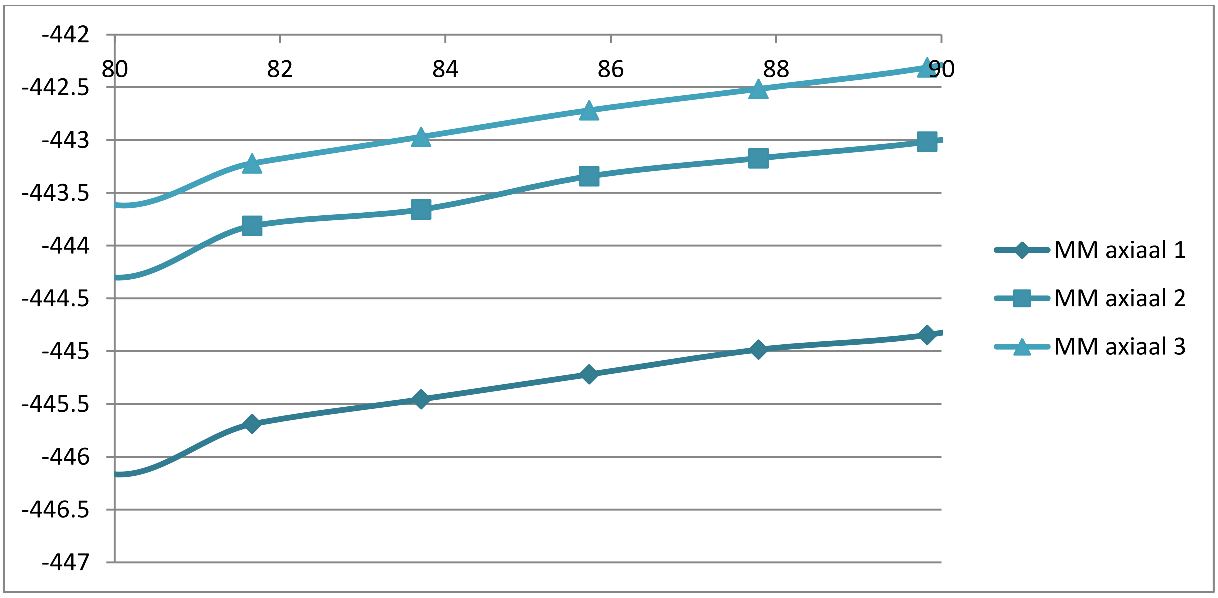

Figure 12.23 Difference between the MM strain gauges

An even more detailed observation (Figure 12.23) of the MM strain gauge behaviour shows the minimal difference between the individual gauges. This illustrates once again the consistency between the various MM strain gauges. The difference is minute, and the behaviour of the rail during the slow relaxation of the pressure cylinder is captured in detail.

12.1.6.5 Temperature test – calculation of α

The temperature test was executed to be able to determine the exact coefficient of expansion for rail steel. Unfortunately, due to the LVDT problems during the compression test doubts have arisen about the correctness of the LVDT measurements. Because in this situation the rail is free to expand it is not going to experience any bending (in theory), therefore a simple averaging of the compensated LVDT measurements should give an indication of the total average elongation of the rail.

In Figure 12.24 the displacement of the rail versus the average rail temperature is displayed as measured during the temperature test.

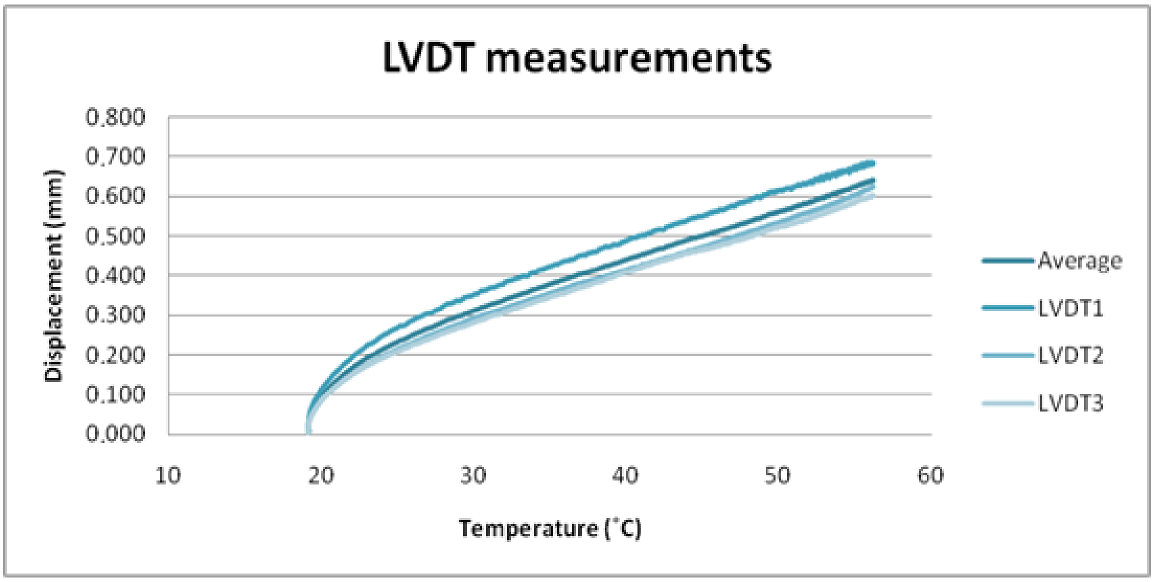

Figure 12.24 LVDT measurements during the temperature test

For calculating the thermal coefficient of expansion, the linear behaviour is of importance, and the change in displacement (elongation) per temperature, coupled with the rail length of 1050 mm. The linear behaviour is observed between the temperatures of 30 and 50 degrees Celsius. This behaviour yields a coefficient of thermal expansion for this specific steel of 11.864 E-6 m/m/˚. As this is a very reasonable value, it could be assumed that the measured expansion by the LVDTs might be correct.

12.1.6.6 Poisson ratio

Using the MM strain gauge output the Poisson ratio of the steel can be calculated very precisely. The MM strain gauges are positioned in the axial direction and in the tangential direction, orthogonal to the axial direction. The impact of bending on the axial strain is now known, using this and the measured tangential strain the Poisson ratio of the steel can be determined. Using a linear approximation of the measurements yields a Poisson ratio of 0.287. The following graph (Figure 12.245) was taken from the first lab test, with a combined temperature and force load. The time span observed is during the application of the load.

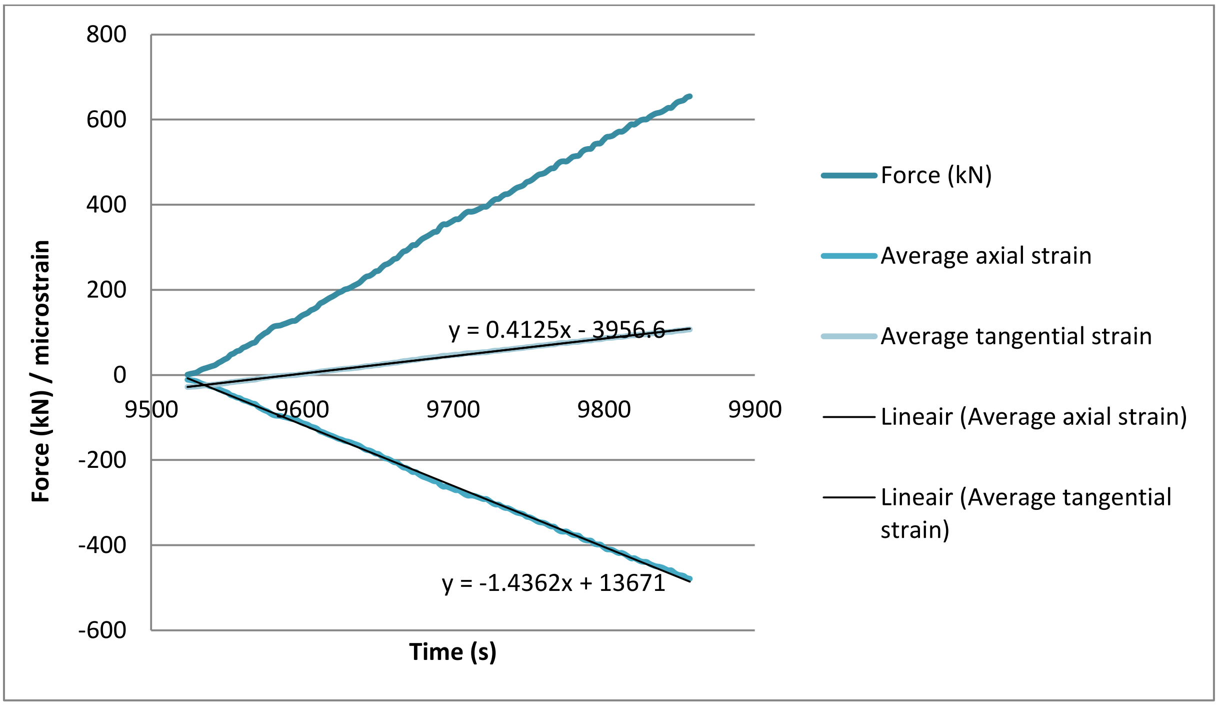

Figure 12.25 Axial, tangential strain and their linear relationships

12.1.6.7 DVRT

The DVRTs were tested in this setup as well. Their performance and accuracy were very good, but as strain gauges, they do not work so well. Of all of the measurements with the DVRTs, only two readings were within a reasonable accuracy (during the last compression test). Reasons for this are the improvised strain measuring set up, and a certain amount of temperature influence seems to be manifesting itself in this setup. This has no consequences for the use of DVRTs during the practical test, as they are used to measure the displacement of the sleeper and rail during cutting of the rail. As this is a very fast procedure significant (air) temperature changes will not occur, and the displacement measurement will focus on the rapid change of displacement, therefore these sensors are very well tailored for these measurements. Other things we have learned during the use of these sensors are how to set them up and how to configure the data logging software. Another important observation was the accuracy limit of the wireless transmitter. The wireless transmitter works using “bits”, a term used by the manufacturer for indicating in how many pieces the entire range of the sensor is divided. The number of “bits” used by the wireless transmitter is 4000. With a range of 4 millimetres, this means that over the 4 millimetres 4000 data points are used to indicate the displacement of the sensor. In other words, the maximum accuracy of the measurements is reduced to 4 millimetres divided by 4000. This means the maximum accuracy during the first practical test is limited to 1 micrometre. This is still more than enough, but it is less than the accuracy when the sensors are connected using a wire.

12.1.7 Accuracy

In Figure 12.26, the averaged behaviour of the three Bienfait and the three MM strain gauges is plotted versus the theoretical strain values. This graph is based on the third compression test, consisting of a single load applied. The horizontal axis is the time.

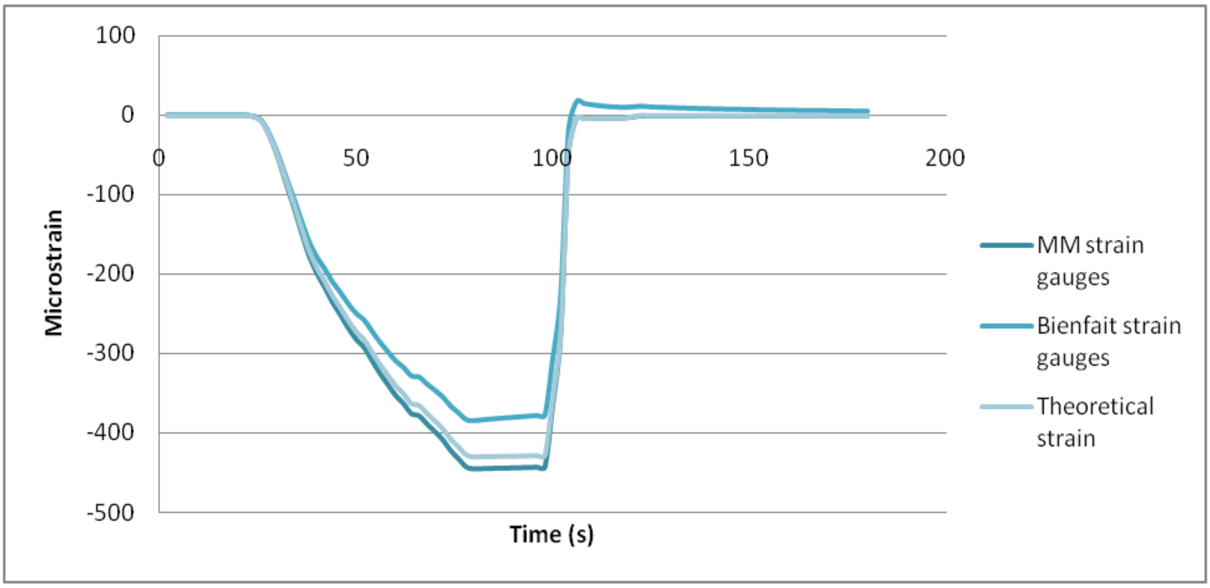

Figure 12.26 Average MM and Bienfait strains vs. theoretical strain third compression test

A number of conclusions can be drawn from this graph, which is very representative for the entire set of load tests conducted.

The first is the obvious difference between the Bienfait and the MM readings. The Bienfait sensors consistently measure lower strains during the load cycle than the MM sensors measure, or the theory predicts.

The second observation is the little peak after unloading in the Bienfait readings. This occurs every load cycle, and might suggest creep in the bonding layer between the steel and the strain gauge. An enquiry at Bienfait revealed that the cause of this deviation is the fact that the glue that bonds the protective cover to the rail is strong enough to make this protective cover work as a stiffener. In other words, due to the protective cover the strain reading is decreased because the cover starts carrying a load. The peak is caused by “sliding” of the glue, due to the high shear forces present. The third loading during the second compression test shows that the peak is higher when the load is applied over a longer period (Figure 12.27).

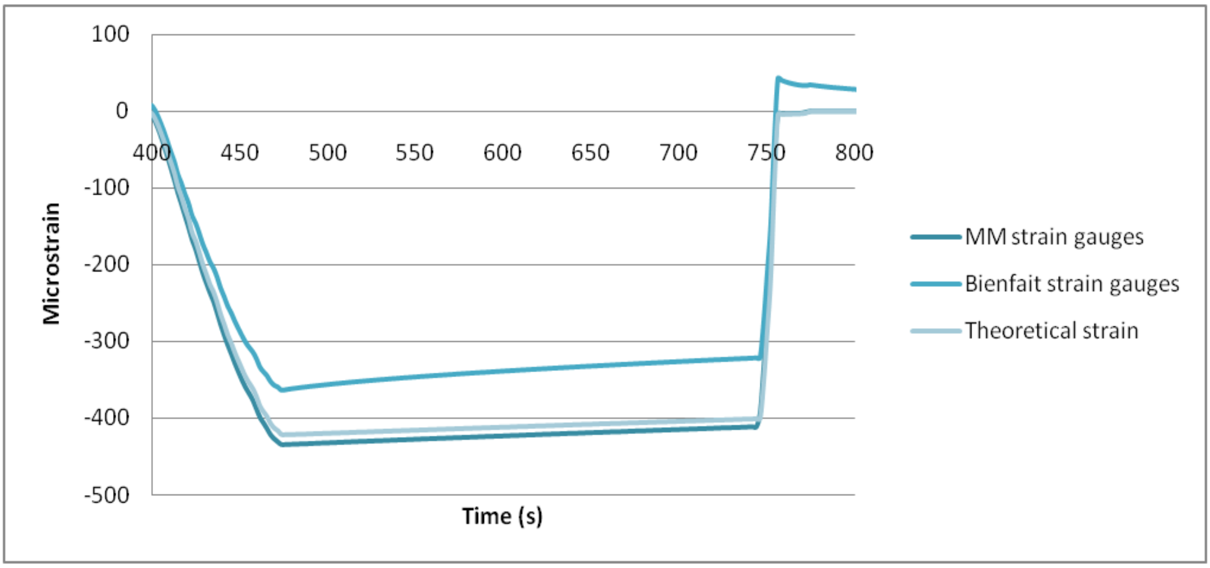

Figure 12.27 Bienfait strain gauges vs. MM strain gauges second compression test, third loading

The last observation that can be made is that the MM strain gauges measure a higher strain than the theoretical strain predicts. This can be explained easily by observing the assumed values for the area and stiffness modulus, a minor deviation of one of these values of only 2.5% can explain this difference. Such a deviation is very likely, and is one of the reasons it would have been preferable to have a proper displacement measurement so these values can be established with a higher certainty.

The performance of both types of strain gauges was analysed based upon the three compression tests. The total number of load cycles of these tests was seven (the load cycles from test one are valid for the strain sensor readings, just not for the LVDT readings). The deviation from the theoretical strain was calculated as the error of the measurement. This was plotted in a histogram with the average error. (chapter 12.1.8) The author is aware that the number of tests and sensors are not in any way sufficient to make any definite claims or statements, as the amount of samples is simply too low to state anything about the behaviour of the sensors in general. However, time and finances are limited, and a larger sample rate than three (sensors) and these seven load cycles was not practical. The author wishes to state explicitly that the sensor choice was based upon the performance of the two pairs of three sensors, and that these cannot be considered a proper representation of all the sensors of that type.

12.1.8 The measurements compared to the theory

An overview of the distribution of the error between the Bienfait reading and the theory is plotted in Figure 12.28. The first thing that can be observed is that the maximum error (79.35) is large, and that there is a single spike around the zero error region. The strain reached during the compression test was around 400 µm/m, giving an indicating of how large the errors are. This is a result of the measurements during the load cycle where the load is zero. Another thing that can be observed is the lack of large negative errors. There are a view around the 0 region, which relates to the zero stress situation (no force, no strain, therefore a lot of data points with a low error). This is due to the Bienfait measurements always being smaller than the theoretical values. The error is established by subtracting the Bienfait reading from the theoretical value.

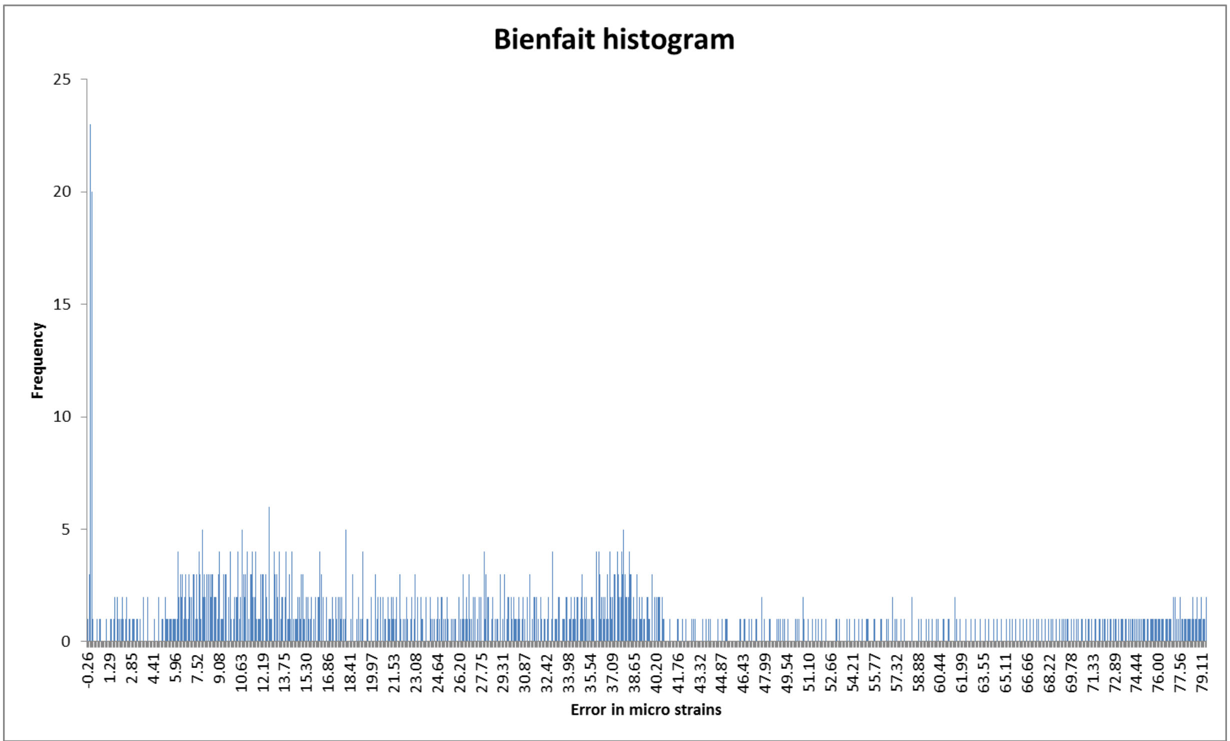

Figure 12.28 Overview of the errors and the frequency they occur

The average error is 29.76 microstrain compared to the theoretical values. The chance of the error being within 6 microstrains (half a degree Celsius of free expansion) of zero is 10%. The chance for it being within 12 microstrains (a full degree Celsius) is 27%. These values can be calculated by observing the amount of data points within these margins in the graph.

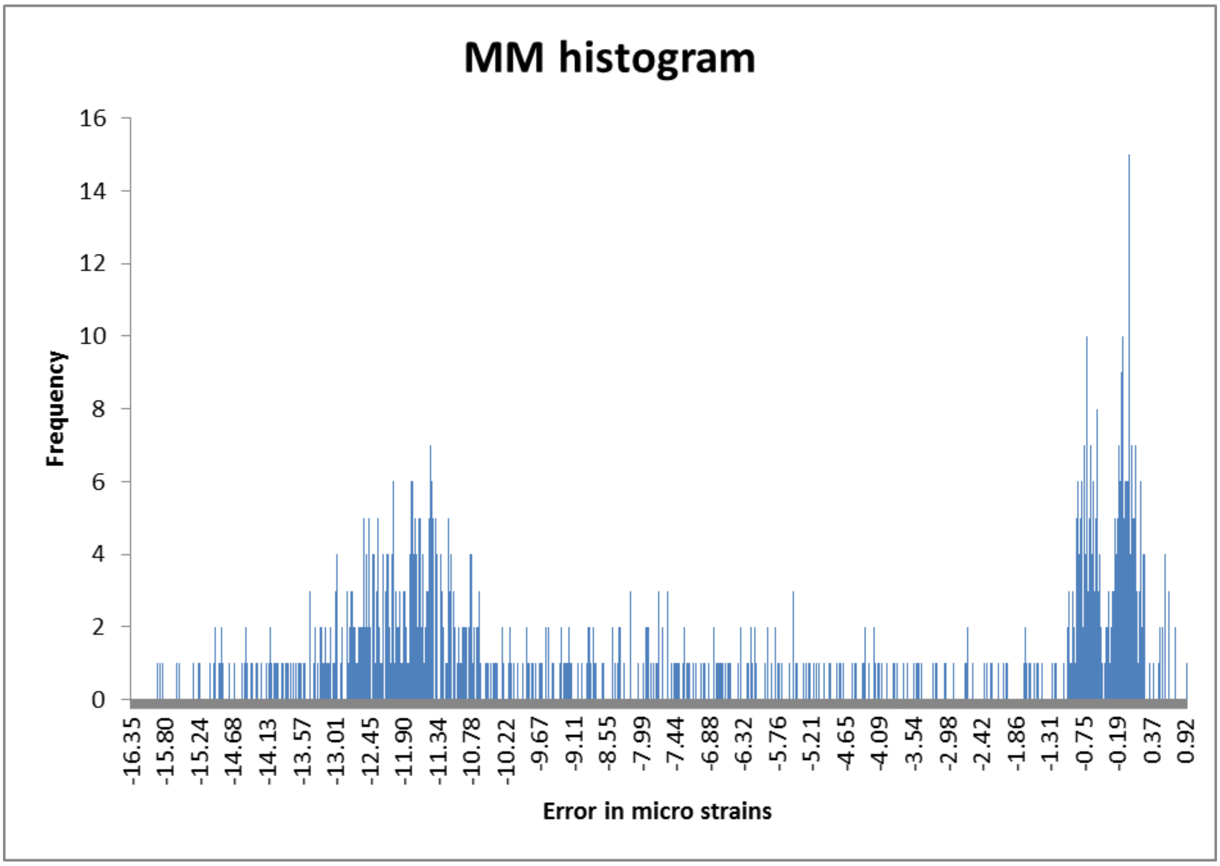

Figure 12.29 Overview of the errors and the frequency at which they occur

The first thing that can be observed from the MM error distribution (Figure 12.29) is that the maximum error is much lower as with the Bienfait, and that there are two clusters around the zero error region. This is a result of the measurements during the load cycle where the load is zero. The error is largely negative, as the MM readings tend to be larger than the theoretical values.
The average error is -6.82 microstrain compared to the theoretical values. The chance of the error being within 6 microstrains (half a degree Celsius of free expansion) of zero is 43%. The chance for it being within 12 microstrains (a full degree Celsius) is 78%. These values can be calculated by observing the amount of errors within the set margins.

Clearly, the MM strain gauge has a better accuracy when its readings are compared to the theoretical output. Unfortunately for the Bienfait sensors, the observed creep seems to put them off quite a bit (chapter 12.1.7).

Assuming that the theoretical variables stiffness modulus E and area A are imperfect, while the MM readings are accurate (they are after all tested and commonly used strain gauges, used in a wide variety of applications) the theoretical strain can be fine-tuned according to the measured strains. This is the step that should have been performed using the external displacement sensors, which would have yielded a second set of data concerning the rail material. Unfortunately, this is not an option. Using the force – strain relationship and the measured strain the stiffness and surface area of the rail are adjusted. This yields a new set of errors for the strain gauge, which are obviously much lower, as the theory is made to conform to the measurements. The corresponding distribution is displayed in Figure 12.30

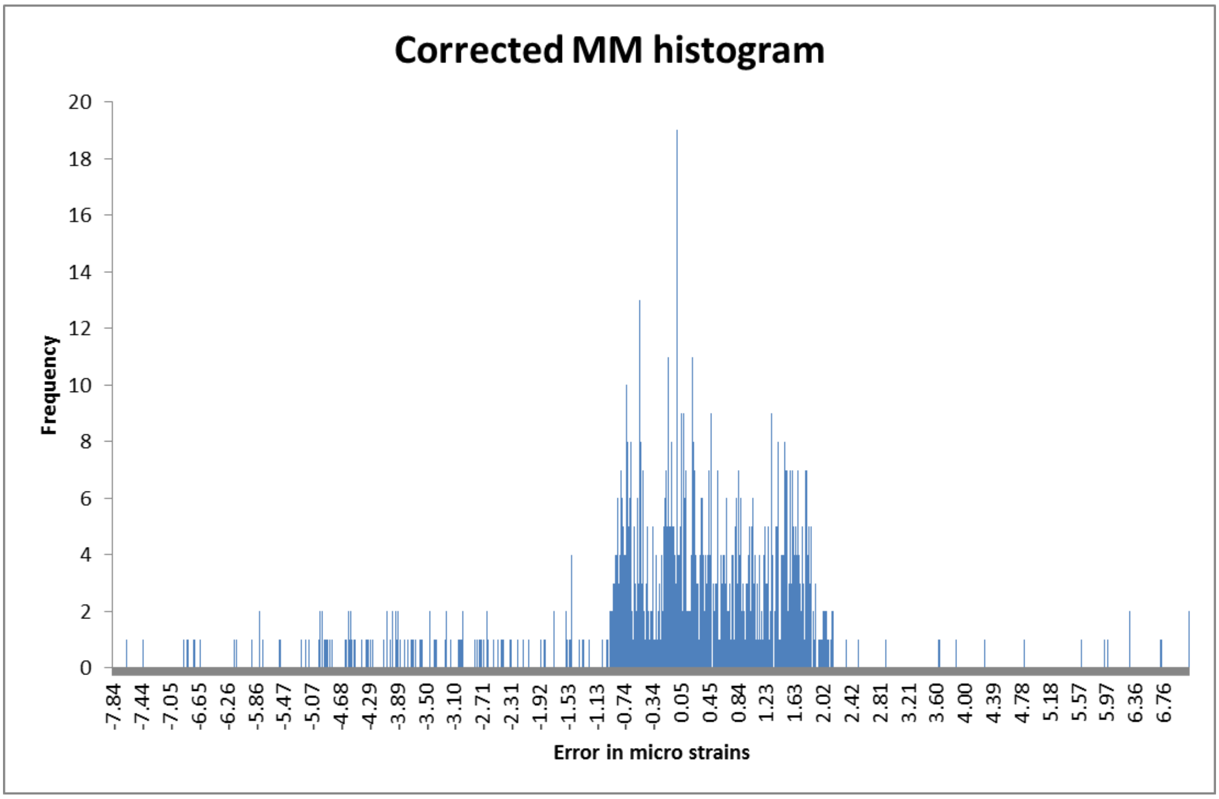

Figure 12.30 Overview of the errors and the frequency at which they occur

This distribution has an average error of 0.01 microstrains. The chance for these readings to be within +12 and -12 microstrain is 100%. The chance for them to be between +6 and -6 microstrain is 98%, a very good result.

At this point, it is interesting to establish how accurate the strain gauges are. ProRail has expressed the wish to measure the strain accurately up to 12E-6 m/m. Using the distribution in Figure 12.30 it can be estimated that the MM strain gauges do indeed have this accuracy, at least in lab conditions, when assuming that the variables for the theory are erroneous. The chance for the readings to be within +6 micrometres and -6 micrometres of zero is 99.87%.

This leads to the conclusion that the MM strain gauges would be useful for the practical test, and the Bienfait sensors unfortunately would not. This is unfortunate, seeing as the Bienfait systems were already geared towards practical use (combining strain gauge and temperature sensors) and are easy to apply. It would have been an excellent device to use in practice. However, based on these test results the strain gauges cannot be recommended for our test. Maybe some improvements to the accuracy can be made, but due to time limits, the Bienfait strain gauge cannot be used in our practical test. A different Bienfait protective casing, one that is applied using silicone kit instead of very stiff glue, has been used to protect the MM strain gauges (of which the accuracy has been established).

12.2 The first in-situ test - planning

The goals of this test were to provide insight in the development of stresses (by measuring strain) occurring in a replacement piece of rail while it is being connected to the current track, and to provide means of long-term monitoring to ProRail. This meant measuring the strains during every step of replacement, with a particular focus on the behaviour of the specimen during welding. For the long term monitoring the sensors were connected to data loggers that will keep measuring the strain. Predictions are that no changes in strain can be measured, but ProRail would like to verify this.

12.2.1 Set up

As the first out of three practical tests situations, the first one was focused on testing the equipment using a piece of straight track. The principle and the equipment must prove themselves on a “simple” situation before they can be implemented in the more complicated turnout. This test would focus on providing insight in the strains that occur during installation, with a separate focus on the effect of the thermite welds on the strains in the rail. For the second test, the sensors are to be set up in such a way that this test will determine whether the behaviour of the entire piece of track can be monitored by a single sensor in the future. By using seven sensors for the longest piece (30 meters), it is also possible to determine whether the strain is constant in the entire replacement piece. Should it not be, the seven sensors are more than enough to determine if the deviation in the strain is linear or nonlinear (Figure 12.31)

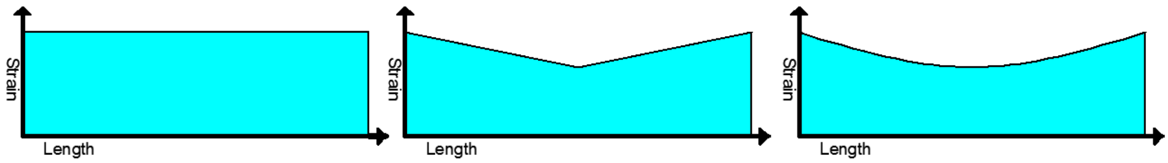

Figure 12.31 Possible strain distributions in replacement rail

During these tests, the installation procedures of ProRail are followed. By measuring the strain the stress in the rail can be determined (chapter 4.5). This will allow feedback on the installation procedures prescribed by ProRail. Measurements are conducted by MicroMeasurement quarter bridge strain gauges (tested in chapter 12.1), coupled with temperature sensors. At the weld locations the displacement of the original rail is measured by displacement sensors, these are of the DVRT type. These measurements determine what happens to the old rail, and what the neutral temperature of that rail was before installing the replacement rail. This is done by measuring the amount the rail retreats when cutting (spring back). Using the stress/strain relation, this can be converted to the neutral stress present in the rail at the time of cutting. It is in essence a more precise approach of the cutting method as described in chapter 7.1.1.

The measurements are logged by wireless data loggers, which send the information to a website. This way the long term monitoring is easy to achieve and only requires a battery replacement every now and then. The estimated battery life is two weeks.

The measuring set up is illustrated in Figure 12.32. A DVRT mounted on a pole in the ballast next to the sleepers, measures the displacement of the sleeper. Another DVRT mounted on the sleeper measures the displacement of the rail relative to the sleeper. By measuring the rail temperature, and using the relation between the length of the rail where the fasteners are loosened and the thermal coefficient of extension of steel, the neutral temperature of the “old” piece of rail can be calculated (chapter 4.5). This is particularly useful for the test with the 30-meter replacement rail, as it is not required by the ProRail guidelines to unfasten any connections for short replacement rails (under 20 meters). It is usually assumed that the adjacent rail has the correct neutral temperature, but for a test upon which new guidelines might be based it is important to measure and know this for sure.

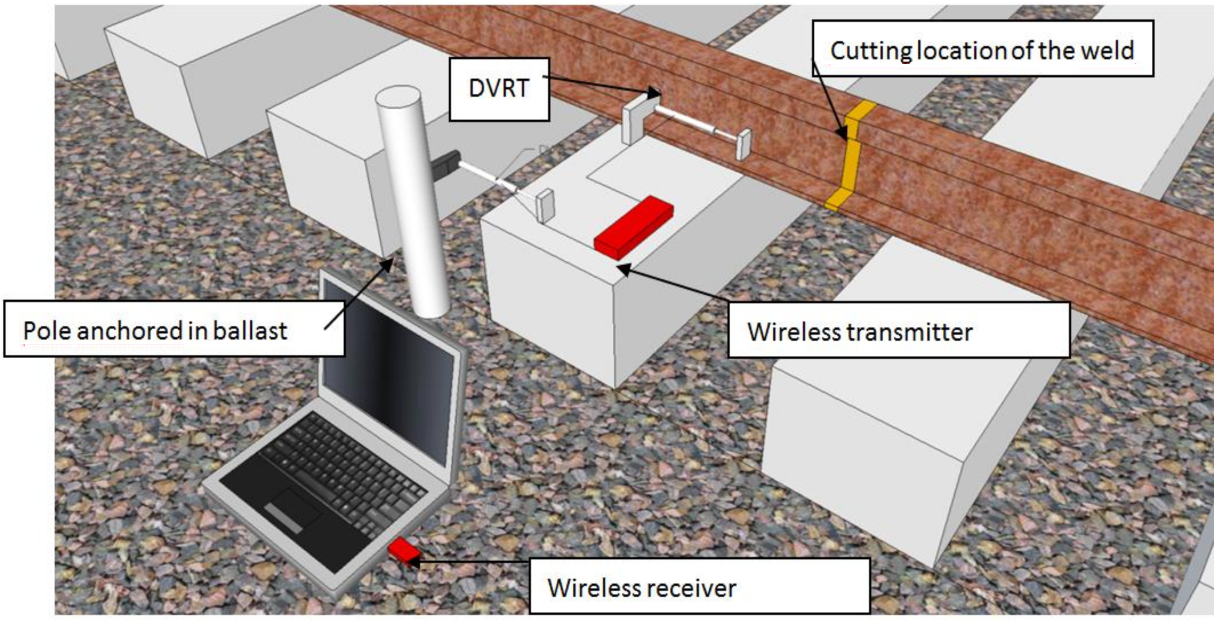

Figure 12.32 Displacement measuring set up

Two separate replacement pieces are tested, in two separate nights. One has the maximum transportable length of 30 meters, the other the minimum replacement length of 6 meters. Shown below are the sensor locations on the 30-meter long replacement rail, viewed from the top. The arrows are the sensor locations.

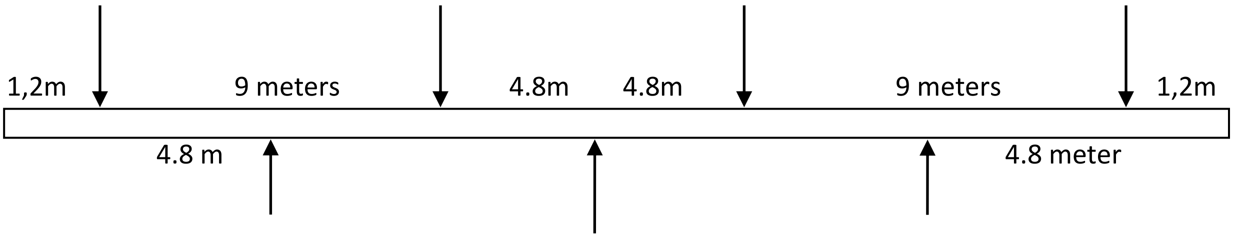

6-meter replacement rail top view:

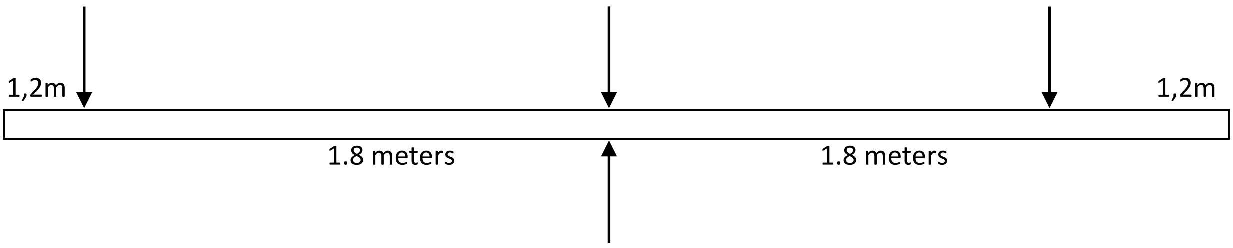

This set up positions every sensor in the area between two sleepers, while also allowing measuring any bending in the horizontal plane. Furthermore, they enable determining the shape of the strain distribution. The two outermost sensors are positioned as close to the weld as possible, without risking them being damaged. At the 30-meter replacement rail two strain gauges are placed outside of the replacement rail, on the rail already present on each side. These allow for detailed information on the strain in the old rails. Next to this, the displacement of the old rail is monitored by applying a line every other sleeper and measuring the distance the rail moves compared to these sleepers. This set of data also provides information on the anchorage length of rail, and how much force is transferred by friction to the sleepers per meter of rail.

Every sensor location contains both a strain and a temperature sensor. This means that two data channels are required for every location.

12.2.2 Preparation

12.2.2.1 General preparation

A number of preparatory steps need to be taken prior to execution of the test. These are:

- An appointment must be made with the safety expert of ProRail
- The track-manager, inspector and line-experts need to be informed
- A meeting with the contractor must be held
- A safe location for the permanent data loggers must be found
- The equipment must be bought and/or borrowed

12.2.2.2 Preparing the test track

Prior to the placement of the replacement rail with sensors, the sensors must be installed. Due to time constraints during maintenance this must be done beforehand. These actions were performed on the terrain of the contractor. These actions consist of selecting the replacement rail, marking it with a telephone number (in case of issues with the rail), and placing the sensors. For placing the sensors a dry area is necessary, any moisture could ruin the adhesion between the strain gauge and the rail and by extension the measurement results. The location of the sensors is marked using paint (Figure 12.33).

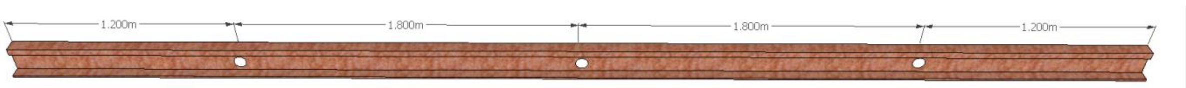

Figure 12.33 Sensor locations marked

After marking the locations where the sensors need to be placed these areas are grinded clean. After grinding, the precise location and height of the strain gauge is determined. This exact location must be sanded down using a fine grade of sandpaper (Figure 12.34).

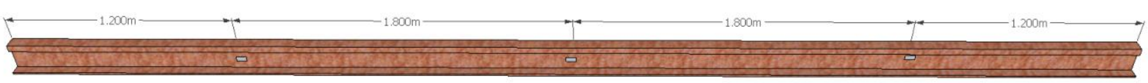

Figure 12.34 Sensor locations grinded down

After sanding, the location needs to be cleaned using a solvent. The strain gauge is then be applied (Figure 12.35). After this step, the protective casings are applied using silicone kit. The rail is now ready for transport.

Figure 12.35 Sensors fitted on the rail

12.2.3 Placement of the rail

12.2.3.1 Placement of the sensors and laptops

After towing the replacement rail to the appropriate location on site, the strain gauges can be connected to their cables. After placing the replacement rail in its final location a reference measurement was made.

Data acquisition set up for the 6-meter replacement rail:

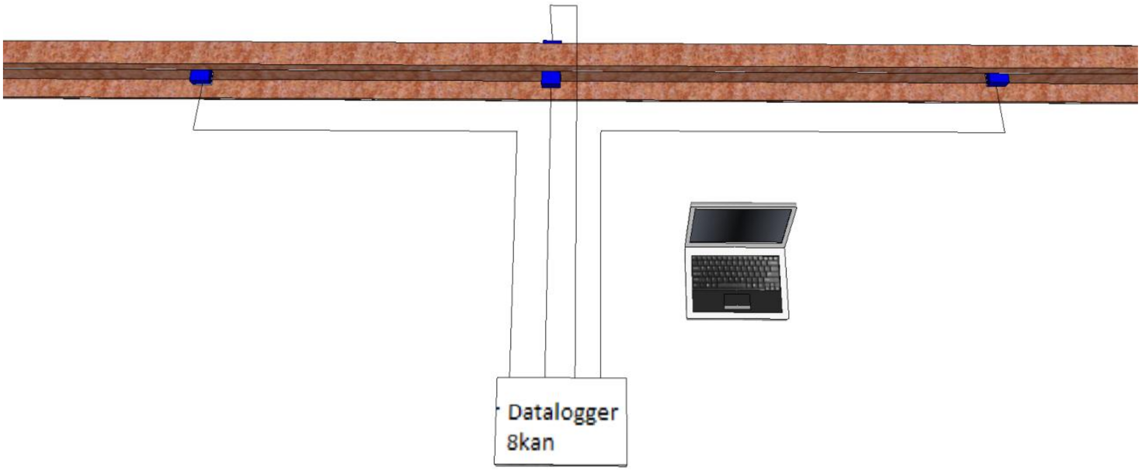

Figure 12.36 6-meter data acquisition

Data acquisition set up for the 32-meter replacement rail:

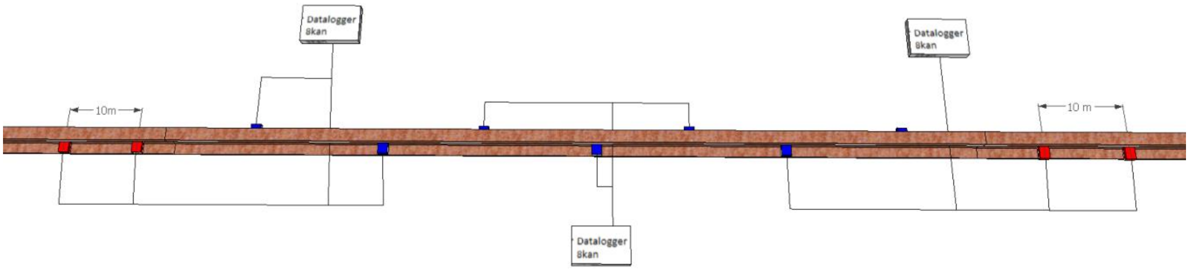

Figure 12.37 30-meter data acquisition

In Figures 12.36 and 12.37, the blocks are the data loggers. The data loggers can be read out on a website, as their data is send to a central server via GPRS. This setup tries to minimise cable lengths. Increasing the cable length is not preferred as it could increase measurement errors as environmental impacts are increased.

Strain gauge positioning

The middle block in the 30-meter replacement rail will contain a strain gauge rosette (Figure 12.38); this rosette will allow ProRail to study the behaviour in the principle directions. Rosette strain gauges are in essence three separate strain gauges positioned at 45-degree increments. This way the behaviour in each direction can be isolated. This rosette strain gauge will provide an anchoring point for the analyses of the results.

The other strain gauges are quarter bridges positioned in horizontal direction, to measure the horizontal strain. These strain gauges are compensated for temperature changes, and the corresponding expansion in all directions (horizontal and vertical). A thermal load will not provide a signal from the strain gauge. This is only the case when the gauge is applied to a piece of steel that can expand freely. When the strain gauge is applied on a fixed piece of steel with prevented expansion, as is the case here, it will output a negative relation equal to the thermal expansion of steel.

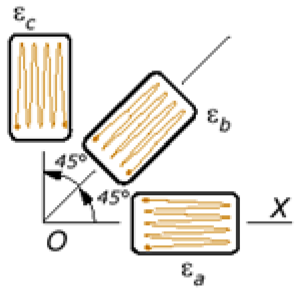

$$\begin{cases} \varepsilon_x = \varepsilon_a \\ \varepsilon_y = \varepsilon_c \\ \varepsilon_{xy} = \varepsilon_b - \dfrac{\varepsilon_a + \varepsilon_c}{2} \end{cases}$$

Figure 12.38 Rosette strain gauge [20]

Frequency of measurement

The data loggers measure with a frequency of two times per minute. After the placement, when the long term observation starts they are set to measure the strain and temperature once every 300 seconds to preserve the battery. Because the weld process is a very interesting moment a higher data density was deemed advisable, therefore a higher sampling rate is needed.

The data loggers have been selected to allow the measurements to continue over the course of several weeks or months and with luck even years. This is not strictly part of this thesis and research, but ProRail would like to monitor the strain for a longer period.

12.2.3.2 The displacement measurement:

Before the rail is cut, the displacement sensors are placed. Four displacement sensors are needed; two to measure the sleeper displacement and two to measure the rail displacement with respect to the sleeper. This measurement is done at each side of the replacement rail, therefore requiring four sensors. Upon cutting the rail the temperature of the rail is measured, this allows calculating the stress free temperature of the old rail by estimating the anchorage length and the formula's in chapter 4.5. Furthermore, it will provide displacement data during the cooling of the welds, thereby allowing calculation of the weld shrinkage. All four sensors are connected to wireless transmitters, and can be read out by a single laptop with a wireless USB receiver.

After completing this setup on both sides of the rail replacement, the replacement rail is moved into its final position. At this moment the displacement sensors need to be connected and running. For the read out of the data loggers, another laptop with wireless internet must be present. The data loggers provide their data to the GPRS network directly. This data can then be read out on a website, this is to facilitate the long-term measurements, but does require a laptop with wireless internet to be present to be able to read the values.

When all the measurements are up and running the welds can be closed (Figure 12.39). It is important to protect the DVRTs when this happens, the molten steel and thermite can easily damage the sensitive equipment. This is the reason why the DVRTs are placed at 2 sleepers distance from the weld location.

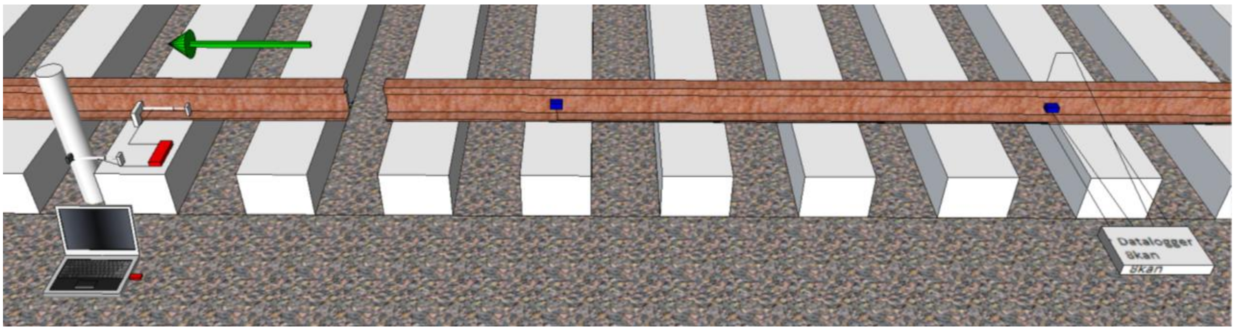

Figure 12.39 Situation at rail stressing

When the weld has cooled down the high sampling data loggers can be switched to the long-term measuring frequency via the website.

12.2.3.3 Data loggers

Due to the two needed channels per location, a single 8-channel data logger is required for the 6 meter replacement rail, while three 8 channel data loggers are needed for the 32 meter piece. These data loggers are placed outside the obstruction free zone determined by ProRail for railways. They are mounted on a pole at 40-50 centimetres above ground or connected to the support structure of the high voltage cable. It is important to thoroughly electrically isolate these data loggers from the ground. The rail is an electrically isolated system, which is not earthed. It is very important that this test set up does not ground the rail, as this will disturb rail operation and will cause lightning strikes (which often strike the rail) to shortcut sensors and data loggers. The current insulation required by ProRail is an electrical insulation up to 4 kilovolts. A round piece of insulation with build in wire threads will allow easy assembly and electrical insulation. This type of insulation is widely used by ProRail and were bought from Voestalpine Railpro.

12.3 The first in-situ test - execution

The sensors were applied on the rail on the 10th of June outside on a Strukton rail maintenance area. The replacement rail was then moved to the test location by crane on the 15nd of June. Installing took place in the night of the 15nd of June.

12.3.1 Location

The test location is in Amsterdam, between station Amsterdam Sloterdijk and Amsterdam Central. The ProRail rail designation is km 180.1 on track SW. The sensors are on the outer rail, near the entrance to a location for vehicles to enter and exit the track. Using Figure 12.40 as a reference, the track on the left is a straight track for a couple of kilometres. On the right is a curve in the track, which diverts the trains towards the outer tracks of Amsterdam station. This is illustrated in Figure 12.40 and 12.41, Figure 12.42 gives a site overview.

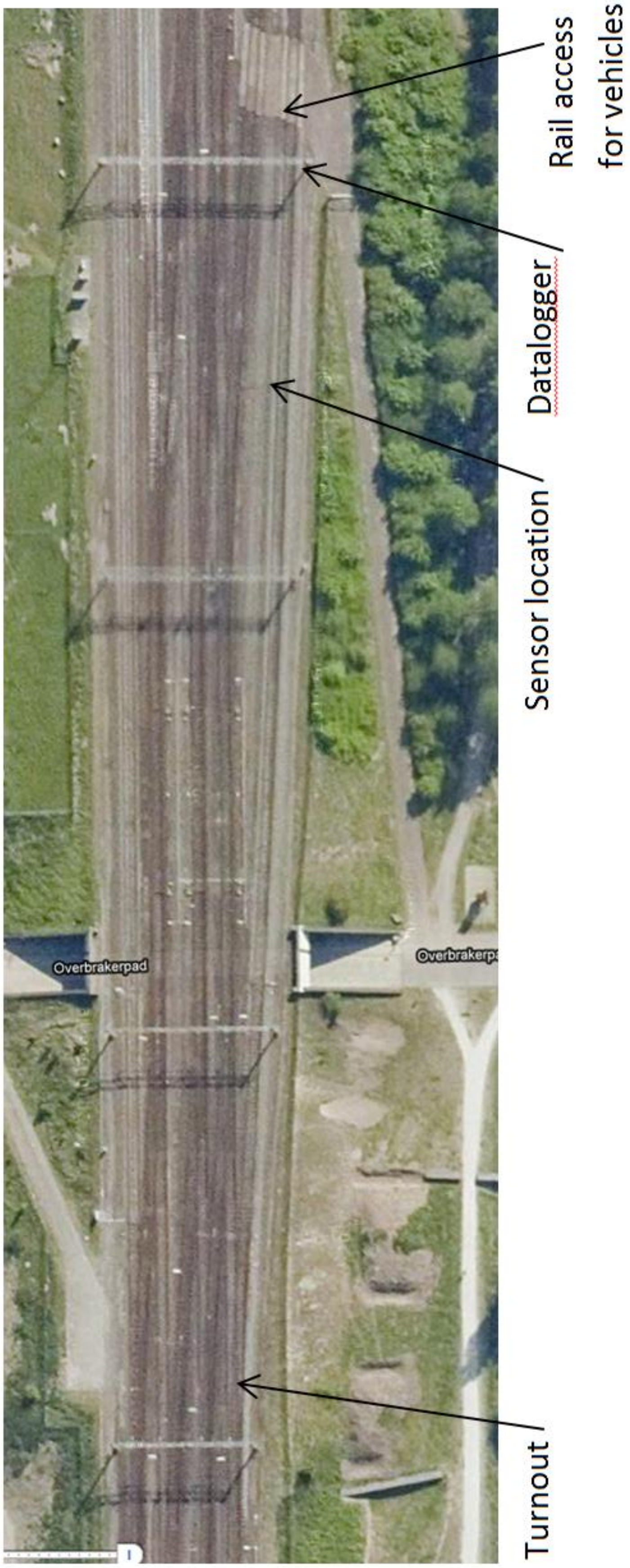

Figure 12.40 Situation overview

Figure 12.41 Track alignment

Figure 12.42 Situation after instalment of the sensors (discoloured bit of rail) and a site overview

In the digital report this space contains a movie of the track viewed from the train cabin and shows the downhill curve. Running direction is from Sloterdijk to Amsterdam Central.

12.3.2 Installation procedure

The strain gauges (Figure 12.44) had been installed at a material depot of Strukton. This was an outside area, in which the replacement rail had been lifted on to a container (Figure 12.43). This provided the Stork employees with a comfortable working height. Luckily, weather conditions were good, moisture was not a problem during instalment. The replacement rail was transported to the maintenance site by crane. The strain gauges were protected with an extra layer of wood to prevent direct collisions (Figure 12.43).

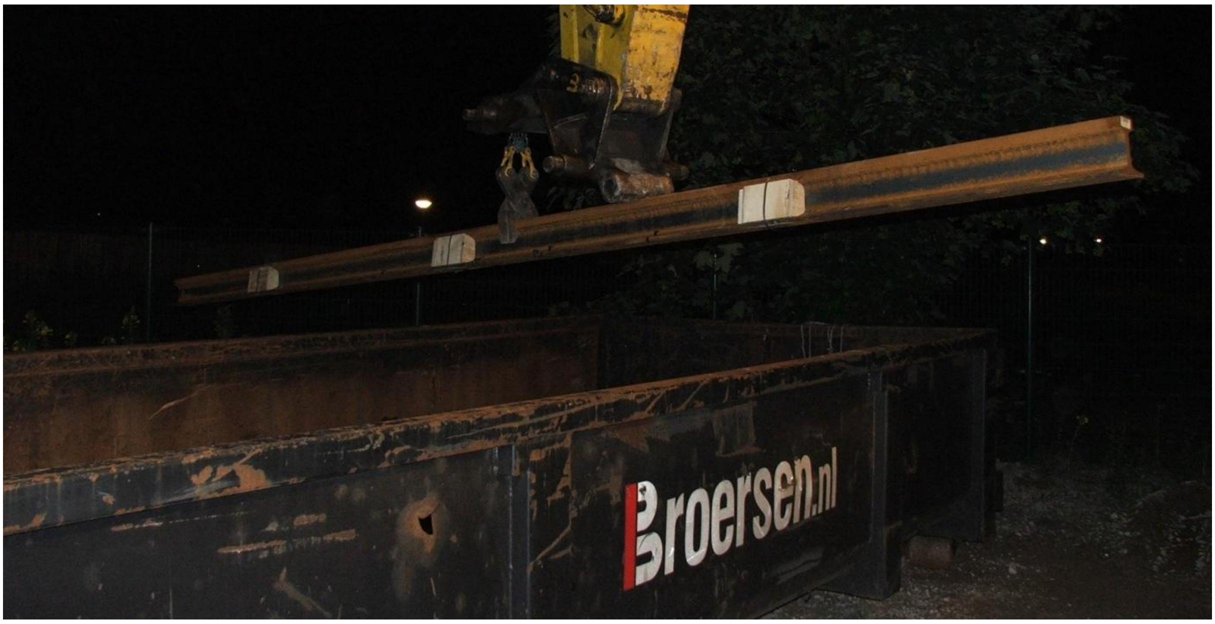

Figure 12.43 The crane lifting the replacement rail from the container

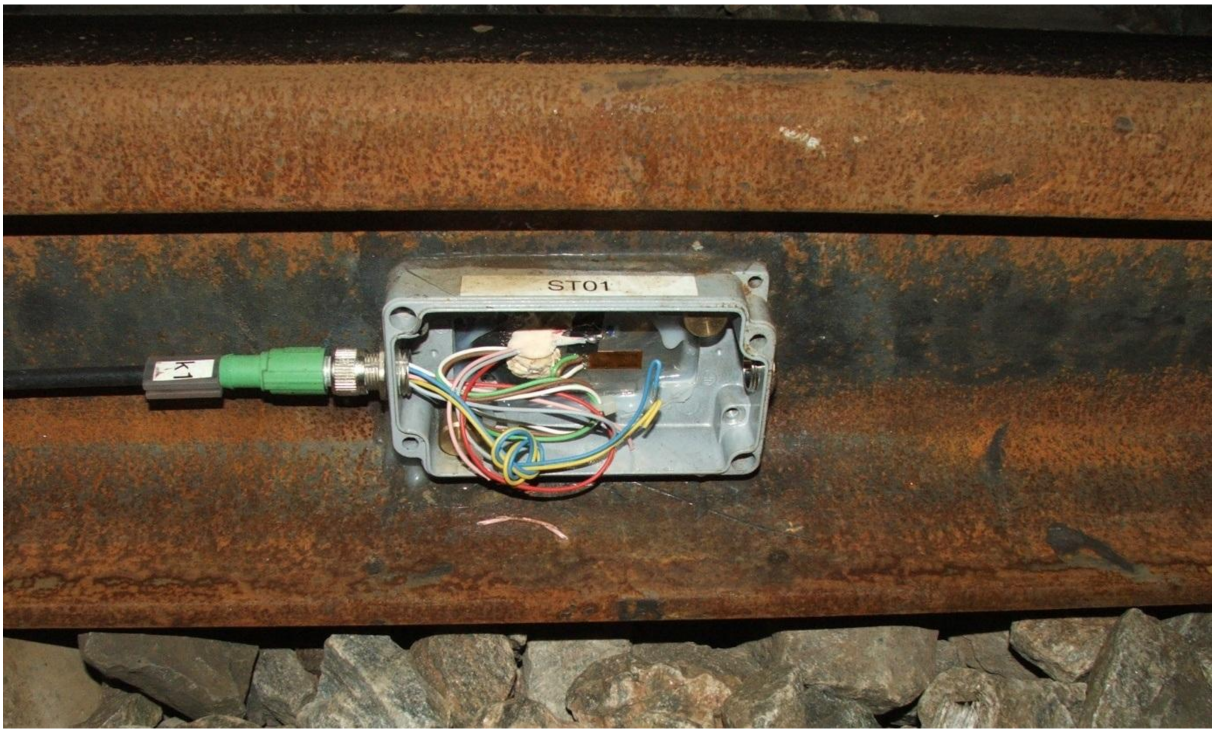

Figure 12.44 The inside of the sensor protection. The brown rectangle is the strain gauge (quarter bridge); above it is the temperature sensor (PT1000)

Conditions during the test were good, it was dry and the air temperature was about 17 degrees, the rail temperature was equal to the air temperature. The first step was marking the location where the replacement rail would be installed. After marking the location, the displacement sensors were installed on the sleepers by the Stork employees (Figure 12.45). To place this sensor the fastenings on this sleeper had to be undone (Figure 12.46). Meanwhile markings were made on ten sleepers on each side to measure displacement differences further away in case of displacement. In case of a large spring back, these markings would help determine the distance.

Figure 12.45 Placement by Stork employees

Figure 12.46 DVRT set up overview

During installation, it was noticed that the displacement sensors for measuring the sleeper displacements could not be installed. The installation required a pole to be put in the ballast, but the distance from the pole to the sleeper was too large to place this sensor, furthermore the pole would prevent heavy equipment to move over the rail, as the tires of the crane were wider than expected. A solution has already been engineered for the test on the 30-meter rail. A close up of the DVRT setup is provided in Figure 12.47. The only sleepers with removed connections were the ones with the DVRTs.

Figure 12.47 DVRT set up, DVRT detail

After installing the displacement sensors and starting the data logging (Figure 12.48), the replacement piece was unfastened. Upon completion of unfastening, the rail was cut in two locations. The air and rail temperature at this time was 17 degrees; no visible spring back was seen. Agitating the rail with a hammer (to release any stored energy constrained by friction) produced no further results.

Next, the replacement rail was placed in position and fastened; logging from the strain gauges and temperature sensors was started. The data logger was not positioned in its final location (figure 12.49) yet, but was kept close by to be able to make adjustments.

Figure 12.48 Data logger position during cool down

Two temperature sensors were malfunctioning and did not start working during the test; the other two perform as expected. After placing the rail the welds were made and allowed to cool. During cooling contact with the strain gauges and temperature sensors in the middle of the replacement rail was lost. These 4 sensors (2 strain, 2 temperature) started working again after the data logger was reset.

When the weld temperature was down to 200 degrees, due to time restraints, the displacement sensors were uncoupled, and the data logger was moved to its final position. The cables were fastened to the rail using cable clamps.

Figure 12.49 Final position of the data logger

In the digital version of the rapport, this page will contain a movie detailing the execution

13 Test results

13.1 Rail replacement

The results of the measurements during rail replacement are discussed first. At a later stage, the results of the long-term measurements are reviewed. The results are based upon the measurements taken in the in situ test described in chapter 12.3.

13.1.1 Basics

The location of the sensors is illustrated in Figure 13.1.

← Amsterdam Sloterdijk, turnout Amsterdam Centraal, maintenance vehicle access →

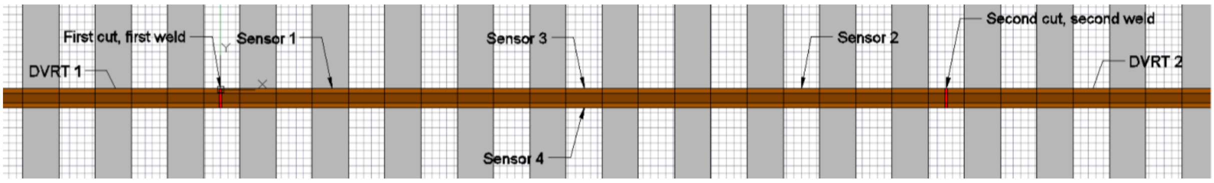

Figure 13.1 Situation overview

Another processes needs to be explained and be understood by the reader prior to examining the data. Furthermore, all the information in chapter 8 is of importance.

Measurement to microstrains

It needs to be explained how the change in resistance of the strain gauge is translated into the corresponding strain value. The data loggers record the change in resistance as a certain value of mV/V (millivolt per volt). This is the direct notation of the change in resistance caused by the strain gauge over a constant agitation signal. A length increase of the strain gauge causes the mV/V output to increase, while a shortening causes the output to decrease. The maximum and minimum values for the mV/V output are 2.099 and -2.099 respectively.

To translate the mV/V output to the corresponding strain, the relation between the two must be known. This relation was established using a calibrated tool provided by Stork FDO Inoteq. This tool simulates a strain gauge; it allows the user to select the desired strain and provides the corresponding resistance. A data logger was connected to this device, and set up for measuring 350-Ohm strain gauges (the kind used during this test). The device was adjusted to simulate a 350-Ohm strain gauge as well. Several strain outputs were selected on the device, and the corresponding mV/V output was logged by the data logger. This data allowed determination of the change in mV/V for a certain change in strain, and thus provided the factor with which to convert the data logger readings into strain. This factor was found to be 0.0004980 mV/V per microstrain.

13.1.2 Strain gauge

The strain gauge results are the most interesting aspect of the measurements; therefore, they are discussed first. They yield the most insight in the mechanics. In Figure 13.2 the strain gauge output is visualized from the moment of connecting to the data logger until 36 hours later. After this moment the data logger broke down, which is discussed in chapter 13.1.5.

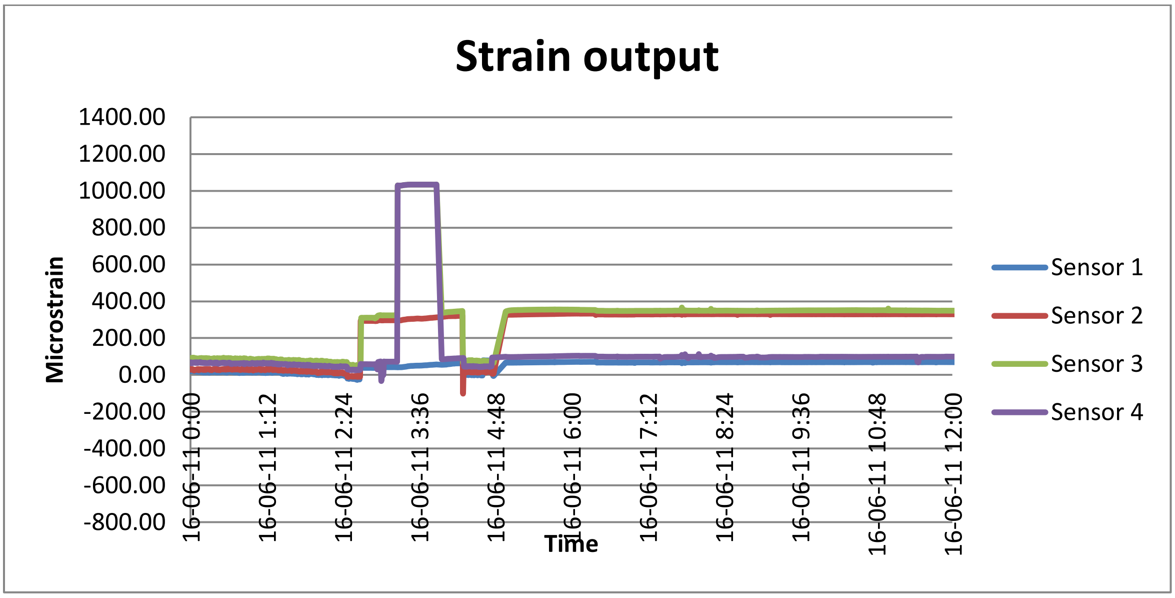

Figure 13.2 Strain gauge output (unaltered)

As one can observe, there are several moments of interference (peaks and valleys). One is caused by a malfunction (the peak), the other by a required moving of the data logger (to a safer location further away), and the necessary disconnection of the sensors to the data loggers for this (the valley, a signal of 0). When the graph is focused upon the cool down period of the welds the graph becomes as presented in Figure 13.3. From this graph, several distinct situations can be identified.

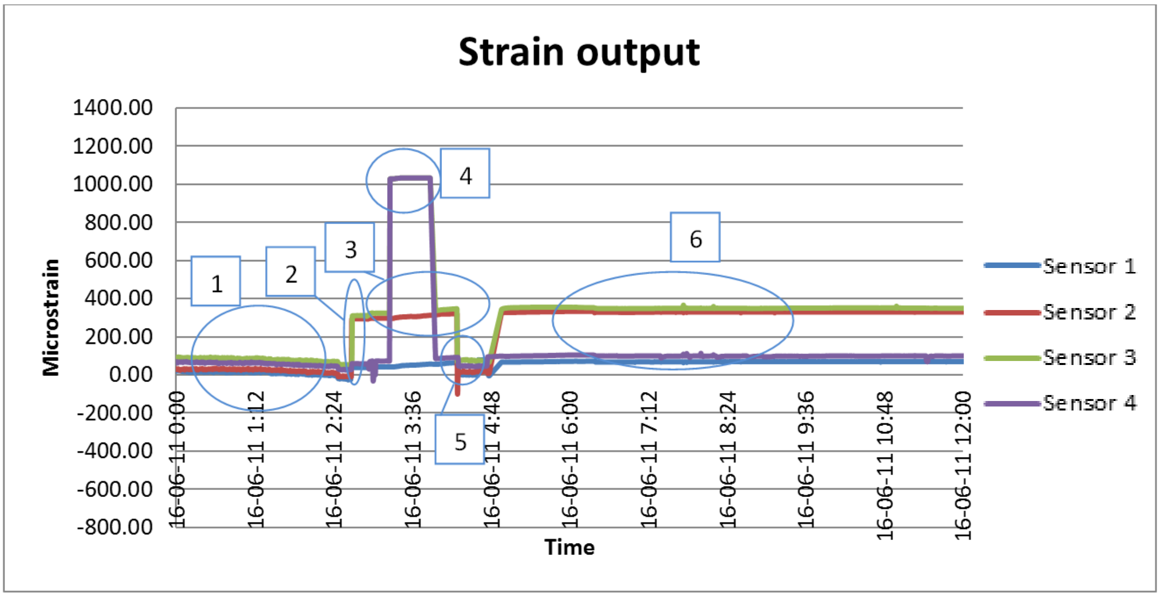

Figure 13.3 Distinct situations during measurement

Area 1

This is the output recorded by the data logger on the night of the rail of the rail replacement, before it was connected to any sensors. The data logger was brought to the site already switched on. This data is not constant due to movement and temperature changes causing interference, which once again illustrates how sensitive the measurements are. This is caused by the high accuracy required during measurements, making the system very sensitive to small influences.

Area 2

At this point in time the sensors were connected to the rail, and all strain gauges were found to be operating. The rail was then moved to its final position (it was outside of the track) and placed on its supporting plates and rail pads. The move has a small influence on the measurements from the strain gauges. Once again, the very high sensitivity translates into measurements caused by even very slight bending of the replacement rail. The point after positioning the rail in its final position is taken as the zero measurement in analysis later on.

Area 3

The first weld was made at 3:13 AM, with the second one following closely at 3:21 AM. This is the start of the cooling down period and the start of stress build up in the replacement rail.

Area 4

During the cooling down period (about two minutes after welding) two of the strain gauges stopped providing data. After switching the data logger off and back on these strain gauges reported data again, this was however only attempted at a late state to make sure at least some data was collected from the two working strain gauges. This was done in case the turning off and on of the data logger might cause even more strain gauges to stop working.

Area 5

Due to time limitations, the data logger had to be moved to its final position on the support of the high voltage cable. The rail had to be cleared in order to allow train traffic again. In order to do this all cables had to be disconnected, to allow them to be fastened to the rail in a proper fashion.

Area 6

This is the start of the long-term measurements, and the end of the strain build up due to the cooling down of the welds.

When filtering the incorrect output (due to breakdowns or disconnections), the data in Figure 13.4 are the remaining data points. In addition, when correcting all the data for the zero measurements, Figure 13.5 , the results are as follows. Due to the constant temperature, the only temperature compensation to be applied is the compensation curve.

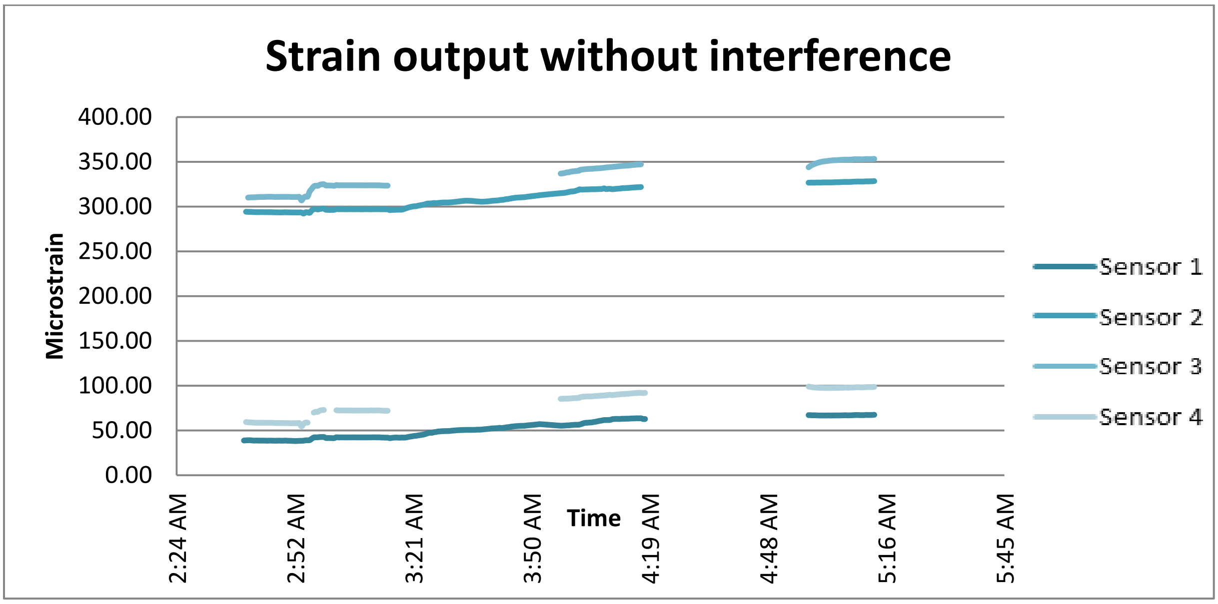

Figure 13.4 Strain output without interference

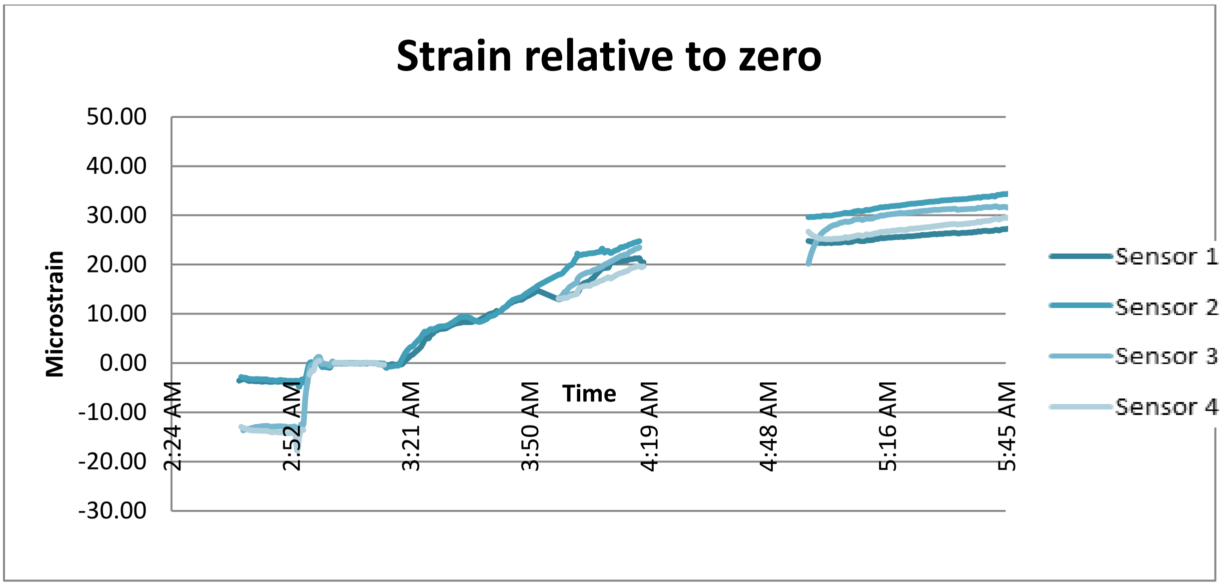

Figure 13.5 Strain output relative to zero measurement

As one can see from these graphs, many data points had to be discarded. Several trends can still be discerned and some statements can still be made, even though it has to be noted these are stated with a certain caution in mind. A single measurement with equipment that has performed sub-optimally does not provide a strong base for definite statements.

The first weld took place at 3:13 and the closure weld at 3:21 AM, this second point has been taken as the zero reference as it is where the strain starts to increase. This will yield the best approximation to the total strain increase due to cooling down. Strain increase before this point is due to shifting of the rail into position or (heavy) equipment being manoeuvred over the locations of the strain gauges.

What can be concluded is that during the cooling period the strain increases with about 28 microstrains (with an average of 27.7 microstrains). This is roughly equal for all the locations on the rail. The strain appears to be highest in the strain gauge closest to the last weld and lowest in the strain gauge closest to the first weld. The difference is small; however, it does appear to be present for the last half hour. These measurements are evidence for two things.

1) The rail slides through its connections and distributes the strain evenly. Almost no longitudinal force is applied on the sleepers under the replacement rail.
2) The neutral temperature of the rail is increased by 27.7/12 = 2.3 degrees Celsius. This is lower than expected, as discussions with Strukton indicated the increase would be approximately 14 degrees. When observing the behaviour of the adjacent rail it would appear much of the force due to weld shrinkage is applied to the adjacent rail, instead of the replacement rail, see also chapter 13.1.3.

To calculate the total elongation of the replacement rail the average strain value from the sensors is calculated and multiplied by the replacement rail's length. This leads to an increase of length of 0.166 mm. Together with the measured displacement of the stock rail by the DVRT (chapter 13.1.3) this comes down to a total movement of 0.9 + 0.8 + 0.17 =1.87 mm. Divided over two welds this yields an average shrinkage of 0.93 mm per weld.

13.1.3 DVRT

Due to unforeseen limitations, the DVRTs that were supposed to measure displacement between the sleeper and a fixed point could not be installed. Even though care was taken to place the poles providing the fixed points outside of the width of the sleepers, the height of the poles was a problem. Placing them at that location would cause obstruction of the wheels of one of the cranes on site; these were wider than the profile of free space for trains. The data of the sleeper displacement was therefore not collected. It is therefore possible that the displacement measured by DVRT 1 and 2 is not the entire displacement due to the weld shrinkage. It is however assumed that the sleepers do not move, due to the relatively high temperature and the consequentially low forces.

The DVRTs measuring the displacement difference between rail and sleeper were installed, and were in place and measuring for cutting of the rail, welding, and cooling down of the rail. Upon cutting the rail, no visually distinguishable displacements were observed. The displacement sensor DVRT 1 suggests a slight movement of about 0.12 mm that starts to occur after cutting has started (02:47AM). DVRT2 suggest a movement of 0.05 mm when the second cut is made. Because it is not yet known how far into the rail force and strains are redistributed, these values cannot tell us much about the exact neutral temperature in the adjacent rail. It can however be concluded that this neutral temperature is close to the current temperature (16 degrees C), as a larger difference would translate into larger displacements. Another reason for the lack of spring back is the fact that the ProRail guidelines allow the fastening of rails adjacent to the replacement rail to remain in place for replacement pieces smaller than 20 meters. No spring back was therefore expected, not with such relatively high temperatures as on this night (17 degrees C, compared to the theoretical 25 degrees C of neutral temperature in the rail). Reports have been made about fastened rail springing back, but only during cold nights. The measurements are therefore conforming to the expectations.

During the welding and grinding process, the DVRTs were protected using protective cloth. After the welds were made, the cooling down period started and the DVRTs remained measuring. Over the course of the following one and a half hour, the weld cooled down to approximately 200 degrees. The displacements measured would increase some more due to further cooling of the weld. Unfortunately, due to the need to continue train traffic the DVRTs had to be removed at this stage.

In the cool down period displacements of 0.9 (Figure 13.6) and 0.8 mm (Figure 13.7) were measured on either side respectively. The measurements for DVRT2 show some irregularities; it appears that some data has been lost. This is probably due to a connection error. The measurements performed by the DVRT are an absolute value of displacement (not relative to the previous measurement); therefore, it can be assumed with some caution that the displacement in the gap would have been constant as it has been in the minutes before the data loss occurred. It will therefore be assumed that the value of 0.8mm is indeed correct.

Extrapolation of the movement due to the weld cooling from 200 degrees to the current air temperature would suggest a further 0.1 to 0.2 mm to occur.

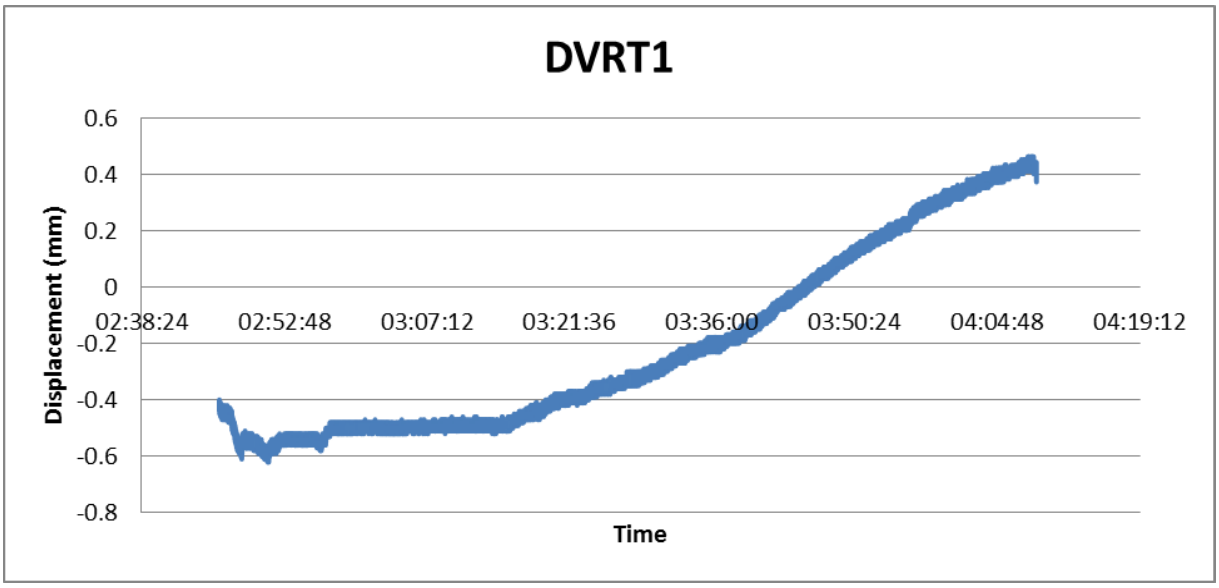

Figure 13.6 DVRT1, closest to the first weld

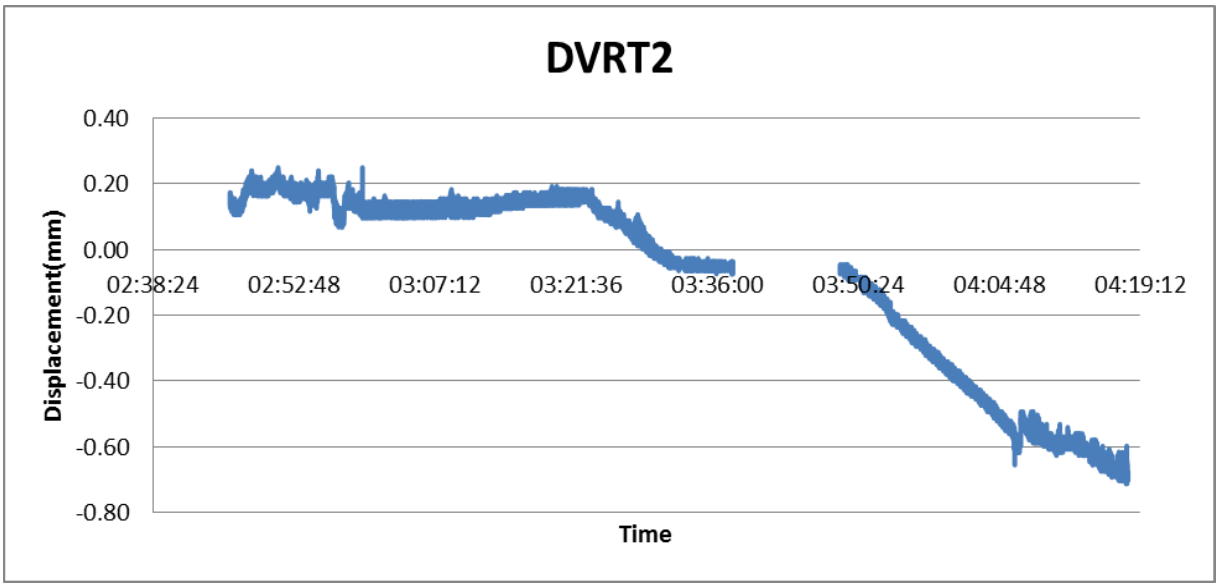

Figure 13.7 DVRT 2, closest to the second weld

When combining this data with the strain measurements in the replacement rail it is obvious that most of the weld shrinkage is accommodated by the adjacent rail, not by elongation of the replacement rail itself. Several factors can be of influence on this behaviour, but no definite statements can yet be made. This would require more data, as will be collected during the 30-meter rail test.

The first possible factor is the clamping force in the connections. The replacement rail connections were fastened on site before welding. The connections of the adjacent rail have not been fastened again, and it is feasible that they have relaxed during their lifetime. This would mean that the force in the replacement rail would be more readily transferred to the sleepers (and thereby the ballast) than would be the case in the adjacent rail, preventing a large strain build-up in the replacement rail.

This brings attention to the second influencing factor, the ease at which the adjacent rail appears to move towards the cooling weld. The key to understanding the behaviour at the weld is the relation between strain and displacement. This relation is centred on the length of the object in which the strain is present. Observing the situation during the test, the shrinkage (strain and force) of the weld cooling down is divided over the adjacent rail and the replacement rail. The replacement rail is only 6 metres long; a token force of 100 kN would generate an elongation of this rail of 0.4 mm. It is unknown over what length the piece of rail adjacent to the weld is influenced by the weld. Assuming this influence spreads as far as 30 meters, due to the ease at which the rail appears to be sliding through its connections, this would mean that a token force of 100 kN would lengthen the 30-meter rail by 2 mm. This process could go a long way towards explaining the measurements. However, it requires knowledge about the influencing length on the adjacent rail. This will only become available once the 30-meter rail test is executed, as strain gauges are mounted at a 10 meter interval on the adjacent rail to measure exactly this influencing length.

Furthermore, this phenomenon is very likely to be influenced by a large number of situational variables, such as the horizontal and vertical alignment of the adjacent rail, the type of connections, the type of sleepers, ballast condition, wear and tear on the rail (influencing the surface area) and very importantly, the neutral temperature in the adjacent rail.

13.1.4 Temperature

The temperature data collections during the rail replacement were also plagued with malfunctioning sensors and interruptions. For instance, only two of the temperature sensors were functioning. Furthermore, one of these two suffered from the same malfunction as two of the strain gauges, and all of them were disconnected during the moving of the data logger as well. However, there are enough data points left to be able to determine the temperature of the rails to be around 16 degrees during the exchange of the rail (Figure 13.8).

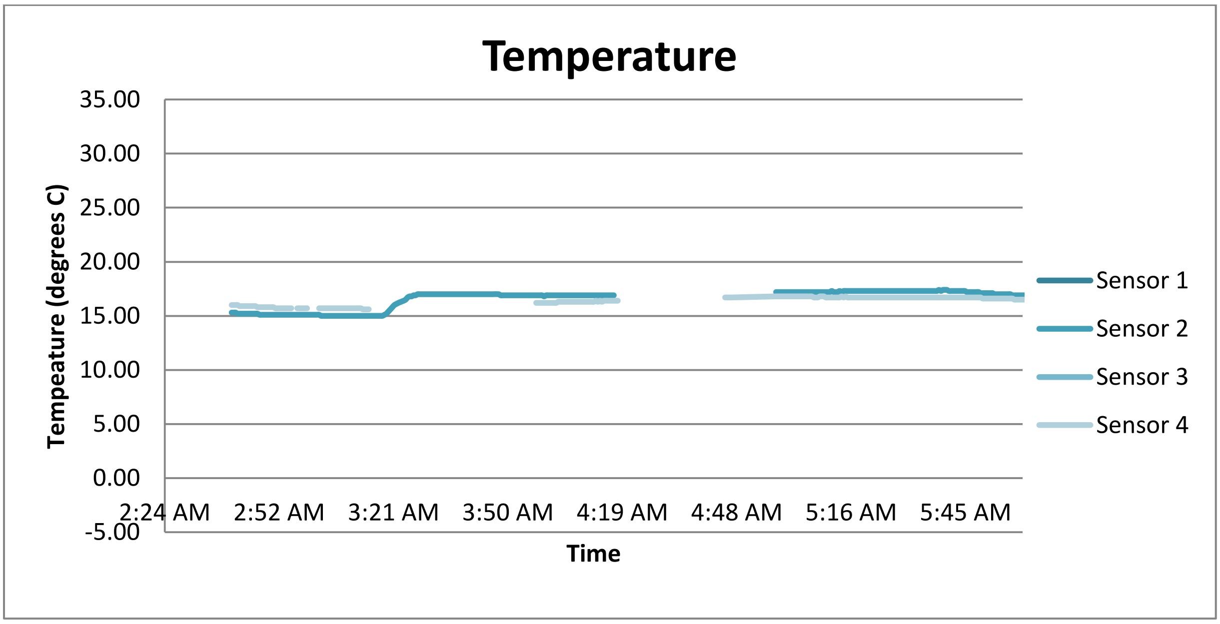

Figure 13.8 Temperature during replacement

Even though the temperature sensor was located close (1.2 meters) to the weld no influence from the weld can be detected. This was confirmed by the thermal imaging camera (figure 13.9); the rail on the left of the inner rectangle has a temperature of 17 degrees. This indicates that the temperature transfer from the weld to the adjacent rail is indeed local. The location of the weld and sensors is displayed in Figure 13.10.

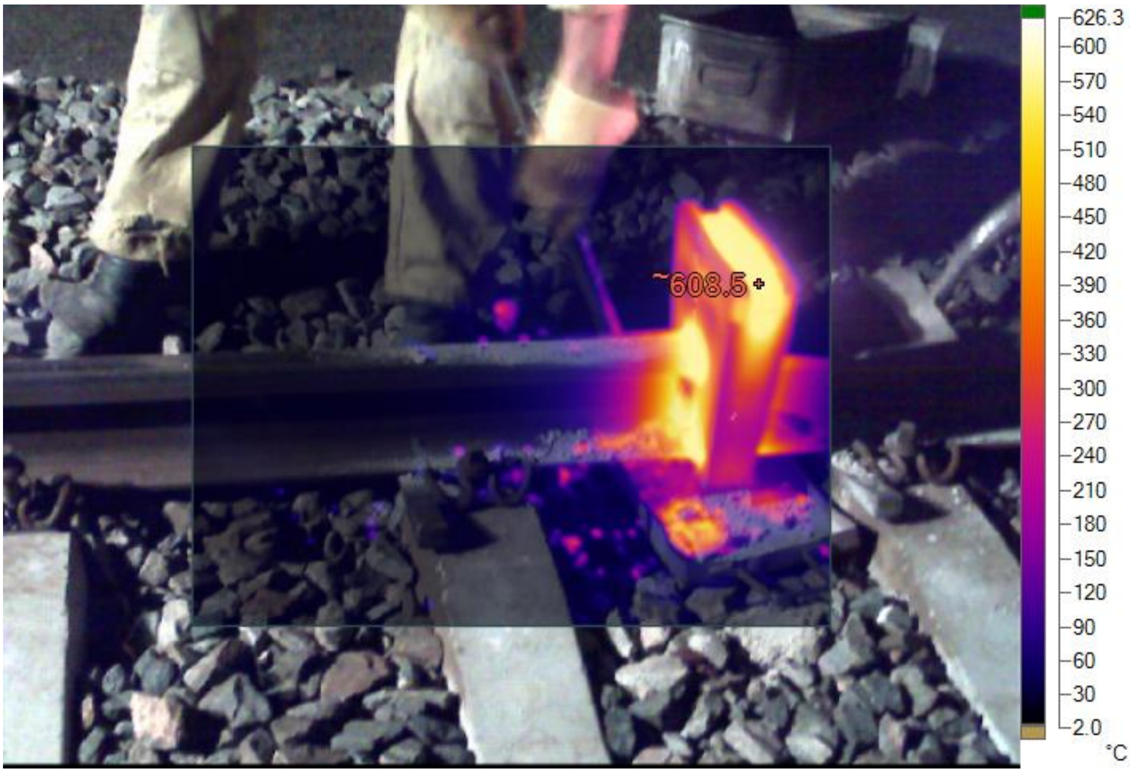

Figure 13.9 Thermal image of the weld cooling down

Figure 13.10 The DVRT on the left, the weld in the middle, and the strain and thermal sensor to the right (1.2 m from the weld)

13.1.5 Incidents

Broken temperature measurements during replacement

It is the opinion of the Stork FDO Inoteq employees that connections to the temperature sensors (PT1000) might have been broken. Because of the bad experience with the temperature sensors so far, it has been opted to replace the two broken ones, and the one with less than perfect behaviour (as became clear in the long-term measurements) with new sensors. The risk of the last good working sensor failing was deemed too high. This replacement was done on Sunday July 10th. In this night, temperature sensor 1 was replaced completely; furthermore, the other malfunctioning temperature sensors had their connections checked and were electrically isolated from the rail (one of the sensor connectors was touching the rail). After this maintenance the site was left with all four temperature sensors working. Unfortunately, the replaced temperature sensor ceased functioning the afternoon after the sensor maintenance.

Broken strain measurements

All the strain gauges seem to be in good condition. The malfunctions during the replacing maintenance could be attributed to the data logger, which seemed to have crashed during the crucial stage. This was resolved by resetting it.

Broken data logger

After starting the long-term measurements, the data logger broke down on the 17th of June. No data was transmitted by the data logger; this was due to an empty battery. Due to the weekend, the data logger was not repaired until June 22nd, after which data was received for 12 hours, and from only 2 strain gauges. After this period all data received appeared to be non-sense. During the battery replacement, some moisture was detected inside the data logger. 12 hours after this maintenance bad weather broke out and the data logger seized functioning. Upon inspection, the data logger was found to be full of (condensed) moisture. It was replaced by a different data logger, on which special care was taken to protect it against moisture. This data logger seemed to be working well, except for a 2-day period in which four channels (2 strain gauge and 2 temperature) were not functioning. It appears to be working well since that period (all channels are working, except for the broken temperature sensors). It has to be noted that the weather since the last malfunction has been good.

13.2 Long term measurements

When observing the long-term measurement data it is advisable to recollect the processes described in chapter 13.1.1. As an example, the measurements for the first 36 hours after the installation of the replacement rail are presented in Figure 13.11, as well as the corresponding temperature measurements.

As can be observed, the strains show a movement downwards during the warmer days when compared to the stresses at night. After 17:00 on the 17th of June, the data logger stopped transmitting for the first time. For more information about the data logger breakdowns see chapter 13.1.5.

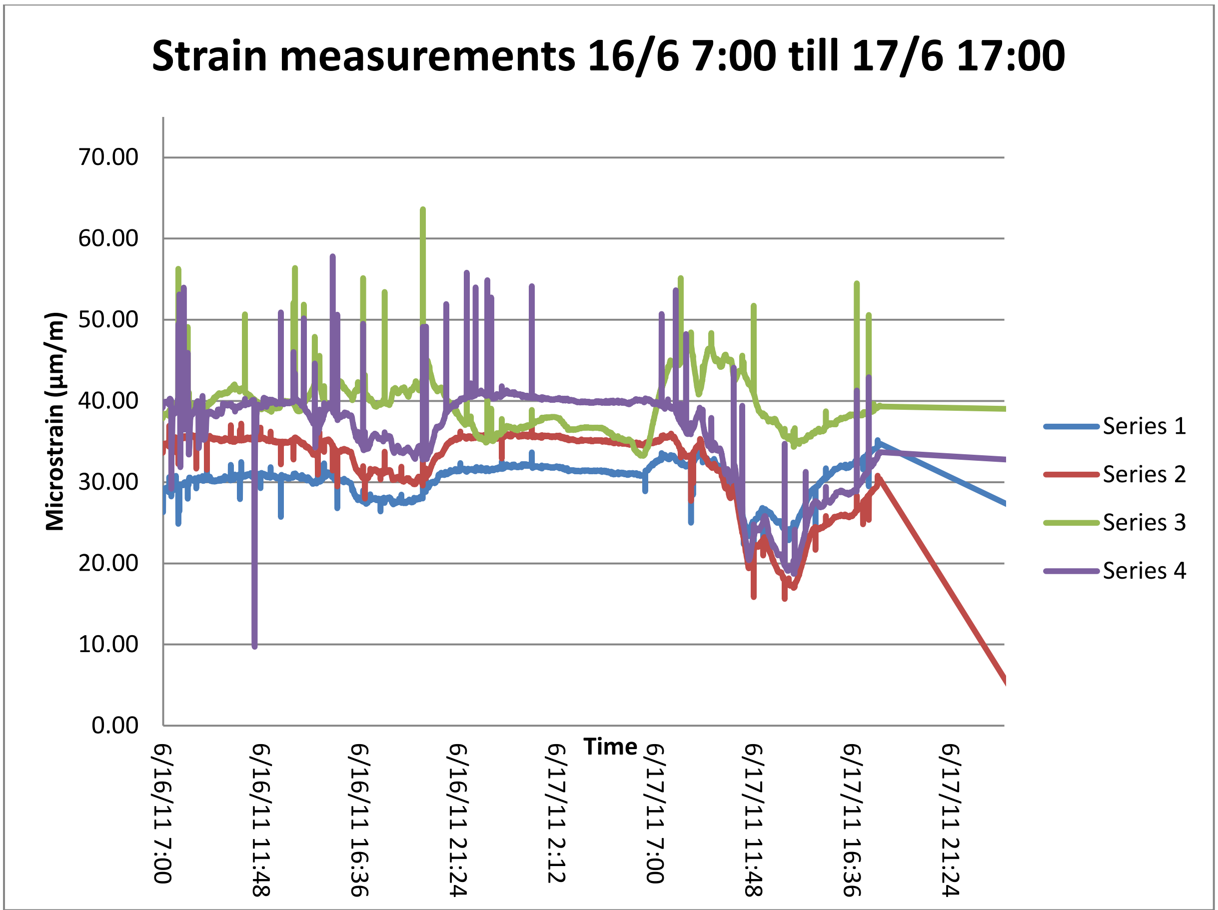

Figure 13.11 Strain measurements 16/6 until 17/6

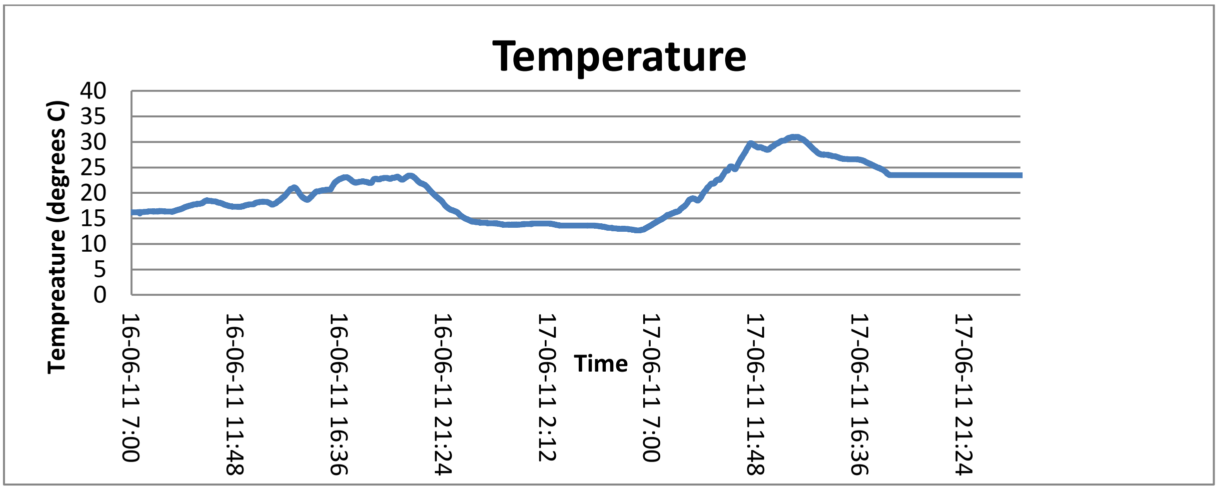

Figure 13.12 Temperature measurements 16/6 - 17/6

The measured strain changes are very small. For example, the temperature difference between the night from the 16th to 17th and the day of the 17th is 17 degrees C (Figure 13.12); at the same time the difference in strain measurements is at maximum -20 (series 4). This indicates that the rail is almost fully free to expand; the 20 microstrain of deviation from the constant value can be converted into a value of roughly 30 kN of compressive force present in the rail. At the same time the strain in the rail due to free expansion is equal to 17 x 12 – 20 = 184 microstrain.

To verify whether this behaviour is persistent in time, the outputs during the 17th of July are visualised in Figure 13.13 and the corresponding temperature in Figure 13.14.

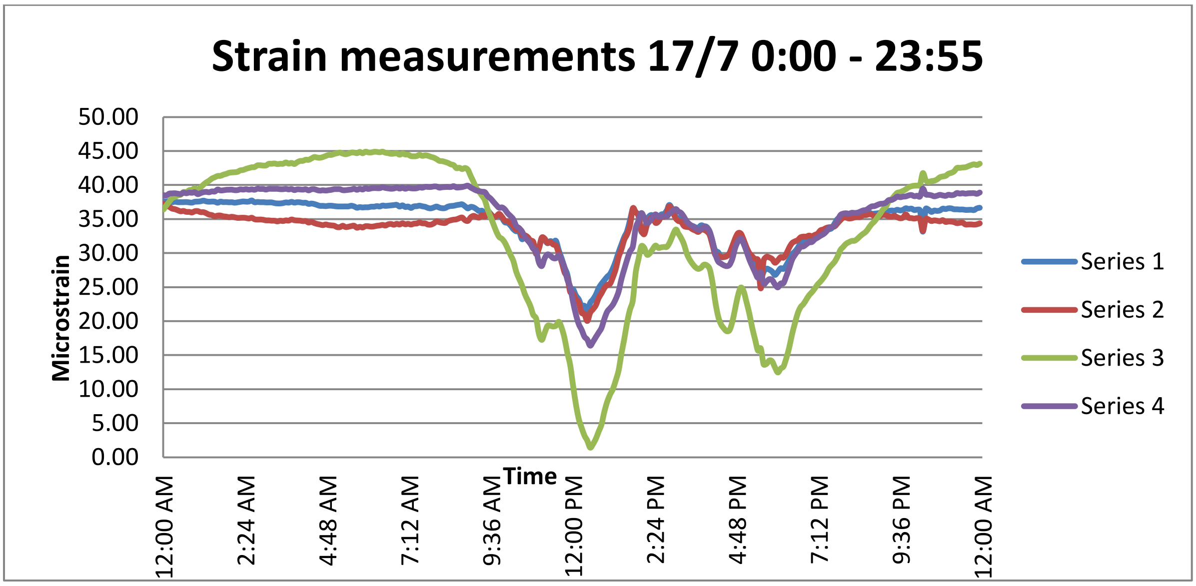

Figure 13.13 Strain measurements 17/7

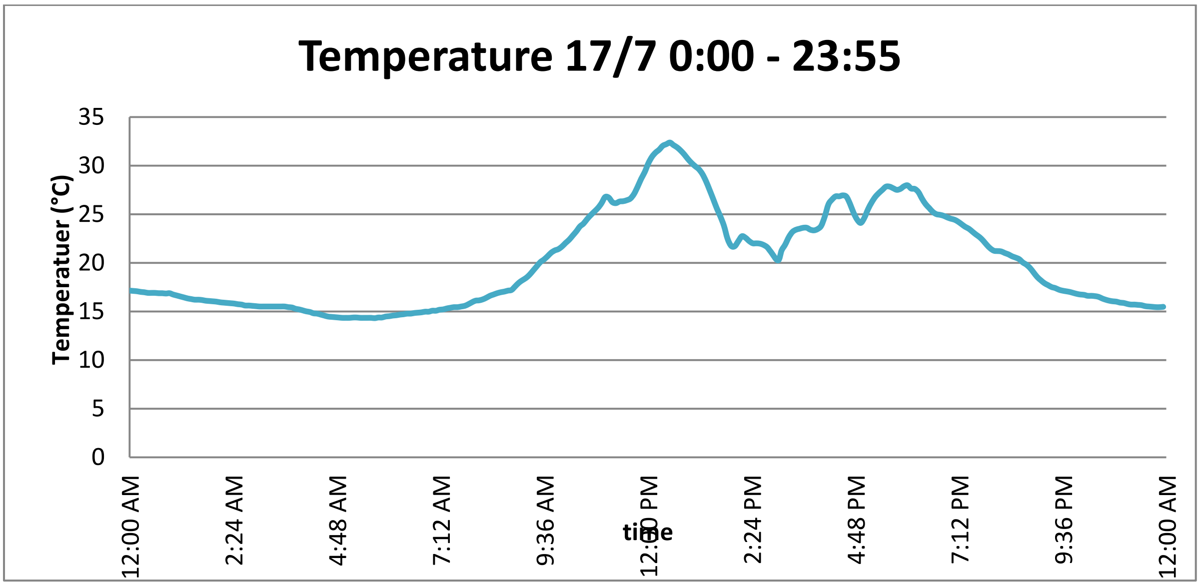

Figure 13.14 Temperature measurements 17/7

Comparing the data of the two days confirms very similar behaviour, with a similar temperature difference similar same strain changes are found. Series 3 does seem to have changed its behaviour; its amplitude is larger than those of the other series are. This could be due to local bending phenomena, where the rail at the location of strain gauge 3 is bended outwards. This in turn increases the measured strain value. This suggestion is further backed by the inverted behaviour of the gauge during cooling, showing an increase in elongation.

Converting the difference of measured strain between strain gauge 3 and 4 (both on opposite sides of the rail) would lead to a curve radius of around 800 meters. This is invisible to the naked eye when present over a length smaller than 4 meters. This length was estimated based on the strain reading of strain gauges 1 and 2, which do not suggest bending at that location (they are on the same side as strain gauge 3).

The largest deviation from a constant measurement is in series 3, in which a temperature change of 17 degrees equals a change in strain of about 40 microstrains. This is on average a relation of 2.3 microstrains per degree, the other relations exhibit even lower coefficients. Even though the influence on temperature changes has been investigated for all sensory components (strain gauge, cable and data logger), and was deemed very small, it cannot be stated that temperature influences are completely irrelevant. These readings might very well be caused due to the temperature influence. It is of great importance to note that, should any significant forces manifest themselves; the deviation from the zero measurement would be many times larger than observed at this point.

For now, it is assumed[1] that these deviations are not caused by temperature influences. The deviations found during temperature influence tests were so small they were deemed unlikely to be the cause. These deviations were found to be:

- For the cables around 2 microstrain per 40 degrees
- For the data logger 0.5 microstrain per 20 degrees (provided the temperature change is relatively slow)
- For the strain gauge, the influence is close to zero when using the compensation curve.

To validate whether the earlier established strain-temperature relation holds for the entire temperature range observed during the long-term measurements the following graph (Figure 13.15) are used. In it is plotted the strain reading of strain gauge series 1, versus the temperature reading at that time. Series 1 is displayed because it has the best consistency of all data sets.

Obviously, the strain-temperature relation does not represent a linear thermal expansion coefficient. In fact, the relation seems to be mirrored around the maximum strain at 19 degrees temperature, with a slope going down on each side. Unfortunately, no data is yet available at lower temperatures to indicate the behaviour on the left side of this point.

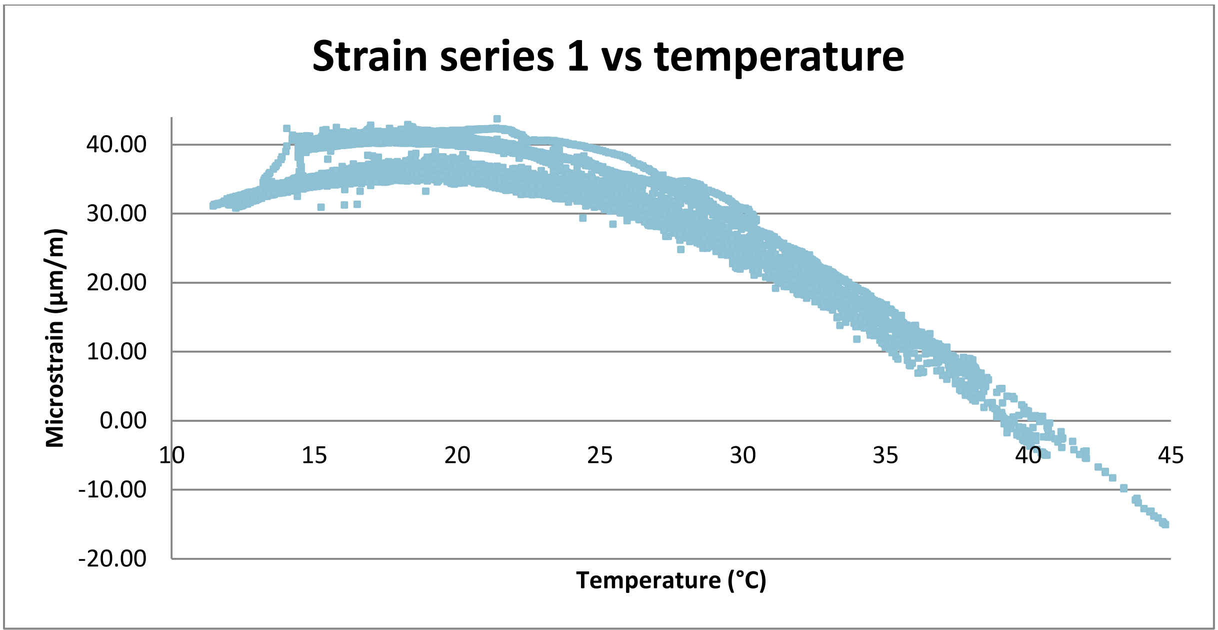

Figure 13.15 Strain series 1 plotted versus the temperature

Even though the graph appears to be very similar to a temperature compensation graph, no definite statement can be based upon this apparent similarity. The non-linear relation might be explained just as well by friction or other mechanical influences that restrain the first expansion of the rail, but are

[1] For the 30-meter rail test, it is advised to place a strain gauge and a temperature sensor on a piece of steel that is free to expand. When this piece of steel is in turn connected to the data logger it can be verified whether there is any temperature influence (deviation from the constant value), and if this is the case, how much this influence is. It is important to use the same type of strain gauge, cable length and data logger for this reference measurement.

of lesser influence once expansion has started. Nevertheless, the temperate-strain relation is found to be so small for temperature up to 30 degrees, that it can be stated with relative certainty that the rail is almost unhindered in its expansion. At higher temperatures, the relation between measured strains and temperature becomes more profound, as displayed in the table below.

Temperature range (°C)	10-15	15-20	20-25	25-30	30-35	35-40	40-45
Strain increase per degree of temperature increase	-0.979	-0.12	0.739	1.598	2.457	3.316	4.175

This relation suggests that at lower temperatures it is easy for the rail to “dissipate” the extra length caused by heating, but that at higher temperatures this becomes more problematic. As a result, at higher temperatures the increase of force due to temperature increases starts to become significantly higher for every degree of warming. A coefficient of 0 indicates free expansion, while a coefficient of 12 indicate a fully fixed situation in which the rail is unable to expand. In the Figure 13.16 the extreme measurements (coefficients of 0 and 12 micro strains per degree of changes) are plotted next to the measured values. The blue constant line indicates sensor output should the rail have been able to expand freely, the orange line indicates sensor output should the rail have been fully fixed. The observed piece of rail therefore appears to be able to expand almost freely at low temperature, as indicated in the table as well. The larger deviation in the green line (sensor 3) indicates a very slight bending of the rail piece.

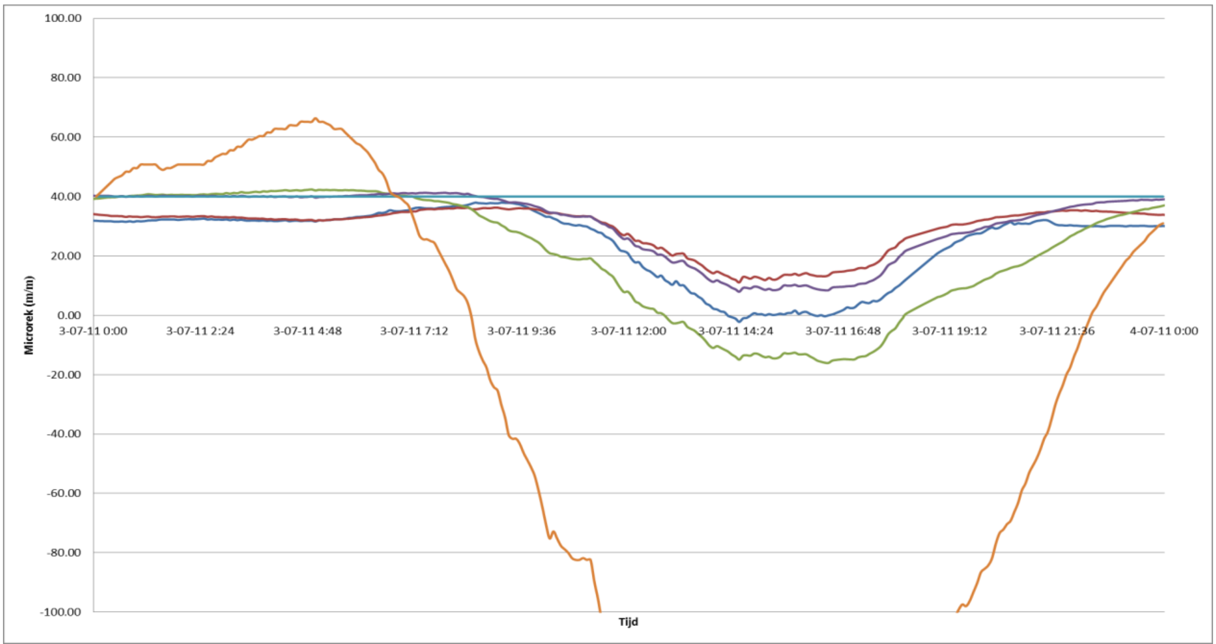

Figure 13.16 Extreme measurement possibilities compared to actual measurements

14 Conclusions

This chapter will discuss the answers to the research questions. These answers are based primarily on chapters 7, 8, 11 and 13.

For easy referral, the research questions are repeated first. These are taken from chapter 3.3. Their order is based upon the order in which they are handled during this research.

Research questions

- What is the best workable method to determine the neutral temperature? (chapter 7)
- Which type of sensors can help ProRail accomplish its goal, what are the drawbacks and costs of these sensors, and which implementation offers the best practical alternative? (chapter 8 and 9)
- What are the critical locations in turnouts and turnout complexes with respect to stresses in the rail? (chapter 11)
- How is rail temperature loading distributed in stresses and deformations? (chapter 13)
- Does the theory match the practical experiments? (chapters 11 and 13)

First, the established answer to the research questions is discussed. These will then be correlated to the sub goals. Lastly any other remaining remarks and conclusions are drawn.

- **What is the best workable method to determine the neutral temperature?**

There are many methods that can be used to determine stresses in rail, and these are discussed extensively in chapter 7. However, due to the restrictions imposed by the rather hostile rail environment and ProRail most of these have to be discarded. These restrictions were; no destructive actions were allowed on the rail, the need to maintain a database should preferably be avoided, and the measurements were not allowed to influence the train movements. Most of all, the applied measurement technique would have to be robust enough to survive the harsh conditions on the rail track. These include maintenance operations and all weather effects. Of all the possible methods all but one were discarded based on these limitations.

- **Magnetic method:** Current practice requires the rail operation to be halted, as the sensor envelops the rail.
- **Vibration method:** No suitable system had yet been introduced on the market that was robust enough.
- **X-ray method:** A very sensitive system, which requires expensive equipment.
- **Deformation method:** The accuracy of this system was not yet proven to be high enough.
- **Ultrasonic methods:** A need for a reference database and the current practice require rail operation to be halted were downsides to this method.
- **Lifting method:** A partly destructive method that requires rail operations to be halted and is hard to apply to turnout elements.
- **Cutting method:** A very destructive and expensive method

The best practical method is the deformation method, in which the stresses in a rail can be determined by measuring the strain and the temperature of the rail. These two parameters are sufficient to establish the stress situation in the rail using formula (6) in chapter 4.5. The best sensor for this obviously is the strain gauge, of which it has been established that they have enough accuracy and can be sufficiently protected to endure in situ conditions. Even though some difficulties were had with the data logger in this particular research, there are plenty of alternatives and possible solutions to prevent similar problems in the future. These solutions will of course be implemented in the 30-meter replacement rail test.

Lastly, it is conceivable that the magnetic and ultrasonic methods will be miniaturized further in the future, making it worth to reconsider them at a later point. At the moment however, these still need to be placed on the rail, to envelop the rail and allow for measurements. This can only be done during maintenance periods in which train traffic is suspended.

- **Which type of sensors can help ProRail accomplish its goal, what are the drawbacks and costs of these sensors, and which implementation offers the best practical alternative?**

When using the deformation method to establish stresses in the rail both a strain gauge and a temperature are required. Without the temperature sensor, it would not be possible to account for the portion of temperature influence that is converted to stresses in the rail. A strain gauge alone would only provide data concerning the portion of temperature influence that is converted into extension of the rail.

In this Thesis, it was proven possible to measure the longitudinal strain with sufficient accuracy using only a quarter-bridge strain gauge. Furthermore, it was proven that these strain gauges are reliable and robust enough to be used for long term measurements, measurements have been on-going for almost two months at the time of publishing. During this time the strain gauges have performed well, the only problems encountered were with the temperature sensors. For more detail regarding these problems, please refer to chapter 13.1.5. Even though the applied method has been proven both practical and workable, improvements can still be applied. For the suggested improvements concerning stress measurements, please refer to chapter 15.1.

- **What are the critical locations in turnouts and turnout complexes with respect to stresses in the rail?**

Unfortunately, no turnout complexes have yet been modelled. However, using the finite element calculations as a guide the most promising locations for strain gauges in turnouts can be identified. This is done based upon the relation between stress and strain. Take note that these locations are solely based on the theoretical calculations and that a practical test on a turnout still has to be performed to validate these results.

To illustrate the following statements, the uncorrected strain diagram belonging to the calculated model with realistic preconditions is displayed in Figures 14.3 and 14.4. The uncorrected outcomes are used because temperature compensated strain gauges will not output temperature strains. Figures 14.1 and 14.2 are provided to facilitate the identification of locations on the graphs.

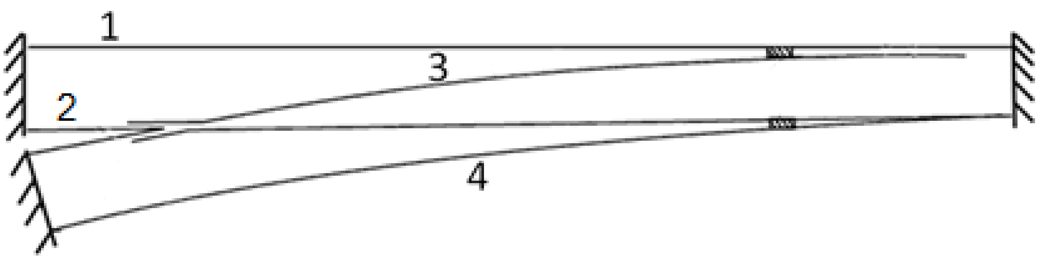

Figure 14.1 Numbering and position overview to clarify the strain graphs

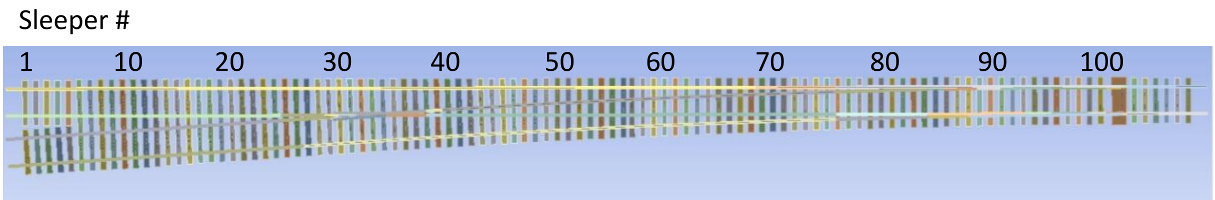

Figure 14.2 Top view of the turnout for reference

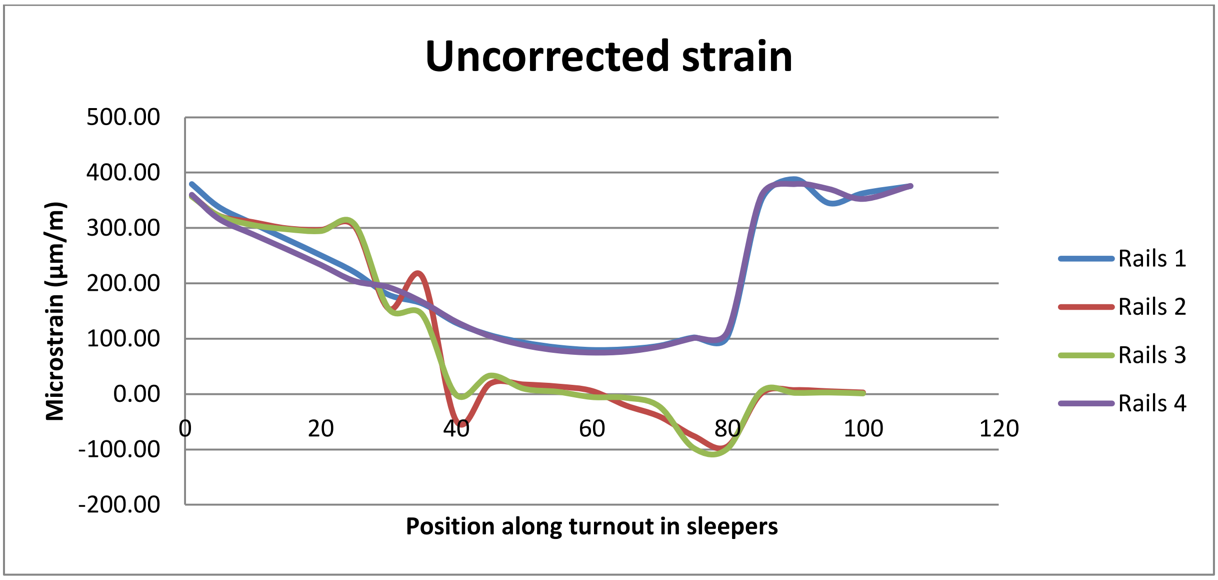

Figure 14.3 Strain after placement (before temperature increase)

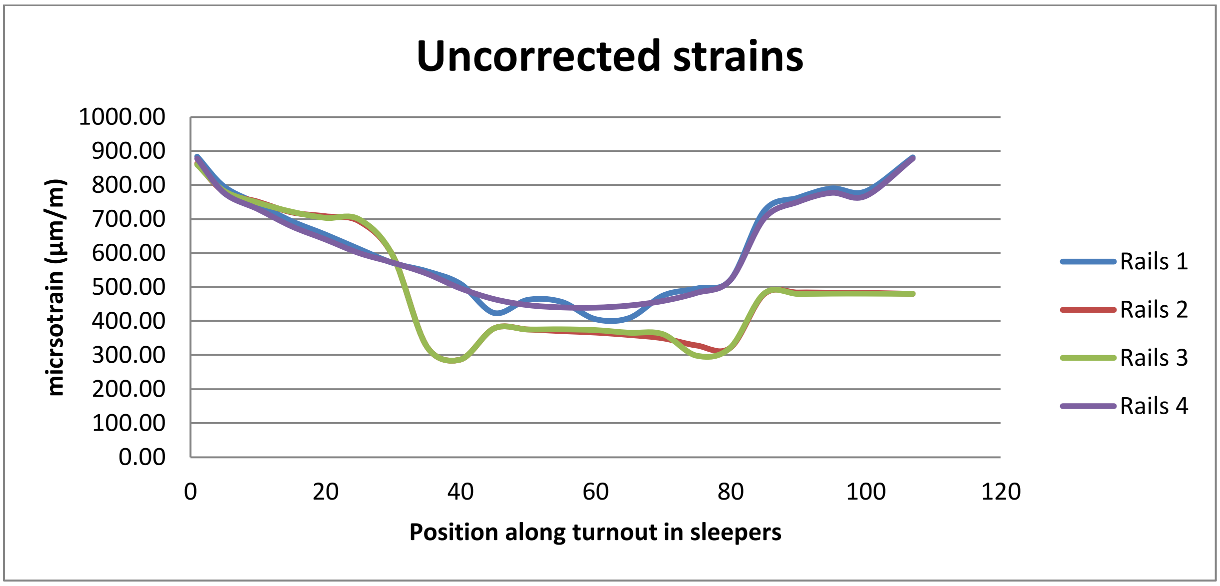

Figure 14.4 Strain after a temperature increase

Two interesting locations can be identified, which are both in the centre of the turnout.

1) On the closure rails (chapter 4.3). Due to the pre heating of this middle section the largest strain displacement in the entire turnout, take place in the centre of the turnout. As an added bonus, when strain is measured on this location the effect of the preheating can be measured, as well as the amount of preheating can be precisely determined. This makes it the best location for both long-term measurements as the location for checking if the placement procedure is done in a satisfying fashion.
2) On the stock rail next to the closure rail, the same changes in strain can be observed as these are coupled to the strains of the closure rail by means of the sleepers and the ball and claw system.

Both locations can be used for long term monitoring of turnout behaviour. Both locations also have a very clear and very direct correlation to the amount of stress in the turnout, as the stress distributions resemble the uncorrected strain distributions very closely. Furthermore, it is advisable also to measure the strain at each of the three turnout ends, this will allow verification of the strain build-up due to the preheating of adjacent rail and the cooling of the weld, providing a full picture of turnout strain behaviour, and coupled with this, the stress distribution.

- **How is rail temperature loading distributed in stresses and deformations?**

Theoretically, an increase of thermal load should have an increase in stresses as its consequence. This is because it is assumed that the rail is unable to extend or compress, due to fixed points along the rail length (turnouts and bridges) and its connections to the sleepers preventing movement relative to the sleeper. The practical experiment showed that the opposite is true, thermal expansion in length direction does not appear to be a problem to rail track, at least on this particular location.

This previous statement is true for temperatures up to around 20 to 25 degrees C. An increase in thermal loading is “divided” over an increase in rail length, and an increase in stress in the rail. When temperatures increase farther, the expansion of the rail becomes increasingly difficult, resulting in a larger portion of the thermal load being converted into stresses.

The replacement rail observed during this research seems to be in a very favourable position with respect to thermal loadings. Its close proximity to a curve downhill is probably the cause of this positive arrangement. This curve will take up a portion of the expansion and stresses caused by thermal expansion and will transfer it sideways or further downhill. During this research, it has become clear that it is easy for rails to move through its connections, thereby facilitating the transfer of stresses and strains towards more critical locations such as curves and slopes.

For this particular replacement piece of rail the temperature – strain relation as found in the data is displayed in table 1 below.

Table 1 Strain increase as present in the data

Temperature range (°C)	10-15	15-20	20-25	25-30	30-35	35-40	40-45
Strain increase per degree of temperature increase	-0.979	-0.12	0.739	1.598	2.457	3.316	4.175

To calculate the forces in the rail one has to consider that every increase of strain in table 1, measured by the data logger, is actually the temperature compensation signal of the strain gauge and not an expansion of the rail itself. Using this fact, the forces and elongation of the replacement rail can be calculated and are presented in table 2.

Table 2 Overview of temperature influence on parameters in real life

Temperature range (°C)	10-15	15-20	20-25	25-30	30-35	35-40	40-45
Force increase per degree (kN)	-1.43	-0.18	1.08	2.33	3.58	4.84	6.09
Strain in the replacement rail (μm/m)	12.98	12.12	11.26	10.40	9.54	8.68	7.82
Elongation of the replacement rail (mm)	0.08	0.07	0.07	0.06	0.06	0.05	0.05

From table 2 it is clear that the higher the temperature is, the more the increase per degree of temperature rise approaches 0 for the strain and elongation, and the theoretical value of 17.5 kN for the force.

- **Does the theory match the practical experiments?**

Unfortunately, due to time limits, delays and budget cuts only two aspects of the relation between theory and practical experiments can be discussed at this moment. The first is the theoretical predictions of the behaviour of the replacement rail; the second is the theoretical prediction of the behaviour of a length of track subject to a change in temperature. The relation between a turnout in situ and the theoretical model cannot yet be specified.

The replacement rail.

Three theoretical predictions were made with respect to the replacing of a rail.

1) The weld shrinkage is about 1.5-2 mm

This was confirmed by the displacement and strain measurements during the weld cool down period. However, the found shrinkage was found to be slightly lower as suggested. This could be due to the variation in weld thickness; a small connection gap would require a small weld, which would shrink less than a large weld due to a large gap. The connection gap in this particular case was found to be relatively small.

2) Due to the weld shrinkage, the neutral temperature of a replacement rail would increase.

This too was confirmed, measurements indicate an increase in neutral temperature of 2.3 degrees C for a 6-meter rail. It is expected that a 30-meter rail, which is 5 times the length, would experience a neutral temperature increase 5 times smaller. This will be confirmed by the 30-meter replacement rail test, which unfortunately can no longer take place in the span of this research, but has been prepared and all equipment has already been bought during the course of this research.

3) The adjacent rail would not be able to move due to the fixation of the sleeper-rail connections, thereby all of the weld shrinkage would be transferred to the replacement rail

This statement was found to be false, the adjacent rail during the 6-meter replacement rail test moved towards the rail with an amount of 0.8-0.9mm on both respective sides. In fact, most of the weld shrinkage was compensated by this movement, and only a relatively small fraction was applied to increasing the strain in the replacement rail (replacement rail extension was about 0.17mm in total, so about 10% of the force build-up due to weld shrinkage was transferred to the replacement rail). The fixation by the sleeper-rail fasteners was overestimated, and it appeared to be quite easy for the adjacent rail to move through it. These findings suggest a review of the current guideline practice to loosen the fastenings on either side of a rail replacement of up to 30 meters could be considered. This requirement might be able to be reduced or even omitted. This of course warrants more research to be done with respect to this particular phenomenon, as it is very dependent on the type of fasteners used.

15 Recommendations

There are a number of recommendations that need to be done. There are of course the two required practical tests, the 30-meter replacement rail and the turnout, of which it is suggest in the strongest possible way to execute these, regardless of future budget cuts or other obstacles. The 30 meter replacement rail test will be able to validate all results obtained so far, and will clarify even more of the processes that occur during rail replacement;

- Establishing the total rail displacement due to welds (rail and sleeper) instead of just the rail-sleeper displacement
- Clarifying the effects of the guidelines for replacement pieces larger than 20 meters (which differ greatly from the guidelines for a 6 meter piece)
- Establishing the length of the adjacent rail in which the forces due to welds are present (i.e. finding the so called anchor length by extrapolating the length over which the strain increase due to welding reaches zero)
- Confirming whether the heating or stretching techniques deliver the required increase of neutral temperature

The reasons for the practical test on the turnout to be executed are:

- To validate the theoretical model
- In conjunction with the previous point, to establish the force distribution in the turnout as a result of temperature changes
- To establish the force distribution in the turnout as caused by the welding of the separate turnout components.
- To establish the amount of force transferred to the sleepers and thereby the substructure as a result of these temperature forces.

For the theoretical model, after it is validated, it is recommended:

- To expand it to model crossings and turnout complexes
- To investigate the theoretical fixed connections to the adjacent track, theoretically these are correct (chapter IV.ii), but the practical test shows these might be more like free expansions.
- To improve and update the parameters used for the model (the spring values for ballast and connections are taken from previous research are out-dated and based upon old ballast types and connections)
- To research the difference between turnouts with different radii
- To improve modelling of non-crucial components such as the point machine and check rails.
- To research the effect of a curve adjacent to a turnout

For the application of sensors on the rail, it is recommended to research a more robust way of measuring the strain, or even better, of directly measuring the force. Once again, the reader is referred to the conclusions for a suggestion as to how these measurements can be improved greatly.

It is recommended to attach a “dummy” strain gauge on a piece of steel able to expand freely for use in the 30-meter rail test. This will allow absolute temperature correction. It is also recommended to measure the behaviour of rail in a less favourable position, between two fixed points or at the bottom of a slope. This will in all likely hood reveal a much more critical relation between temperature and force.

The last recommendation is to share the found knowledge with the contractors, engineering firms and other rail network companies, and to use these findings and their cooperation to improve rail maintenance guidelines even further. This will in turn lead to lesser breakdowns and maintenance operations on the rail, increasing passenger comfort and reducing total maintenance costs.

15.1 Improved strain sensor implementation

Not so much a recommendation as a suggestion to improve workability and practicality of stress measurements the following method is suggested.

At this moment, strain gauges coupled with temperature sensors, are still the best proven and workable method to determine the neutral temperature. They are a non-destructive type of measurement and can be attached relatively easy. However, due to recent developments ProRail is no longer completely opposed to minor destructive methods. In one of the internal discussions, it was no longer considered unthinkable to drill a hole in the rail, which it unfortunately was at the start of this research. This change in viewpoint opens up an excellent opportunity for further research by integrating a strain gauge measurement inside the rail. A short description of the, in the opinion of the author, ideal solution for the future shall be provided.

The solution proposed comprises a cylindrical instrument that is placed inside a small hole in the web of the rail. When a hole is drilled inside a structure subject to tension or compression the hole deforms, as illustrated in Figure 15.1 (not to scale). Using this knowledge, it is suddenly possible to measure the force in the rail via the relation between the compression of the hole and the force in the rail. A similar concept has already been tried in Italy, but it was applied to determine axle loads. The benefit of this set up is that the stress in the rail can be measured directly, without the need for a reference temperature measurement and the corresponding calculations.

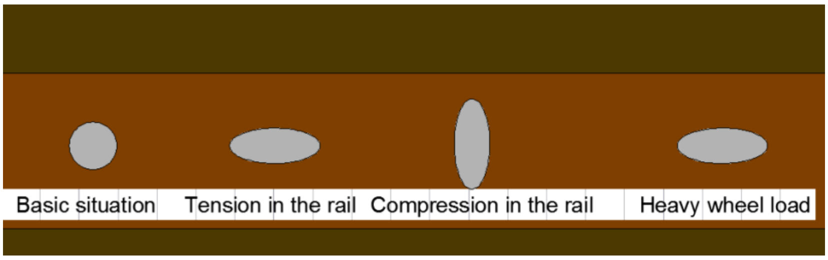

Figure 15.1 Deformation of a hole subject to compression and tension (not to scale)

In the proposed instrument, two strain sensors and a temperature sensor would be implemented. The two strain gauges are to be positioned vertically and horizontally, measuring both the compression and extension of the hole. Very stiff glue would be used to position the sensor, to measure the strain as directly as possible. The temperature sensor would provide feedback to determine the force relation/temperature relation for this particular piece of rail; it is not needed to calculate the stress. Because the deformation of the hole can be very accurately and easily calculated, for instance with the help of a software package such as Ansys®, the relation between deformation and force can be easily determined. A simple laboratory test would confirm these calculations, and almost all equipment for this test is already available to ProRail. Readymade sensors for measuring the forces and deformations are also already available on the market.

There might still be room for further improvement by using the newly developed SAW sensor system, applying these sensors as both strain gauges and temperature sensors would allow all of the data to be read wirelessly. For instance by a device mounted on a moving train, or a handheld device operated by an inspector.

A first quick inquiry into the strains that would occur in a hole with a diameter of 20mm suggests values of 21 microstrains per degree C of temperature change. 21 Microstrains per degree C is well within strain gauge accuracy as established during this research. Forces should therefore be able to be determined well within a single degree (of temperature) of accuracy.

16 References

Publications

[1]. *Measuring axial forces in rail by forced vibrations: experiences from a full-scale laboratory experiment.* **Johnsonn, E and Kjell, G.** 2009, ImechE vol 223 part F.

[2]. *Achieving neutral stresses in a renewed switch and crossing*. **S Boogaerdt.** 2009, TUDelft Master Thesis.

[3]. *Stability of continuous welded rail.* **M.A. Van**, 1997

[4]. *Modern railway track second edition*. **Coenraad Esveld**, 2001

[5] *profile programm,* **Voestalpine**

[8] *Thermal imaging of railways to identify track sections prone to buckling*, **I Chapman, J E Thrones, S P White**, 2006

[9] *A model for predicting the effect of temperature force of continuous welded rail track***, Y luo**, 1999

[10] *Investigation of the influence of track maintenance on the lateral resistance of concrete tie track,* **T Sussman, A Kish, M Trosino**, date unknown

[11] *Risk analysis based CWR track buckling safety evaluations,* **A Kish, G Samavedam,** date unknown

[19] *LONGSTAB theoretical manual*, **Esveld**, 2004

Internet websites:

[6] http://www.wikipedia.org

[7] http://www.halcrow.com/Global/Images/climate_change/rail_buckle_512.jpg

[12] http://www.Volkerrail.co.uk/bin/ibp.jsp

[13] http://www.lesico.com/english/List.aspx?Item=358

[14] http://www.thermit-welding.com/images/technology/02.jpg

[15] http://www.ndt.net/article/dresd97/szelazek/fig3.gif

[16] www.thermit-welding.com

[17] http://www.goldschmidt-thermit.com/en/index.php

[18] http://esveld.com/

[20] http://www.efunda.com/formulae/solid_mechanics/mat_mechanics/strain_gage_rosette.cfm

17 Table of Figures

Figure 4.1 Typical track structure [4] 17
Figure 4.2 UIC 54E1 rail profile, sizes in mm, scale 1:1 [5] 18
Figure 4.3 Old fishplate joint [6] 19
Figure 4.4 Thermite weld 19
Figure 4.5 Buckling example [7] 20
Figure 4.6 Hooke's law basic situation [6] 23
Figure 4.7 Force and expansion in continuous welded rail near an open end according to plastic shear theory [4] 24
Figure 4.8 Rail elongation by heating (using heating blankets) [12] 24
Figure 4.9 Rail elongation by hydraulic jack 25
Figure 4.10 Igniting the thermite 26
Figure 4.11 Hydraulic shearing device (left) and grinder (right) [4] 26
Figure 4.124 Mobile flash butt welding equipment [13] 27
Figure 4.135 A turnout and its important parts [4] 28
Figure 7.1 Cut and marking method 34
Figure 7.2 Stress measuring by the lifting method [14] 35
Figure 7.3 Deformation measurements with a strain gauge 35
Figure 7.4 Ultrasonic measurements [15] 36
Figure 7.5 overview of the SAW system 36
Figure 7.6 Principle behind x-ray stress measurements [1] 37
Figure 7.7 Principle behind the electromagnetic stress measurements 37
Figure 8.1 Using a zero stress reference 39
Figure 8.2 Using a stress measurement as reference 39
Figure 8.3 Overview of the strain development when placing a replacement rail 41
Figure 8.4 Strain gauge outputs 42
Figure 10.1 Model overview 47
Figure 10.2 The spring stiffness determination 48
Figure 10.3 Left to right: geometry, rotational load, displacement in X direction 48
Figure 10.4 Railpad material 49
Figure 10.5 Straight track model, with a force on both rail ends. 50
Figure 10.6 Force displacement relation of the non-linear spring element 52
Figure 10.7 Springs in the model 53
Figure 10.8 Turnout overview 54
Figure 10.9 Sleeper material 55
Figure 10.10 Rail material 55
Figure 10.111 Slide plates 57
Figure 10.12 Modelling methods properties 59
Figure 10.13 Ball and claw system of this turnout 61
Figure 10.14 Turnout with fixed supports on all sides 62
Figure 10.15 Heated turnout with fixed supports on all sides 62
Figure 10.16 Cooled down turnout with fixed supports on all sides 62
Figure 10.17 Heated turnout with 2 out of 3 supports fixed, and one free 62
Figure 10.18 Turnout constructed according to the ProRail guideline 63
Figure 11.1 Rail numbering 64
Figure 11.2 Top view of the turnout for reference 64
Figure 11.3 Data request location 64
Figure 11.4 Strain variation over the height of the rail profile 65
Figure 11.5 The boundary conditions for the model 65

Figure 11.6 Uncorrected strain distribution in the model ... 66
Figure 11.7 Stress distribution in the model ... 66
Figure 11.8 Corrected strain ... 67
Figure 11.9 Displacement in length direction, along the turnout length ... 68
Figure 11.10 Lateral displacement in the model ... 69
Figure 11.11 Boundary conditions of the model ... 69
Figure 11.12 Corrected strain in the model ... 70
Figure 11.13 Stress in the turnout model ... 71
Figure 11.14 Displacement in length direction in the model ... 71
Figure 11.15 Displacement in lateral direction ... 72
Figure 11.16 Displacement in the lateral (z) direction at the crossing. Red is maximum (positive) displacement, blue minimum (negative). Scale 1:200, displacement scaling 100x. ... 72
Figure 11.17 Boundary conditions of the turnout ... 73
Figure 11.18 Comparison of strain between linear and non-linear supported model ... 73
Figure 11.19 Stress comparison between linear and non-linear supported model ... 74
Figure 11.20 Comparison of displacement in length direction between the linear and non-linear supported models ... 74
Figure 11.21 Comparison of the lateral displacement between the linear and non-linear model ... 75
Figure 11.22 Corrected strain output in the turnout model ... 77
Figure 11.23 Stress distribution in the turnout model ... 77
Figure 11.24 Displacement in length direction in the turnout model ... 78
Figure 11.25 Lateral displacement in the turnout model ... 78
Figure 11.26 Corrected strains in the turnout model ... 79
Figure 11.27 Stress distribution in the turnout model ... 80
Figure 11.28 Stress distribution comparison between basic construction and following of the guidelines ... 81
Figure 11.29 Displacement in length direction in the model ... 82
Figure 11.30 Displacement in lateral direction in the model ... 82
Figure 12.1 Loading and temperature cycle ... 86
Figure 12.2 Strain distribution during laboratory test ... 87
Figure 12.3 Sensor placement ... 88
Figure 12.4 DVRT "strain" set up ... 88
Figure 12.5 The temperature distribution during the first lab test (combined temperature and mechanical load) ... 89
Figure 12.6 The load over time during the first lab test (combined temperature and mechanical load) ... 89
Figure 12.7 Temperature distribution ... 90
Figure 12.8 Test rail ... 90
Figure 12.9 The load cycles during the second compression only test ... 91
Figure 12.10 The LVDT readings during the first compression only test ... 91
Figure 12.11 Temperature distribution during the third laboratory test (temperature load only) ... 92
Figure 12.12 Temperature compensation curve prescribed by the manufacturer ... 93
Figure 12.13 LVDT placement and displacements ... 94
Figure 12.14 Deformation ... 94
Figure 12.15 Double bowl structure ... 95
Figure 12.16 Loading plate deformation ... 95
Figure 12.17 Strain gauges output during temperature changes ... 96
Figure 12.18 Strain gauge output with heating current influence ... 97
Figure 12.19 Difference between Bienfait and MM strain gauges under temperature changes ... 97
Figure 12.20 Strain gauge outputs under loading ... 98
Figure 12.21 Strain gauge output variation under zero load ... 98
Figure 12.22 Strain gauge readings under maximum load ... 99

Figure 12.23 Difference between the MM strain gauges 99
Figure 12.24 LVDT measurements during the temperature test 100
Figure 12.25 Axial, tangential strain and their linear relationships 101
Figure 12.26 Average MM and Bienfait strains vs. theoretical strain third compression test 102
Figure 12.27 Bienfait strain gauges vs. MM strain gauges second compression test, third loading 102
Figure 12.28 Overview of the errors and the frequency they occur 104
Figure 12.29 Overview of the errors and the frequency at which they occur 105
Figure 12.30 Overview of the errors and the frequency at which they occur 106
Figure 12.31 Possible strain distributions in replacement rail 107
Figure 12.32 Displacement measuring set up 108
Figure 12.33 Sensor locations marked 109
Figure 12.34 Sensor locations grinded down 109
Figure 12.35 Sensors fitted on the rail 110
Figure 12.36 6-meter data acquisition 110
Figure 12.37 30-meter data acquisition 110
Figure 12.38 Rosette strain gauge [20] 111
Figure 12.39 Situation at rail stressing 112
Figure 12.40 Situation overview 114
Figure 12.41 Track alignment 115
Figure 12.42 Situation after instalment of the sensors (discoloured bit of rail) and a site overview 115
Figure 12.43 The crane lifting the replacement rail from the container 116
Figure 12.44 The inside of the sensor protection. The brown rectangle is the strain gauge (quarter bridge); above it is the temperature sensor (PT1000) 116
Figure 12.45 Placement by Stork employees Figure 12.46 DVRT set up overview 117
Figure 12.47 DVRT set up, DVRT detail 117
Figure 12.48 Data logger position during cool down 118
Figure 12.49 Final position of the data logger 119
Figure 13.1 Situation overview 121
Figure 13.2 Strain gauge output (unaltered) 122
Figure 13.3 Distinct situations during measurement 122
Figure 13.4 Strain output without interference 124
Figure 13.5 Strain output relative to zero measurement 124
Figure 13.6 DVRT1, closest to the first weld 126
Figure 13.7 DVRT 2, closest to the second weld 126
Figure 13.8 Temperature during replacement 128
Figure 13.9 Thermal image of the weld cooling down 128
Figure 13.10 The DVRT on the left, the weld in the middle, and the strain and thermal sensor to the right (1.2 m from the weld) 129
Figure 13.11 Strain measurements 16/6 until 17/6 131
Figure 13.12 Temperature measurements 16/6 - 17/6 132
Figure 13.13 Strain measurements 17/7 132
Figure 13.14 Temperature measurements 17/7 133
Figure 13.15 Strain series 1 plotted versus the temperature 134
Figure 13.16 Extreme measurement possibilities compared to actual measurements 135
Figure 14.1 Numbering and position overview to clarify the strain graphs 138
Figure 14.2 Top view of the turnout for reference 138
Figure 14.3 Strain after placement (before temperature increase) 138
Figure 14.4 Strain after a temperature increase 139
Figure 15.1 Deformation of a hole subject to compression and tension (not to scale) 143

Appendix

Table of contents

I. Metallurgy III
 i. General steel introduction III
 ii. Weld ability of steel IV
 iii. Rails manufacturing V
II. Interview with Ruud van Bezooijen Id2 engineering VI
 i. Algemeen VI
 ii. Las VI
 iii. Railpads VI
 iv. Belangen VI
 v. Rotatie liggers VII
 vi. Nieuwbouw VIII
 vii. Schaduw en zon VIII
 viii. Ankerlengte/relaxatie VIII
 ix. Vastzet richting bij verwarmen IX
 x. Locatie van verwarmen IX
 xi. Metallurgie IX
 xii. Bogen X
 xiii. Wissel X
 xiv. Verbetering RLN120 XI
 i. Normal elastic strain (y-direction) XIII
 ii. Thermal strains XIII
 iii. Normal stress (y-direction) XIV
 iv. Displacement x direction (vertical) XVI
 v. Displacement Y direction (longitudinal) XVII
 vi. Displacement in z direction (lateral) XIX
 vii. Conclusion XX
IV. Short investigations into model behaviour XXI
 i. Linearity of the model XXI
 ii. Fixed connections XXI
V. Sensitivity analysis XXIII
 i. Stresses XXIII
 ii. Stresses XXV
 iii. Displacements in the length direction XXVI
 iv. Displacements in the lateral direction XXVII
 v. Conclusion XXVIII
VI. Practical situation at a temperature increase of 60 degrees XXIX
 i. Stresses and strains XXIX
 ii. Displacements XXX
VII. Comparison between the two possible modeling solutions for the switchblade. XXXI
VIII. Strain gauge application XXXIV
IX. Lab test execution XXXIX
X. Stork lab rapport (Dutch) XLI
XI. Model results LI
XII. DVRT mounting trial test, and preliminary conclusions LII
 i. Description of DVRT mount trial test. LII
 ii. Conclusion LV

I. Metallurgy

Thermite welding is a crucial part of CWR rail practice. To get a weld of good quality it is of importance to tune the weld procedure to the desired result and the steel qualities and types of the rail. To this end, an introduction into the metallurgical qualities and processes is a valuable extra.

i. General steel introduction

Steel properties can be varied greatly by its chemical composition and production conditions. The definition of steel is by weight mostly iron with <2% carbon and containing other elements. The Figure below is the iron-carbon phase diagram. This Figure describes different microstructures in the steel. The forming of these structures is a function of the carbon content and the temperature at which the steel is heated.

Austenite is a structure in which all the carbon is dissolved in the austenite. When it is cooled down slowly the austenite transforms into pearlite, which is a combination of ferrite and cementite, in which the cementite (chemical compound Fe_3C) is deposited in a lamellar structure. Pearlite is a strong crystal structure, which gives steel its strength.

Rapid cooling causes Martensite to form in the steel solution. The fast cooling traps carbon atoms that do not have time to diffuse out of the crystal structure. Martensite is a brittle structure, with needle like shapes. These needles cause large stress concentrations in the steel structure, having a negative effect on fatigue behaviour. Martensite can be easily transformed back to austenite by heating the steel. Martensite is not in the Figure below, as it is not an equilibrium phase. Depending on carbon content, Martensite forms at a temperature between 350 and 200˚C.

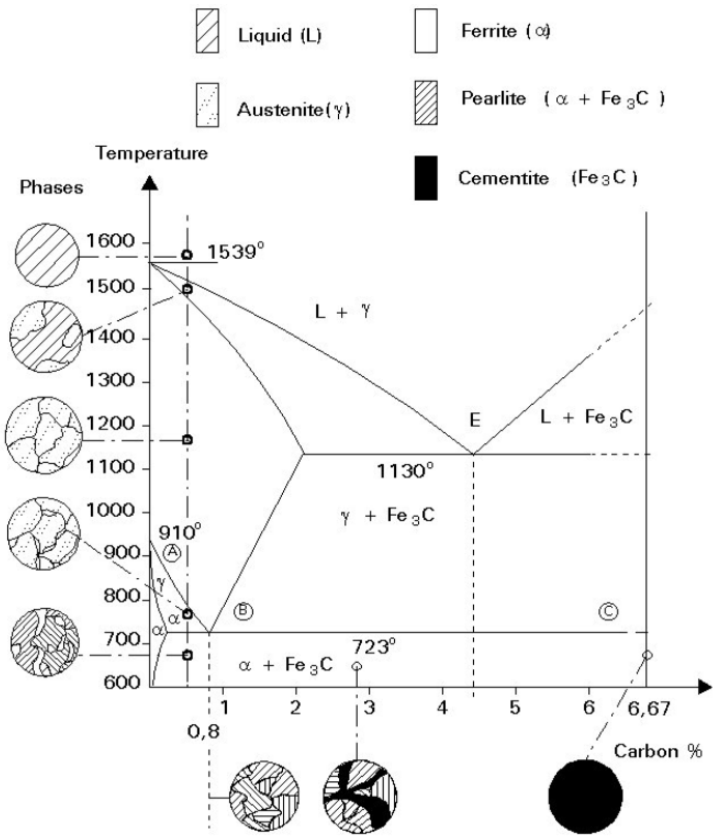

A cooling curve is shown in the Figure below. This curve is valid for an R260 material, which is the steel grade for most rails. In the outer rail in curves and for certain special constructions such as turnouts R 350 HT and 1% Cr steels such as MHH (Micro head hardened and R370LHT are used due to their higher resilience to wear. The Figure below shows the cooling curve of a batch of steel. The closer this curve approaches the right side of the nose of the curve, the finer the pearlite structure becomes and the better the properties are. The benefit of the rolling process is illustrated as well.

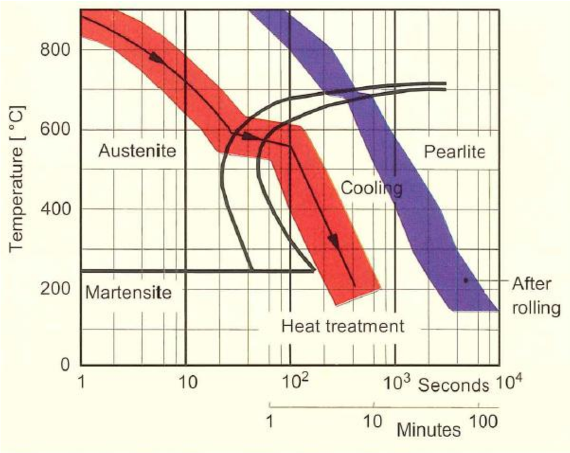

Figure 10.26: TTT-diagram for grade R 260 (900 A) with cooling curve for heat treatment

In the Netherlands R260 Mn steel is used instead of R260, this contains between 0.03 and 0.035% extra manganese. The reason for this is that R260Mn has a higher resistance to a type of pit corrosion, which occurs when the rail is placed in a moist environment. These pits are very likely to reduce the fatigue life of the rail.

ii. Weld ability of steel

The weld ability of a steel product is judged based on its tendency to cold cracking and the toughness of its heat-affected zone. Increasing the content of alloying elements decreases the weld ability, while a fine grained steel increases the weld ability. This fine grain can be achieved by rolling the steel under a press. This forces the grains to elongate which leads to recrystallization of the grains to a finer distribution. Another way to achieve this is normalising the steel, which comprises reheating the steel to the austenitic region, and cooling it slowly causing the austenite to disappear while a fine pearlite forms in its place. This also increases the tensile strength of the steel.

The rate of cooling influences the susceptibility to cold cracking. Preheating the rail reduces the cooling rate, as the hot weld material does not come into contact with cold material, but with the pre-heated material. Cold cracking can be even worse in head hardened or special grade rail (for example R370LHT), in these situations, the cooling process has to be adjusted to the specific material in use. Otherwise, the crystal structure of the material can be disturbed, causing the loss of its beneficial properties. When welding, the cooling curve must conform to the one illustrated earlier, lest Martensite should form.

During the welding process, part of the heat affected zone is welded to over 720 degrees C, causing pearlite to be transformed into austenite. By subsequent cooling, the austenite should retransform into pearlite. Whether or not this actually happens depends on the steel's chemical composition and the rate of cooling. Faults can therefore not only occur in the weld itself, but could also occur in the heat-affected zone.

Another possibility is to "upgrade" Martensite that has formed. This procedure allows the Martensite to be used in benefit of the strength and wear resistance. This can be done by allowing the weld to cool to a maximum of 180˚C, then heat it to 450˚C and to keep it at this temperature for a certain amount of time. The Martensite will then transform into a structure with a lower energetic condition and become globular in shape (instead of needle like). This will reduce the chances on cracks in the steel, while preserving the wear resistance of the steel.

iii. Rails manufacturing

Rails are produced by casting batches of steel that is hot rolled into the rail shape. After cooling, the rails have to be cold rolled to compensate for the deformation of the rail during cooling. This deformation is caused by the railhead cooling at a different rate than the rail foot. The batching process at which the steel is produced means that there are small differences in chemical make up between two rolling batches. Within a single batch there are differences as well. The chemical composition of the molten steel in the bottom of the ladle differs slightly from that in the top.

II. Interview with Ruud van Bezooijen Id2 engineering

i. Algemeen

Ruud is al jaren werkzaam in de railbouw, als projectleider en lascoördinator en is nu eigenaar van zijn eigen ingenieursbureau en raillasbedrijf. Tijdens dit gesprek zal Ruud zijn observaties en theorieën met betrekking tot het voegloos en op neutraaltemperatuur brengen van het spoor met ons delen. Ook worden eerder uitgevoerde onderzoeken die van belang zijn besproken.

ii. Las

Het eerste onderwerp was de las zelf. Ruud gaf aan dat er metingen verricht waren op 25 lassen door Harry Voets van BAM en van Etikhoven van Movaris in opdracht van Prorail. Dit in het kader van het voegloos maken van spoor, uit deze metingen is gebleken dat lassen 2 mm krimpen tijdens de afkoelperiode.

iii. Railpads

Het volgende besproken onderwerp waren de railpads, en hun gedrag als de bevestigingen losgemaakt zijn. In theorie moet los gemaakte rail vrij uit kunnen zetten en inkrimpen, dit is ook het idee achter het losmaken van de bevestigingen alvorens rails door te snijden. Ruud heeft geobserveerd dat de railpads aan de rails en de liggers “blijven plakken”, de pad heeft (vaak) een u vorm waardoor deze niet uit de stoel kan verplaatsen. Hierdoor wordt er dan wel een kracht over gebracht op de liggers. Ruud merkt hier over op dat dit er voor zorgt dat als er getrokken wordt op kracht, dat de kracht in de rails dan niet overeen zal komen met de kracht die de trekapparatuur aan geeft. Ruud zijn oplossing hiervoor was om de rail “door te trekken” tot de railpads losschieten, daarna de kracht er weer af te halen, en dan op de juiste kracht de rails alsnog aan te trekken.

Commentaar van ProRail: Het is daarom dan ook gebruikelijk om bij het opzetten/neutraliseren van de spoorstaven deze op rolletjes te leggen waardoor de spoorstaaf los van de nieuwe onderlegplaatjes of van de inmiddels losgemaakte onderlegplaatjes kan verplaatsen.

Een andere oplossing is met een zogenaamd mes aan de arm van een atlas de pads onder de rail vandaan te rijden.

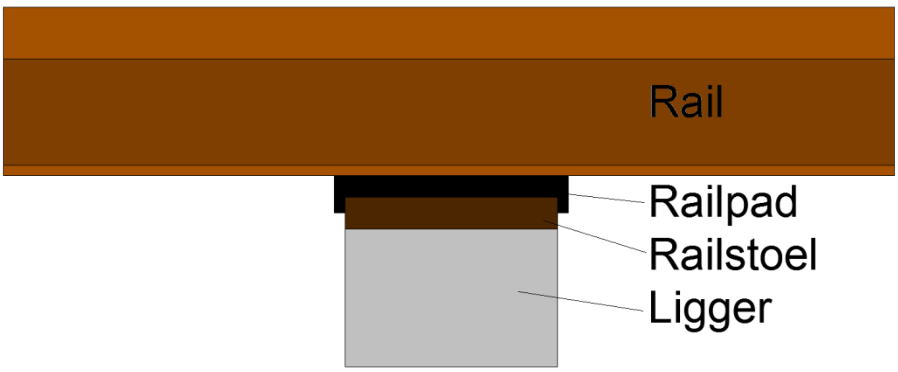

iv. Belangen

Ruud benadrukt dat er belangen verschillen spelen in de railbouw, en dat hij hier graag iets van terug zou willen zien in mijn afstudeerverslag. Hierbij is het volgens Ruud van belang dat er aandacht besteed wordt aan de discussie die gaat over het op kracht of op neutraal temperatuur. Hierbij is het voor ProRail logisch om op neutraaltemperatuur te specificeren, maar omdat de aannemer praktische waardes nodig heeft is het voor de aannemer het makkelijkst om op bijvoorbeeld kracht of verlenging te werken.

Commentaar van ProRail: Een aannemer heeft een groot financieel belang bij goede resultaten. Het hydraulisch verlengen gebeurt wel echter altijd op basis van de theoretische verlenging incl het aftekenen. Alleen op kracht is niet betrouwbaar vanwege de eerder beschreven problematiek van ontstaan van wrijving bij ook evt. scheve dwarsliggers. Bij de korte stukken spoorstaaf neutraliseren wordt eigenlijk praktisch altijd verwarmen toegepast. Bij grote aantallen pastukken wordt ook de SuperPuller[trekken en stomplassen] toegepast

v. Rotatie liggers

Vervolgens werd naar aanleiding van onze eerste praktijkproef de situatie besproken waarbij er een van de twee railstaven doorgesneden wordt. Er wordt in deze situatie aangenomen dat beide rails op de correcte neutraaltemperatuur zijn van 25 graden. Bij het lossnijden gebeurt volgens Ruud zijn observaties, en volgens het theoretisch model, het volgende:

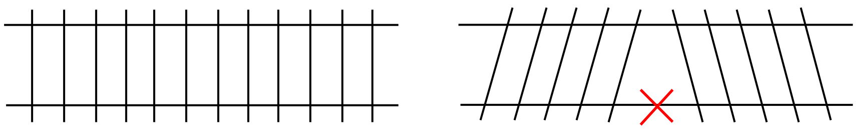

Bij het kruis wordt de rail doorgesneden. De rail hier trekt zich terug, en trekt daarbij de liggers mee, welke op hun beurt roteren om de andere bevestiging. Bij het praktische experiment is dit redelijk vanzelfsprekend, aangezien alle bevestigingen nog vast zaten. Ruud heeft dit echter ook geobserveerd bij situaties waarin de bevestigingen losgehaald waren. De spanningen die door de "plakkende" railpads overgedragen kunnen worden zorgen voor een zelfde soort verplaatsing.

Als de ligger ten opzichte van de rails roteert manifesteert zich een ander fenomeen. Hiervoor moeten we in detail kijken naar hoe de rail in de railvoet zit. Links staat een bovenaanzicht van een 54E1 rail geplaatst in een willekeurig bevestigingsplaatje. Rechts staat wat er gebeurd als de ligger ten opzichte van de rails roteert. In deze situatie komt de rail in contact met de bevestiging. Op deze punten ontstaan dan hoge spanningen en daardoor kunnen door wrijving grote krachten overgedragen worden. Als gevolg van deze krachten kunnen verplaatsingen van de rails doorgegeven worden aan de liggers, en vice versa. Hetzelfde gebeurd uiteraard ook als de rail in zijn bevestiging roteert.

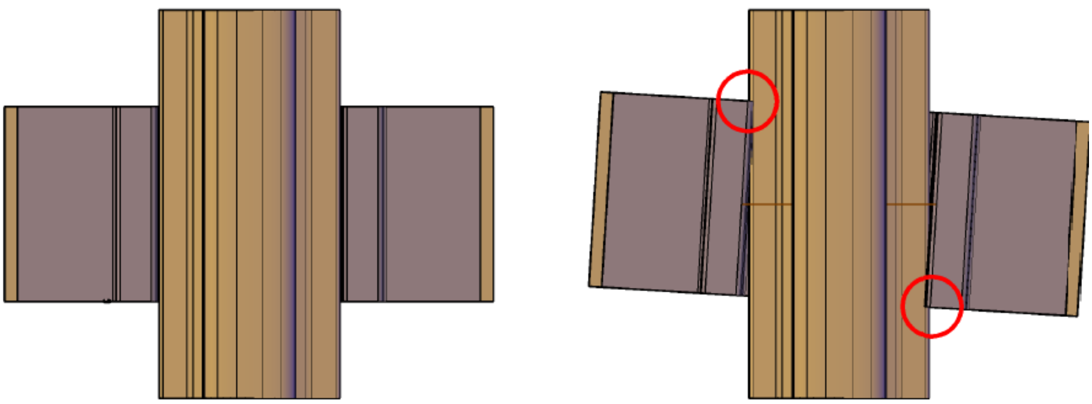

Dit fenomeen is ook in bogen een erg interessant fenomeen, het uitzetten van de rails door warmte drukt deze in een boog ook opzij, waardoor er een wrijving met de bevestigingen ontstaat. Als er dan bij een temperatuur hoger dan de neutraaltemperatuur in de rail een snede gemaakt wordt kan deze wrijving ook voor verplaatsingen zorgen. Het is overigens gebruikelijk om in bogen verwarmingsapparatuur in combinatie met fixeerapparatuur te gebruiken.

Omdat bij nieuwbouw aan beide railstaven tegelijk getrokken wordt zal dit fenomeen daar niet voorkomen, er wordt met dit fenomeen rekening gehouden. Bij onderhoudswerkzaamheden gebeurd dit echter niet.

vi. Nieuwbouw

Het volgende besproken onderwerp is in de nieuwbouw situatie, daar wordt door de voorschriften voorgeschreven dat de rails elke 10 dwarsliggers door een roller ondersteund moet worden. Ook moeten elke 30 meter bij verwarmen, of elke 60 meter bij hydraulisch trekken, streepjes op de rails en de bevestigingsplaat gezet worden om te controleren of er genoeg verlenging in de rails is aangebracht. Door ProRail is vervolgens een tabel aangeleverd waarin de verlengingsafstanden, de theoretische krachten, en de toe te passen krachten vermeld staan voor verschillende lengtes van het nieuw aangelegd spoor. Hierbij is de theoretische toe te passen gebaseerd op de wet van Hooke, en de toe te passen kracht is voor elke lengte en temperatuur 20 kN groter. Deze 20 kN is toegevoegd om weerstands en wrijvingsverliezen op te heffen. Het is alleen vreemd dat dit voor elke lengte constant is, voor langere lengtes zijn de wrijvingsverliezen namelijk hoger. Dit heeft te maken met het feit dat de rollers niet wrijvingsloos zijn.

Commentaar door ProRail: Het toevoegen van de theoretische kracht was om het voor de aannemer wellicht wat makkelijker te maken, het trekken op streepjes is nog steeds de voorgeschreven methode.

vii. Schaduw en zon

De volgende situatie is een passtuk vervanging of bij nieuwbouw / vernieuwing waarbij de ene spoorstaaf in de schaduw ligt, terwijl de andere spoorstaaf in de zon staat. Hierbij is de spanningssituatie in de ene staaf boven de neutraaltemperatuur, en de andere eronder. Als je in deze situatie een of zelfs beide rails lossnijdt dan kunnen de liggers gaan roteren. Na het plaatsen van de passtukken en het sluiten van de las zullen deze liggers geroteerd blijven liggen. Ruud suggereert dat dit te voorkomen is door de rails voor het snijden te fixeren met behulp van de trekapparatuur. Deze trekapparatuur moet dan wel langer zijn dan het passtuk. Bij nieuwbouw of vernieuwing is het mogelijk dat de schaduwspoorstaaf verwarmd moet worden terwijl de zonnekant boven de $25^{0}+3^{o}C$ ligt. Dan moet er na afkoelen in de nacht een passtuk worden geplaatst om de overmatige verlenging op te heffen.

viii. Ankerlengte/relaxatie

Vanuit het onderwerp van verplaatsende liggers komen we uit op de ankerlengte. Ruud verteld dat hij tijdens een proef geobserveerd heeft dat de ankerlengte maar 3 liggers zou zijn. In deze proef zijn metingen uitgevoerd voor het introduceren van de stomplas machine. Hierbij is op een stuk spoor de rails losgemaakt, en is deze op de correcte neutraaltemperatuur gebracht. Vervolgens is de las gesloten. Hierdoor werd gegarandeerd dat de begin situatie voor de test een correcte neutraaltemperatuur had. Hierna is een aantal maal een stomplas aangebracht in dit stuk spoor.

Hierbij is geobserveerd dat bij een temperatuur verschil van ongeveer 10 graden de verschuiving tussen rail en ligger bij het lossnijden van de rail alleen op de eerste 3 (houten) liggers plaats vond. En niet over de gehele aangenomen ankerlengte. Op basis van deze metingen stelt Ruud dat de relaxatielengte van het spoor veel korter is dan doorgaans aangenomen wordt, en dat de gehele kracht in de rail over deze 3 liggers overgedragen kan worden in het ballastbed.

Commentaar door ProRail: wel kan door aanstoten dit effect over een grotere lengte optreden.

ix. Vastzet richting bij verwarmen

Hierna ging de discussie over de vastzet richting bij spoor dat door middel van verwarmen op neutraaltemperatuur wordt gebracht. Elke 30 meter wordt een markering aangebracht om te controleren of de rails voldoende uitgezet is. De verwarmingstrein rijd over het spoor van markeringspunt tot markeringspunt. Achter de trein worden de rails vastgezet. Een betere manier zou kunnen zijn om te wachten tot de trein voorbij het markeringspunt is, en om dan vanuit het markeringspunt terugwerkend de liggers vast te zetten. Dit zorgt ervoor dat de (losliggende) rails de kans heeft om een constante spanningsverdeling aan te nemen. Bij het achter de trein aan vastzetten loopt men het risico dat de spanning varieert naar gelang de snelheid en de warmte van de trein.

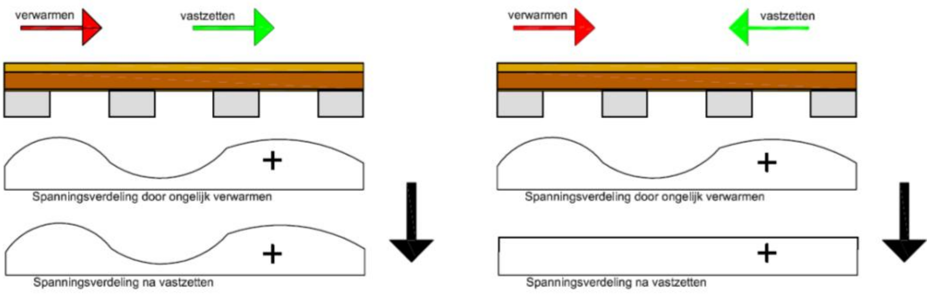

x. Locatie van verwarmen

Uit de voorstaande discussie volgt een discussie over de verwarmingslocatie van de verwarmingstrein (bovenop de railkop), het zou wellicht beter zijn om vanuit het web te verwarmen. Hierdoor is de warmteverdeling in de raildoorsnede constanter, wat voor minder spanningsconcentraties in de rails zorgt. Een verwarming van alleen de bovenkant zorgt er bijvoorbeeld voor dat de rails krom gaat staan.

xi. Metallurgie

Vanuit deze discussie volgt een uitleg over de staaltypes, metallurgie en de overwegingen voor gebruik van andere staalsoorten in bochten en puntstukken. Er wordt uitgelegd waarom de R370LHT en de MHH (micro head-hardened) stalen niet te snel mogen afkoelen, en dat bij het verwarmen van de rail de temperatuur onder de 500 graden moet blijven. Een temperatuur van boven de 723 graden en snelle afkoeling zorgt voor een verandering van de staalstructuren waardoor het staal brosser kan worden. Dit kan gebeuren als de verwarmingswagen te lang op dezelfde plek stil staat. Daar bovenop komt nog dat het metaal dan te snel afkoelt en dat hierdoor brosse structuren zoals Martensiet zullen ontstaan.

xii. Bogen

In bogen is de situatie anders dan op recht spoor. De voorschriften stellen nu dat er midden in de boog een sluitlas geplaatst moet worden. Dit betekent dat er in het harde R370LHT of MHH (micro head hardened) staal in de buiten boog op locatie een las gemaakt moet worden. Dit is lastig, omdat hierbij rekening gehouden moet worden met de juiste afkoelingsperiode om te zorgen dat het staal niet van structuur veranderd. Ruud zou graag zien dat de voorschriften het toestaan om de boog van tevoren op locatie te lassen of deze in zijn geheel naar de locatie te vervoeren. De sluitlas zou hij dan het liefst op het rechte deel spoor na de boog plaatsen omdat de staalkwaliteit daar R260Mn is welke bij luchtkoeling perlitisch wordt. Zijn suggestie is dan om aan één kant de boog aan te sluiten en het geheel met de boog mee te verwarmen tot de boog goed ligt, aan het andere eind van de boog wordt dan de sluitlas geplaatst.

De huidige situatie waarbij in het midden van een boog een sluitlas geplaatst moet worden is volgens Ruud onwenselijk omdat voor het maken van een las een recht stuk rail nodig is. Op dit rechte stuk rail wordt de trekapparatuur geplaatst welke de rails fixeert. Dit omdat in het geharde staal voor de buitenrails er scheuren in de las kunnen ontstaan door krimp.

Dit zorgt er (in kleinere boogstralen) voor dat de rails de onderstaande vorm aanneemt. De rail is uit zijn kluisjes (helingplaten) gekomen en is moeilijk terug te plaatsen bij lage temperaturen. Hierdoor ontstaat een zwakke plek in de voor knik gevoelige bogen. De groene vorm is de boog met een recht stuk voor de las. Hierbij wordt aan beide kanten de rails tegen de bevestigingsplaten gedrukt en zorgt het daarmee voor een piek in de laterale krachten op het ballastbed, wat het risico op uitknikken vergroot.

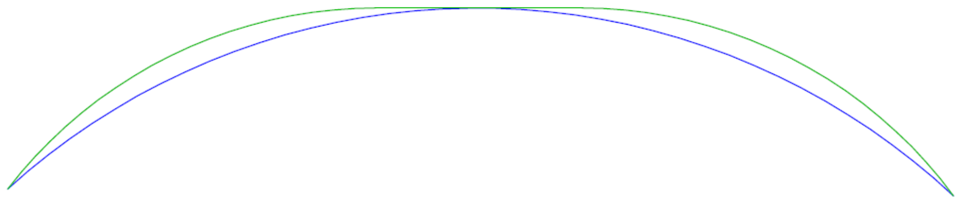

xiii. Wissel

1. *Vervorming*

Als laatste werd er gesproken over het gedrag van een wissel. Begonnen werd met een uitleg over de lasvolgorde en waarom deze van binnen naar buiten is. Deze uitleg wordt geïllustreerd met behulp van onderstaand figuur. Bij het maken van een las krimpt op die locatie de rail ongeveer 2 mm. Dit zorgt er voor dat er aan die kant aan de ligger getrokken wordt en deze roteert. Omdat in wissels de liggers erg lang kunnen zijn zorgt deze rotatie voor een grote verplaatsing, en daarmee wordt de wisselgeometrie veranderd. Onderstaande figuur geeft weer wat er gebeurd als er van buiten naar binnen gelast wordt

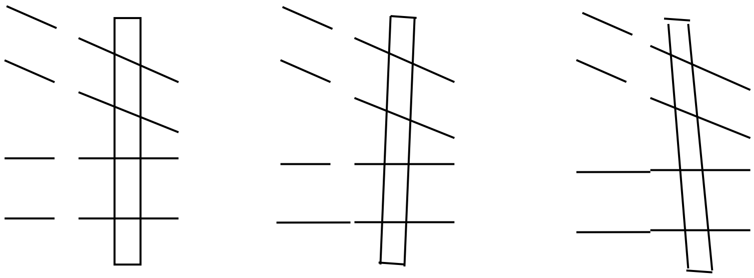

Eerst wordt de buitenste rail gelast, hierdoor trekt de ligger een beetje scheef. Vervolgens wordt de andere buitenste rail gelast, waarbij de ligger roteert om de bevestiging van de ligger die al vast gelast is. Dit vervormt de ligger geometrie. Dit effect is kleiner als er van binnen naar buiten gelast wordt.

Vroeger was dit effect nog veel erger, toen werden er houten liggers gebruikt, en de wissels ter plekke gebouwd. Als de lasser dan eerst de buitenste doorgaande spoorstaaf laste zaten er tussen de buitenste en binnenste lassen een verschil in het aantal lassen. Dit komt doordat op de binnenste spoorstaaf meer elementen verbonden moeten worden, waardoor er een verschil ontstaat in de hoeveelheid krimp. Dit verschil in krimp zorgt dan voor het scheeftrekken van de wissel. Dit is bij nieuwbouw van huidige wissels niet meer van toepassing, omdat deze veelal in stukken aangeleverd worden waarbij de doorgaande spoorstaaf evenveel lassen nodig heeft als de binnenste spoorstaven. Dit staat hiernaast geillustreerd. Er moet een las komen op elke scheiding van de wisselonderdelen, er zit dus geen verschil in per spoorstaaf.

2. *Lijmlas*

Vervolgens ging de discussie verder over lijmlassen. Deze mogen in de wissels van Prorail niet toegepast worden. Dit gebeurt echter wel. Belangrijk bij lijmlassen is dat ze niet open gaan staan. Daarom gebruikt Ruud een lasvolgorde waarbij hij de lijmlas als eerste legt, waarna de thermietlassen van de spoorstaven aan weerszijden gemaakt worden. Doordat deze krimpen ontstaat er druk in de lijmlas en zal deze niet open kunnen gaan staan.

xiv. Verbetering RLN120

Als laatste volgt een discussie over hoe Ruud graag zou zien dat wissels aangelegd mogen worden. Dit komt neer op het plaatsen van de wissel delen en deze aan elkaar lassen. Hierdoor vormt de wissel één geheel en is haar geometrie vastgelegd. Vervolgens worden de wisselbenen aan de spoorstaven bevestigd, waarbij het Ruud zijn voorstel is om een aantal liggers afstand te nemen, op deze liggers de bevestigingen vast te maken, en vanaf daar met een verwarmingswagen de spoorstaven op neutraaltemperatuur te brengen. Op deze manier zorgt het verwarmen van de rails dat de rails uitzet in de richting van de wissel vandaan, waardoor de wissel niks “merkt” van deze verwarmingen. Het aantal liggers dat als afstand genomen wordt stelt Ruud op 14, dit zou de ankerlengte moeten zijn. De ankerlengte is de lengte spoor waarin de neutraaltemperatuur krachten vanaf 0 opgebouwd kunnen worden. Door deze lengte afstand te nemen is verzekerd dat de wissel niks merkt van temperatuurverschillen in de aansluitende sporen.

Na afloop van aanleggen is het spoor dat naar de wissel leidt op de juiste neutraaltemperatuur. De wissel zelf heeft als neutraaltemperatuur dan de temperatuur waarop de wisseldelen aan elkaar werden gelast. Dit wijkt af van de neutraaltemperatuur en zal doorgaans lager zijn. Dit betekent dat de spanningen in de wissel zomers hoger op kunnen lopen dan in recht doorgaand spoor, maar de redenering is dat deze krachten kunnen worden opgevangen doordat de wissel veel stijver en zwaarder is dan doorgaand spoor en daardoor minder snel zal uitknikken.

III. The impact of omitting the lateral springs

The reason for this investigation is the arduous task of applying every spring manually to any new models being made. If these springs could be omitted the process of creating new models could be significantly faster, this is useful when creating models for turnout complexes. A focus is on the behaviour in the y-direction, as these are the most significant stresses and are the focus of this research.

i. Normal elastic strain (y-direction)

The top results picture is of the model with springs (the grey cylinders), the bottom one is of the model without these springs. All other properties are similar.

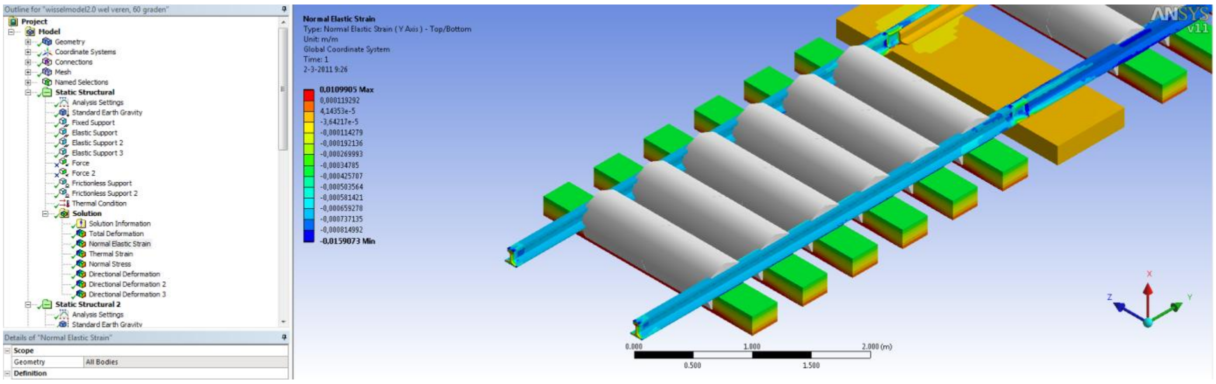

Figure III.1 Strain distribution with springs

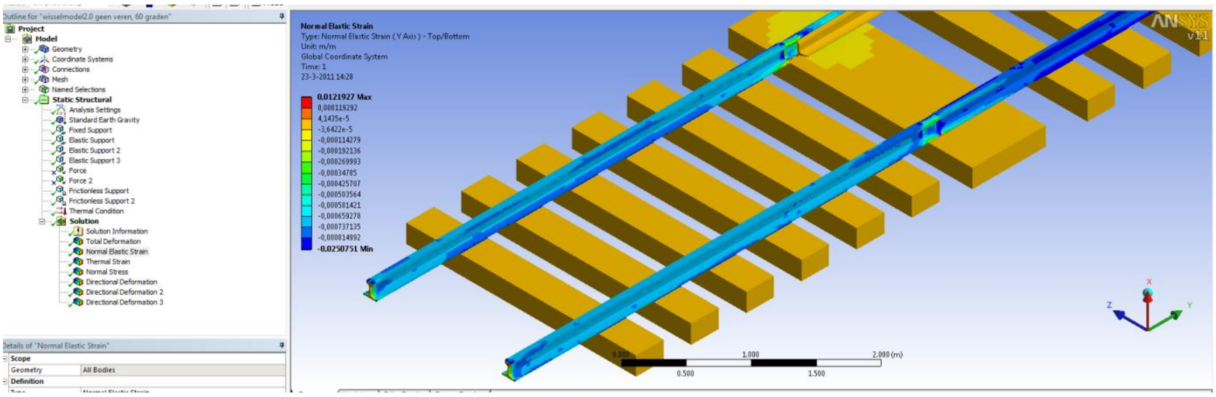

Figure III.2 Strain distribution without springs

One can see that the resulting strains in the sleepers are not the same. The strains in the rails however appear to be somewhat similar. This goes for the entire length of the turnout, but is not shown here.

ii. Thermal strains

The thermal strains are of course identical, as they are independent of any springs applied and are a result only of material properties

iii. Normal stress (y-direction)

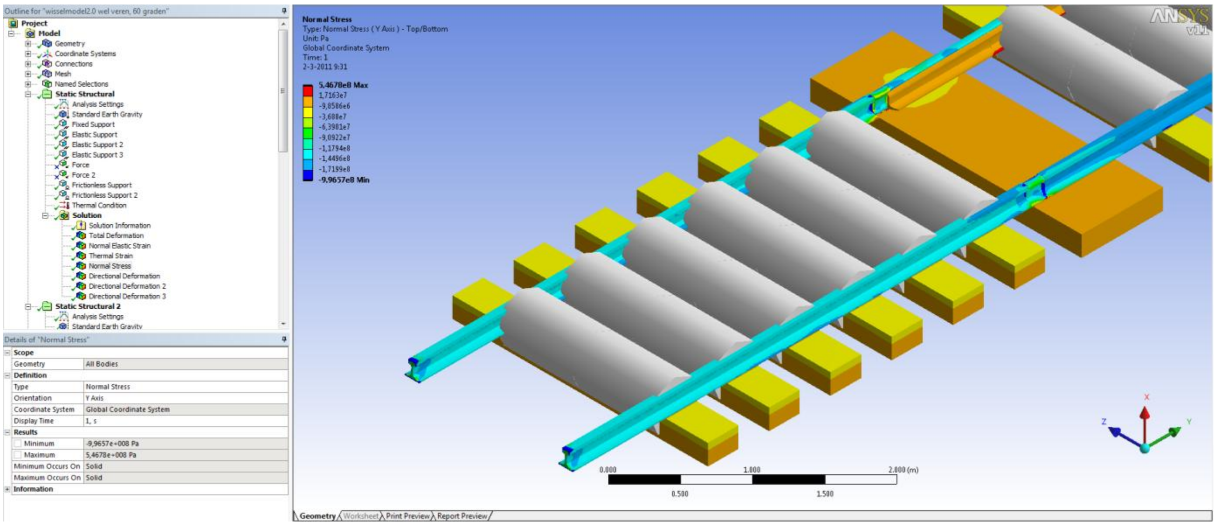

Figure III.3 Normal stresses with springs

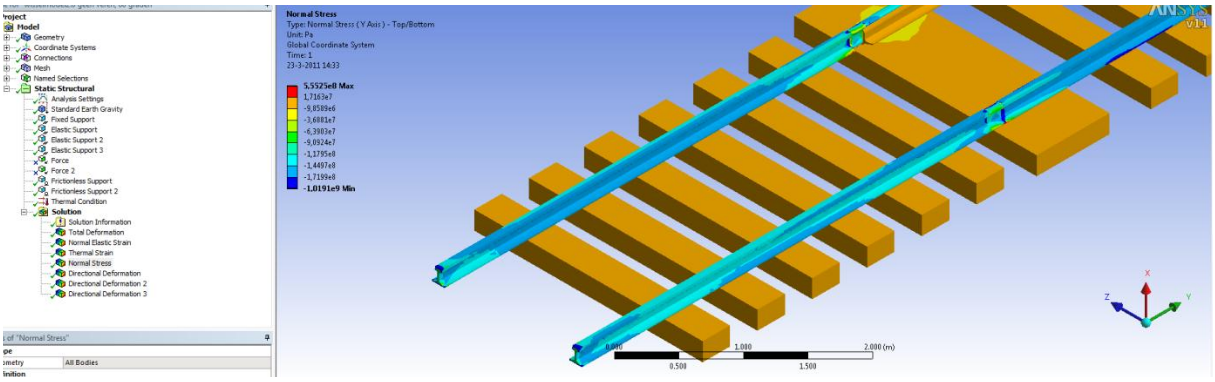

Figure III.4 Normal stresses without springs

Once again, the sleeper results are not identical, but the rail stresses are largely similar. This goes for the entire turnout. The ball and claw area is highlighted below.

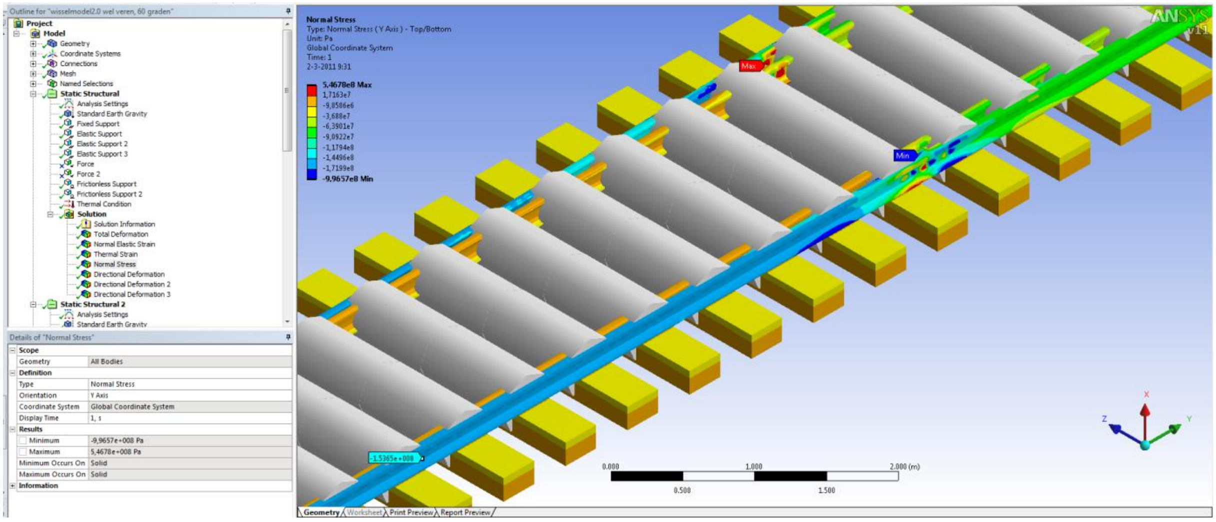

Figure III.5 Normal stresses near ball and claw with springs

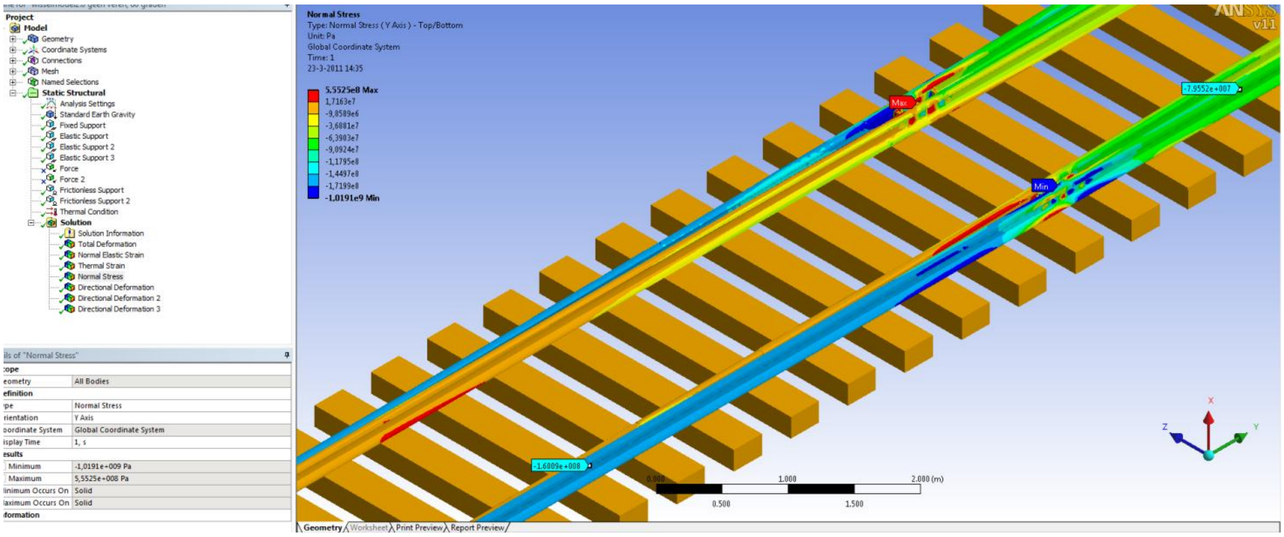

Figure III.6 Normal stresses near ball and claw without springs

iv. Displacement x direction (vertical)

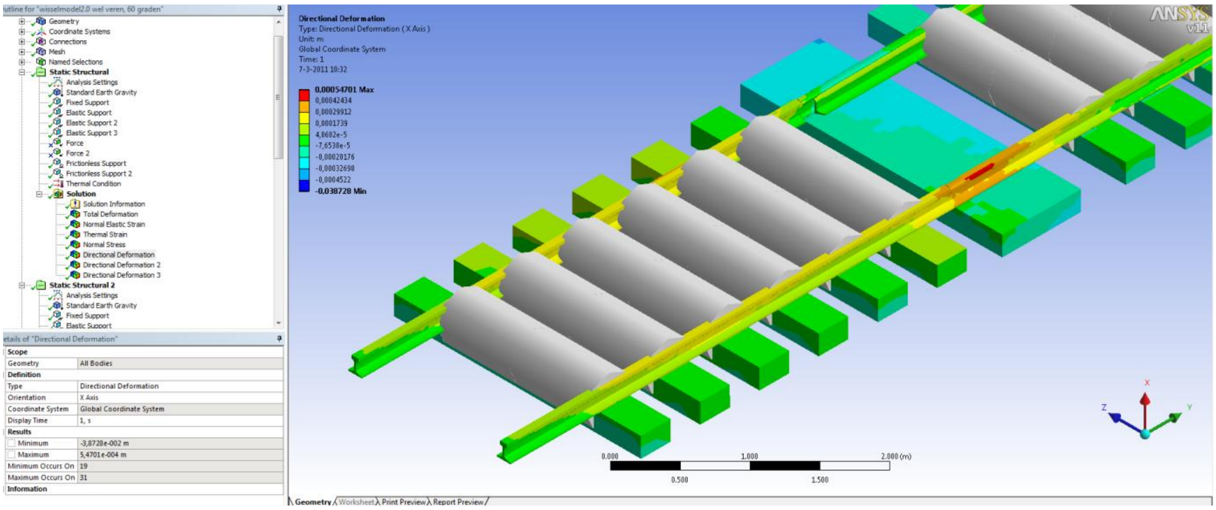

Figure III.7 Displacement in the x direction with springs

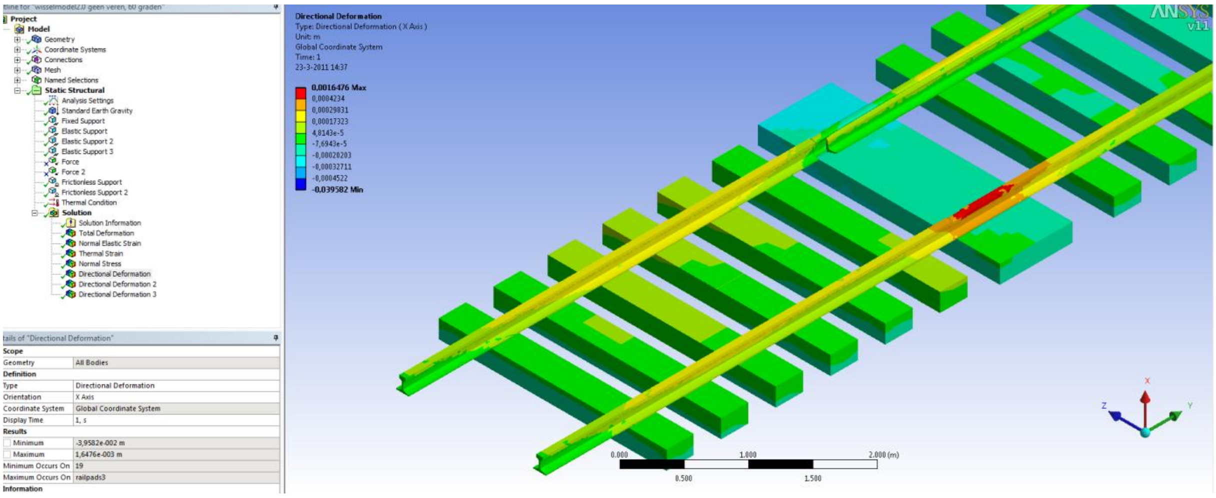

Figure III.8 Displacement in the x direction without springs

These displacements are almost similar as well. The maximum is different, but this is a value inside a railpad, and therefore not of interest.

v. Displacement Y direction (longitudinal)

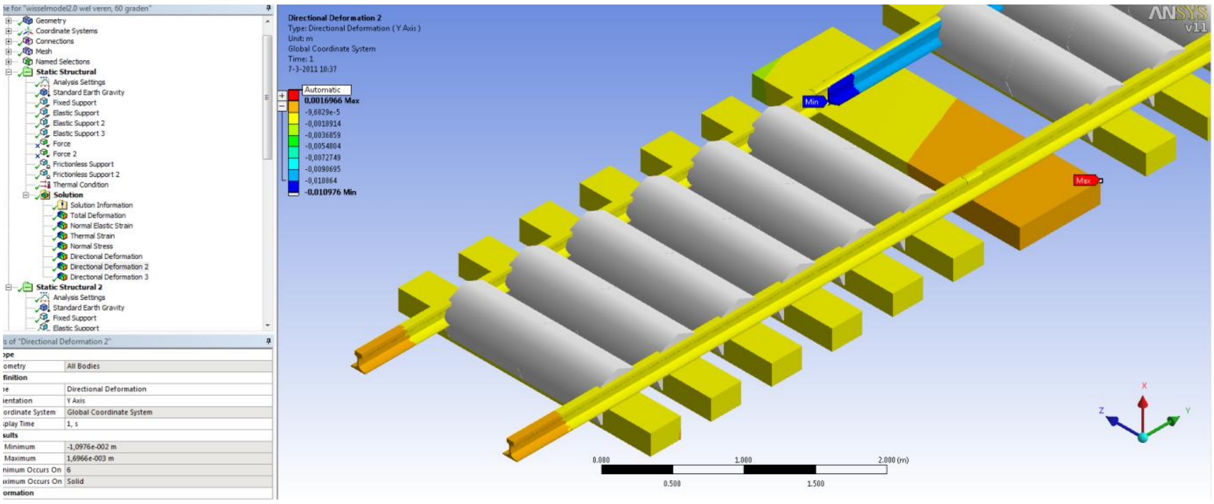

Figure III.9 Displacement in the Y direction with springs

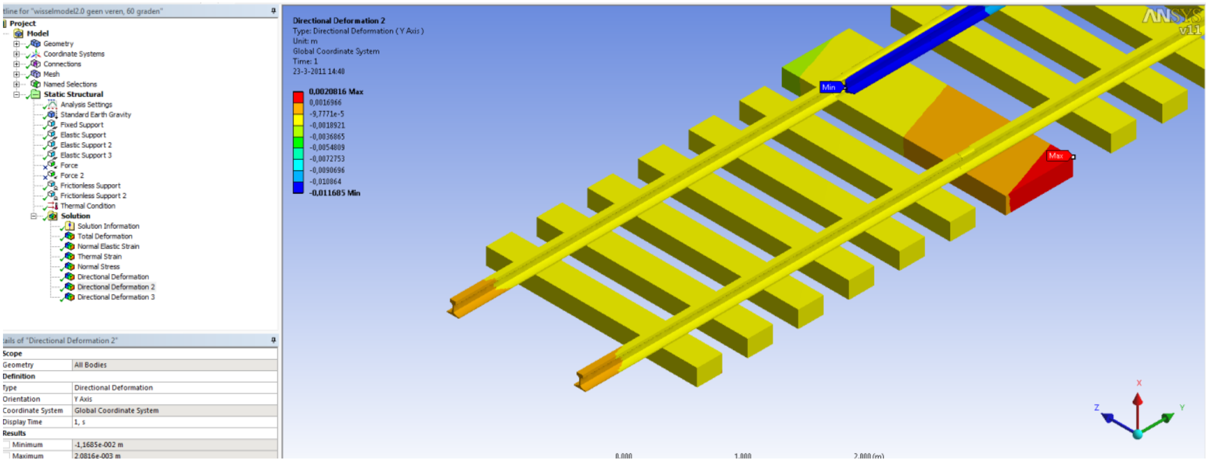

Figure III.10 Displacement in the y direction without springs

The differences are somewhat more profound in this direction, but still within an acceptable margin.

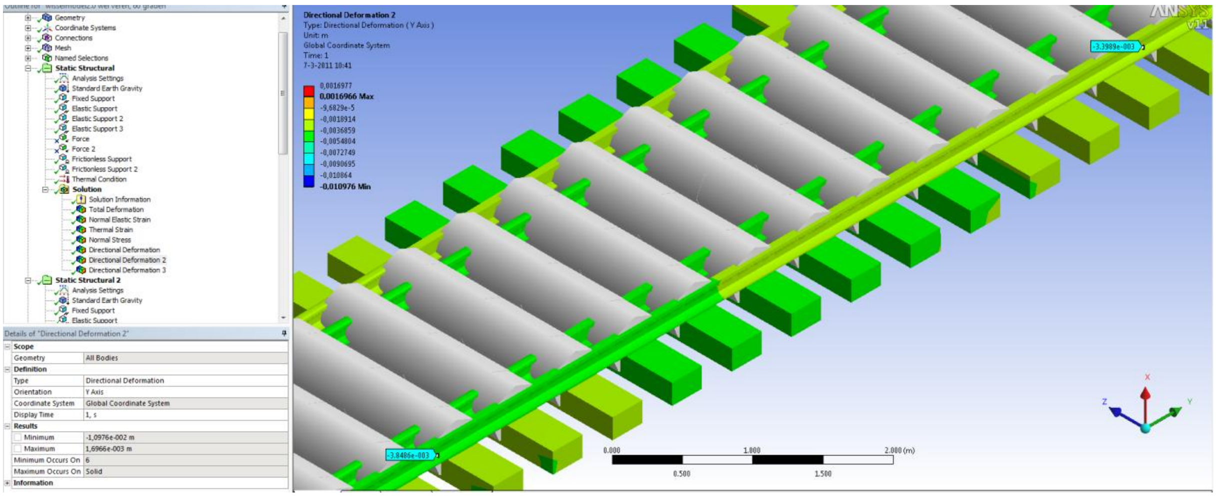

Figure III.11 Displacement in the y direction at the largest deviation section with springs

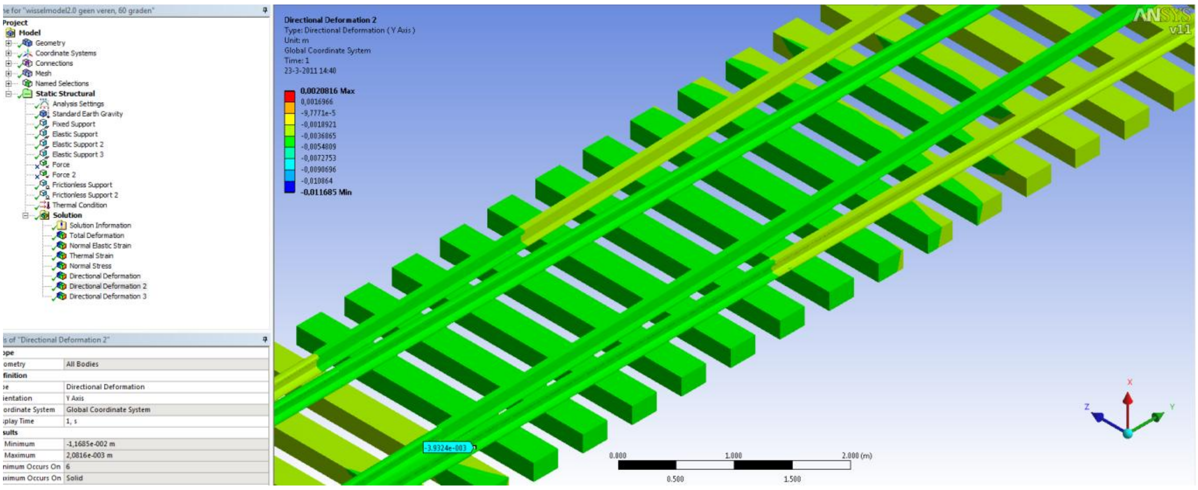

Figure III.12 Displacement in the y direction at the largest deviation section without springs

The biggest differences are found in this area, but these results are still largely similar, the sleeper displacements of the model without springs are somewhat larger (there are more dark green sleepers)

vi. Displacement in z direction (lateral)

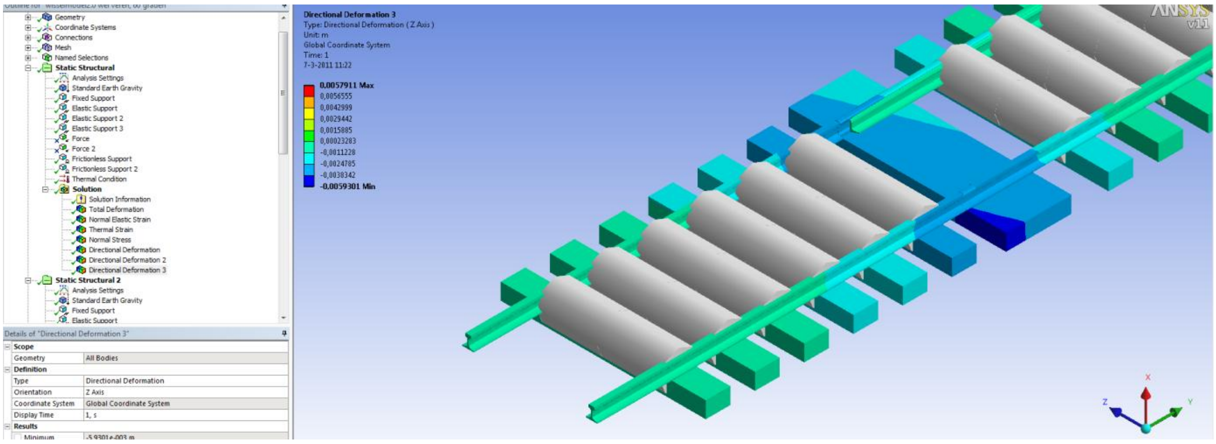

Figure III.13 Displacement in the z direction with springs

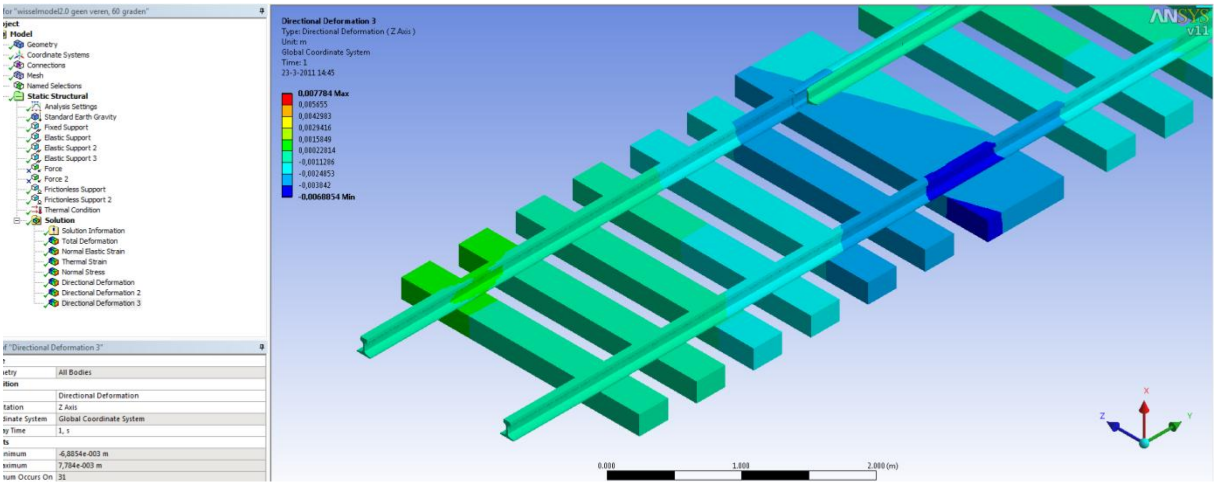

Figure III.14 Displacement in the z direction without springs

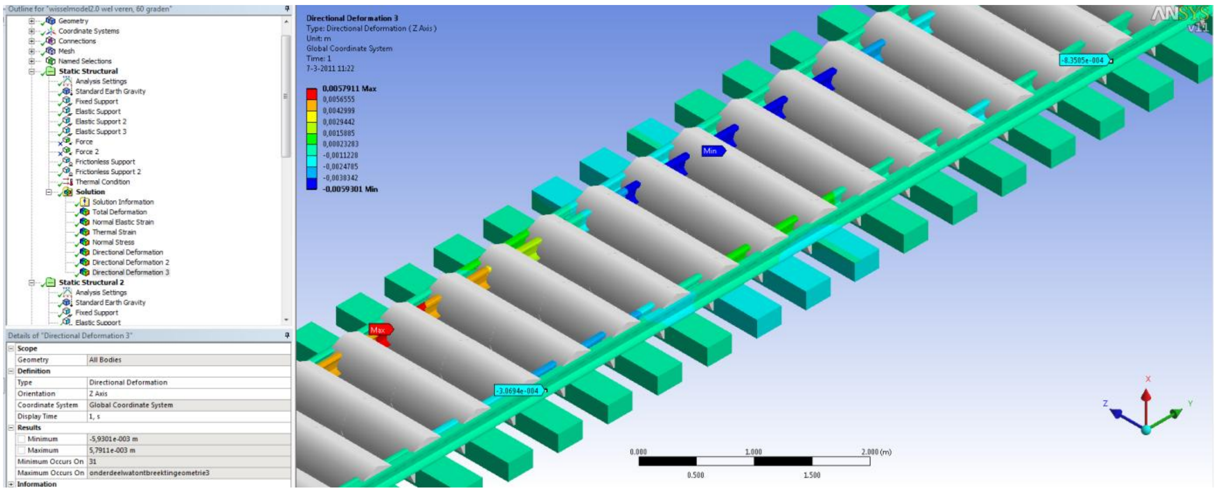

Figure III.15 Displacement in the z direction with springs, near the ball and claw

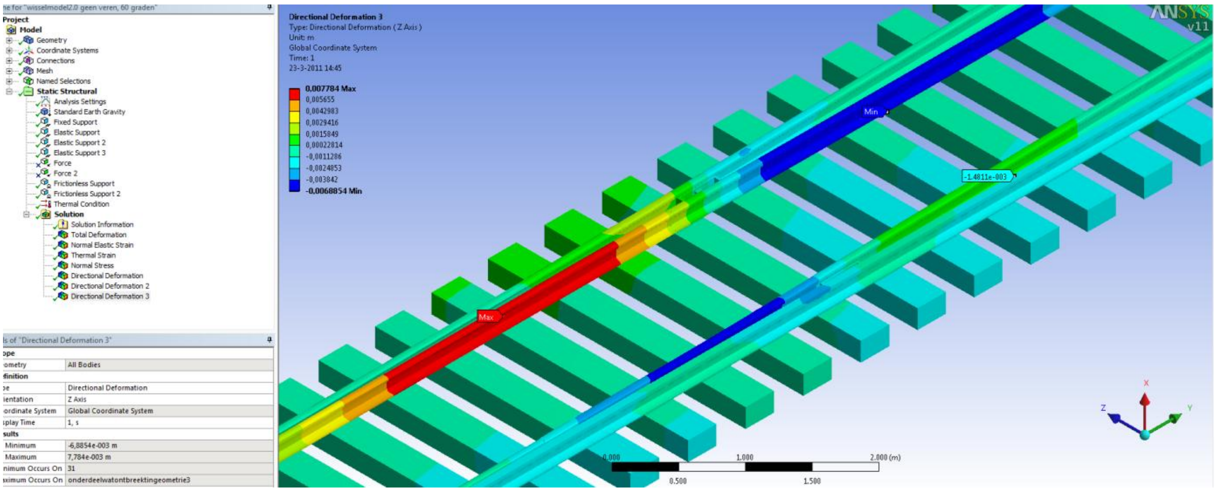

Figure III.16 Displacement in the z direction without springs, near the ball and claw

The differences in this direction are beyond an acceptable margin. They are still largely similar, but well beyond a 10% deviation.

vii. Conclusion

It is possible to use the models without springs, if it is agreeable to have a lesser accuracy and the displacement of the sleepers or the displacement in the lateral direction (z direction) is not the focus of the inquiry. This would allow for fast construction of models detailing large turnout complexes, as all that needs to be done is copy and rotating one turnout until the complex is made, and to add a couple of sleepers or crossings where necessary.

IV. Short investigations into model behaviour

i. Linearity of the model

A number of investigations into the predicted behaviour of the turnout were conducted. The first is the verification of the linear scaling of the behaviour of the turnout. This was done by using the full model, with fixed connections at the three turnout ends, and applying three different temperatures to it. The starting temperature of the model is 18 degrees, and the three applied temperatures are 58 degrees C (+40), 38 degrees C (+20) and -22 degrees C (-40). Comparisons were made by checking the same spots for each temperature. Displacement, stress and strain were compared.

The locations of the comparisons are:

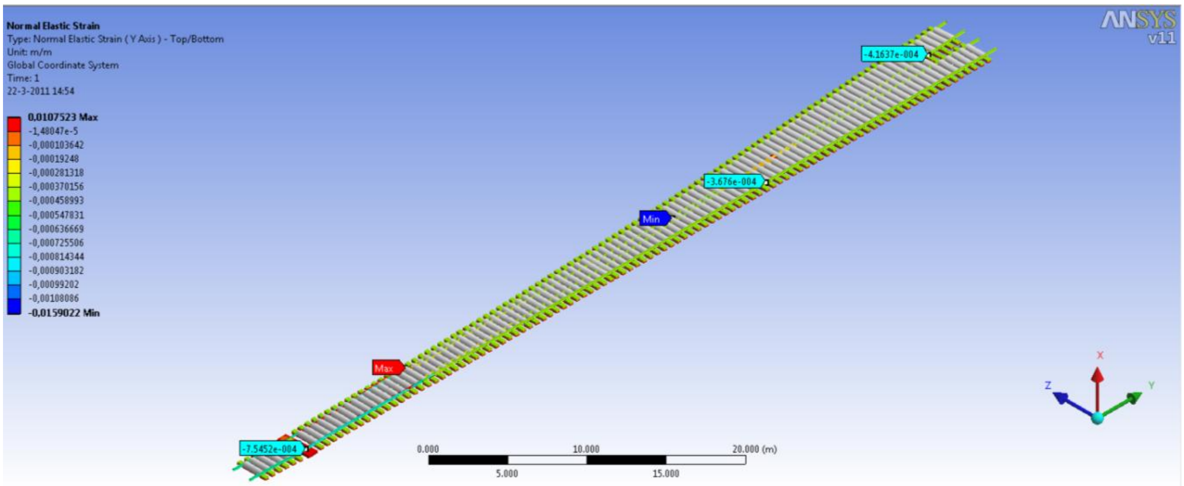

An overview of the outcome is given below:

	Normal elastic strain			Thermal strain	Normal stress		
Location:	1	2	3	constant	1	2	3
+40 degrees	-7,55E-04	-3,68E-04	-4,16E-04	4,80E-04	-1,52E+08	-7,35E+07	-8,34E+07
+20 degrees	-3,79E-04	-1,84E-04	-2,08E-04	2,40E-04	-7,54E+07	-3,67E+07	-4,17E+07
0	0	0	0	0	0	0	0
-40 degrees	7,42E-04	3,67E-04	4,16E-04	-4,80E-04	1,53E-08	7,35E+07	8,34E+07

These verify the linearity of the model (no non-linear behaviour occurs due to geometry of the structure). This outcome is as predicted, but this model is only valid and verified (using models by S Boogaerdt and M.A. Van) for sleeper displacements up to 5 mm.

ii. Fixed connections

To verify the fixed connections at the ends of the turnout one must understand that in reality the rail continues here. A simulation of a piece of track yielded the resulting force inside the rail due to temperature changes. Applying this force at one of the turnout ends instead of a fixed connection yielded a displacement of approximately zero. The force observed in the fixed fixation corresponded to the one calculated to be present in the rail. Fixed connections are therefore deemed suitable to model the connection to continuing rail.

V. Sensitivity analysis

In this chapter each of the three branches of the turnout are loaded by a force of 170 kN in turn, these three situations will provide insight into what loading case causes the highest strains and stresses. This will provide the worst case situation, upon which to model the exceptional situations, such as one branch not being connected.

- Stock rail out loaded:

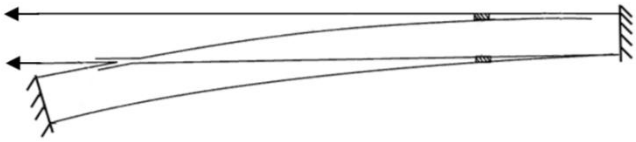

- Turnout branch loaded

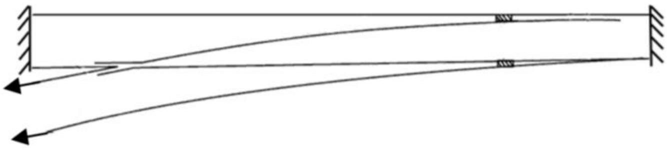

- Stock rail in loaded

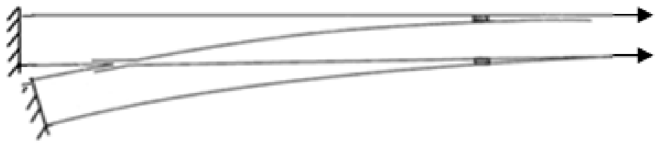

i. Stresses

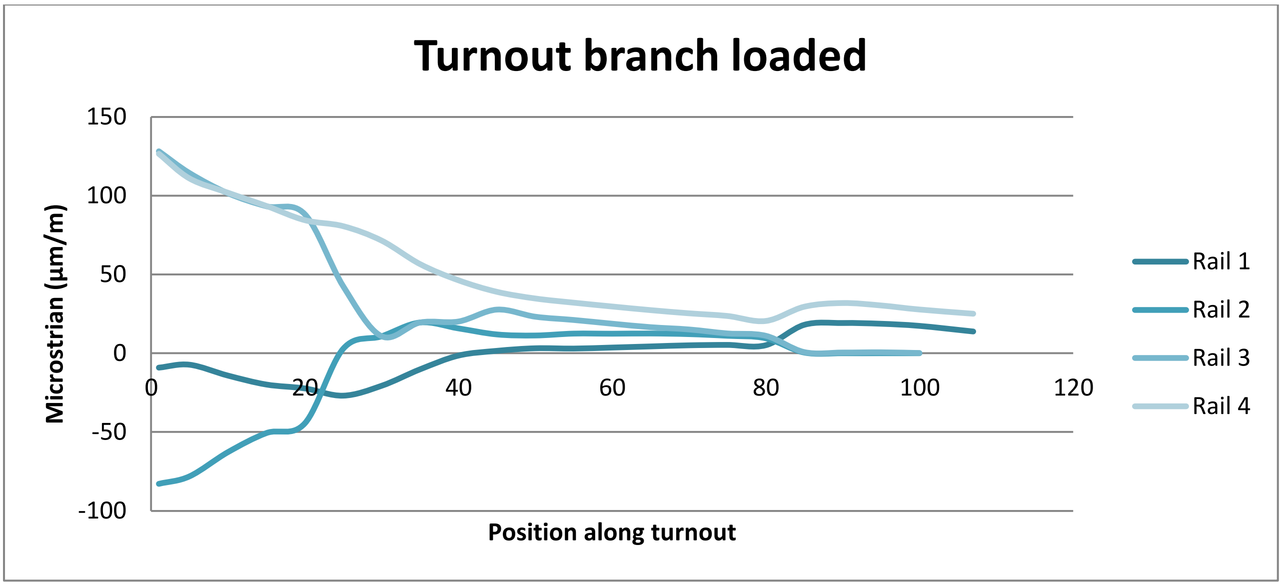

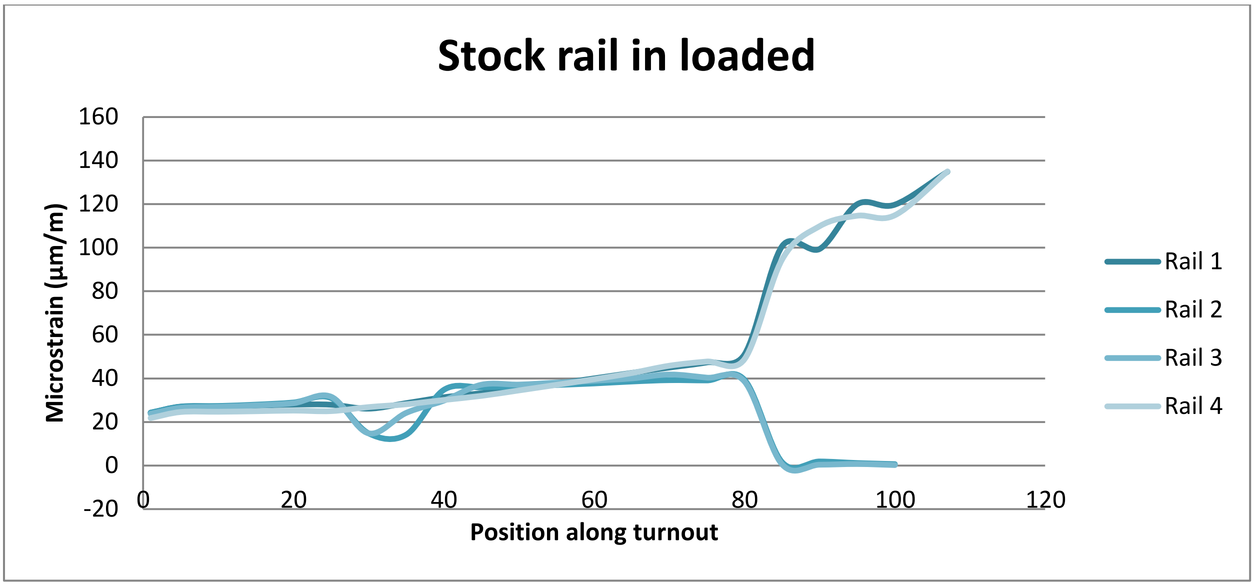

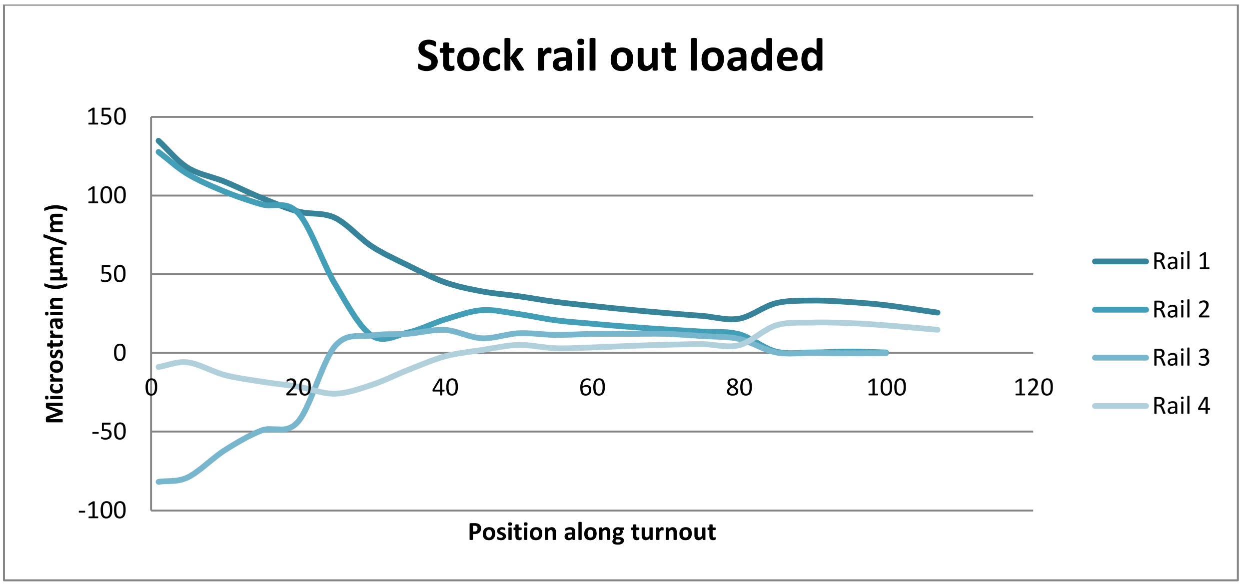

A number of conclusions can be drawn from these graphs. Firstly, the strain distribution between the situations with the loaded branch and the loaded stock rail out are almost perfect mirrors of each other, however with different rails undergoing the strain distributions. Rails 4 and 1 and rails 2 and 3 are switched around. In the situation with the load on the incoming stock rail, the only portion of the turnout under a large strain is the stock rail until the ball and claw system.

ii. Stresses

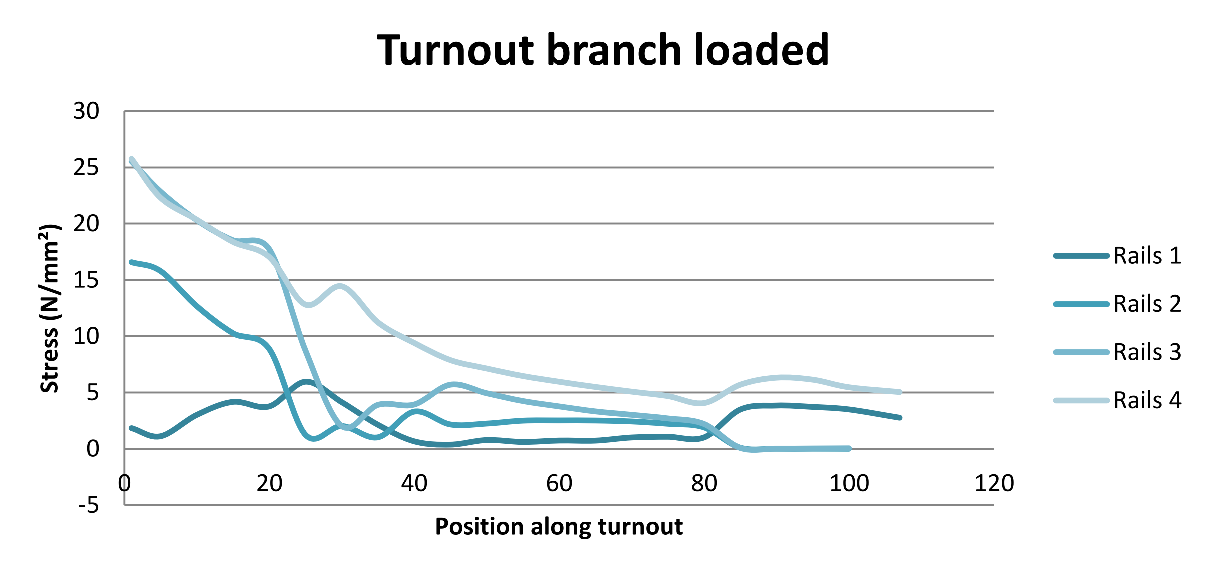
Turnout branch loaded
Stress (N/mm²)
30
25
20
15
10
5
0
-5
0
20
40
60
80
100
120
Position along turnout
Rails 1
Rails 2
Rails 3
Rails 4

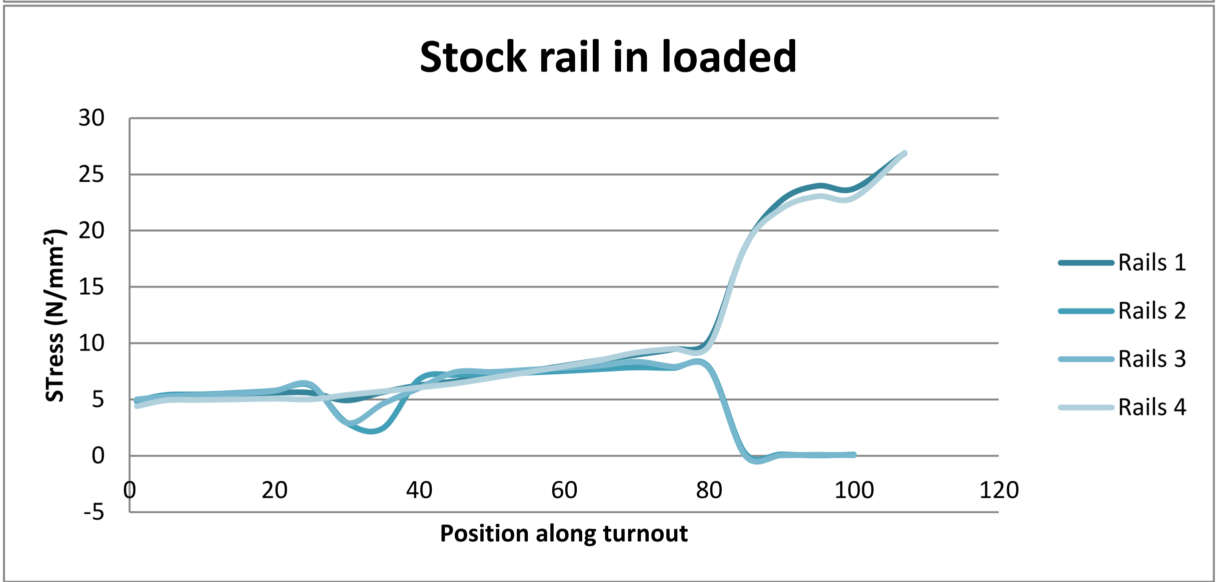
Stock rail in loaded
STress (N/mm²)
30
25
20
15
10
5
0
-5
0
20
40
60
80
100
120
Position along turnout
Rails 1
Rails 2
Rails 3
Rails 4

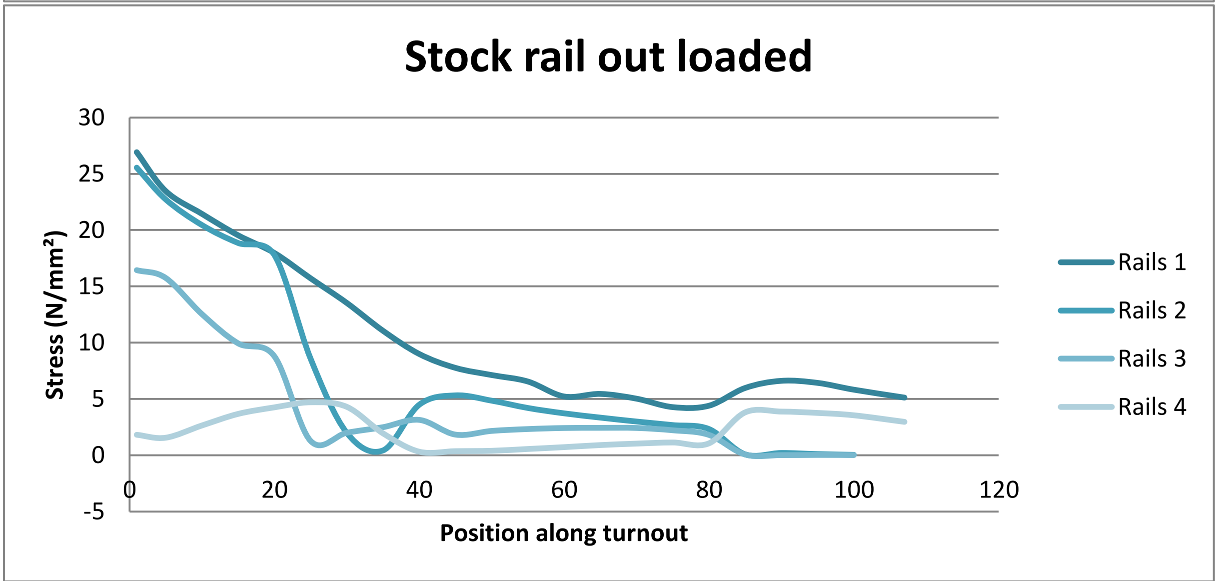
Stock rail out loaded
Stress (N/mm²)
30
25
20
15
10
5
0
-5
0
20
40
60
80
100
120
Position along turnout
Rails 1
Rails 2
Rails 3
Rails 4

iii. Displacements in the length direction

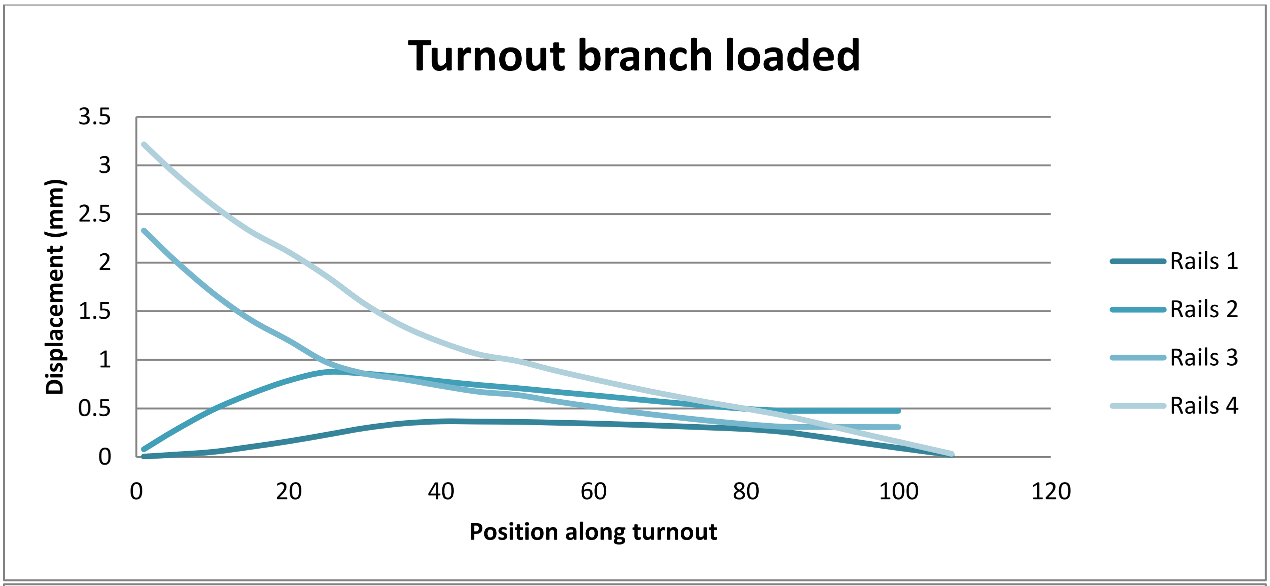

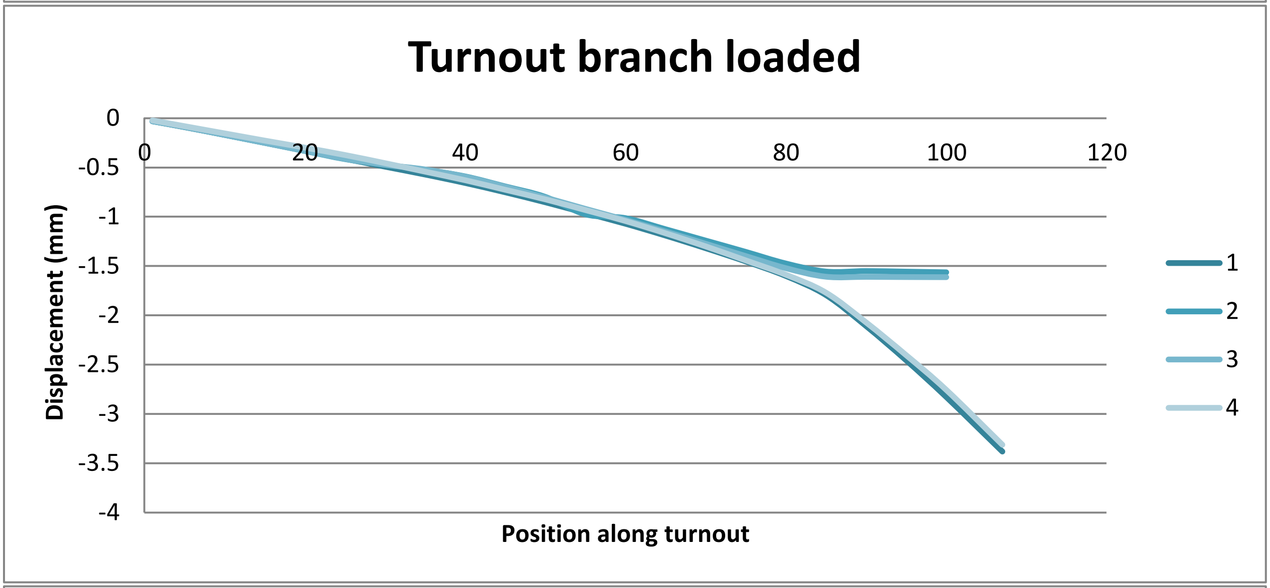

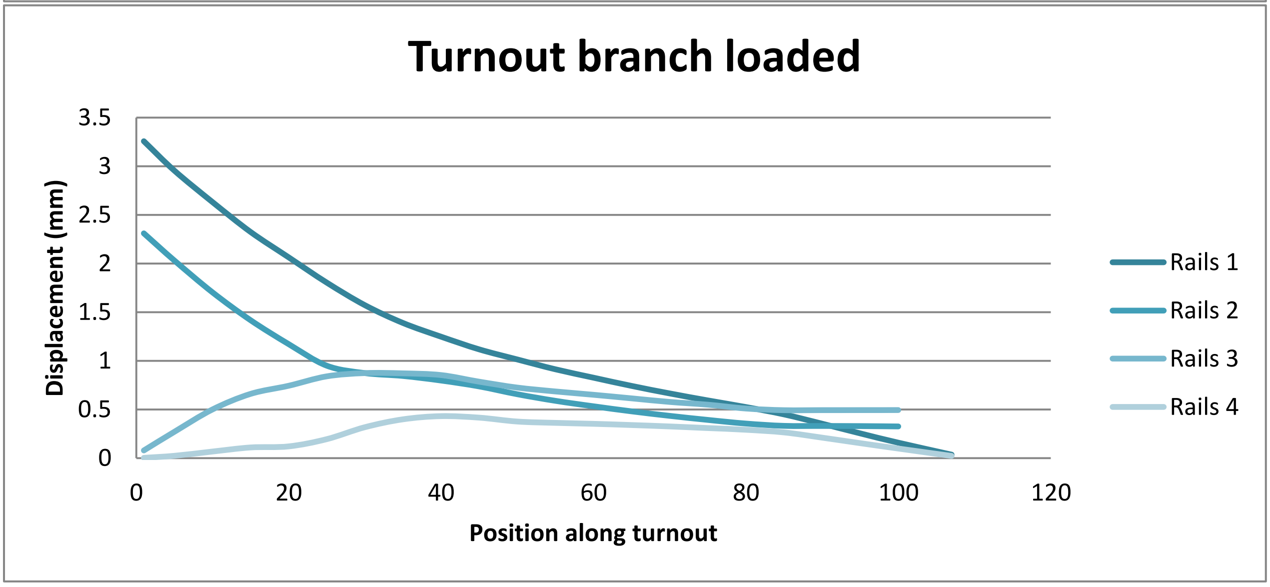

iv. Displacements in the lateral direction

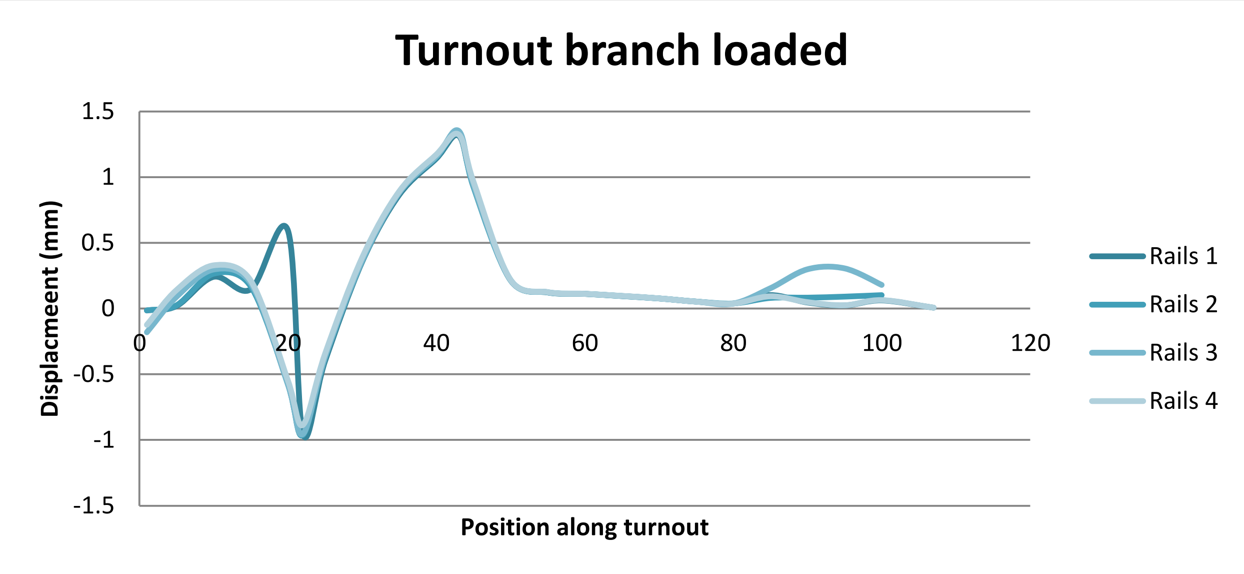

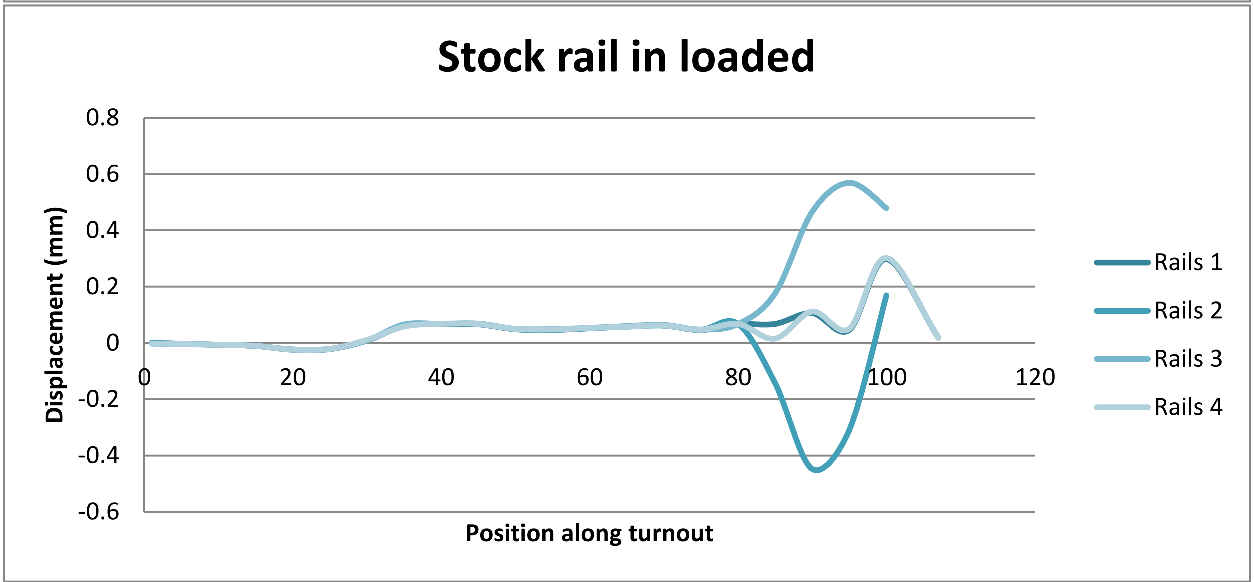

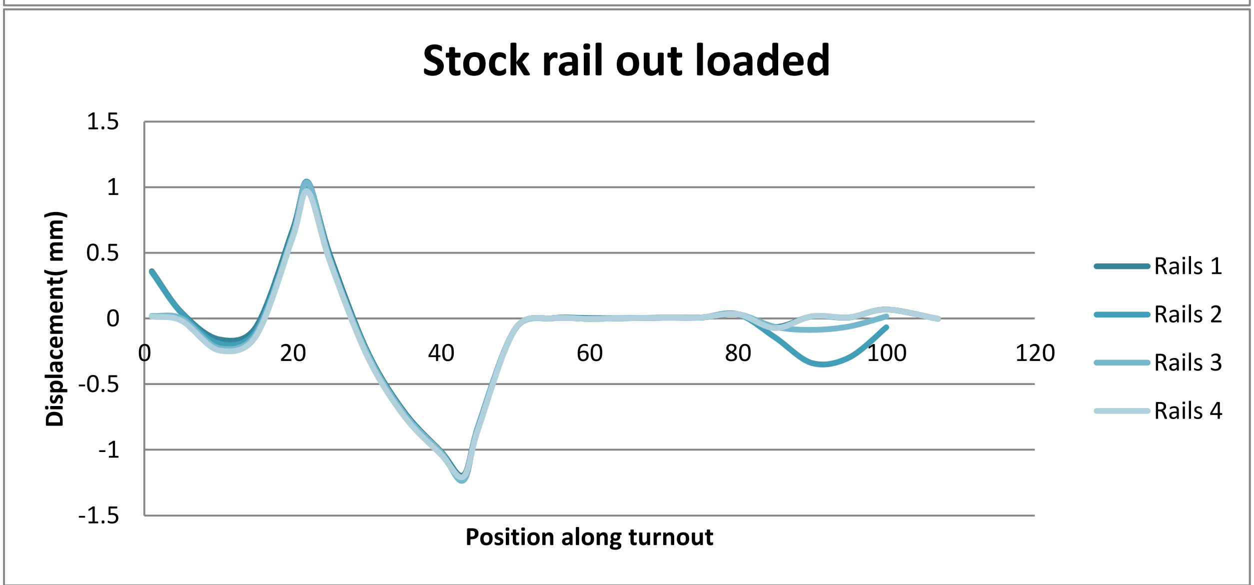

v. Conclusion

The stresses and both displacement graphs confirm the observations made in the strain graphs. Focus of the other models will be towards the situation in which the turnout branch is not connected, as this is deemed the most likely scenario.

VI. Practical situation at a temperature increase of 60 degrees

To increase insight in what happens with strains and stresses in the turnout that is constructed according to the guidelines another model was calculated in which the temperature increase was set at 60 degrees. The closure rail (chapter 4.9) was set to 60-28 = 32 degrees, while the rest of the turnout was heated to 60 degrees.

i. Stresses and strains

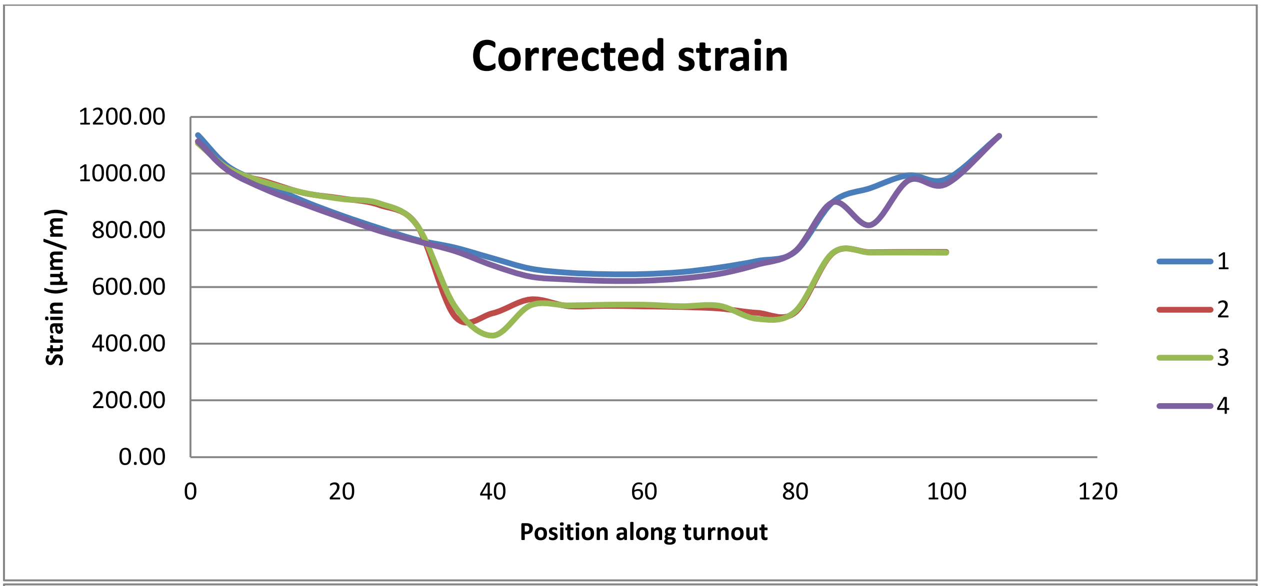

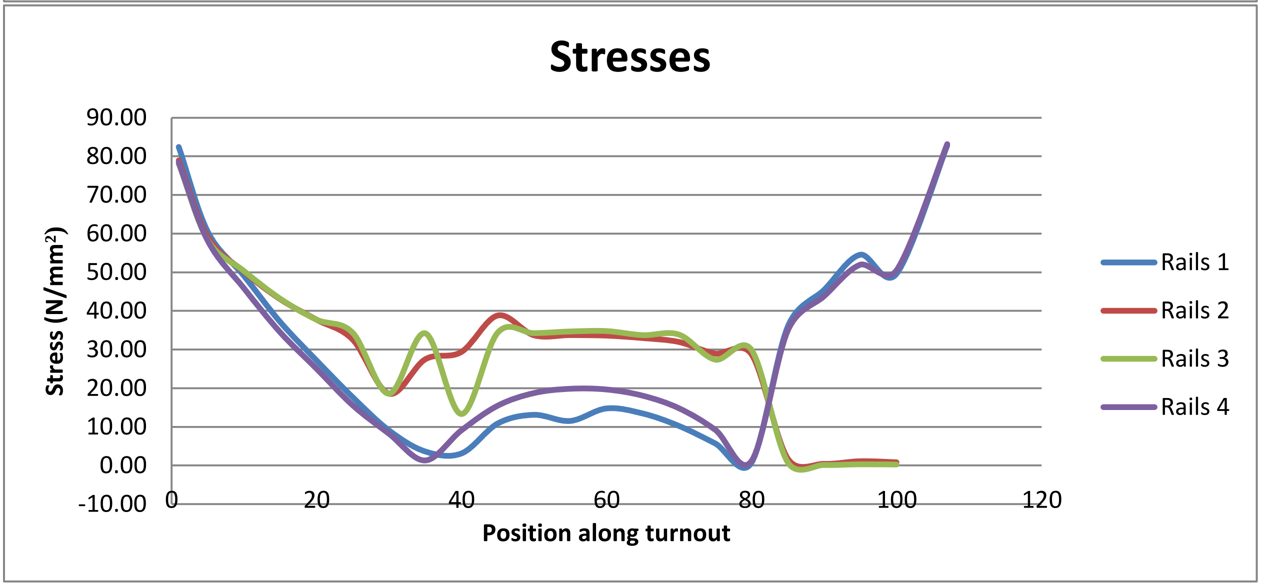

The strains in this situation are increased even further, this increase is linear. The stresses remain largely the same, with a slight increase all over. In the stock rail the stresses do increase noticeably, but the curve stays “anchored” around the common crossing, as these points are unstressed by the counteracting force from the “prestressed” (due to the heating up) closure rails (chapter 4.3).

ii. Displacements

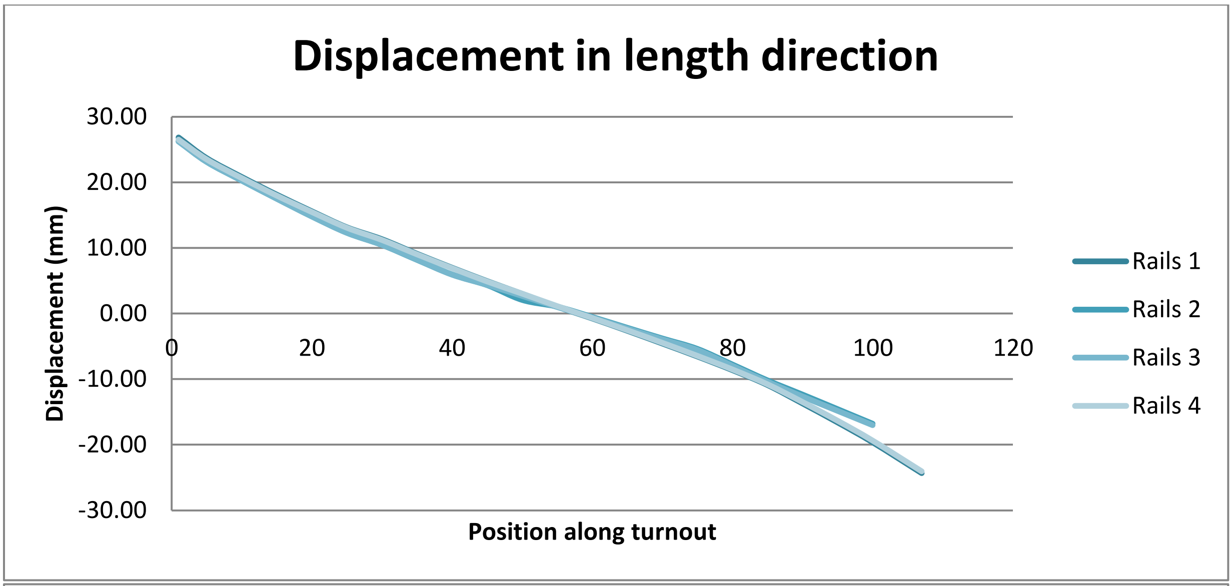

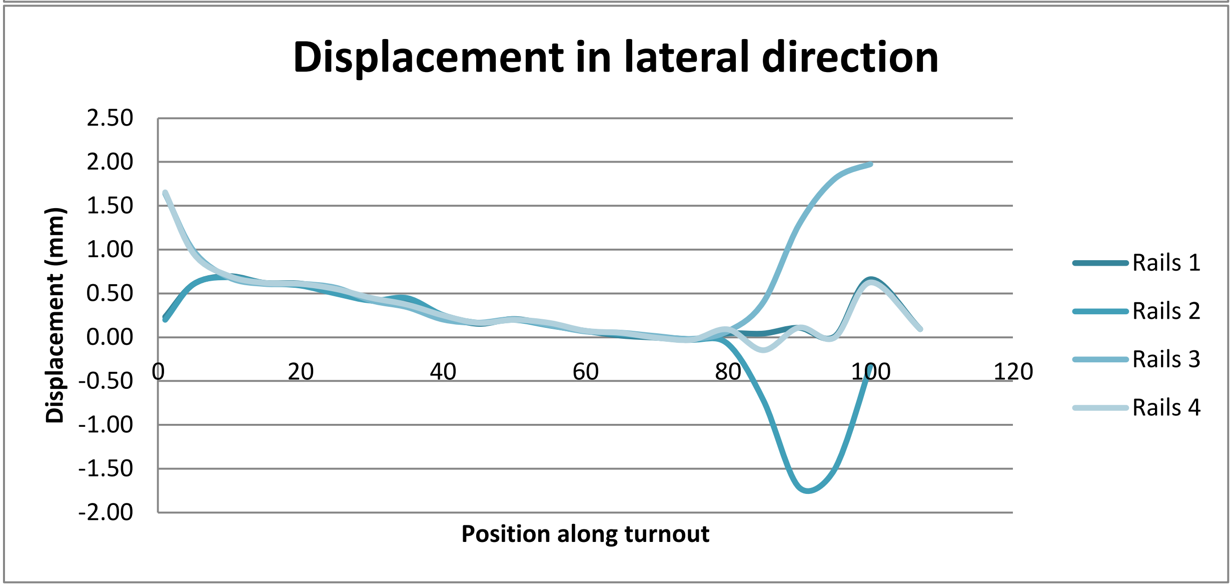

The displacement graphs show predictable behaviour, the displacements increase. The zero point of the displacement in length direction is shifted somewhat to the left, showing that the stresses and forces in the turnout start to become dominant over the “prestressing” of the closure rail.

VII. Comparison between the two possible modeling solutions for the switchblade.

As discussed in chapter XX there are several ways to model the switchblade end. It has been opted not to restrain the lateral switchblade movement, except from where it is held in position by the point machine. To verify the correctness of this decision a model was made and calculated using a frictionless contact setting between switchblade and stock rail. This type of contact allows movement until both model entities touch each other, at which point forces will be transferred from one rail to the other.

On the following pages in Figure III.17 and Figure III.18 the strain and stress distributions in the turnout are displayed. Focus is put on the right sides of the graphs; the left sides are very similar except for some minor variations due to the manual data extraction. Situation A is the plot of the situation with the frictionless contact zone, while situation B is the situation without this contact zone. Tracks 2 and 3 are the switchblades themselves, while tracks 1 and 4 are the corresponding stock rails. Due to the large amount of data presented, the Figures have been giving a full page each.

Examination of the plot near the switchblade shows that the change in strain for the frictionless situation is less abrupt, and contains greater variation along the switchblade length. This is a logical result of both rails connecting, and transferring forces and displacements to each other. In the lesser realistic version, where both rails can pass through each other, the strain is very close to zero, as there is no force transferred to cause change in strain. A similar difference can be found in the stock rail, the change in the amount of strain is more gradual when the more realistic conditions are used, and the reached values are slightly lower for the realistic model (some of the force is now carried by the switchblade, which was not the case before).

These observations are reflected in the stress plots, the changes in stress are more gradual for the more realistic situation, while the stress in the strain does not reach the absolute zero as nicely as it does without contact modelling.

Some minor differences can be observed, however these do not cause incorrect behaviour or other effects when the contact zone is not modelled. This confirms the earlier quicker check at which the force in the switchblade was gauged (around 2 kN) and deemed to be of little consequence. For the purpose of this research, the contact area can be omitted without any consequences on the behaviour of the turnout. Should further research be done concerning the behaviour of the switchblade it is strongly suggested to omit the rest of the turnout and to improve on the switchblade boundary conditions.

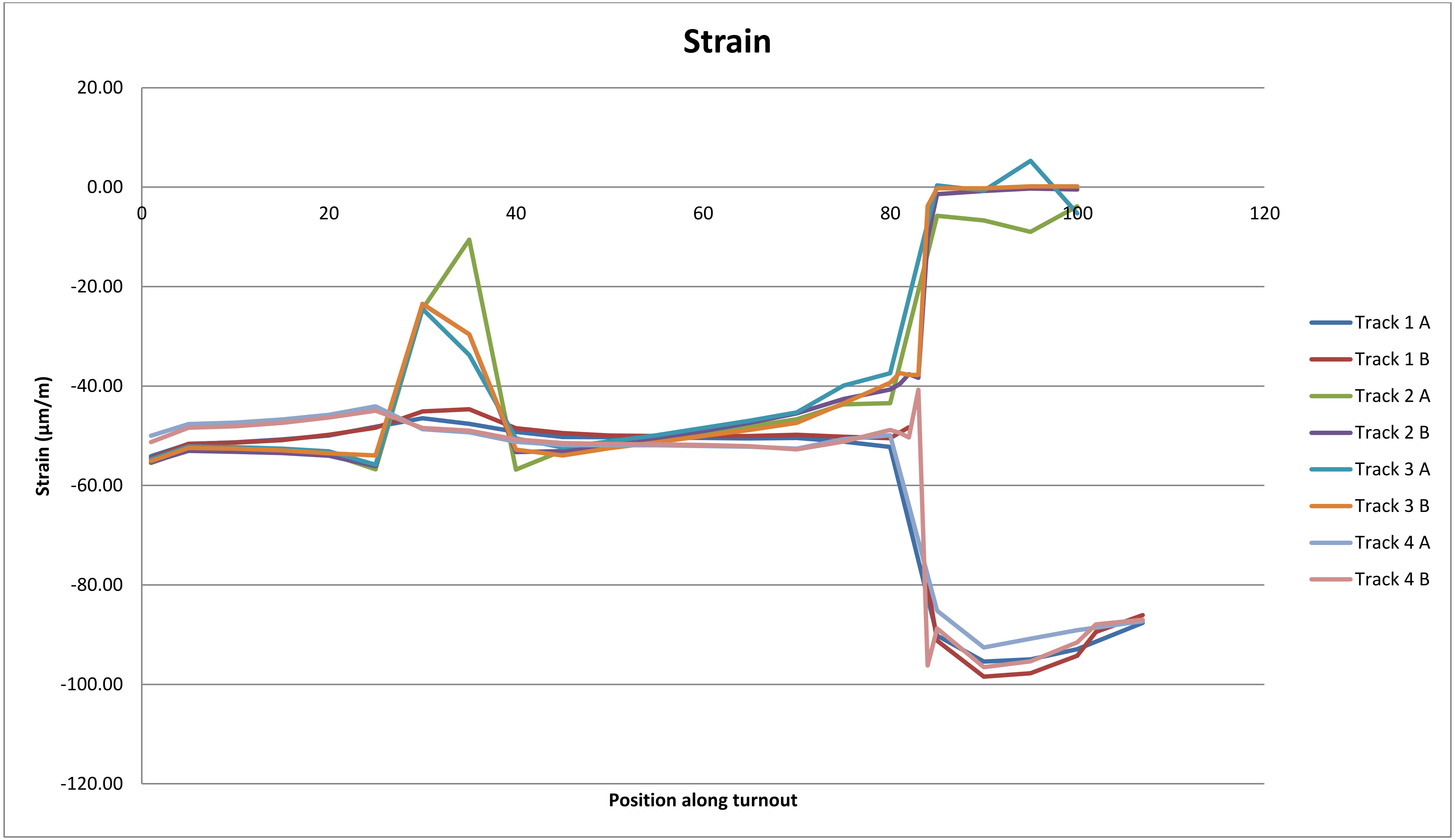

Figure III.17 Strain comparison, situation A is with frictionless contact areas

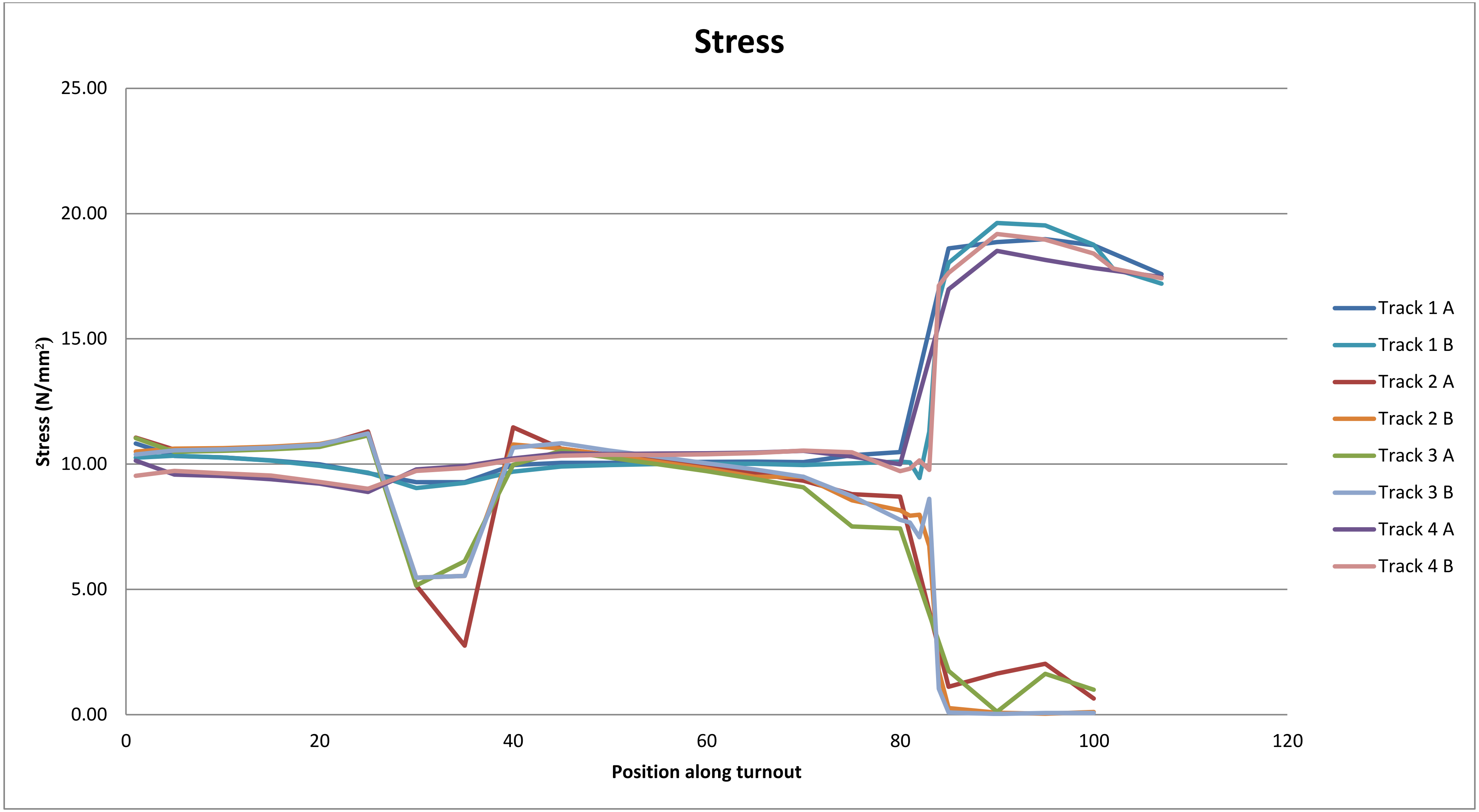

Figure III.18 Stress comparison, situation A is with frictionless contact areas

VIII. Strain gauge application

Firstly the rail needs to be grinded, first roughly and then with a sanding paper with a fineness greater than 250.

Figure III.19 grinding the rail

Figure III.20 Sanding down the strain gauge locations

The next step is to clean the surface using acetone.

The surface is then prepared using a preparation agent; this removes the oxidants from the surface. This is then neutralised using a different solution.

Figure III.21 Left to right, accelerator, preparation agent, neutraliser

The strain gauge is transferred to a piece of non-stretching sticky tape using tweezers.

Figure III.22 Strain gauge on sticky tape

This tape is then applied to the cleaned surface, and pealed back on one side.

Figure III.23 Pealed back tape

An accelerator is applied to the strain gauge and the surface; this is to speed up the hardening process.

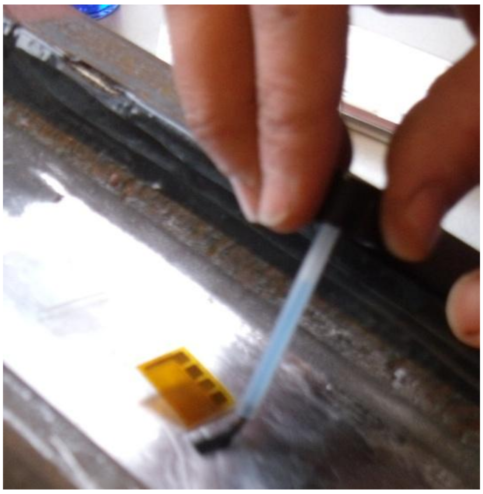

Figure III.24 Applying the accelerator

Glue is then applied on the strain gauge and it is pressed firmly against the surface.

Figure III.25 Applying the glue

After keeping the pressure on the strain gauge and surface for about a minute the glue is left to harden. The last step is removing the tape. The wiring can now be soldered to the strain gauge and connected to the data logger.

The application of Bienfait sensors goes similarly, except the accelerator and the glue are not applied as such. With the Bienfait system the (two component) glue is mixed by a glue-gun, and then applied directly to the strain gauge. The casing is then pressed against the metal and is held there by build in magnets. The wiring is already soldered to the strain gauge and can be connected via a socket on the casing.

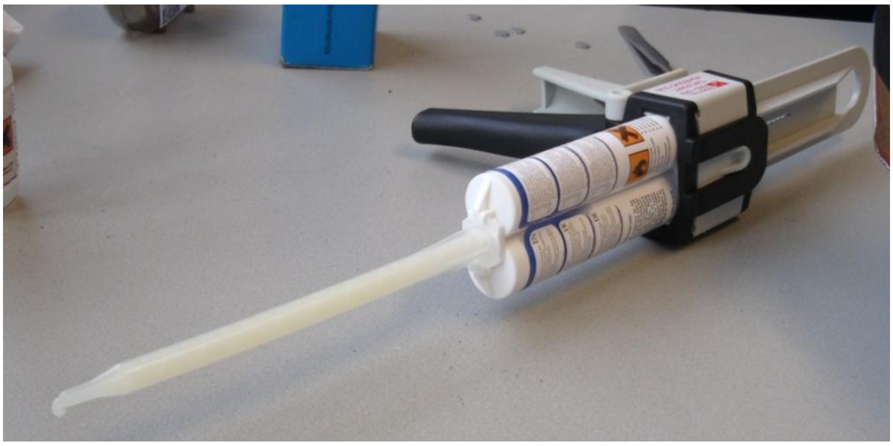

Figure III.26 Bienfait glue (mixing) gun

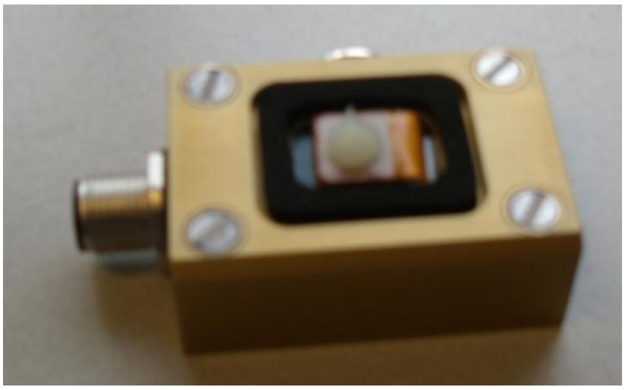

Figure III.27 Bienfait casing with glue. The four round surfaces in the corners are the magnets

IX. Lab test execution

Figure III.28 LVDT set up

Figure III.29 test set up

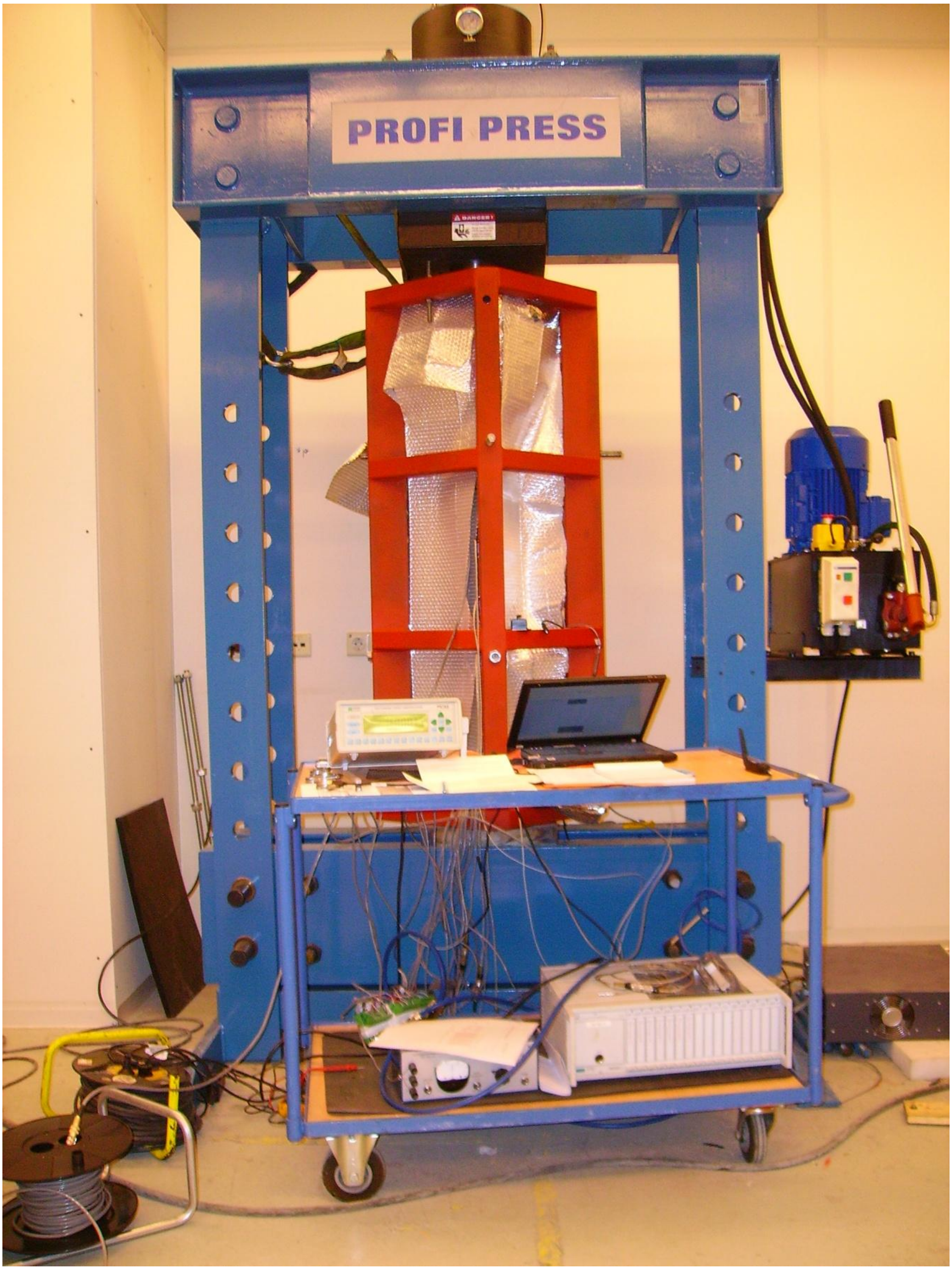

Figure III.30 Test set up with thermal isolation and all equipment

X. Stork lab rapport (Dutch)

Stork | FDO Inoteq

System Engineering, Product Testing and Materials Technology

Amsterdam : Czaar Peterstraat 229, 1018 PL

Postbus 379, 1000 AJ

Hengelo (Ov) : Langelermaatweg 10, 7553 JD

Postbus 194, 7550 AD

Telefoon : 020 556 3 555

LABORATORIUM TEST
SPANNINGS METING IN RAILS

Rapport

© Copyright Stork FDO Inoteq B.V.

Alle rechten voorbehouden. Niets uit deze uitgave mag worden vermenigvuldigd, opgeslagen in een geautomatiseerd gegevensbestand of openbaar gemaakt, in enige vorm of op enige wijze, hetzij elektronisch, mechanisch, door fotokopieën, opnamen, of enige andere manier, zonder voorafgaande schriftelijke toestemming van Stork FDO Inoteq B.V.

Indien dit rapport in opdracht werd uitgebracht, wordt voor de rechten en verplichtingen van opdrachtgever en opdrachtnemer verwezen naar de 'Algemene leveringsvoorwaarden van Stork FDO Inoteq B.V.' zoals op 27 juni 2005 onder nummer 33194077 gedeponeerd bij de Kamer van Koophandel te Amsterdam, tenzij uitdrukkelijk anders met ons is overeengekomen.

Opdrachtgever : ProRail B.V.
Moreelsepark 3
3511 EP UTRECHT
t.a.v. I. Shevtsov

Ordernr. Opdrachtgever : IP06-2202942

Ordernr. Stork FDO Inoteq : SFI002325P
Rapportnummer : SFI002325P Rev. 0
Auteur : Maarten Vaandrager
Datum Rapport : 1/24/2011
Aantal Bladen : 61

Classificatie :

Distributie : ProRail B.V.

t.a.v	I. Shevtsov	1x
Archief Stork FDO Inoteq B.V		1x

1) Inleiding

ProRail B.V. heeft Stork FDO Inoteq B.V. verzocht om een laboratorium proef uit te voeren op rails. Het doel van de laboratorium proef is het toetsen van de praktische toepasbaarheid van verscheidene meetmethodes voor het meten van spanning in de rails als gevolg van temperatuur fluctuaties en variërende mechanische belasting.

Om de invloed van temperatuursverandering en mechanische belasting op de sensoroutput te meten en te vergelijken met de theorie is een opstelling gebouwd met een stuk rails van 1.05m. Op de rails zijn verwarmingselementen aangebracht en de rails zelf is binnen een hydraulische pers geplaatst.

Dit rapport beschrijft de gebruikte apparatuur en methodes, de redenen voor bepaalde keuzes en de beperkingen van de gebruikte methodes en testopstelling. De dataverwerking van de metingen zijn door ProRail B.V. uitgevoerd en maken geen onderdeel uit van dit rapport.

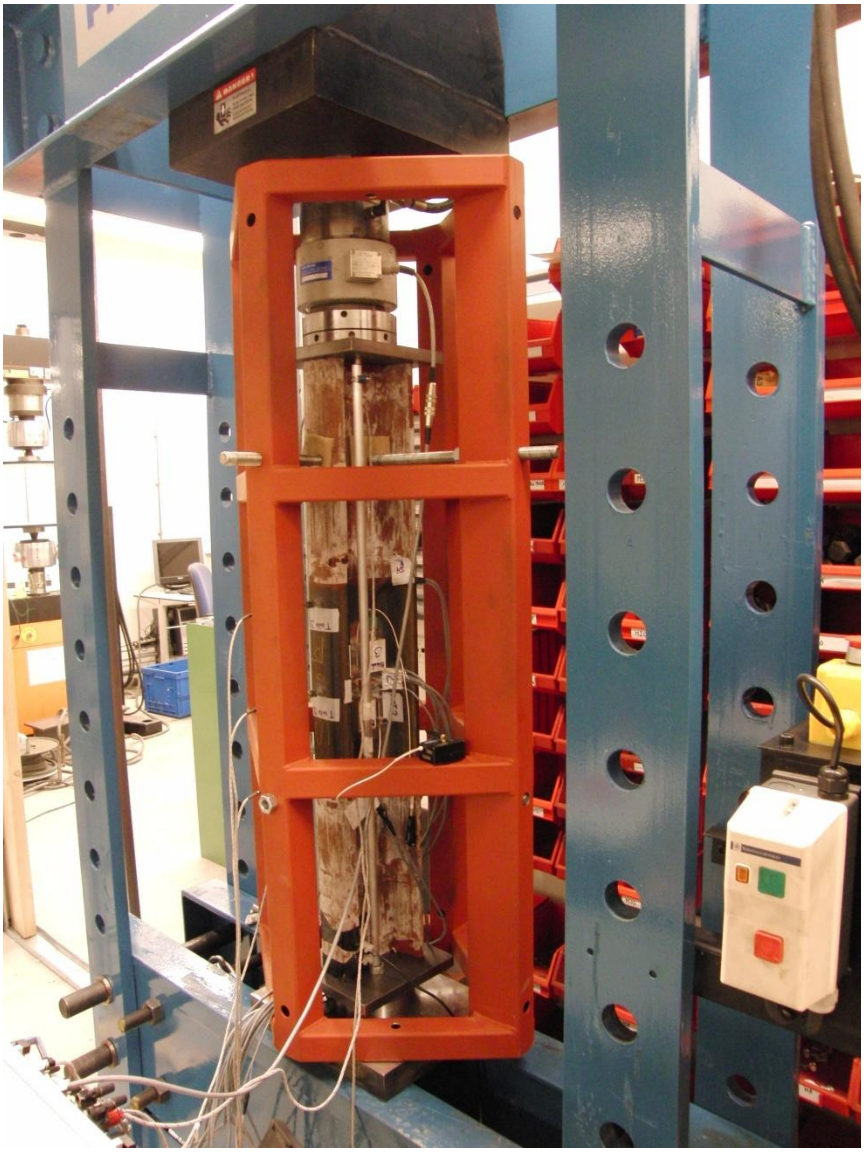

Figuur III.31**.** Testopstelling met pers, verwarming, frame, rails en sensoren

1.1) Apparatuur

De gebruikte apparatuur voor de labproef zijn weergegeven in tabel 1:

ITEM	OPMERKINGEN	REF.
Voeding voor verwarming	Typisch op 50 Volts, 10 amp. (500W)	114-473-18
PICAS meetversterker	Carrier frequency meetversterker voor load cell en LVDT's	114-422-28
HBM datalogger	Meetversterker voor pt100, Thermokoppels K, rekstroken en analoge voltages,	114-422-17
Laptop + usb microstrain basestation	met Catman Easy software and Node Commander 2.0 software	NLAMWS221
AE SG-DVRT-4 + Demod DC amplifier	Max error 2.3% of full scale (4mm)	1224-373
AE SG-DVRT-4 + Demod DC amplifier	Max error 2.6% of full scale (4mm)	1224-374
AE SG-DVRT-4 + wirelessLink	Max error 2.1% of full scale (4mm) 14bits wireless accuracy	1224-375
Anti buckling frame	-	-
3x Bienfait kastjes + pt100	Volle rekstrook brug 350 ohm	-
Rekstroken	Type Vishay General purpose. 350ohm, geconfigureerd als kwart brug	CEA-060250UT-350
2000kN Loadcell HBM	Max 1.5% relative error* over 0-600kN	114-433-27
2mm LVDT 1	Max 0.8% relative error	114-408-16
2mm LVDT 2	Max 0.8% relative error	114-408-1043
2mm LVDT 3	Max 1.2% relative error	114-408-03
20mm LVDT 1	Max 0.1% relative error*	-
20mm LVDT 2	Max 0.4% relative error*	-
20mm LVDT 3	Max 0.2% relative error*	-
3x PT100	Max ±0.2 C absolute error	-
3x Thermokoppels Type K	Max ± 2 C absolute error (can drift)	-
Mechanische pers Profi Press	capaciteit 160 ton	-
Rails	1.05m lang (+/-1mm)Type type 54E1, materiaal R260MN	-

Tabel 1: gebruikte apparatuur. *:Na correctie met factoren

1.2)Test setup
Om de rails onder een belasting te zetten van 600kN is gebruik gemaakt van een 160ton pers en frame om knik te voorkomen. Het frame dient ook als veiligheid voor het geval de opstelling onder compressie toch onstabiel wordt.

Om te voorkomen dat er een moment op de rails geplaatst kan worden zijn onder en boven de rail twee komvormige bolgewrichten geplaatst. Beide hebben het draaipunt van het gewricht naar het midden van de rails. Dit maakt het onmogelijk voor de pers om een moment door te geven aan de rails en zijn de uiteindes van de rails moment vrij.

De verwarming functionaliteit is aangebracht doormiddel van het bedekken van het onderste en bovenste deel (in de lengterichting) met koperdraad. Dit koperdraad is vervolgens met een dikke verf thermisch verbonden met de rails. De weerstand van de draad is in totaal 5 Ohm en levert daarmee bij een voltage van 50 volt en 10 ampère een vermogen van 500 watt.

Op het web van de rails in het midden van de lengte zijn de rekstroken geplaatst. Daar omheen zijn de DVRT's en Bienfait rekstrook kastjes geplaatst. De DVRT's zijn bevestigd met een bevestiging die zodanig is vastgelijmd dat deze over een afstand van 47.3mm meten.

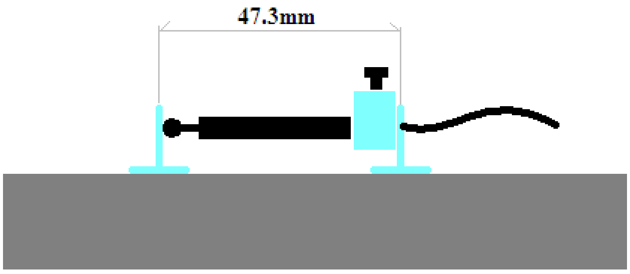

Figuur III.32**.** DVRT bevestiging aan de rails.

De kabels van de Bienfait kastjes zijn ge-rewired om zo een 6 draads aansluiting voor de brug te creëren. Dit maakt het mogelijk om door middel van de logger de meting te compenseren voor de weerstandsverandering van de draad. Ook de enkele rekstroken zijn met dubbele draden uitgevoerd (4 draads) waarmee de invloed van de weerstandsverandering van de draad gecompenseerd wordt.

Drie LVDT's zijn gemonteerd langs de rails op een 1.04 meter lange aluminium staven van diameter x. Gezien de hoge warmtegeleiding en de grote oppervlakte van de doorsnede van de staven wordt aangenomen dat deze een bij benadering uniforme temperatuur hebben. De temperatuur van de staven wordt gemeten met behulp van K-thermokoppels. De meting van de LVDT's samen met de berekende uitzetting van aluminium zou het mogelijk moeten maken om de lengteverandering van de totale rails te bepalen.

Op de rails zijn drie pt100 sensoren bevestigd over de lengterichting die gebruikt kunnen worden om een eventueel temperatuursverloop over de rails te kunnen bepalen.

Er zijn verscheidene proeven uitgevoerd waarbij de rails is opgewarmd tot 50-55 graden en vervolgens is belast tot een drukkracht van 600kN. De opwarming en belasting zijn ook uitgevoerd als individuele tests. De metingen zijn uitgewerkt door ProRail B.V. en de bespreking van de meetresultaten zijn daarom geen onderdeel van dit verslag.

Figuur III.33**.** Beide zijden van de rails en de daarop bevestigde sensoren

De Bienfait reksensoren zijn uitgevoerd als volle brug. Een volle brug is, vergeleken met enkele rekstroken, minder gevoelig voor temperatuurverandering. Ook heeft een volle brug een bridge factor van 2.6. Dit beteken dat een volle brug 2.6 x meer signaal geeft als enkele rekstrook bij dezelfde hoeveelheid rek en dus minder gevoelig is voor externe stoorsignalen. Het nadeel van de volle brug is dat deze gevoelig is voor lengteverandering en dwarscontractie (poisson ratio) maar dat het onderscheid tussen deze niet is te achterhalen. De enkele rekstroken hebben daarentegen het voordeel enkel gevoelig te zijn voor de richting waarin ze geplaatst zijn.

1.3)Beperkingen van de setup

Tijdens het uitvoeren van de test zijn enkele beperkingen van de testsetup naar boven gekomen waar rekening mee gehouden moet worden bij het verwerken van de meetdata:

De LVDT metingen op eindplaten kwam aanzienlijk hoger uit dan verwacht. De oorzaken die mogelijk ten grondslag liggen voor deze afwijking zijn:

1) Buigen van de platen aan de kopse kanten van de rails waarop de LVDT’s steunen. Aangezien de bolgewricht steunen van ronde vorm zijn, de rails een soort I profiel heeft en de 2cm dikke platen hier tussen zitten kan dit tot buiging van de platen hebben geleid. Hoewel miniem zorgt dit al snel voor een significante additionele verplaatsing in de LVDT metingen.

2) Contactoppervlak tussen platen en rails. Na afloop was aan de onder en bovenplaat te zien dat de oppervlakte druk niet gelijk verdeeld is geweest (zie fig. 4). Het gevolg hiervan kan zijn dat het contactoppervlak tussen de rails en de platen substantieel ingedrukt is en voor een additionele verplaatsing heeft gezorgd in de LVDT metingen.

Een betere uitvoering van de LVDT meting zou zijn als deze de verplaatsing zouden meten op eenzelfde wijze als de DVRT's maar dan over de gehele rails in plaats van slechts 47 mm.

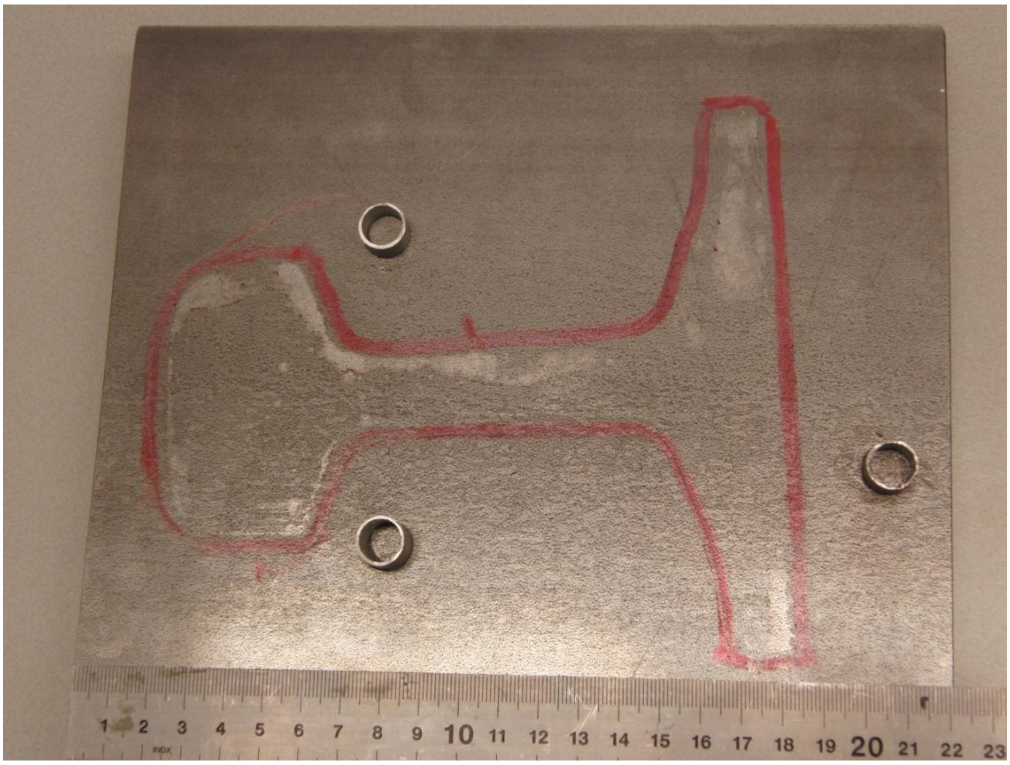

Figuur III.34**.** De 'imprint' van de rails op de plaat laat zien dat de oppervlaktedruk niet gelijk verdeeld was. De cilindertjes zijn de bevestigingspunten voor de LVDT metingen.

Tijdens de tests is een sterker dan verwachte temperatuur gradiënten over de rails gemeten (5 tot 10 graden verloop). Aangezien de temperatuur minder homogeen bleek dan verwacht is het temperatuurverloop niet verwaarloosbaar als de uitzetting van de rails onder invloed van temperatuur berekend moet worden.

De 2000kN loadcell die gebruikt is in de krachtmeting bleek bij vergelijking met een klasse 1 testbank een afwijking te hebben van 5% bij 200kN. Aangezien dit niet acceptabel is, is een hercalibratie uitgevoerd over het bereik van nul tot 600kN. Ook na correctie bleek de maximale relatieve error nog 1.5% te zijn.

De DVRT's zijn ook gebruikt om de uitzetting te meten tijdens het opwarmen van de rails. Echter, deze sensoren zetten zelf ook uit als gevolg van temperatuur en met hoeveelheid die waarschijnlijk in de buurt van de uitzetting staal ligt maar feitelijk onbekend is en dus moeilijk te compenseren, De bolgewricht steunen voorkomen het dat er een buigend moment doorgegeven wordt aan de rails. Ze voorkomen echter niet het ontstaan van een buigend moment dat het gevolg is van het niet op lijn liggen van de drukbelasting en de neutraal-lijn van de rails. Aangezien de rails op het oog is uitgelijnd in de pers en niet op basis van de exacte middel-lijn en neutraal-lijn van de rails is de kans aanwezig dat dit wel plaats vindt. Dit zou de oorzaak kunnen zijn voor verschil in rek meting tussen de twee zijdes van de rails.

Stork FDO Inoteq B.V.

Autorisatie: E. de Rijcke
Afdelingsmanager

Auteur: Maarten Vaandrager
Adviseur Toegepaste Mechanica

Integratie in het afstudeerrapport heeft de opmaak enigszins veranderd. Er zijn geen inhoudelijke wijzigingen aangebracht.

XI. Model results

Due to the large amount of print screens of the model made, and a lack of a sufficiently efficient method of presenting them completely, these model results are omitted from the appendix. A digital copy can be requested.

XII. DVRT mounting trial test, and preliminary conclusions

i. Description of DVRT mount trial test.

The goal was to test whether the DVRT mounting would be influenced by the jolt that occurs upon cutting the rail at temperatures below the neutral temperature. The DVRT was not acquired yet, so an LVDT took its place. The LVDT measuring device is similar in shape and principle, but its exact technology differs a little. The mount would be glued to a sleeper, while the measuring part of the LVDT was positioned against an aluminium profile that was glued to the rail.

Upon arrival at the site, we were informed that the connections would not be loosened next to the welds. We expected the connections to be loosened for 30 meters, to provide a large length of rail to "build up" the shortening of the rail. Improvising on site the decision was made to measure the replacement piece, and how much it jolted back. The replacement piece was approximately 6.5 meters long, and along this length, the connections would be loosened, with an added sleeper. The total length of unfastened rail was estimated to be 12 sleepers, or 7.2 meters. The temperature was -2 degrees, this was determined with the help of a thermal imaging camera. (28 degrees F is about -2.2 degrees C)

Figure III.35 Thermal imaging temperature measurement of rail

Using this data the amount of shortening of the unfastened rail (Δ L) can be calculated:

Δ T = temperature difference between neutral temperature (25) and rail temperature: 27 degrees C

Length of unfastened rail (L): 7200 mm.

Coefficient of thermal expansion of steel (α): 12E-6

$\Delta L = \Delta T * \alpha * L$ = 7200*12E-6*27 = 2.338 mm

Upon making the first cut the zero measurement of the LVDT was established to be 2.379 mm. After cutting and stabilisation of the measurement (due to temperature effects the reading was not yet stable immediately after cutting) the final value was -3.500 mm. This means the LVDT measured a displacement of 5.879 mm closely to the cut position (within 30 cm).

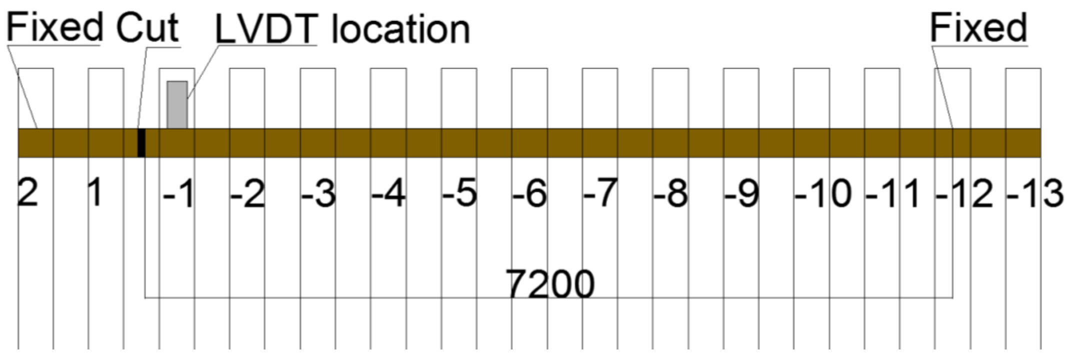

Figure III.36 Overview of the situation, sleepers and only the cut rail are shown

Before cutting, reference lines were chalked on the rail. This was done for 5 sleepers in the direction of the fastened rail, and for 12 sleepers in the direction of the replacement rail (the entire replacement rail length, with the 12th sleeper being the fastened one). These reference measurements indicated that the replacement rail compression was as follows:

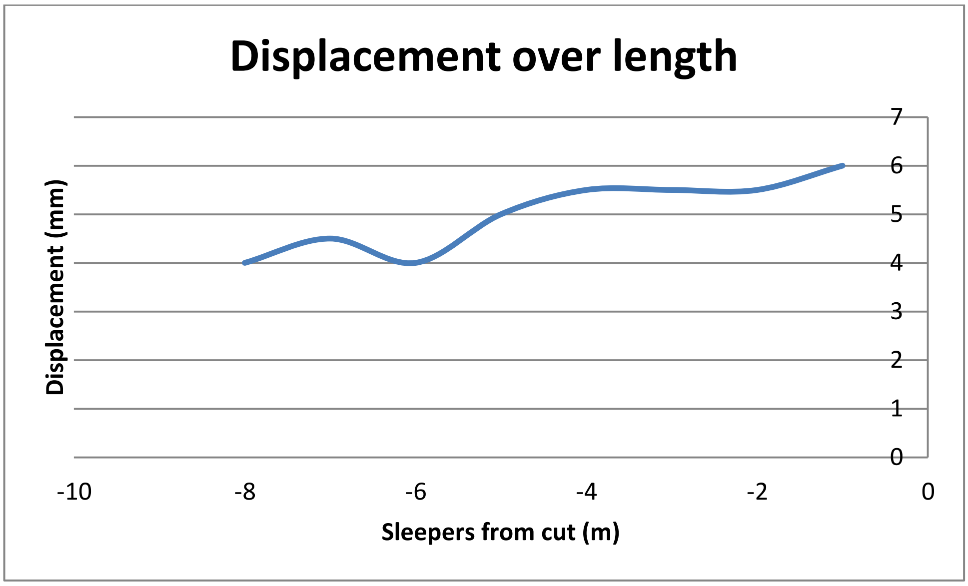

Figure III.37 Displacement measurements using reference chalk stripes

Pictures of the measurements leading to this distribution are added on the last pages of this report. The distribution is not very linear, this is due to the uncertainty in reading the chalk lines. The linearity is assumed to be a decrease of 2 millimetres over 7 sleepers, spaced 60 cm apart. Converting this to the total length (7.2 meters) of the unfastened replacement rail comes down to roughly 2.9 mm of compression caused by the linear contraction due to temperature difference. This means that the neutral temperature of the replaced rail was about 30 degrees Celsius.

32 * 12E-6 *7200 = 2.8 mm

This leaves a further 3 mm of displacement (measured by both the chalk lines and the LVDT) unaccounted for, as well as the 4 mm of displacement on the opposite side (measured on sleeper 1).

A simulation run on the situation clarifies the outcomes:

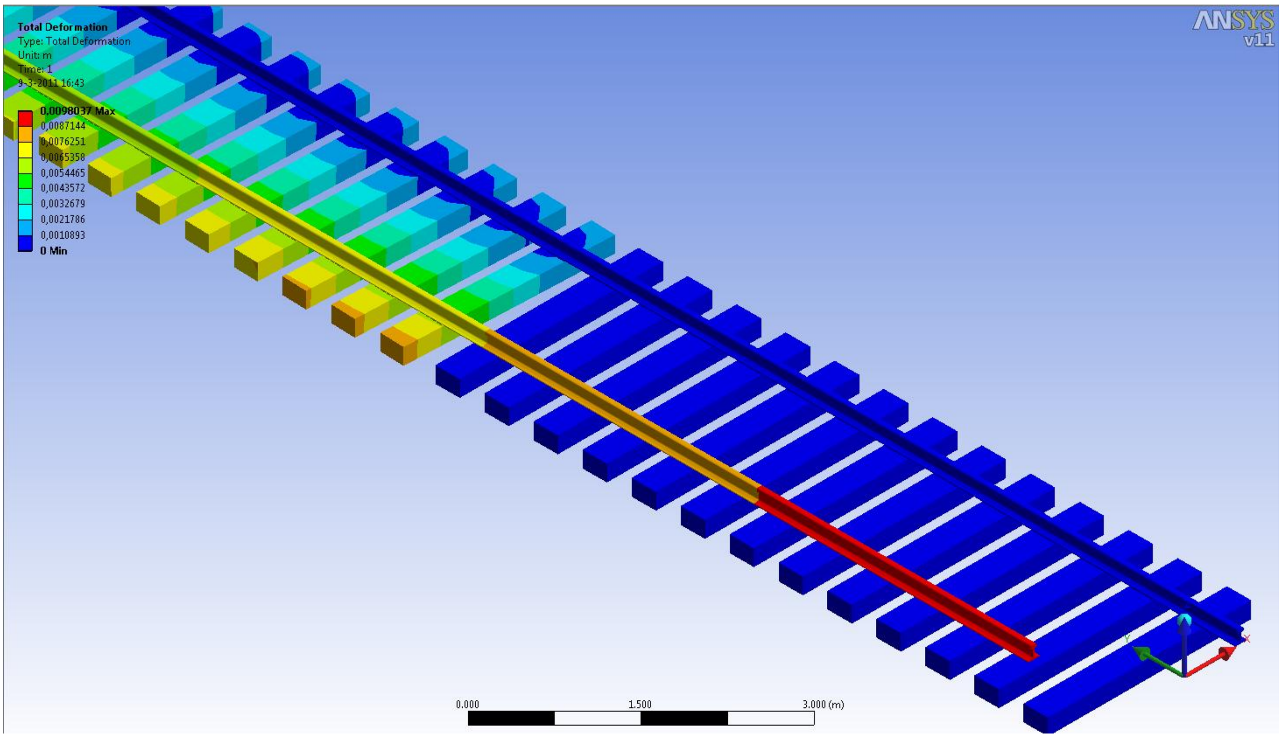

Figure III.38 Simulation run based on a 27 degree temperature difference

This is an overview of the outcome at a neutral temperature of 25 degrees Celsius. It is apparent that the sleepers move as well (they rotate), and that this amount of movement corresponds to the unexplained portion of the results. Furthermore, when a simulation is run with a lower neutral temperature (12 degrees C) the simulation results represent the measurements closely, suggesting that the neutral temperature in the rails is about 12-15 degrees.

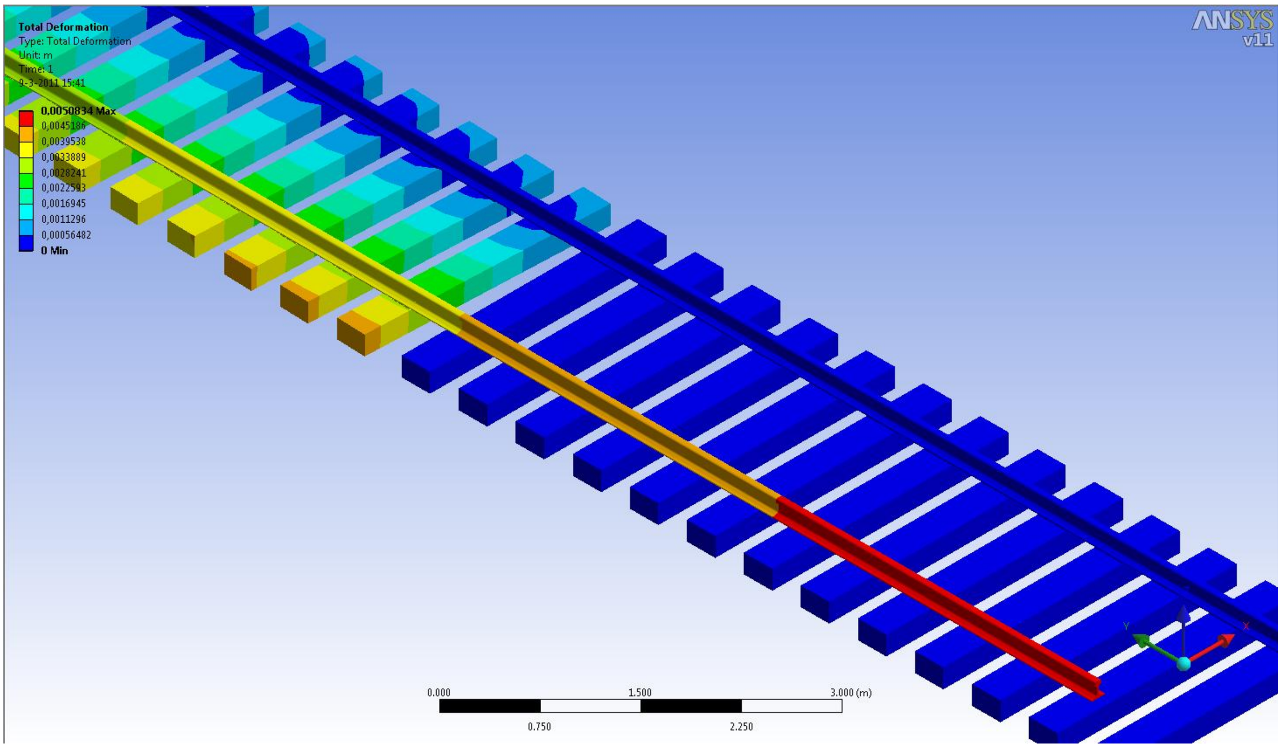

Figure III.39 Simulation at 12 degrees neutral temperature

There are of course uncertainties in the model with respect to the resistance of the ballast. This illustrates that it is important to measure the resistance of the ballast, and the displacement of the sleeper. I would like to suggest placing a strain gauge right after the first fixed sleeper, this way we have the displacement of the sleeper, and the difference in strain due to a single sleeper fixation which will provide us with ballast resistance estimations.

The distance of the cuts was measured as well, the first cut was 1,3 cm wide while the second was 0.3 cm. Because the second cut was performed without tension in the rail it provides us with a base line of the cutting width itself. Subtracting the 0.3 from the 1.3 cm indicates that the total distance the rail retreated was about 1 cm, which corresponds to the added displacement measurements of 6 and 4 mm respectively.

ii. Conclusion

The DVRT mounting performed according to specification, but a longer time for the glue to harden is required. The influence zone (the number of displaced sleepers) is in the order of magnitude of 30-40 sleepers. It is important to measure the sleeper displacement as well, as these displacements appear to be significant. The displacement of the sleepers in the ballast appears to be in the order of magnitude of 3-4 mm (the measurement on sleeper 1 indicates 4 mm). These displacements are therefore important to measure as well. A more precise way to determine sleeper-rail displacement is needed, the chalk lines are too uncertain.

Nothing about the outcomes can be said with certainty, the measurements are simply not precise enough. This will improve when strain gauges are added, sleeper displacements are measured and a more precise method of measuring rail-sleeper displacement is used. A combination of spray paint and a piece of sticky tape might be a good idea, as it provides a clear line to measure, and the angle of the pictures must be aligned straight with these lines as the perspective seems to have an influence as well.

Sleeper 1

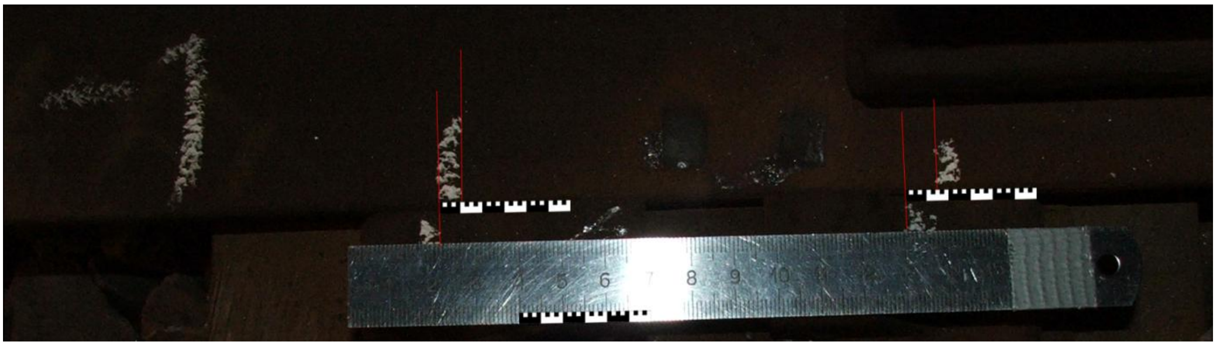

Sleeper -1

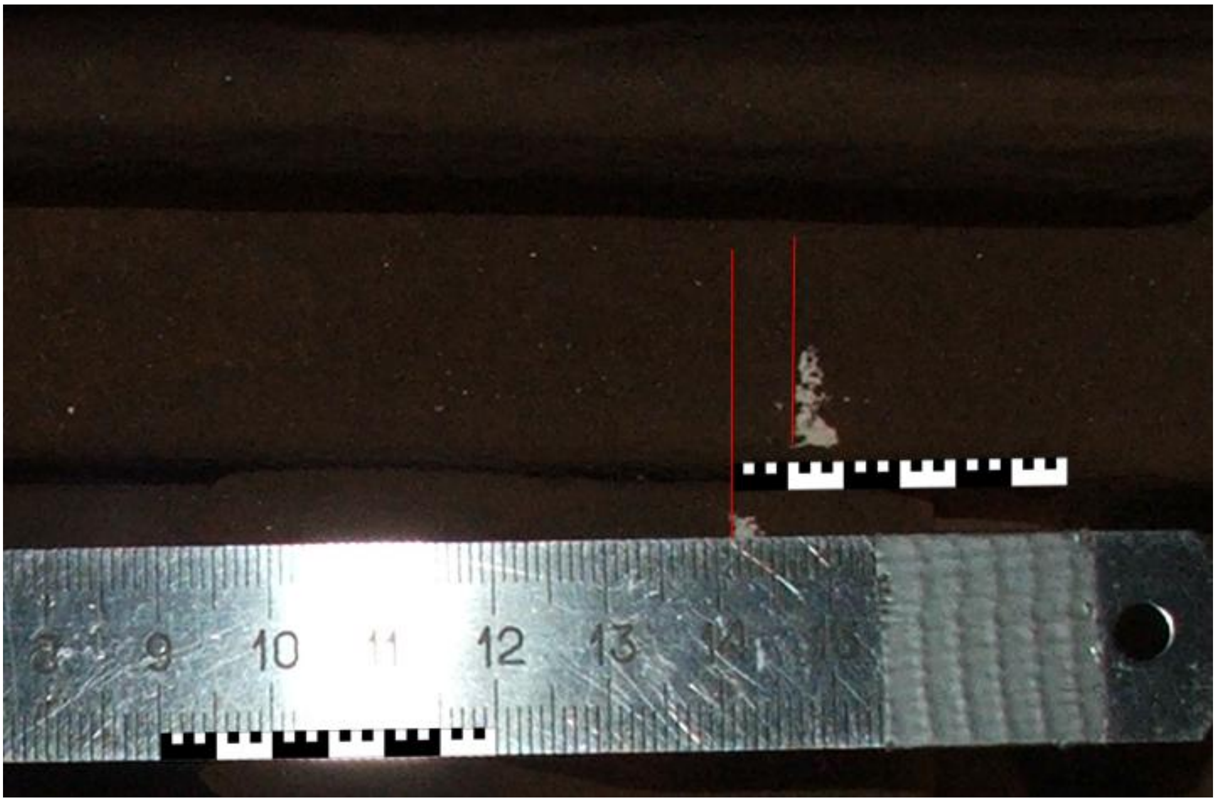

Sleeper -2

Sleeper -3

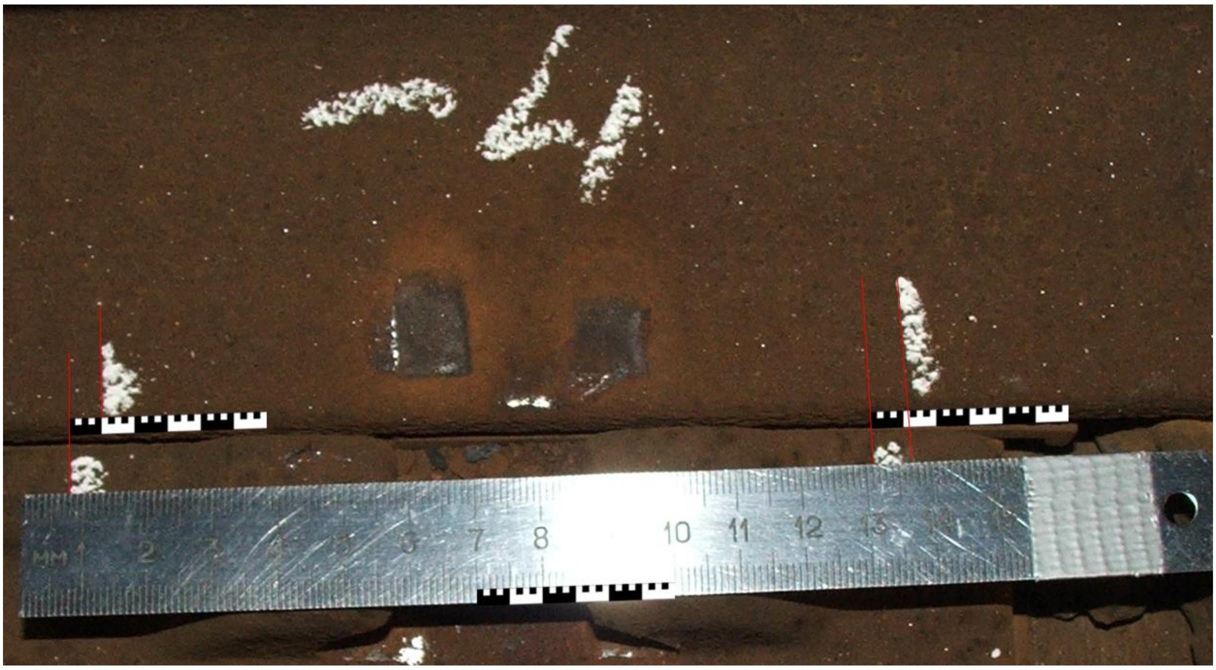

Sleeper -4

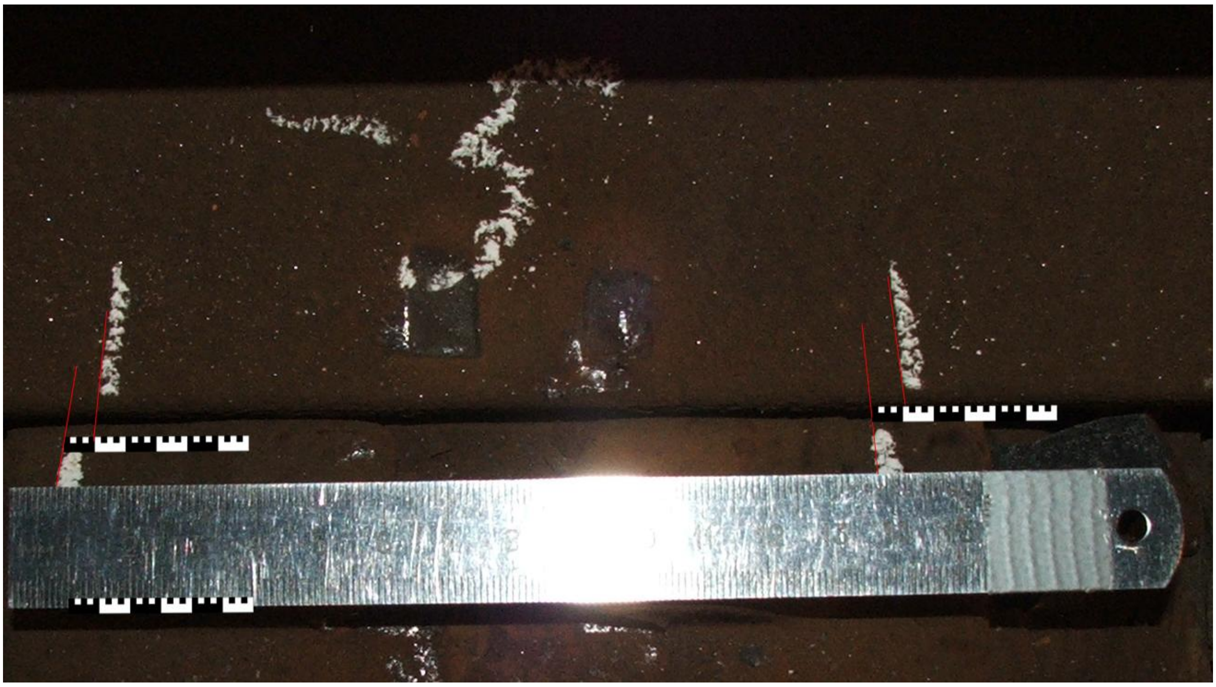

Sleeper-5

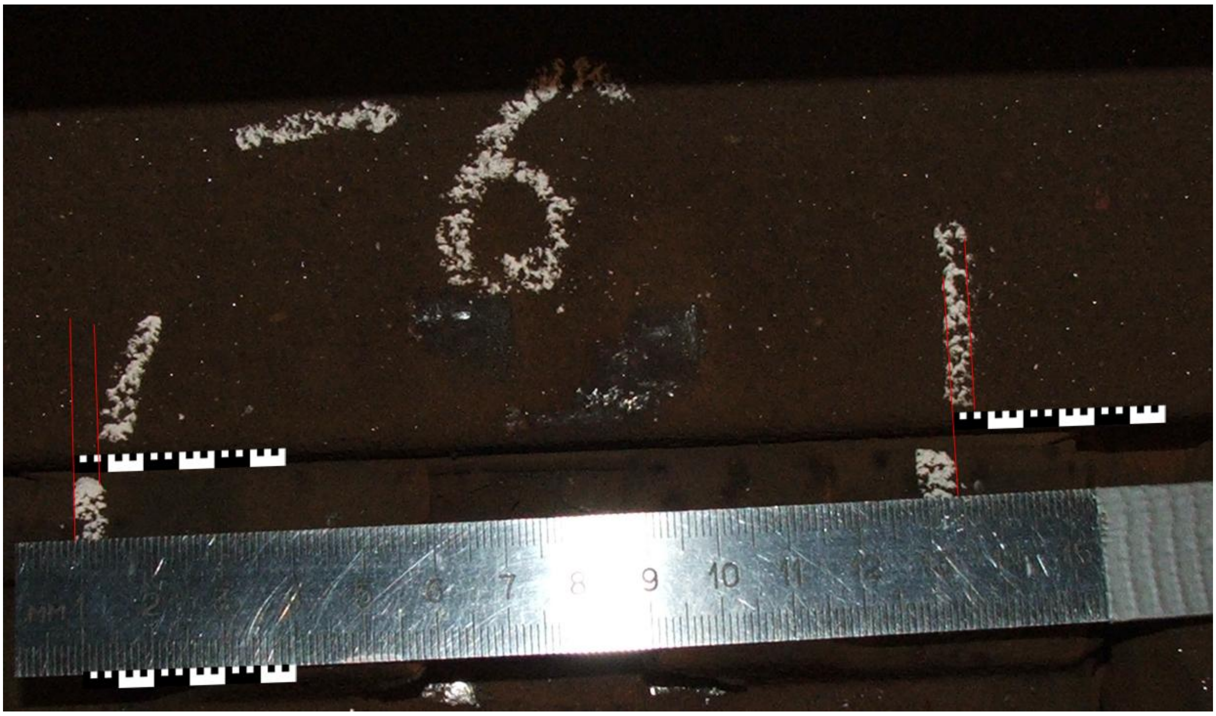

Sleeper-6

Sleeper -7

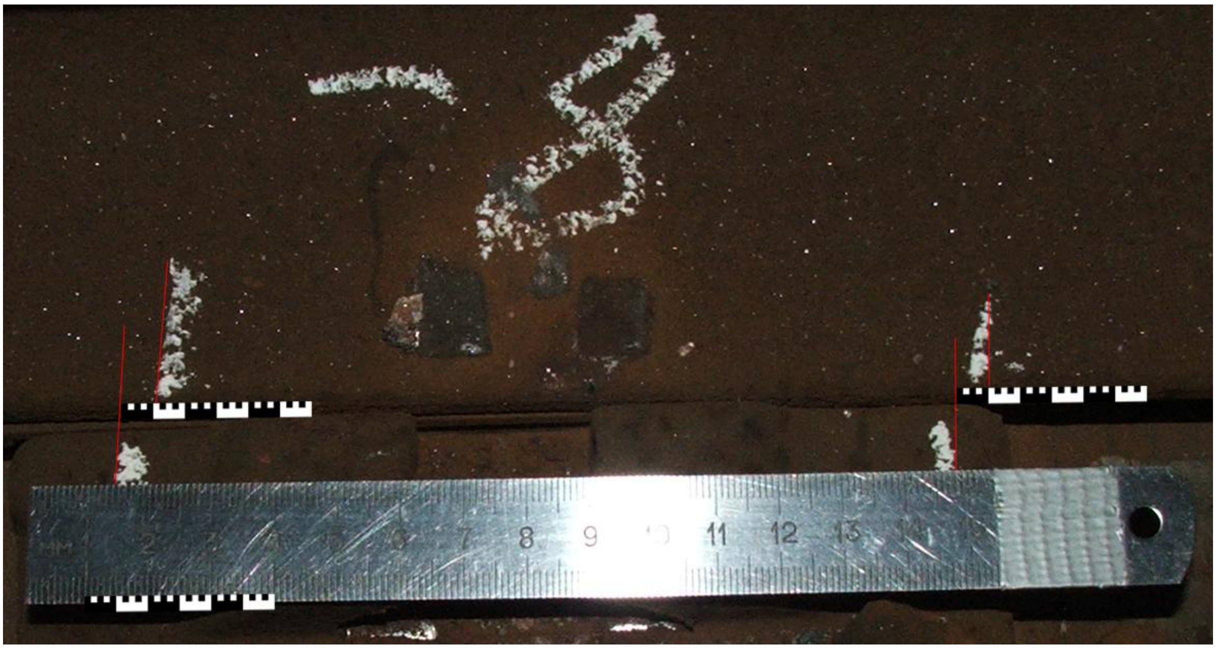

Sleeper -8

Table of figures

Figure III.2 Strain distribution with springs XIII
Figure III.3 Strain distribution without springs XIII
Figure III.4 Normal stresses with springs XIV
Figure III.5 Normal stresses without springs XIV
Figure III.6 Normal stresses near ball and claw with springs XIV
Figure III.7 Normal stresses near ball and claw without springs XV
Figure III.8 Displacement in the x direction with springs XVI
Figure III.9 Displacement in the x direction without springs XVI
Figure III.10 Displacement in the Y direction with springs XVII
Figure III.11 Displacement in the y direction without springs XVII
Figure III.12 Displacement in the y direction at the largest deviation section with springs XVII
Figure III.13 Displacement in the y direction at the largest deviation section without springs XVIII
Figure III.14 Displacement in the z direction with springs XIX
Figure III.15 Displacement in the z direction without springs XIX
Figure III.16 Displacement in the z direction with springs, near the ball and claw XIX
Figure III.17 Displacement in the z direction without springs, near the ball and claw XX
Figure III.18 Strain comparison, situation A is with frictionless contact areas 32
Figure III.19 Stress comparison, situation A is with frictionless contact areas 33
Figure III.20 grinding the rail XXXIV
Figure III.21 Sanding down the strain gauge locations XXXIV
Figure III.22 Left to right, accelerator, preparation agent, neutraliser XXXV
Figure III.23 Strain gauge on sticky tape XXXVI
Figure III.24 Pealed back tape XXXVI
Figure III.25 Applying the accelerator XXXVI
Figure III.26 Applying the glue XXXVII
Figure III.27 Bienfait glue (mixing) gun XXXVII
Figure III.28 Bienfait casing with glue. The four round surfaces in the corners are the magnets XXXVIII
Figure III.29 LVDT set up XXXIX
Figure III.30 test set up XXXIX
Figure III.31 Test set up with thermal isolation and all equipment XL
III.32. Testopstelling met pers, verwarming, frame, rails en sensoren 45
III.33. DVRT bevestiging aan de rails. 47
III.34. Beide zijden van de rails en de daarop bevestigde sensoren 48
III.35. De ‘imprint’ van de rails op de plaat laat zien dat de oppervlaktedruk niet gelijk verdeeld was. De cilindertjes zijn de bevestigingspunten voor de LVDT metingen. 49
Figure III.36 Thermal imaging temperature measurement of rail LII
Figure III.37 Overview of the situation, sleepers and only the cut rail are shown LIII
Figure III.38 Displacement measurements using reference chalk stripes LIII
Figure III.39 Simulation run based on a 27 degree temperature difference LIV
Figure III.40 Simulation at 12 degrees neutral temperature LV